2017

An intelligent, fast-acquisition remote sensing system for locating and measuring burial of subsea power and telecommunication cables

Szyrowski, Tomasz

An intelligent, fast-acquisition remote sensing system for locating and measuring burial of subsea power and telecommunication cables

by

Tomasz Szyrowski

A thesis submitted to Plymouth University
in partial fulfilment for the degree of

Doctor of Philosophy

School of Marine Science and Engineering

September 2016

To my wife Kamila and daughters: Cecylia and Liliana

Abstract

This thesis describes novel methods to localise and estimate the burial depth of subsea cables. The limitation of the current methods is that they can measure the distance to the cable only in a small vicinity, usually up to three metres. The enhancements of the methods were investigated. The output from Neural Network algorithms was tested for its ability to enlarge the detection range and increase its precision.

Following traditional methods, a new approach based on system identification and modelling was inspected. Various models were proposed and enhanced with Kalman filtering for linear models and unscented Kalman filtering for nonlinear models. In the case of subsea cable tracking, Kalman filtering requires precise knowledge of the system dynamics and associated stochastic processes. These requirements are often difficult to satisfy. To overcome this limitation this thesis proposes a novel and effective algorithm based on particle filtering.

The proposed novel approach uses the whole set of sample points collected from the surface above the subsea cable. The algorithm based on a batch of samples allows to eliminate effectively the noise of the readings and estimate the position of the cable from larger distances than the current methods can do.

The novel batch particle filter was implemented in different applications. Depending on the survey requirements and set-up, the method can be used on a single survey line or applied to the area covered by the survey and estimate the three-dimensional section of the cable. The algorithm was tested in a simulation of tracking by an autonomous surface vehicle. Finally, the market analysis for commercialisation of the method was conducted and a new prototype was proposed.

The batch particle filter was tested on experimental data collected in different locations. The results demonstrate that the method is both practical and feasible and can successfully estimate the position of the subsea cable in shallow water.

Contents

List of Figures

Nomenclature

AC – Alternating Current

ADC – Analogue to Digital Converter

AE – Aqua Explorer

AUV – Autonomous Underwater Vehicle

BEP – Best Estimation Point

BMH – Beach Man Hole

BOSS – Buried Object Scanning Sonar

BPF – Batch Particle Filter

CAT – Cable Avoidance Tools

CCR – Current – Channel Response

DC – Direct Current

ECR – Eddy – Current Response

EF – Electric Field

EKF – Extended Kalman Filter

ELF – Extremely Low Frequencies

EMF – Electro - Magnetic Field

EMS – Electromagnetic Searcher

FFT – Fast Fourier Transform

FLS – Fuzzy Logic System

GA – Genetic Algorithm

GIS – Geographic Information System

GPS – Global Positioning System

GUI – Graphical User Interface

HF – High Frequencies

HMM – Hidden Markov Model

ICPC – International Cable Protection Committee

KF – Kalman Filter

LKF – Linearized Kalman Filter

LoG – Laplacian of Gaussian

MF – Magnetic Field

MIMO – Multiple Inputs, Multiple Outputs

NN – Neural Network

PDF – Probability Density Function

PF – Particle Filter

PSD – Phase Sensitive Detector

RGB – Red, Green, Blue

RMSE – Root Mean Square Error

ROI – Region of Interest

ROV - Remotely Operated Vehicle

RTG – Real-Time Tracking Gradiometer

SISO – Single Input, Single Output

SLAM – Simultaneous Localisation and Mapping

SMA – Simple Moving average

SMC – Sequential Monte Carlo

SNR – Signal to Noise Ratio

SSS – Side Scan Sonars

TDOA – Time Difference of Arrival

UI – User Interface

UKF – Unscented Kalman Filter

USV – Unmanned Surface Vehicle

UUV – Unmanned Underwater Vehicle

UXO – Unexploded Ordnances

VIC – Video Imaging Complex

Acknowledgements

Firstly, I would like to thank to my wife Kamila. Without her continuous support and help I would not have achieved this success.

Gratitude needs to be given to the initiator of this project Mr Steve Moore from Subsea Cable Tracking Ltd. His many years of mentoring given in different projects are valuable for all individuals directly benefiting from his support but also for a wide research community who can build on his great experience.

I would like to thank my supervisory team. In particular, a big thank you to my Director of Studies, Dr S. Sharma for his continued support, Prof. R. Sutton, for his valuable insight to this project. I have tended to stray from my academic work most of the time, and without my supervisors' guidance I would have lost sight of my aim long ago.

Through the course of my research I received help from many friends but one in particular, Amit Motwani has helped me on different levels. Without his input the quality of this work would not reach its current standard.

Many thanks to all the staff at the university who provided their support. In particular Francesca Niedzielski for keeping a steadfast eye on my successful progress, the staff at the School Office led by the ever resourceful Barbara Fuller who I am convinced can resolve just about any logistic or administrative quandary us students seem to get ourselves into, and the team from the Graduate School, especially Sarah Kearns for her neverending encouragement.

Finally, I would like to give thanks to my friends and people I met on my research journey, who have always encouraged me in this work, even during the times I was too busy to appreciate their encouragement.

Declaration

At no time during the registration for the degree of Doctor of Philosophy has the author been registered for any other University award without prior agreement of the Graduate Committee.

Work submitted for this research degree at the Plymouth University has not formed part of any other degree either at Plymouth University or at another establishment.

This study was financed by European Social Fund, Combined Universities of Cornwall to promote regional development.

Publications (or presentation of other forms of creative and performing work): 6

Presentation and Conferences Attended: 6

Word count of main body of thesis: 52,694

Tomasz Szyrowski

31st October 2016

Chapter 1. Introduction

Detection of subsea cables plays an important role in many applications, from laying down new connections, through to periodical inspection, damage repairs and the clearing off out of service utilities. This thesis focuses on one of the challenges faced in subsea installations: detecting and estimating the burial depth of subsea cables in shallow water.

This chapter presents an overview of the concept, summarises research objectives, outlines the main contribution of the research and lists publications resulting from the work.

1.1 Motivation of the research

Subsea cables are critically important for the current economy. They provide power and communications links between continents and islands and connect a growing number of off-shore installations. The subsea cables need to be periodically checked, localised and repaired for faults. Localisation of cables is a difficult and costly task as dynamic sea environments keep changing the cables' initial position and their burial depth (Szyrowski et al., 2013a).

The current state of knowledge in estimating the position and burial depth of marine power cables relies mainly on deterministic approaches and mathematical inversion methods (Cowls & Jordan, 2002; Won, 2003; Szyrowski et al., 2013b). A magnetic signal emitted from the cable is sampled at two different points in space. Because of the salinity of sea water it attenuates at a fast rate. The magnetic field signal can thus be measured only in close proximity from the source and in practice the signal can only be measured within a 5 m range (Takagi et al., 1996; Kojima et al., 1997; Szyrowski et al., 2013b). This creates a problem in marine surveys as it has to be performed by a remotely operated vehicle or a specialised diver and thus susceptible to an increase in operational cost and risk to human health and life. The diver can only remain in the water for a short period of time and it is difficult to operate in limited visibility and/or strong currents. In addition, the localisation of the cable based on a human's judgement is susceptible to errors and not reliable in most cases (Ortiz et al., 2000).

There are number of methods that try to solve the problem of cable location. Methods based on visual inspection, acoustics or geo-magnetics provide some means to track subsea cables. Despite advances in

technology all of these methods suffer from many limitations. Visual and acoustic methods can only recognise cables which lie on the seabed. Although magnetic methods can detect buried utilities, often the size of the cable and surrounding magnetic noise render these methods to be unreliable.

Additional complications arise in shallow water. A ship with specialised equipment can only navigate in waters deeper than ten metres. Often this means that along many kilometres off the coast the cable needs to be surveyed with a small boat.

Shallow water has proven to be a difficult and challenging environment. One solution which could meet these requirements is to devise a surveying method from the surface of the sea without engaging a diver or remotely operated vehicle (ROV). This would require a reliable method for mid-range detection which can cope with the uncertain environment. Such methods need to have the ability to reduce the effects of noises originating from various sources such as the engines of the survey boat, communication devices and other sources of magnetic fields.

This thesis introduces a novel stochastic approach based on particle filters to estimate the distribution of an induced electromagnetic field on the sea surface in an uncertain environment and accurately predict the location of the cable.

1.2 Subsea cable tracking method

The method of subsea cable tracking described here relies on detection of the electromagnetic field emitted by an induced alternating current. From all the methods used in subsea surveying, the tone detection method is one of the most reliable (Szyrowski et al., 2013b). Although other magnetic inspection methods can sense the ferromagnetic objects, tone based detection can uniquely characterise the utility from the induced frequency.

In the tone based detection, the alternating current applied to the cable generates an electromagnetic field propagating through the water. The field is sensed by searching coils tuned to a given frequency. Based on the magnitude of the emitted field the cable can be localised and the distance to the cable can be estimated.

Traditionally this method has been used by a diver with a handheld sensors' frame placed on the seabed. The reliability of the survey depends not only on the properties of the environment such as the seabed's condition or water current but is largely impacted by the human factor.

The need to derive a more accurate detection method has led to new developments and a move towards the use of underwater ROVs. They can be used for longer periods of time at greater depth and with better precision but still suffer from many limitations

Irrespective of how the tone induced method is used, whether by the diver or the ROV, the sensors need to be close to the seabed, and no more than five metres from the cable. It is particularly challenging in shallow waters with more features on the seabed, marine growth, and stronger currents.

The methods described in this work use a different approach. The sensors are mounted on the side of the boat and the detection is performed from the water surface. The aim of this set-up is to reduce the survey time, provide better positioning and reduce the risk of underwater operations.

To achieve this goal the method is designed to sense from a larger distance. The processing of collected data is not conducted by a deterministic approach as in traditional methods but instead rely on a stochastic algorithm. This novel approach may seem more complicated and computationally intensive but it provides a good alternative to traditional methods.

1.3 Aim and Objectives of the Research

The main aim of the research reported in this thesis is to address the challenge of shallow water surveys through the design and development of a new fast-acquisition survey system which can be towed or vessel-mounted and be capable of rapidly detecting and remotely measuring the burial depth of subsea power and telecommunication cables

To achieve the main aim various partial objectives were set as described below:

1. To develop a new remote sensing system for locating and measuring burial of subsea cables.
2. To investigate intelligent procedures able to adapt to challenging shallow water environment.
3. To investigate the Kalman Filter algorithm and the possibility of its use in cable tracking.
4. To undertake a market analysis and justify the feasibility of the method.
5. To develop a prototype for the remote sensing method.
6. To develop new algorithm for localisation of the subsea cable in the water depth up to 15 metres from the surface.
7. To investigate and implement new algorithm Batch Particle Filter.

1.4 Contribution of the Research

The contribution of this research includes

1. A general framework for a new method for remote sensing of subsea cables has been formulated. The method has been tested on real world data and has been proven to be an efficient alternative to traditional methods.
2. The implementation of Particle Filters in a novel application has been proposed as new localisation algorithm Batch Particle Filter.
3. Utilisation of the whole distribution of the emitted electromagnetic field has been carried out. The approach is in opposition to the single measurement used in traditional methods. It gives a new approach to particle filters and data acquisition.
4. Proposal of a novel surveying method with the use of unmanned surface vehicles. The combination of batch particle filters and autonomous navigation was tested in simulation. It provides an alternative to costly traditional marine surveys.
5. Investigation of the disadvantages of the usage of Kalman Filtering in tracking and localisation in shallow water environments. Various mathematical models were investigated and tested on experimental data.
6. To the best of author's knowledge, the outcome of this work constitutes a novel approach to subsea cable tracking and has not been used before in a similar configuration.

1.5 List of Publications

The following papers have been published during the course of this research.

Journal articles:

1. Szyrowski, T., Sharma, S.K., Sutton, R. and Kennedy, G.A., 2013. Developments in subsea power and telecommunication cables detection: Part 1–Visual and hydroacoustic tracking. *Underwater Technology*, *31*(3), pp.123-132.

2. Szyrowski, T., Sharma, S.K., Sutton, R. and Kennedy, G.A., 2013. Developments in subsea power and telecommunication cables detection: Part 2–Electromagnetic detection. *Underwater Technology*, *31*(3), pp.133-143.
3. Szyrowski, T., Sharma, S.K., Sutton, R. and Kennedy, G.A., 2015. Subsea cable tracking in an uncertain environment using particle filters. *Journal of Marine Engineering & Technology*, *14*(1), pp.19-31.
4. Szyrowski, T., Motwani, A., Sharma, S.K., Sutton, R. and Kennedy, G.A., 2015. Subsea cable tracking by an unmanned surface vehicle. *Underwater Technology*, *32*(4), pp.217-229.

Peer-reviewed conference papers:

5. Szyrowski, T., Sharma, S.K., Sutton, R. and Kennedy, G.A., 2014, July. Point localisation of a subsea cable using particle filters. In Control (CONTROL), 2014 UKACC International Conference on (pp. 290-295). IEEE.
6. Szyrowski, T., Motwani, A., Sharma, S. K., & Sutton, R. "Localisation of subsea ferromagnetic objects from an autonomous surface vehicle", In Undersea Defence Technology (UDT) Conference, ACC Liverpool, UK, pp 1-9

Conferences and seminars:

7. Szyrowski, T., An intelligent, fast-acquisition remote sensing system for subsea applications. PlyMSEF 'Making Waves' Conference, 18th December 2012. Plymouth Marine Laboratory, Plymouth, UK.
8. Tomasz Szyrowski on An intelligent, fast-acquisition remote sensing system for subsea applications Wednesday 13 March 2013 at Engineering Research Seminar
9. Szyrowski, T on The Python programming language as a freeware alternative to Java, Matlab or R. Wednesday 17 April 2013 at Engineering Research Seminar
10. Szyrowski, T., Particle filters in subsea localisation. 'Making Waves' Conference, Plymouth Marine Laboratory, 28th November 2013, Plymouth, UK.
11. Szyrowski, T.on The use of particle filtering in subsea cable localisation Wednesday 18 December 2013 at Engineering Research Seminar

12. Szyrowski, T., “Subsea Cables in Shallow Waters - Tracking, Installation and Protection” MARSIC Seminar National Oceanography Centre Southampton 05 September 2016

1.6 Thesis Outline

The rest of this thesis is organised as follows:

Chapter 2 presents current possibilities and available choices often used for surveying subsea cables. The chapter is organised into two parts, namely visual and acoustic detection. The knowledge of these methods is important for surveying practices as the methods are often combined to provide the best possible mapping of the utility and its surrounding area.

Chapter 3 extends description of available surveying methods to electromagnetic detection. From all available methods only a few can detect a buried utility. Electromagnetic fields can be detected regardless of the burial depth of the cable. The practicalities of electromagnetic detection are addressed in the following chapter.

Chapter 4 focuses on practical issues of cable detection. It starts with a market analysis and description of current techniques used for estimation of burial depth. In this chapter available techniques are described as the knowledge of them is important for design of new tool.

The chapter 5 gives an overview of the usage of the proposed method, describes the main components of the system and how the system can be incorporated into wider survey.

After this practical introduction, the proposed method is further analysed in the following chapters. Before the new algorithm is proposed, the possible improvements of current methods are considered.

Chapter 6 presents the theory behind the inverse techniques used as industry standards. The chapter evaluates the usage of the method at greater distances from the cable. It also considers improvements of the method by the application of Neural Networks. The experimental data collected in real-world experiments are used to evaluate the method and possibility to carry out enhancements

From the traditionally used inverse method, more focus is given on the modelling of emitted field and its application to source detection. Chapter 7 considers the localisation of subsea cables by means of Kalman

Filters. The chapter examines different approaches to modelling of phenomena and utilisation of different Kalman Filtering algorithms.

After the analysis of tracking methods based on point measurement, a different approach is presented. Chapter 8 describes the method of Batch Particle Filters. In the first section of the chapter describes the method of particle filters and its traditional application. In the following section, it outlines the usage of the proposed algorithm and presents the outcome of its application on both simulated and real world data. After the presentation of the proposed Batch Particle Filters, the details of algorithms are considered and analysed. The chapter concludes with the presentation of the algorithm's usage during a marine survey.

Chapter 9 summarises and concludes the thesis. Although the method can be used for cable tracking, their extensions to other applications are considered. The chapter also proposes directions for future work.

Chapter 2. Image based subsea detection techniques

Traditionally most surveys and spatial analysis techniques were carried out by trained assessors and operators based on the images obtained from the area of interest. In recent years, the trend is to automate those tasks, improve the quality of the images and collect more data frames without human interventions.

Image based detection is not only about analysing camera pictures, it also extends to other mediums. Images are often obtained in the traditional way with photographic equipment capturing a snapshot of the light backscattered from the target object. However, imaging covers much more techniques. Especially in the marine environment light is not always the first medium of choice. More often sensors build images of seabed features based on backscattered acoustic waves using echolocation or laser-beams in the newly developed LIDAR technology.

The following chapter considers the developments of visual and hydro-acoustic sensing and their application to detection of subsea cables laying on the seabed or buried in the sediment.

2.1 Visual

Underwater cable localisation, tracking and examination were traditionally carried out by visual inspection performed by a specialised diver. Technological progress has allowed using more advanced methods. In recent years the task of visual inspection is often completed by use of a ROV with an operator on the surface. Despite this shift in execution, visual cable surveys have many limitations. Often the method is cost ineffective, unreliable and gives uncertain results. The method is time-consuming and prone to error caused by loss of attention or fatigue of the human operator. (Ortiz et al., 2000; Wang et al., 2013)

The trend is to automate the visual inspection of cables and pipelines to provide detection and tracking without human intervention. The surveyed utility can be characterised by its shape and most often to a certain degree by its uniform colour (Chen et al., 2015; Hallset, 1991a). In practice, simple recognition is based on the extraction of geometrical features from a 2D image. The recognition system tries to extract rectangular shapes which can be classified as a part of the pipeline or cable (Hallset, 1991b). In addition, it

is assumed that the utility such as a cable or pipeline is a straight line which can be followed by an Autonomous Underwater Vehicle (AUV) (Ito et al., 1994).

The main challenge for visual subsea cable tracking stems from the subsea environment. Balasuriya et al. (1997) observed that submarine imaging differs from optical sensing on land. Underwater visual sensing has an important limitation. In most cases, underwater visibility is poor because of little or no ambient light. To solve this problem, active light sources need to be used to illuminate an object. As a result, the submarine image contains blurs from the spatial attenuation of higher frequencies and backscatter from the predominance of low frequencies. Figure 1 shows three different images where an underwater cable is difficult to detect as illustrated by Wirth et al. (2008).

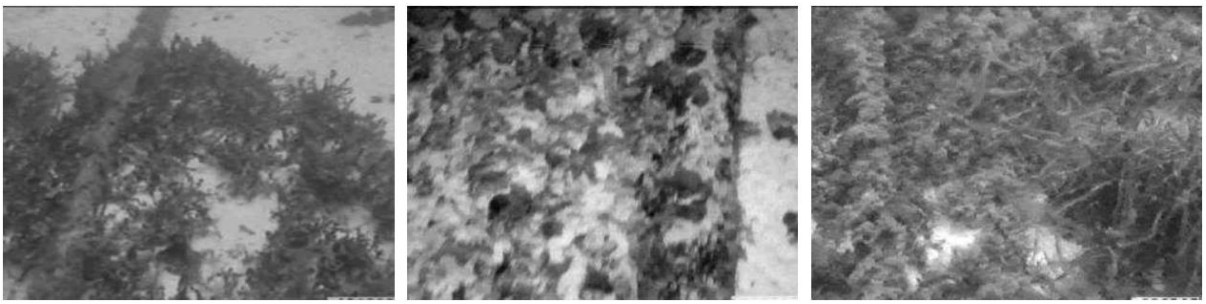

Figure 1 Images of underwater cables in which the cable is difficult to detect. (Wirth et al. 2008)

In addition, Balasuriya et al. (1997) emphasised that because of non-uniform light, the far ranges of the utility appear to be darker, while the parts directly exposed are much lighter. Also randomly moving particles suspended in the water give rise to many bright spots in the resulting image. Such non-uniformity is highly undesirable for recognition algorithms.

2.1.1 Deterministic visual detection

The approaches to visual detection of underwater cables can be categorised into different groups. A review of the available literature shows that that the dominant approaches can be classified into two groups: deterministic and stochastic methods.

Balasuriya & Ura (2000) proposed image filtering to reduce some undesirable features unique to underwater images. The proposed filter is based on the Laplacian of Gaussian (LoG) operator. The LoG, firstly using the Gaussian filter, smoothes the image in order to reduce sensitivity to the noise. Then

secondly, the Laplacian part of the filter highlights regions of rapid changes in intensity. After applying the LoG, the image of an underwater cable produces a high pixel concentration in a particular direction. The position of the model is extracted by transforming the pixel data into a parametric space known as the Hough transform. The line feature introduces a peak in the Hough space and its existing region can be predicted using the uncertainty of the model line and the cable can be distinguished from its background.

A similar approach based on an edge detector has been developed by Ortiz and co-workers. Ortiz et al. (2000) suggested performing an initial cable's localisation and direction before the image processing is performed. Regions with alignments of contour pixels in a preferred orientation are determined from the seabed picture. If among those alignments there are two with a great number of pixels line up with a high degree of parallelism, then the cable is considered to have been located. Otherwise, the next image in the sequence is analysed.

After initialisation as described above, Antich & Ortiz (2003a) tracked the cable by using a Kalman filter. During this procedure, before the next image is processed, the position and direction of the cable are predicted to reduce the region of interest. It not only reduces computation time but also makes the method less prone to error (Simo et al., 2000).

A comprehensive description of visual tracking for underwater cables and pipelines can be found in Asif & Arshad (2006). They argued that underwater visual tracking requires special image processing techniques, different to those used on land. Asif & Arshad, (2006) separated the whole process into six different stages as shown in Figure 2.

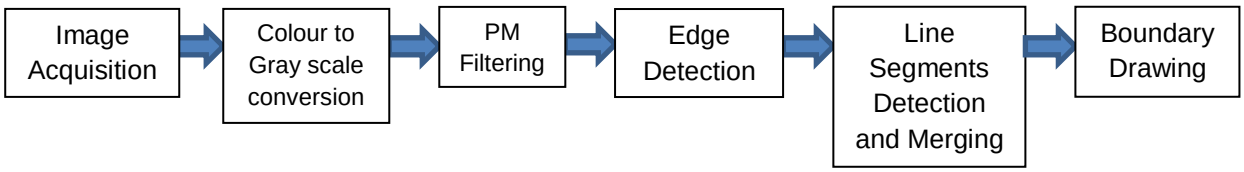

Figure 2 Flow diagram of underwater image processing (Szyrowski et al., 2013a)

They converted a 24-bit in red, green, blue (RGB) image from an onboard camera into an 8-bit greyscale image, where in the resulting image only the red channel from the original image is used. Similar to Balasuriya et al. (1997), they argued that because of dynamic lighting, the resulting image is very noisy.

However, Asif & Arshad (2006) pointed out that Gaussian filters tend to smooth the whole picture together including the edges of the cable of interest. This process can lead to unnecessary difficulties in detection arising from loss of contrast. Instead, they proposed using a Perona-Malik filter, which retains information essential in detecting pipeline and cable boundaries. Application of the above step allows the use of the Sobel edge detector and the Hough transform that has smaller computational requirements.

After detecting the underwater pipeline image, Asif & Arshad (2006) designed a deformable template to represent the perspective view of the long length utility boundaries. The resulting prior shape model was used as the regularisation term in the fitting process. In the described procedures, a second order non-uniform B-spline curve with six control points were used. Asif & Arshad (2006) suggested that in the case of a pipeline, B-spline fitting is better than a polynomial or line fitting. However, the method may be difficult to apply for cables tracked from the short distances necessary in visual inspection. Asif & Arshad (2006) identified that the B-spline fitting it is not suitable for more flexible utilities such as optical cables.

Asif & Arshad (2006) applied their method not just to detection but also tracking underwater pipelines or cables. They used an AUV to track an underwater utility. After detection and modelling the underwater line, the AUV needs to turn in the direction of the utility and perform its tracking. To accomplish this task the model needs to incorporate an expectation of future performance of the cable. Asif & Arshad (2006) used an autoregressive process where a time series modelling strategy takes into account the historical data to predict the current state value. The information about the predicted state and the best fitting curve obtained is merged by use of a Kalman filter. The output of the whole procedure provides the AUV with the most probable position and direction of the following part of the cable. Recognition of underwater objects and its coupling with tracking systems is an additional challenge in underwater cable detection.

Similar difficulties in the cable detection process are pointed out by Narimani et al. (2009). They considered that it is desirable to develop a vision system with the ability to mimic the human mind. Human operators can be reasonably confident that decisions made by such a system can ensure safety and mission completion.

A vision-based system alone is not sufficient for Inzartsey & Pavin (2008). Underwater cable inspection not only relies on adequate detection but also on effective tracking. Inzartsey & Pavin (2008) argued that tracking is the most difficult task in underwater inspections. They implement an integration of methods called video imaging complex (VIC) and electromagnetic searcher (EMS). The VIC algorithm searches the

longest straight line on the presented seabed's image. Inzartsey & Pavin (2008) claimed that data obtained from two sources increase cable detection probability and quality of AUV movement. Figure 3 compares tracking with EM sensors alone and tracking with sensors fusion.

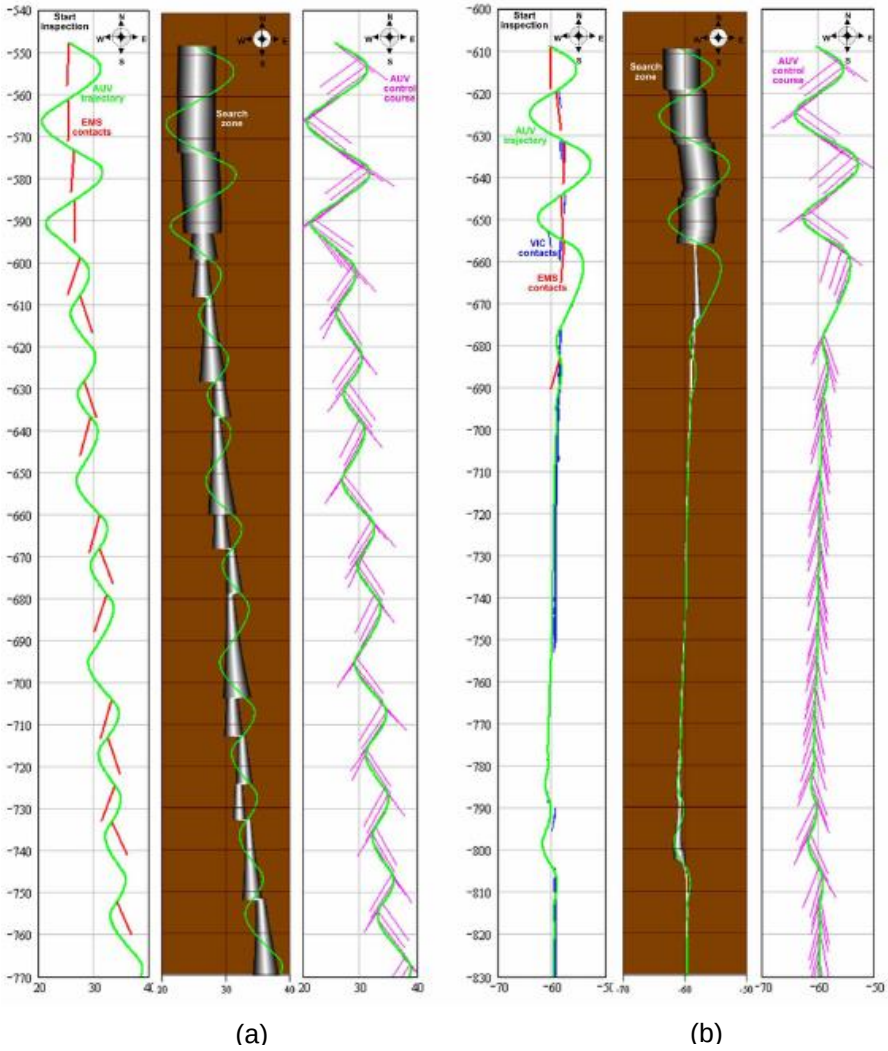

Figure 3 (a): Tracking using EM sensor. (b): Tracking using EMS and Visual Sensor. (Inzartsev & Pavin 2008)

2.1.2 Stochastic visual detection

A different approach to that described above was presented in Wirth et al. (2008). In their opinion, methods such as border detection, line extraction, segmentation or texture description are too deterministic for the marine environment and can fail in ambiguous situations. They proposed to use a stochastic method based on the use of particle filters.

A particle represents a particular (hypothetical) configuration of the cable's variables represented as a state in the state space together with a weight that represents its likelihood called importance weight. In other

words, every particle reproduces a possible shape, alignment, etc. together with a possibility of occurrence. The particle filter sequentially estimates the likelihood of the cable's specific position and orientation (pose). For each image in a sequence, the prior probability density function of the cable parameters is used to estimate the cable's posterior pose. The probability density function is updated by means of the observation model. The most likely cable pose is finally determined from the resulting density.

Figure 4 shows a typical image and applied particle filters.

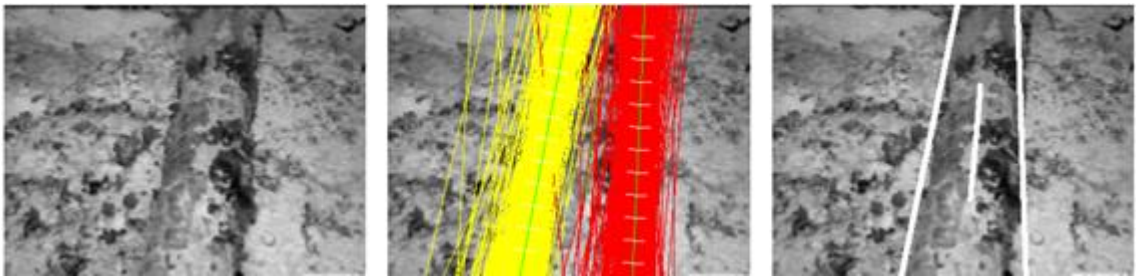

(a) (b) (c)

Figure 4 (a): a typical image of a submarine cable; (b): 500 hypothetical cable poses that are modelled by the particle filter for that image; (c): estimated cable pose (Wirth et al. 2008).

In the tracking procedure, the particles are built for each video frame and the resulting estimation gives a prediction for particles in the next frame. The sample set evolves according to a movement model and an observation model. The movement model describes the transition of the particles from one time step to another. The observation model allows the weighting of particles according to a given observation by matching each particle with an existing template.

A similar approach was presented in Ortiz et al. (2009a). To compensate for some possible errors in estimation of the cable pose, they added new features to the standard structure of particle filters. One of the improvements which reduces the degeneracy error is the introduction of a resampling step when more than half of the samples have a low weight. Another enhancement is to estimate one line corresponding to an axis of the cable instead of estimating both boundaries. It eliminates the requirement of navigation close to the seabed to recognise the thickness of the cable and its borders.

Ortiz et al. (2009a) also improved the observation model, through using a set of filters to determine the particle's weight. The particle is scored with the average of the observation filter responses. To speed up the process, instead of using a filter that is oriented perpendicular to each pose, horizontal- and vertical-mask filters are defined and respective convolution images are computed for the current image after being loaded

Ortiz et al. (2009b) reported a set of experiments to evaluate the method in different marine environments. They claimed that the method was able to cope correctly with all situations. The tracker not only correctly detected the visible image but in addition was able to detect the absence of the cable when the utility was buried.

Figure 5 shows two cables tracked during the experiment.

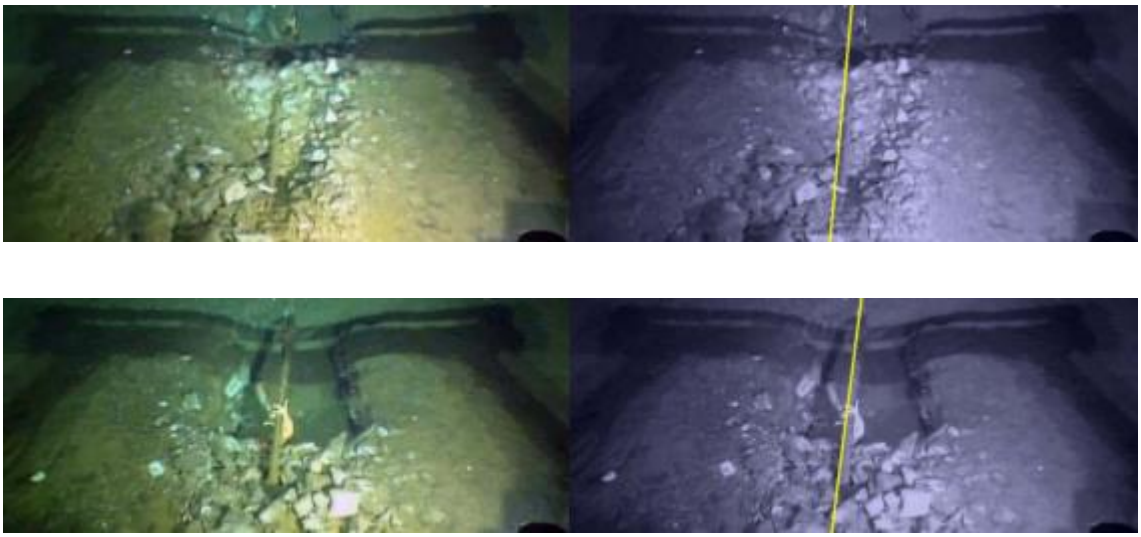

(a) (b)

Figure 5: Tracking results of the video sequence; (a): (left) original frames; (b): (right) processing results: yellow - cable estimate (Ortiz et al. 2009a).

Visual sensing methods can have some advantages. Antich & Ortiz (2003b) pointed out that devices such as magnetometers and sonar require more space and power than a simple visual camera. Greater demands result in higher cost and lower effectiveness of the survey platform. Asif & Arshad (2006) agreed with this position. In their opinion, the power consumption and size of sonar and magnetic sensors disqualify them in a demanding survey environment. In addition, they defended visual recognition as more robust and claim that sonar and magnetometers are often too sensitive to background noise.

Despite all its advantages, the method of visual inspection not only carries a high risk of error but also suffers from a distance limitation. Additionally, for buried power cables and transmission lines, visual inspection is not possible as the utilities are completely hidden.

The next section describes detection and tracking methods based on the use of underwater acoustics as possibly being more suitable for the detection of buried utilities.

2.2 Hydroacoustic

The second group of widely used marine survey methods is based on acoustic location. Acoustic methods are often more precise than their visual counterparts. They are able to penetrate the seabed, enabling the possible use of sonar for detecting buried utilities. However, echolocation suffers from its own limitations. In shallow water sound propagation, reflection and scattering make this method very difficult and often impractical.

Detection and tracking of subsea unburied cables by use of echolocation has been described in Isaacs & Goroshin (2010). They focused on an algorithm capable of detecting segments of prominent straight lines. They agreed that the lines can vary in appearance; they can have different thickness, colour intensity or geometry. Thus, it is desirable to define the general characterisation of cable-like objects, which can be used to detect arbitrary cables. They defined cables as straight line segments with coherent structure but whose intensity may be very close to that of the background.

Isaacs & Goroshin (2010) suggest that one of the best techniques to recognise a straight line is the Hough transform. However, they concluded that because of spurious objects the linear Hough transform does not give satisfactory results. The line predicted from a Hough transform can only estimate the region of interest and this area should be further investigated to determine the existence of the cable. Figure 6 shows a sonar image of the cable on the seabed and its Hough transform.

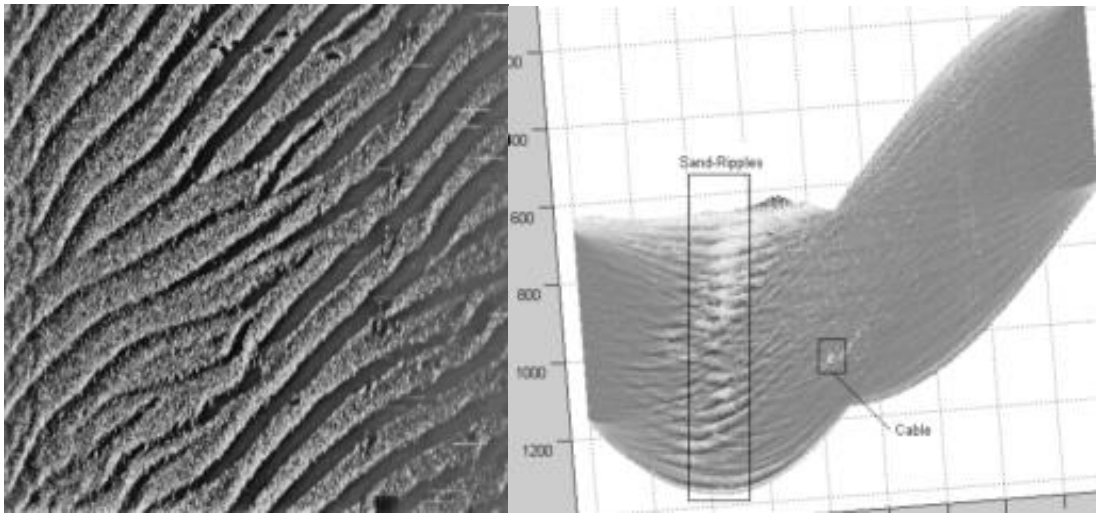

(a) (b)

Figure 6 (a): Sonar Image with sand ripples. (b): Hough Transform of the image (Isaacs & Goroshin 2010)

Isaac & Goroshin (2010) divided the cable detection algorithm into the following steps: noise reduction, edge and line enhancement, thresholding, line detection, classification. The flow diagram of the process is shown in Figure 7. They drew the conclusion that, since their approach can be successful in sonar imagery, it can be applied to most imagery where the cable shows a response.

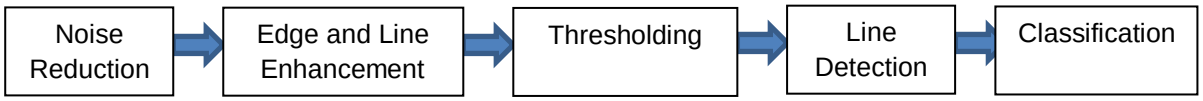

Figure 7 Flow diagram for acoustic sensing (Szyrowski et al., 2013a)

Recognition and tracking of underwater cables based on sonar imagery were followed by Bagnitsky et al. (2011). They drew attention to the configuration of side scan sonars (SSS) for detection of underwater long length objects. The main point is to set up an image resolution high enough to be able to detect thin, lengthy objects. The resolution needs to be kept below some threshold value to be resistant to noise. In their experiments, they used a hydroacoustic SSS which possesses high resolution (up to 0,5°x0,03 m) and has the long range of operation (up to 2x120 m).

The next step after obtaining an image is to apply filtering. Similarly to most image filtering methods, this process is based on brightness of neighbouring elements. The main problem in cable detection comes from the fact that a thin, lengthy object covers only one to five pixels and is often neglected as a noise. To

overcome this problem the sliding window for filtering in cable detection should be as small as 3x3 pixels. Bagnitsky et al. pointed out that a filter cannot change pixel values on the object borders but relieves the image from local extreme. They proposed a filtration algorithm that changes the pixel brightness to the nearest value from the environment if brightness of this pixel does not exceed the threshold above or below any of the surrounding pixels. In the filtration process, they also proposed an algorithm based on a gradient model to determine the probability that the point on the image belongs to the border of a required object.

After obtaining an SSS image, the borders of the cable are recognised by the Hough transform in a similar fashion to recognition made during visual detection.

Bagnitsky et al. (2011) claimed that the method applied to detection by use of an AUV brings satisfactory results, which means that during an experiment the AUV has traced the whole of pipeline with confidence. To use the method during real time tracking SSS needs to be used together with an adequate model of a vehicle's movements. The recognition brings best results if the object is in a high sensitivity zone, located approximately 5m to 40m on each side of the AUV if the vehicle moves approximately 5m to 15m above the sea floor. The main advantage of the method is its low-resources requirements.

2.2.1 Buried object scanning sonar

A traditional SSS can detect and track underwater long length objects lying on the seabed. Conventional sonar, however, cannot cope with cables buried on the seafloor. A solution to this problem can be the buried object scanning sonar (BOSS) proposed by Schock and co-workers (Schock et al., 2001; Schock & Wulf, 2003; Schock et al., 2005).

The sub-bottom profiling imagery comes with a trade-off between penetration depth, and image resolution. Although low frequency acoustic waves can penetrate the seabed into tens of metres they do not provide resolution high enough to recognise small objects. The high frequency penetration can provide decimetre resolution in shallow water but relies on two dimensional imaging difficult for thin objects recognition (Gutowski et al., 2015).

The improvements are made mainly within acquisition techniques. It was considered by Schock and co-workers that conventional single channel reflection sonar is usually not suitable for detecting buried objects. The main reason is that the noise produced by the heterogeneities within the sediments, the roughness of

sediment–water and the sediment layer interfaces are often higher than the amplitude of echoes reflected from the buried targets of interest.

In addition, the compressional wave attenuation in sediments is much higher than in the water. As a consequence, the BOSS needs to operate at much lower frequencies than SSS. In buried objects detection, the following can be observed: higher diffraction around the target, transmission through the target and relatively high acoustic noise caused by backscattering from sediments surrounding the target. The result of the above is a lack of acoustic shadow normally present in acoustic imagery.

In comparison with conventional sonar, the main improvements in BOSS proposed by Schock et al. (2001) are to introduce a multi-channel planar hydrophone array with the operating frequency band of 5–23 kHz. The configuration was designed in such a way that it could be mounted on a small vessel. The project was later redesigned to overcome some limitation of the predecessor and increase performance in recognising the shape of the object. This new configuration contained a receiving array with 252 hydrophone elements mounted with equal spacing on a 1.5m diameter circular disk, and a spherical acoustic source mounted in the same horizontal plane as the receiver. The source generates an FM pulse over the band of 2 to 12 kHz (Schock & Wulf, 2003).

Traditional sonar delivers three-dimensional images but BOSS methods suffer from a limitation in the image produced. Detection of a cable in a SSS image is performed by using a gradient of the border. For the BOSS sonar, there are no measurements of the signal reflected from any non-orthogonal part of the object's surface. The shape of the image has no spherical appearance but instead appears as a point.

Mounting BOSS on a moving platform requires motion compensation. In the original approach, the dimensions of the hydrophone array limit the resolution of the target imagery. To improve the resolution and signal against scattering noise performance Schock et al. (2001) proposed synthetic aperture processing. Synthetic aperture processing coherently sums the data over a sequence of transmissions to improve spatial resolution along the track. The changes in projector and hydrophone positions between transmissions are calculated, and a summation is performed for each 3D location.

Schock et al. (2001) reported good results from conducting experiments. The BOSS scanner was able to detect cylindrical objects buried at a depth of 30cm in the sand. To detect the object some requirements had to be met. The angle of incidence for the object of interest has to be less than 45 degrees. Objects were

buried on the seabed for at least one month before the experiment was conducted to allow normal sediment to settle.

2.2.2 Bio-inspired sonar

An interesting approach has been presented by Capus et al. (2010). They used a sonar design based on that of a bottlenose dolphin. It covers a frequency range 30-130kHz and has a frequency dependent beam width considerably wider than typical imaging sonars.

Capus et al. (2010) claimed that the wideband sonar allowed excellent detection of cables with a diameter of 25mm or less. It was able to differentiate between different types of material of the cables or thin pipes. In addition, wideband sonar could detect cables on different sediment backgrounds or even when buried.

The differentiation between cable types was based on the scattering theory of thin cylindrical shells. A cable model could indicate predicted positions for spectral notches derived from the reflection from the cable's shielding with relatively low impedance. The model could also predict the second wave from the propagation of the acoustic wave around an inner metallic layer. In this approach, Capus et al. (2010) were interested in the shape of the response rather than its size.

Figure 8 indicates the predicted positions for spectral notches derived from reflection from the cable's shielding with relatively low impedance, and the second wave from the propagation of the acoustic wave around an inner metallic layer.

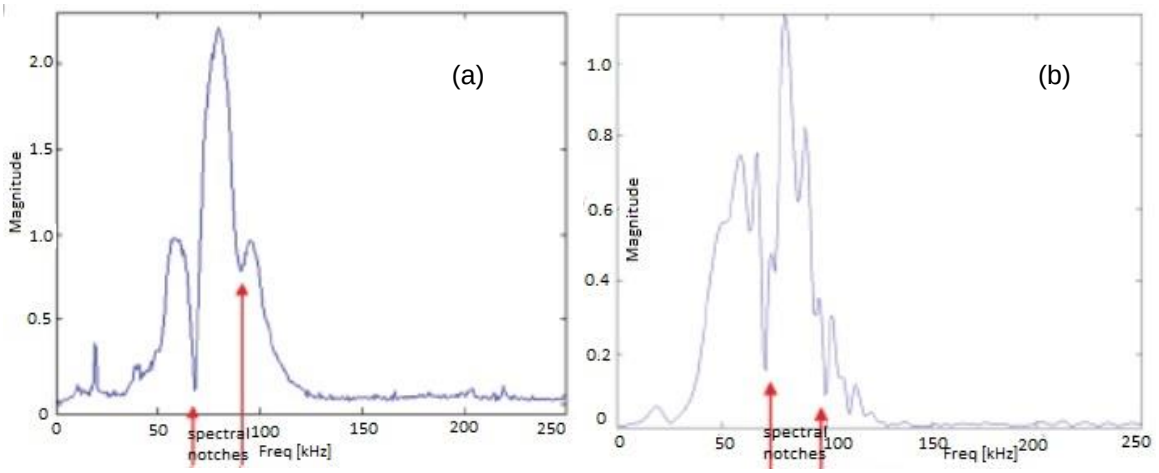

Figure 8 Differentiation of a cable's type (a): in free water (b): on the tank floor (right). Red arrows indicate prediction of location based on spectral notches. (Capus et al., 2010)

In the experiments conducted, Capus et al. (2010) measured the impact of different seabed types on the ability to detect cables. The conclusion drawn is that the rougher the sediment, the higher the reverberation level. The grazing angle plays an important role in determining the reverberation noise level. For rough sediments, a lower grazing angle will provide better results. From the experiment in the water tank, Capus et al. (2010) concluded that the detection was also affected by cable curvature, tank wall returns, disturbances in the sediment surface and ambient noise sources. Capus et al. (2010) proposed to minimise these issues by improving post-detection filtering and noise suppression.

Capus et al. (2010) made the point that a single observation cannot be reliable in discriminating between different responses. A robust recognition is achieved by integrating returns over a series of pings. This procedure also determines the most likely track of the cable.

Capus et al. (2010) concluded that, since the discussed method can differentiate between types of the detected line, it can also detect a buried utility. By using different pulses, Capus et al. (2010) focus on the part of the spectrum, which is of particular interest.

In the presence of a buried target, some responses within the frequencies of the wideband sonar were generated by the target. Detection of the utility relies on classification of spectral features. Capus et al. (2010) noted that for the mid-water response, characteristic notch spacing is well-preserved. Because of this observation, Capus et al. (2010) were able to predict precise notch location shifts with burial.

To track variations in responses for different targets they used the concept of spectral texture. Capus et al. (2010) adopted Haralick's co-occurrence feature sets. These methods are widely used in image processing and its description can be found for example in Clausi (2002). In the procedure used by Capus et al. (2010), the feature's values are calculated from normalised, quantised spectra which give information about detailed variations in spectral content, although quantisation process can remove important information.

The next step is a tracking of changes in the values of the features. To track the changes variations in the target aspect were analysed. Capus et al. (2010) proposed using the hidden Markov model (HMM). The model is based on probabilities of observing the particular feature values given some particular state of the target. For classification, the HMM integrates returns over a range of target aspects.

Capus et al. (2010) were able to see similarities in response from smooth objects and rougher objects after receiving just one wideband target echo. After 10 received pings, the aspect of the object can be accurately estimated, and therefore the objects can be firmly identified.

High resolution acoustic and optical surveys performed by underwater robots make many tasks possible and feasible; however, they suffer many limitations. Whitcomb (2000) pointed out that by no means is this method the same as its land, air or space counterparts. Rapid attenuation of acoustic or optical waves restricts the range of the sensors.

The methods of acoustic detection for underwater buried objects are criticised by Pei et al. (2010). In their opinion, buried object detection is especially difficult in shallow water. Pei et al. (2010) suggested that seabed environments, especially in the coastal region, are difficult to carry out using acoustic surveys. Transitioning from the air/sea and sea/bottom interfaces, complex bottom topographical profiles, and buried objects present a difficult environment for acoustic detection.

In addition, they suggested that the coastal region has a high density of synthetic clutter that may cause a high false alarm rate using the acoustic sensor alone.

2.2.3 Hydro-acoustic localisation – practical notes

Echolocation techniques were used during a commercial survey in South America 2014 and 2015. The survey was performed in a shallow water area where three existing cables were already connected to a beach man hole (BMH) and a new cable was planned to be installed on top of them. The surveyed area was between three metres water depth and 300 metres from the beach to 11 metres of water depth and eight kilometres from the beach.

In addition to identifying cables in operation, the region was known as likely to contain non-operational cables left by the US-Army. The unidentified cables could pose a hazard for the cable's operation and all measures needed to be taken to determine their existence.

Prior to the sonar survey, the existing, known cables were localised with an electromagnetic detection described in Chapter 3. The hydroacoustic survey aimed to confirm these results and to ensure that there were no additional hazards such as wrecks or other seabed features.

A proprietary SSS system known as “Klein System 3000” was mounted by an experienced hydrographic surveyor on the side of the survey boat. The Klein 3000 system is an advanced, dual frequency SSS rated for demanding military and government surveying applications. The system is composed of a towfish, a transceiver processor unit, a tow cable, and a “Klein sonar workstation”, an industrial PC and the “SonarPro” Software for data display (Klein Marine Systems, Inc., 2016).

The survey was planned as a hydrographic line covering all the areas of interest. Among some small artefacts, the survey uncovered a previously unidentified wreck of a fishermen’s boat, a large part of a mast with rigging and lines on the seabed thought to be parts of the non-operating cables.

Figure 9 (a) shows the SSS setup on the survey vessel. The required space, power consumption and constant attention of the surveyor makes the SSS operation very demanding and difficult. Figure 9 (b) shows real-time screenshots of the SSS software showing the seabed with an unidentified line. Figure 9 (c) shows another part of the line after initial post-processing. The longest uncovered line was 800 metres long and at the time of the survey was thought to be an old US-Army cable.

The conducted survey was followed by a diving operation to confirm the survey findings. The diving team made several dives in the area where the lines were discovered. They reported no cables on the seabed. The lines appeared to be the trace of a dragged anchor left in the muddy seabed. All lines reported as a cables were false.

The SSS survey can uncover different structures on the seabed but care needs to be taken in interpreting the findings. The recognition relies mainly on the experience of the surveyors. At the moment there are no reported methods to successfully differentiate the cable from other long lines like hawsers or in the case of the described survey a trace in the muddy seabed.

The visual and acoustic methods of subsea detection are often the first choice in a marine survey. Recent technological progress has provided many advances and significantly improved the ability of underwater detection. However, these methods suffer one very difficult to overcome limitation: they cannot sense a buried utility, which is not accessible by light or acoustic waves.

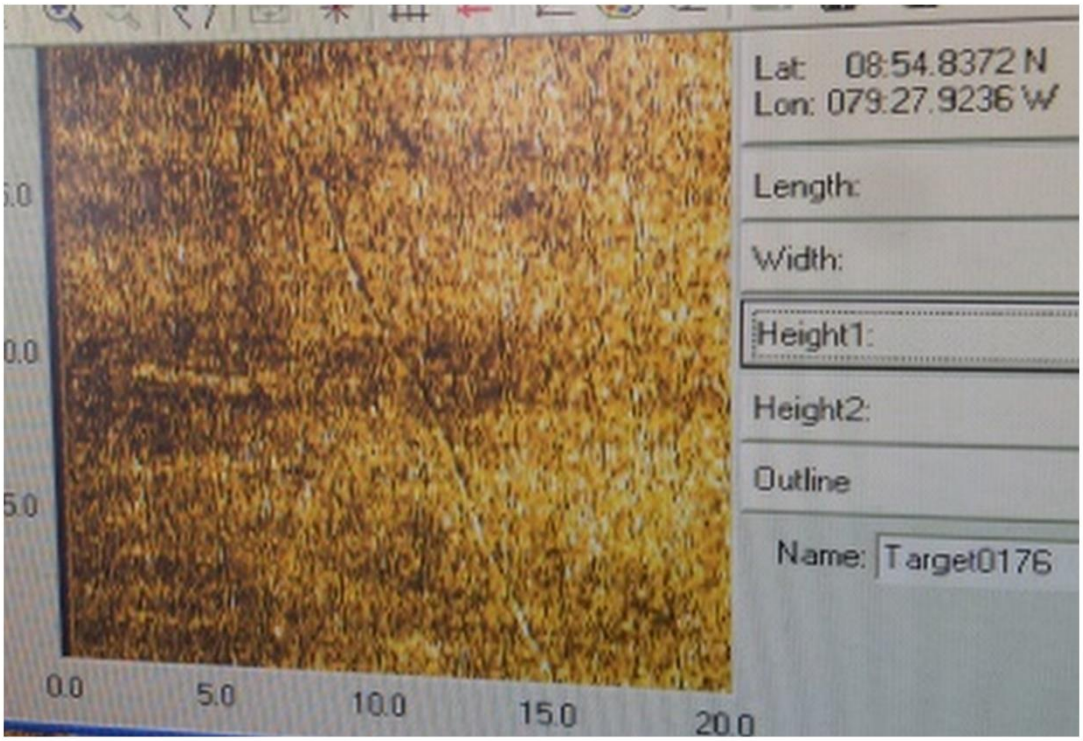

(a)

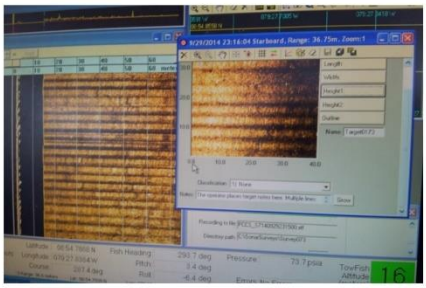

(b)

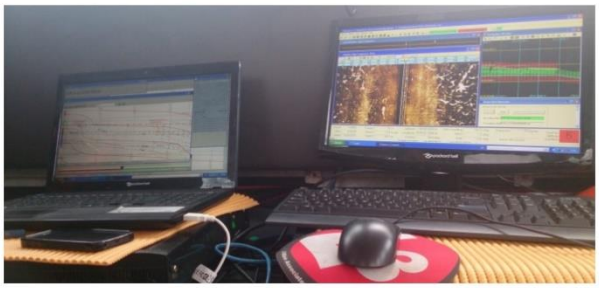

(c)

Figure 9 Hydroacoustic survey (a): post processing output. (b): real time display. (c): Computer setup during the survey.

In the next chapter a different approach based on magnetic detection will be presented. The magnetic field equally penetrates the seawater and the seabed. The emitted field can be detected even if the cable is hidden under the ocean floor.

Chapter 3. Magnetic and electromagnetic subsea cable detection

Despite their advances and benefits, the visual tracking and hydro-acoustic methods suffer limitations and often are unsuitable in the case of buried cables (Ortiz et al., 2000; Capus et al., 2010). Sensing of magnetic and electromagnetic fields are the most appropriate methods for detection of hidden underwater utilities, such as buried transmission lines. These techniques are described in more detail in the following section.

Magnetic an electromagnetic sensing is not limited to one approach. The subject is often confused among practitioners and surveyors understanding and linking different techniques to different names. What connects all the methods is a link between magnetic sensor's readings and changes in the sensed field. What differentiates the methods is the source of the field, its frequency, amplitude, direction of the vector field and other characteristics. Before describing these methods, some aspects of the fields emitted from the cable will be described.

The electromagnetic sensing of underwater ferromagnetic materials is not limited to the search for cables and pipelines. In recent years there have been new developments in underwater unexploded ordnances (UXO), which can be applied to detection of objects such as a ferromagnetic transmission line. Therefore, for completeness of the review it is worthwhile to include important developments in UXO detection.

3.1 Fields emitted from the cables

A primary aspect of magnetic detection is the response of the sensor to the magnetic field. The main source of the magnetic field is from moving electric charges but it is not the only form of magnetism. The magnetic sensors react to the Earth's magnetic field caused by its mass.

Submarine cable detection techniques use all possible steps to take advantage of magnetic detection. Most of them will be described in this section. Out of them all electromagnetism gives the most reliable results and will be the method focused on in this review.

3.1.1 Low frequency, alternating Electromagnetic Fields

The magnetic (MF) and electric (EF) fields around a submarine cable originate from the electric currents and charges which either exist in the cable or are induced in the surrounding waters. The fields can be determined by solving Maxwell's equations (Olsen & Wong, 1992). The MF from a distribution of current at any point in space can be determined by the formula:

$$\boldsymbol{B} = \nabla \times \int_{All\ space} \frac{\mu_0\ \boldsymbol{J}(t - \frac{r}{c})}{4\pi r}\ dv \qquad (1)$$

where $\boldsymbol{B}$ is the magnetic flux density, c is the speed of light, $\boldsymbol{J}$ is the distribution of current in space, r is the distance from source to field point, μ_0 is the permeability of free space and $\nabla \times$ is the curl operator. Equation (1) can be used to determine any field from any distribution of currents.

For the purpose of submarine cables surveys, the frequency of the time varying current is often in range of 25 – 100 Hz. The use of these extremely low frequencies (ELF) is mainly determined by the relation between frequency and attenuation of the MF in sea water. However, the use of ELF has another implication for determining the MF within distances of up to 50 metres.

In the ELF range the methods of quasi-static fields can be used. The quasi-static method first derives the static MF, which after is described as oscillating in amplitude at the frequency of the sinusoidal source current. The spatial distribution of the field maintains the same shape but its amplitude varies in time with the source.

For the high frequencies (HF) the method does not necessarily hold (Olsen & Wong, 1992). For HF the magnetic and electric fields are calculated by geometric optic methods, where the visualisation is such as ray of light passing through space. Both methods have their origin in Maxwell's equations. The exact solution of Maxwell's equation reduces to different approximations in the case of ELF and in the case of HF.

To illustrate these characteristics a small loop of sinusoidally oscillating current I can be considered. The parameters of the loop are: a as the radius of the loop, $k = 2\pi/wavelength$ as the wavenumber, f as the

frequency with its angular counterpart $\omega = 2\pi f$ and r as the distance from the loop, where $a \ll r$. The magnetic field in free space, originating from this loop current can be described by a set of three equations:

$$\boldsymbol{B_\theta} = \frac{\mu_0 I\, a^2}{4}\left(\frac{\cos(\omega t - kr)}{r^3} - \frac{k\ \sin(\omega t - kr)}{r^2} - \frac{k^2 \cos(\omega t - kr)}{r}\right)\sin\theta \qquad (2)$$

$$\boldsymbol{B_r} = \frac{\mu_0 I\, a^2}{4}\left(\frac{\cos(\omega t - kr)}{r^3} - \frac{k\ \sin(\omega t - kr)}{r^2}\right)\cos\theta \qquad (3)$$

$$\boldsymbol{B_\Phi} = 0 \qquad (4)$$

The three terms in equation (2) are identified respectively as the "static" $(1/r^3)$ term, "induction" $(1/r^2)$ term and "radiation" $(1/r)$ term. In the quasi-static method, only the first two terms are grouped together and considered. In equation (3) the radiation term does not exist and the equation is completely quasi – static.

The motivation for the quasi-static approach is the rate of decay with distance from the source. The terms in the quasi-static approach decay at least as fast as the square of the distance. These terms dominate for small distances. For example, for the 60Hz source, the ratio of the quasi-static field amplitude and the radiation field amplitude is proportional to $1/k^2r^2$ which for the wavelength of 5000km is 63300000. The radiation field can be ignored. For a quasi-static field, since $kr \ll 1$, equations (2) and (3) become:

$$\boldsymbol{B_\theta} = \frac{\mu_0 I\, a^2}{4}\sin\theta\ \cos(\omega t) \qquad (5)$$

$$\boldsymbol{B_r} = \frac{\mu_0 I\, a^2}{4}\cos\theta\ \cos(\omega t) \qquad (6)$$

For the analysis of the MF from a submarine cable, the cable can be modelled as an infinitely long current carrying wire as depicted in Figure 10. The total MF can be calculated by adding the MF created by the individual dipoles lined up along the z-axis.

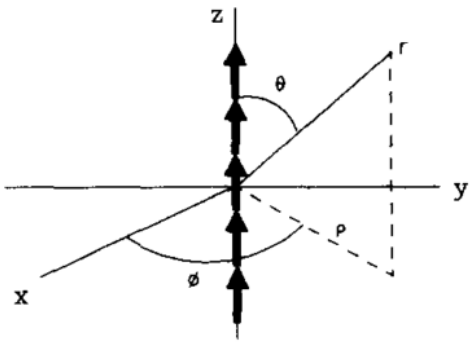

Figure 10 Infinitely long current carrying wire

The equation describing such a situation is:

$$\boldsymbol{B_{\Phi}} = \frac{\mu_0 I a^2}{4\pi}\left\{\int_{-\infty}^{\infty} \frac{I(z')\cos\left[\omega t - k(\rho^2+(z-z')^2)^{\frac{1}{2}}\right]\rho\, dz'}{(\rho^2+(z-z')^2)^{3/2}} - \int_{-\infty}^{\infty} \frac{k\, I(z')\sin\left[\omega t - k(\rho^2+(z-z')^2)^{\frac{1}{2}}\right]\rho\, dz'}{\rho^2+(z-z')^2}\right\} \quad (7)$$

where $I(z')$ is the current along the z-axis, $\rho = (x^2 + y^2)^{1/2}$ and $\sin\theta = \rho/r$

Equation (7) is difficult to evaluate but the MF from a uniform current $I(t)$ along an infinite long wire can be solved with use of the Ampere's law. Assuming that current is constant in space but varies in time:

$$\boldsymbol{I}(t) = I\cos(\omega t) \quad (8)$$

For the electric current density $\boldsymbol{J}$ and circle of radius C centered on the wire, with the surface S which includes the wire depicted in Figure 11, Ampere's law in integral form is:

$$\int_C \boldsymbol{B}\cdot\boldsymbol{dl} = \mu_0 \int_S (\boldsymbol{J} + j\omega\,\epsilon_0\,\boldsymbol{E})\cdot\boldsymbol{ds} \quad (9)$$

The left-hand side of equation (9) is equal to $2\pi\rho B_{\Phi}$ and other components of the MF are zero. On the right hand side the integral gives the total current on the wire $(I\cos(\omega t))$. If the term $j\omega\,\epsilon_0\,\boldsymbol{E}$ can be ignored, the equation for MF becomes:

$$\boldsymbol{B}_{\boldsymbol{\Phi}} = \frac{\mu_0 I \cos(\omega t)}{4} \qquad (10)$$

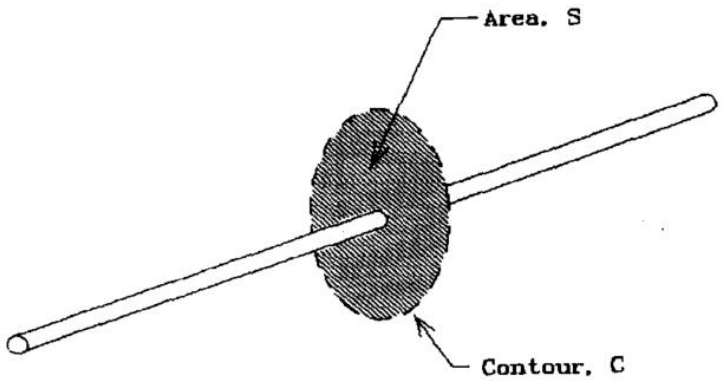

Figure 11 The MF centred on the wire

The same quasi-static solution can be obtained exactly for $k\rho \ll 1$. Using equation (8), equation (9) can be solved by the Bessel functions of order 1, first and second kind. For $k\rho \ll 1$ the Bessel functions can be approximated as $J_1(z) = z/2$ and $Y_1(z) = -2/\pi z + (z \ln(z/2))/\pi$. Thus equation (9) becomes:

$$\boldsymbol{B}_{\boldsymbol{\Phi}} = \frac{\mu_0 I k}{4}\{J_1(k\rho)\ \sin(\omega t) - Y_1(k\rho)\ \cos(\omega t)\} \qquad (11)$$

In both (10) and (11) the same term dominates for the ELF range and MF can be analysed using a quasi-static approach.

The above calculation assumes the MF distribution to be in free space or at least in the air or earth. The much higher conductivity of sea water leads to much greater complex wavenumber for electromagnetic waves (King, 1989):

$$k_1 = \beta_1 + i\ \alpha_1 \sim (i\omega\mu_0\,\sigma_1)^{1/2} = (1+i)(i\omega\mu_0\,\sigma_1/2)^{1/2} \qquad (12)$$

where k_1 is the complex wavenumber for sea water and $\sigma_1 \sim 4\ S/m$ is the typical conductivity of the sea water. The associated wavelength $\lambda_1 = 2\pi/\beta_1$ is much shorter in the sea water that in the earth. Despite the fact that the wavelength reduces in the salt water, King (1989) also pointed out that for long wires the internal resistance per unit length becomes dominant and the radiation resistance can be neglected. Channels susceptible to dissipation of electric or electromagnetic energy are called lossy in opposite to ideal, lossless channels. The insulated conductor should be seen more as a lossy transmission line and no longer as an antenna.

3.1.2 Distribution of MF from the cable

In most of cases the underwater cable can be considered as a straight horizontal wire of infinite length, parallel to the water surface. Similar assumptions often are considered in analysis of the electromagnetic fields from overhead power transmission lines.

The electromagnetic fields under overhead power transmission lines are regularly studied in connection with human health. Studies started in 1979 suggest that exposure to MFs has a positive correlation with human cancer (Tao & Zahedi, 1998; Said et al., 2004). Although the main reason for studying MFs from transmission lines is to reduce the field, the studies deliver models for MF distribution.

There are significant differences between transmission lines and submarine cables. The main difference is that for the purpose of the marine survey, the electromagnetic field originates from the pulse induced in the shielding of the cable. In the case of transmission lines, the field is an effect of the transmitted current. The field from a transmission line can be reduced by various factors, which rarely applies to submarine cables.

Said et al. (2004) list the main variables which affect the MF for transmission lines. The most important factor is the magnitude of the phase current. The current on a line varies proportionally to the demand for electricity. Unless the current is known precisely it is difficult to determine values of associated MF. The pulse induced in the submarine cable is known precisely and the current flowing in the shielding can be calculated. The MF from the submarine cable is stable over the time.

The second factor given by Said et al. (2004) is the height of the transmission line. The MF decreases with the distance from the source and the height of the line above the ground level is an important factor. In a similar way, the MF from submarine cables decreases with the distance from the cable. In addition in the

marine environment, magnetic attenuation caused by salt water contributes to reducing of the MF on the sea surface.

Three phase transmission lines often have bundles of two or more conductors. The MF on the ground level is a sum of the fields produced by the currents in all conductors. Placing conductors close together can greatly reduce or even eliminate the MF. In marine surveys, the current is induced in the single additional conductor or the shielding of the cable. The phase and the frequency of the current are chosen to have no interference with other currents and to produce the maximum possible MF on the sea surface.

The MF density caused by the current *I* flowing through the straight conductor with length $\overrightarrow{dl}$ can be calculated by using Biot and Savart's law (Dezelak et al., 2010).

$$\boldsymbol{B}_{\mathbf{P}} = \frac{\mu_0 I}{4\pi r_P} (\overrightarrow{dl} \times \overrightarrow{r_P}) \quad (13)$$

The problem of different geometries of the current carrying wire was considered by (Olsen et al., 1988). He proposed to approximate the current path by straight line segments with a constant current. The description of this approximation is depicted in Figure 12. The MF at point *P* can be described by the equation:

$$\boldsymbol{B}_{\mathbf{P}} = \mu_0 \sum_{i=1}^{N} \frac{I_i}{4\pi |r_{iP}|} (\sin\theta_{i1} + \sin\theta_{i2})\, a_i \times a_{iP} \quad (14)$$

where *N* is the number of segments, I_i is the current on segment i, $|r_{iP}|$ is the length of the vector from the center of segment i to point *P*, a_i is a unit vector in the direction of segment i and a_{iP} is a unit vector in the direction of vector r_{iP}.

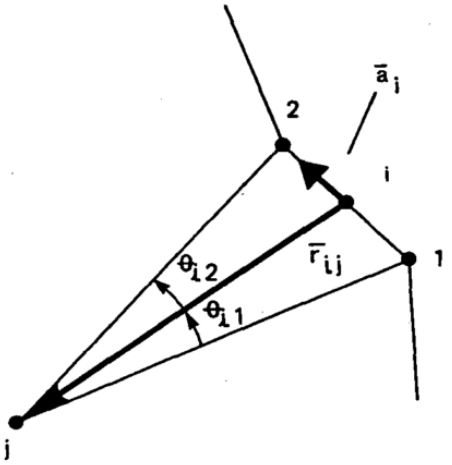

Figure 12 Discrete approximation of the Biot-Savart Law

The analytical solution for the MF from the single current carrying conductor can be obtained by using a 3-D Integration Technique (El Dein, 2009) based on Biot-Savart law as:

$$\boldsymbol{B}_{\mathbf{P}} = \mu_0 \int_l \frac{\vec{I}(l)\, dl \times \overrightarrow{a_P}\ (l)}{4\pi\, |\overrightarrow{r_P}\ (l)|^2} \qquad (15)$$

where l is the parametric position along the current path, $\vec{I}(l)$ is a line current, $\overrightarrow{r_P}\ (l)$ is a vector from the source point $S = (x_s, y_s, z_s)$ to the field point $P = (x_P, y_P, z_P)$, $\overrightarrow{a_P}$ is a unit vector in the direction of $\overrightarrow{r_P}\ (l)$ and dl is a differential element in the direction of the current. The variables from equation (11) are illustrated in Figure 13.

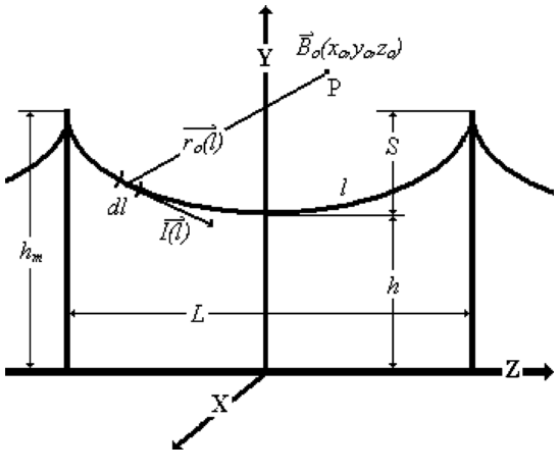

Figure 13 Overhead electric lines and Integral form of Biot-Savart Law

The calculation of the MF from overhead transmission lines assumes that the line is surrounded by air with zero or negligible conductivity. This is not the case if the line is buried in the soil. Gard (2002) considered the MF from the buried cables, where the conductivity and permittivity are different from that in the air. He considered the cable as a series of straight line sections where the magnetic flux is radially symmetric and can be considered as resembling cylindrical shells. He described the magnetic flux density by:

$$\vec{\boldsymbol{B}} = \frac{\mu_r \mu_0 I}{2 \pi r} \ \overrightarrow{\alpha_\phi} \qquad (16)$$

where $\overrightarrow{\alpha_\phi}$ is the tangential unit vector in a cylindrical coordinate system and μ_r is the relative permeability of the soil.

Equation (16) translated to Cartesian coordinate system becomes:

$$\vec{\boldsymbol{B}} = \frac{-\mu_r \mu_0 I(y+d)}{2 \pi (x^2 + [y+d]^2)} \ \overrightarrow{\alpha_x} + \frac{-\mu_r \mu_0 Ix}{2 \pi (x^2 + [y+d]^2)} \ \overrightarrow{\alpha_y} \qquad (17)$$

For the frequencies between 10 and 100Hz Dunbar et al. (2011) suggest that to some extent the attenuation rate follows the rate predicted by the expression for attenuation for a “good conductor”.

$$\alpha = 8.686 \ (\pi f \mu_0 \sigma)^{1/2} \ \text{dBm}^{-1} \qquad (18)$$

Dunbar et al. (2011) also consider the magnetic noise in the marine environment. From conducted experiments, they argue that the noise level is likely to have values in the order of 300 (dB).

All the calculations assumed the current to flow within an infinitely thin wire. For the purpose of marine surveys the thickness of the cable can be neglected. The distance between the cable and the sea surface often exceeds three metres which is dictated by the safe depth of operation of a marine survey boat. Taking into account that the thickness of modern submarine cables is 0.069m it is safe to assume that the distance is measured from the centre of the cable.

3.1.3 Sea water impact for MF distribution

Difficulties around the propagation of the MF in sea water are well known and have been studied for nearly one hundred years. (Bogie, 1972) lists four properties of sea water, which affect the magnetic propagation.

One of these factors is conductivity, with its typical value of 4 Siemens per metre (S/m) for sea water and the value of 0.001 S/m for fresh water. Conductivity depends upon factors like salinity, temperature, pressure or excitation frequency.

Permeability is usually taken as its value for free space ($4\pi\ 10^{-7}$ Henrys/m). The permeability for non-ferromagnetic substances such as sea and fresh water can be negligible.

Permittivity is correlated with frequency but for polar liquids can be considered constant for frequencies below 10^9 Hz. The permittivity of free space varies between 78 and 81

The last factor is polarisation. Sea water is an electrolyte and unless the flowing current is alternating, the polarisation has an impact on the magnetic propagation.

Sea water also reduces the velocity of propagation. For a frequency of 1 Hz the velocity can be similar to the velocity of sound, 1500 m/s. Lastly, the electromagnetic radiation incident at the air-water interface is reflected nearly in the whole range and only a small quantity dependent on frequency, polarisation and sea-state is refracted. Figure 14 shows different attenuation rates for different frequencies.

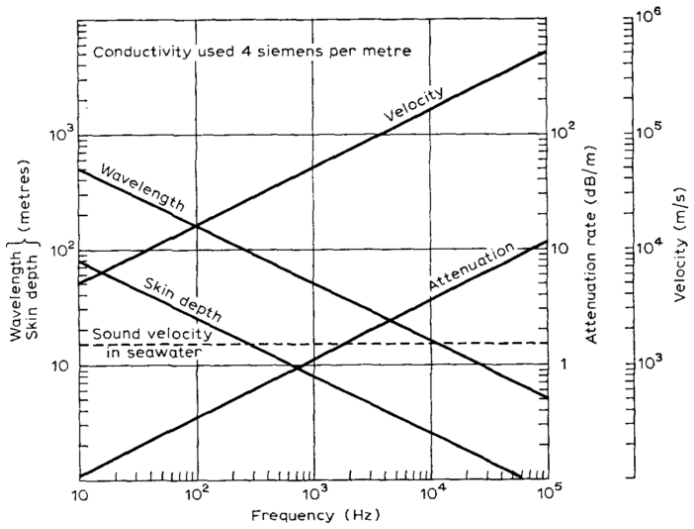

Figure 14 Dependency between frequency and attenuation (Bogie,1972)

A comparison of the attenuation in different types of water was conducted by Abdou et al. (2011). They point out that the complex propagation constant γ is described by the attenuation constant $\propto$ and phase constant β.

$$\gamma = \propto + j\beta \quad (19)$$

King (1993) approaches the attenuation problem by analysing the single electromagnetic pulse. He observed that the velocity of the electromagnetic wave is greatly reduced in sea water in comparison to air. It also depends on the width of the pulse and therefore the electromagnetic frequency. King (1993) draws the conclusion that the exponential attenuation of propagation in seawater decreases with the frequency.

Properties of the propagation of electromagnetic waves in the sea water were considered by Somaraju & Trumpf (2006). They draw attention to the fact that most models of the permittivity of sea water are empirically obtained as the best fit to experimental data. They proposed a physical, realistic model, similar to one used on plasma's physics. Although Somaraju & Trumpf (2006) focus on high frequencies from 1 GHz onwards, they conclude that lower frequencies propagate further. Somaraju & Trumpf (2006) point out that the frequencies might not be the only factor important in electro – magnetic field (EMF) analysis. For small EF strengths the conductivity of the sea water might decrease drastically and therefore have a large impact on EMF propagation.

The propagation of ELFs between 30Hz to 3 kHz in the layered structures consisting of mud, water and air was analysed by Johnson et al. (2011). They focus on the usefulness and robustness of simulation methods used in the analysis of ELF propagation problems. Johnson et al., (2011) compared the numerical analysis with experimental data showing excessive error between the two. They explain the error being due mainly by inhomogeneity in the medium and non-uniformity of the mud saturation. They experiment shows that it is difficult to precisely calculate an attenuation rate and the marine environment needs to be considered as more complex that its aerial counterpart.

The theory of magnetic and electromagnetic fields is used in many different approaches and survey techniques. The range of possible methods will be described in the next sections.

3.2 Geomagnetic

Distortions in the Earth's MF have been used for ferromagnetic object detection for nearly a century (March, 1953). The methods are widely accepted in the industry and are often seen as the first choice for wreck detections, subsea mining and recently for contaminated seabed and UXO detection (Weiss et al., 2007). It is not a surprise that geomagnetic sensing has been adapted to cable surveys. The ferromagnetic material in submarine cables is often small in comparison to other artefacts but the cables have been successfully surveyed in many occasions.

Marine magnetic surveys rely on detecting small changes in the strength and direction of the MF and is popularly referred to as a magnetometer survey. In the marine industry the magnetometer is known as an instrument to measure the MF naturally produced by the mass of the Earth. Ferromagnetic objects such as iron produce magnetic anomalies around them, which can be visualised as MF bends (Holt, 2014).

The important shortcoming of the survey is the fact that magnetometers do not sense the ferromagnetic objects directly. They can only measure changes in the Earth's MF. As Holt (2014) points out, it is very difficult to distinguish if an observed distortion comes from a submarine cable, pipeline, debris or even minerals with magnetic properties located on or under the seafloor. Another important property of magnetometers is their omnidirectional measurement. There is often no difference if the ferromagnetic object is directly under the instrument or if the magnetic distortion originates by the effect of a passing boat.

Holt (2014) further advises that the Earth's MF is not constant in time and space. The strength of the field is measured in Teslas (T) but values of the Earth's field vary gradually from 60,000 nT in parts of northern Canada to 24,000 nT in Brasil. These values change in time, what is known as the diurnal effect caused by the rotation of the Earth within the magnetosphere. These daily cycles cause the magnetic measurement at the same place to be different in the morning and in the afternoon.

The background MF and connected magnetic noise are important for marine surveys. All the information needs to be considered during survey planning and preparation, such as magnetometer calibrations. The smallest anomaly, which can be reliably detected, is about 5nT. This value translates into a minimum detection distance to an object with known mass. For example, an anchor with a 100 kg iron mass cannot be detected from a distance of more than six metres.

The standard survey procedure is to display a measurement output as a time series filtered in real time with a moving average. The chart should report the same values in the area with no magnetic objects and the filtered time series should be flat after reducing background noise. If the magnetometer passes the object the time series plot shows a “wiggle” indicating the presence of a ferromagnetic target.

The size of the distortion does not always follow the same profile. It largely depends upon the magnetic target’s orientation and the direction in which the instrument passes the target. Figure 15 taken from Holt (2014) shows that the produced anomaly can be clearly visible if the sensor flies above the target in the direction of magnetic peaks (line C) but can be not recognisable if the sensor passes above the target with a perpendicular course (line D).

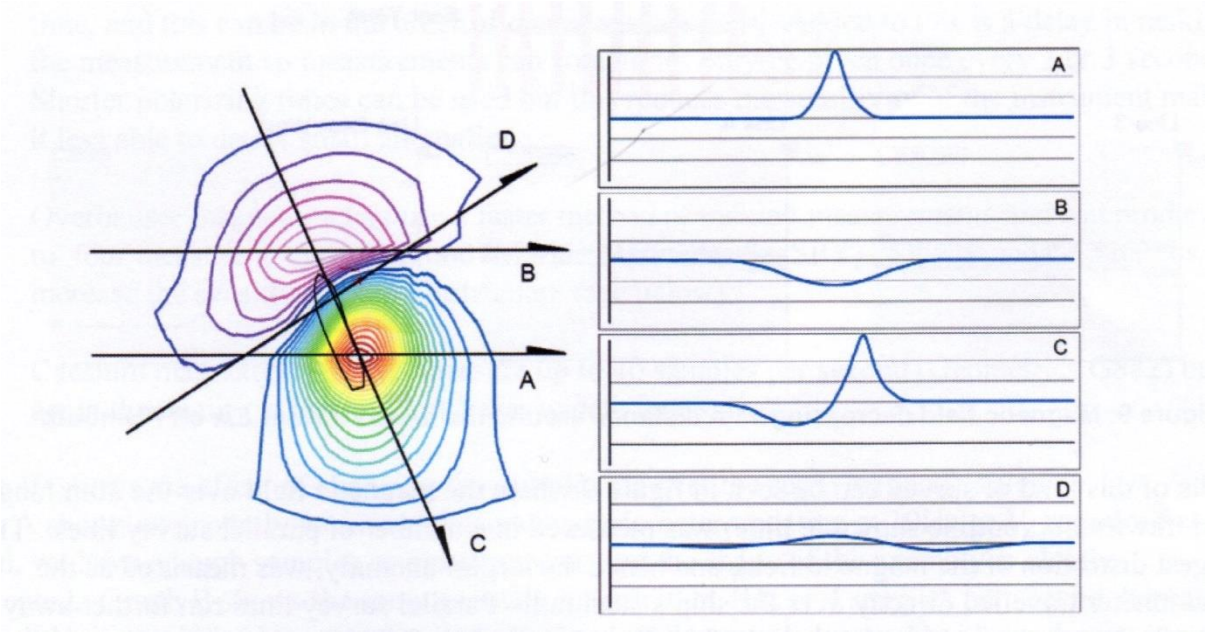

Figure 15 Distorted magnetic field above a wreck. Line A: the sensor passes across the positive peak. Line B: the sensor passes across the negative peak. Line C: the sensor crosses both peaks. Line D: the sensor passes between the peaks (Holt, 2014)

Different approaches are taken to improve magnetometer surveys. The most common one is to arrange magnetometers in an array of sensors towed behind a research vessel. Towing a magnetometer eliminates the signal from the magnetisation caused by the towing vessel (Gee, 2002). Another measure taken to assure an effective survey is the magnetometer calibration. The measurements of the sensors are corrupted by different sources of errors. Zhang & Gao (2009) specify error factors such as random instrument noise,

constant biases, scale factor deviations, non-orthogonality of the sensor axes. To reduce the error the instrument needs to be precisely calibrated before the survey and the readings need to be compensated for the inaccuracy.

Despite the drawbacks of magnetometer surveys Holt (2014) reports good results in cable detection. Holt (2014) considers the cables and pipelines as much longer than wider and he suggests this characteristic results in anomalies bigger than expected.

Figure 16 taken from Holt (2014) shows the magnetometer readings above the cables in Plymouth Sound. The readings show large but narrow anomalies above the group of cables. As Holt (2014) points out the power cables can additionally increase the distortion of the field resulting in unusual large signals. Figure 16 (B) shows a huge anomaly of 150,000 nT above power cable.

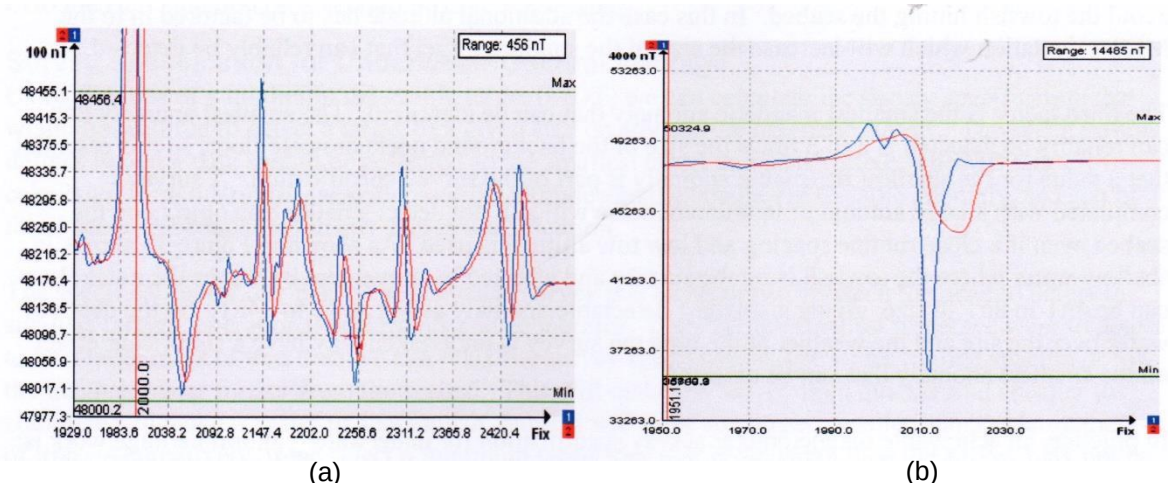

(a) (b)

Figure 16 (a): Series of cables giving large magnetic anomalies. (b): The Large anomaly of 14485 nT over power cable (Holt, 2014)

Magnetometer surveys of telecommunication cables can be very difficult for the reason that the main part of the cable is non-magnetic. Typically only the armour is made of iron and produces a magnetic signature.

The techniques were used during one of the commercial surveys in 2014. The survey was carried out in South America during preparation for installation on new telecommunication cable. The magnetometer Geomatrix G-882 was deployed and towed behind the survey vessel. Figure 17 (a) shows the magnetometer's deployment during the calibration process and Figure 17 (b) shows a computer screen with a display of raw and filtered readings.

(a)

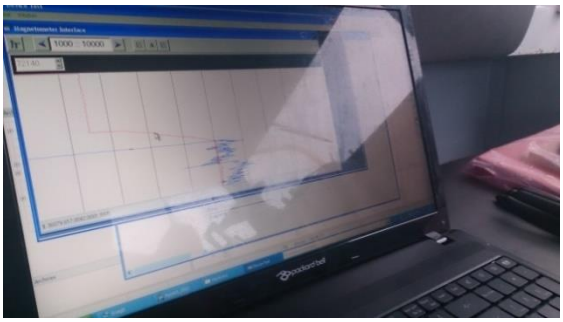

(b)

Figure 17 (a): Magnetometer deployment from the surveying vessel. (b): magnetometer readings during calibration

The performed survey gave satisfactory results and the target cables were identified. It also revealed many problems which need to be considered during the survey.

The magnetic signature of the locally sourced survey boat was very large. To avoid interference the magnetometer was towed behind the vessel at a large distance of 40 m. Although there exist techniques to control the towed fish, deploying addition sensors during a small survey is often not cost effective. As a result, the survey was performed only during high tide, in waters deeper than five metres.

The positioning of the magnetometer in relation to the boat was used by calculating a layback which could be questioned for precision. Magnetometers' deployment and recovery might be difficult in some conditions resulting in the risk of equipment damage or injury of personnel.

The most important drawback was the amount of false readings and uncertainty in the target detection. The produced outcome was heavily dependent upon the experience of the surveyor and post-processing. The survey was demanding in terms of both costs and time necessary to produce acceptable results.

Despite its disadvantages, often a magnetometer survey might be one of the few possible to perform. The technique does not require access to the cable ashore, which is necessary for tone detection surveys.

3.3 Electromagnetic detection

Applications relying on sensing distortions to the Earth's MF are often too general to precisely localise buried submarine cables. In many situations the EMF emitted from the utility gives better and more reliable results.

The following sections will focus on different methods of seabed objects localisation based on the electromagnetism resulting from moving electric charges and electric currents.

3.3.1 Direct current detection

Most EMF sensing methods are based on detecting the MF from an Alternating Current (AC). However, in long distance transmission, the AC current suffers a significant decay in current strength. For many applications a Direct Current (DC) is used instead.

Takagi et al. (1996) proposed a deterministic approach to detect DC subsea cables by use of AUVs. The application of fluxgate magnetometers instead of the widely used searching coils allowed them to sense a DC MF directly from the cable. Based on the inverse methods described below, they were able to localise the utility from short distances.

Takagi et al. (1996) suggested three methods for detecting underwater DC power cables. The first of these methods used a single fluxgate magnetometer and can be used as an aid to search for a cable on the seabed. This method measured a magnitude of the static magnetic field. The second method could measure the position of the cable and the direction in which it is lying. Calculations were subsequently carried out using the outputs of two fluxgates, which were mounted a fixed distance apart. The third method removed ambiguity, improved accuracy, and gave the 3D position of the cable. This method contained two vertically aligned gradiometers.

The position of the cable was calculated in relation to a sensing platform. Takagi et al. (1996) used two coordinate systems. One of the systems $X_{(0)}\ Y_{(0)}\ Z_{(0)}$ was fixed to the cable and the second system $X_{(3)}\ Y_{(3)}\ Z_{(3)}$ was assigned to the platform.

For the three-axis fluxgate magnetometer, the MF in the cable's coordinate system consisted of three values, one for each coordinate axis. The magnitude of the MF measured by each of the three axes of the sensor could be calculated by trigonometric equations.

To obtain the correct values for the DC current source, the calculation needed to be corrected for the background noise. The magnitude of the MF from the induced DC current was normally very weak compared to the Earth's MF and the magnetic noise from the platform. Additionally the vehicle's pitching and rolling resulted in an overall error. The platform's pitching and rolling caused inconsistencies of sensitivities, distortions of orthogonality and offset of the magnetometers.

To circumvent these problems, Takagi et al. (1996) proposed a compensation matrix and an offset vector. The values of the matrix and the vector are obtained from calibration by orientating the survey platform in the static, uniform and stable MF.

The problem was more easily solved by using two magnetometers. They could be placed in such a way that the corresponding axes were in the same direction. The gradiometer setup not only allowed the position of the cable to be calculated but also allowed the background noise to be cancelled. For the described gradiometer, a difference vector between two corresponding readings needed to be calculated.

The calculation left ambiguity about the position of the cable. A survey platform can be on the left side of the cable or on its right side. To resolve this ambiguity, two gradiometers containing two separate magnetometers per device were used. This arrangement allowed the position of the cable to be identified by use of Euler angles. Thus allowing the rotation of the platform, that moves in the reference to the cable's coordinate system, to be calculated.

Takagi et al. reported successful sea trials where the magnetometers were mounted on the large-sized ROV "MARCAS-2500". The ROV was able to detect the fluctuation in the MF from a distance of 20m. After detecting the MF, the ROV moved towards the source of the field and used the second method to estimate the position of the cable of interest.

The sea trials confirmed that a cable with a direct current of one ampere can be detected from a distance of up to eight metres. Additionally, the position of the cable can be calculated at a distance of up to four metres.

3.3.2 Active coils for cable tracking systems

A different approach to that described above is to actively induce a current within the target being detected.

The waveform of the resultant MF signal depends upon the geometry of the source and its proximity. A diagram of the MF and its response in eddy currents is shown in Figure 18. The detected signal from the eddy currents decays rapidly. The relation between the amplitude of the signal and the distance from the target r is an important drawback.

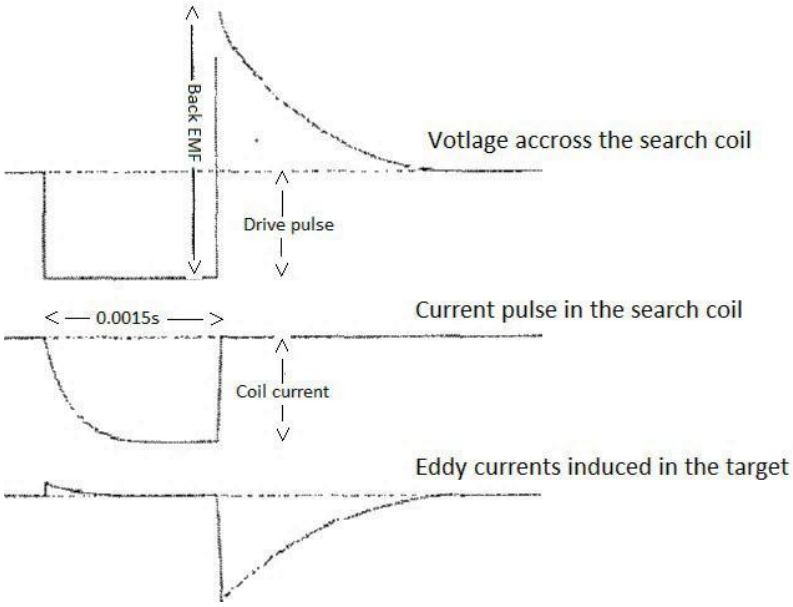

Figure 18 Diagram of induced magnetic field and eddy current response. (Cowls & Jordan, 2002)

The inducting coil can be considered as a dipole emitting the MF whose strength decays with r^{-3}. The target source can be considered a straight wire with the induced MF as circular loops and the same rate of decay. In this situation an aggregated signal decay is proportional to r^{-6}. Practically it means that a 50% improvement in the range requires about a ten-fold increase in the transmitted induction voltage or a very large improvement in the signal to noise ratio (SNR).

In subsea applications, the conductivity of the seawater largely determines the detection limit. The induced MF results in formation of eddy currents not only in the target but also in the surrounding seawater. The conductivity of the seawater is much less than the conductivity of the target, therefore the eddy current decay in the seawater is much faster than the decay from the source.

The fixed contribution of the seawater and conductive materials from the platform is measured by recording the voltage on the coils with no target presented. In measurements of the impact of seawater some, but not always valid, assumptions are made. For example, Cowls & Jordan (2002) assumed that the voltages caused by the seawater, on all three different coils, are the same. This is not always true. The coils are not necessarily the same distance from the source and the seawater is not necessarily homogeneous as an electromagnetic medium.

Cowls & Jordan (2002) pointed out that calibration is not the only procedure for removing the seawater influence. Cowls & Jordan (2002) were able to separate the signal by modelling the decay time of the eddy currents in the target and experimentally obtain the decay time in the seawater.

They used finite element modelling to determine two types of eddy currents in the target. One of them, a saddle, is roughly circular and is parallel to the excitation current in the coil, with a decay time of $130\mu s$. The second of the eddy currents is axial and travels along the target and its decay time is about $1ms$.

Given the above data, Cowls & Jordan (2002) were able to fit two exponential curves into their experimental data. After obtaining the models for the eddy currents in the target, they performed an experiment to find the seawater contribution. They found that the seawater response follows an approximate exponential curve with a decay time of $59\mu s$. Cowls & Jordan (2002) decomposed a complete waveform into a target response and a seawater response by using a linear least square fit.

The theory was successfully applied in a commercial method called “TSS”. The above procedure gives a better seawater response rejection and it is claimed to improve the range of the TSS method by 50%. However, from the experiment it was found that the water response below a depth of $100m$ did not behave in the predicted way.

There were two reasons for this discrepancy. First, the seawater signal decay is not truly exponential. Second, as the platform moves, the MF from the seawater eddy currents not only decreases in amplitude but also in decay time. Both of these reasons suggest one conclusion; the response from the seawater eddy current is not linear and can only be approximated by the linear least square fit.

Cowls & Jordan (2002) agreed that linear rejection of the seawater response is difficult to apply. They claimed that were able to improve the range of detection by simply eliminating the seawater contribution from the overall signal.

Cowls & Jordan (2002) tested this approach in water at a depth of 24m. With 100 measurements taken, they claim they rejected the seawater contribution by up to $5\mu V$ compared to the normal seawater contribution on the level of $70\mu V$. They state that the presented method can improve the range by 20% for a typical sized target.

The parameters are specific for the water's depth, salinity and uniformity. Also, although Cowls & Jordan claim some satisfactory results, the experiments were conducted in relatively close proximity to the target. The experiment used to obtain these parameters was conducted at a distance of up to five metres from the sea bottom.

If the method is to be used at a distance of up to 60m from the target, it will require a significantly improved error rate and a better understanding of the seawater influence on the measurements to reduce its contribution.

3.3.3 Underwater unexploded ordnance (UXO)

Pulse induction is a general method of detecting ferromagnetic objects and is widely used in underwater mine hunting and detecting unexploded ordnance (UXO). The UXO detection and discrimination techniques are a vibrant area of current research involving subsea EMF. Developments in the detection of ferromagnetic underwater objects can be directly transferred to the field of sensing and tracking of the electric and telecommunication cables.

The problems specific to the detection of underwater UXO objects were presented in Clem & Lopes (2003). They drew attention to the conductivity of sea water. The electromagnetic field induced in the salt-water generates an electric current channel around the target. This perturbation excites secondary electric currents that are characteristic of the target that can be detected by the receiver. This situation leads to a phenomenon labelled as the current-channel response (CCR), in contrast to the better-known eddy-current response (ECR). Clem & Lopes (2003) argue that under certain conditions the CCR will be stronger than the ECR.

Clem & Lopes (2003) also argue that most analyses focus on targets suspended in the water column. These investigations fail to take into account the impact of the EM wave scattering at the bottom interface and wave propagation into the sea floor for the case in which the target is buried.

Clem & Lopes (2003) point out that certain assumptions which are normally used are not necessarily true. These assumptions can be categorised into four groups: (1) the sensor is moving in level flight at a constant speed through the water; (2) the water and sediment are homogenous; (3) the sea floor interface is flat and (4) the air-water interface can be ignored.

They present different types of sensors, among them different types of magnetometers, able to detect ferromagnetic UXO objects, but they drew the conclusion that the best result can be achieved by means of sensor fusion.

The developments in underwater metallic UXO detection by use of electromagnetic field induction techniques are reported by Sulzberger and co-workers (Sulzberger et al., 2006; Alen et al., 2005).

Sulzberger et al. (2006) and Allen et al. (2005) conducted a set of experiments with a real-time tracking gradiometer (RTG) mounted on an unmanned underwater vehicle (UUV) - Bluefin 12.

The RTG contained four 3-axis fluxgate magnetometers located within a 3-axis Helmholtz coil. Three of these sensors were located at the vertices of an equilateral triangle. These three magnetometers form six gradients, only five of which are independent. A fourth, centrally located, 3-axis sensor was used as a reference sensor to provide feedback to the three gradient-generating sensors. The reference sensor responded to the ambient magnetic variations and produces the “nulling corrections” for sensors that are generating the gradients. This feedback greatly reduced the motion response in the compensated sensors and allowed them to operate in a nominal low-field environment (Sulzberger et al. 2006).

Allen et al. (2005) reported good results from the conducted experiments. They reported that they were able to detect a target in a 10m range with a 95% confidence. Nevertheless, they pointed out that the determination of the precise position of the buried underwater targets by use of a UUV is difficult in practice. The Bluefin 12 used in the experiments was umbilically-connected with a surface vessel. The global positioning system (GPS) on the vessel gives a precise position on a surface, and from that reading, the position of the UUV can be approximated.

Allen et al. (2005) also pointed out that shallow water detection is very problematic. In their opinion, a single sensor technology is not sufficient because of the wide range of target characteristics and environmental conditions encountered in marine environments. They proposed the use of a carefully selected suite of complementary sensors such as magnetic gradiometers and BOSS. The main problem in using magnetic sensors is their short range and large signals produced when they are in motion in the Earth's magnetic field (Allen et al., 2005).

Similar research to develop an AUV with electromagnetic pulse induction for detection of underwater ferromagnetic UXO objects was undertaken by Pei & Yeo (2006; 2009) and Pei et al. (2010). Magnetic and electronic modules of an AUV are shown in Figure 19. Pei & Yeo (2006; 2009) and Pei et al. (2010) investigated the use of a similar RTG magnetometer setup but focused their attention on target parameters calculation, correct noise reduction and integrating the sensor with a moving platform.

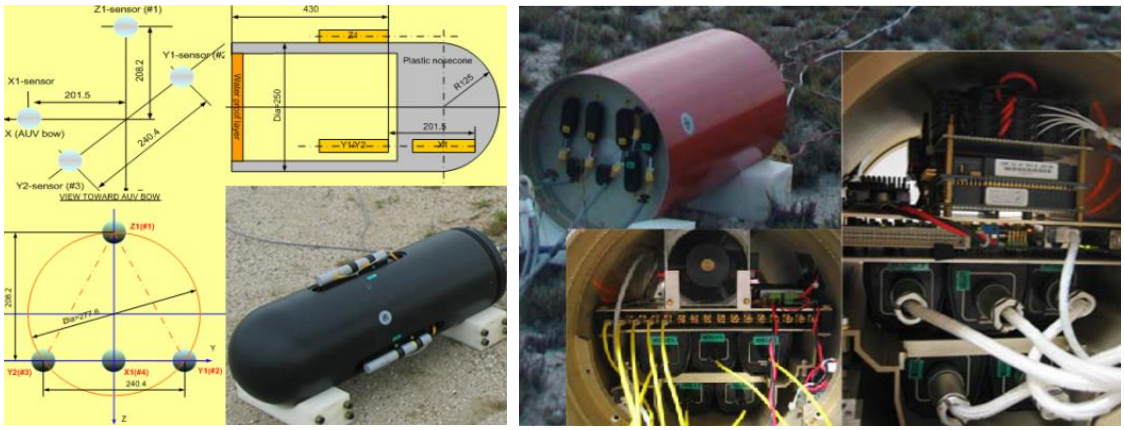

(a) (b)

Figure 19 (a): AUV's Magnetometer module. (b): AUV's Electronic module (Pei & Yeo 2009)

Pei & Yeo (2006; 2009) suggested that magnetic anomaly detection is an effective way of sensing, especially in underwater buried target detection and localization. A method such as inversion can derive the range, bearing and magnetic moment of the target of interest. Pei & Yeo (2006) invert information related to a magnetic object. The target's magnetic parameters are determined via an iterative search process by means of magnetic gradient field target pattern matching. The initial location of the object is determined by an inversion of the dipole model. Pei et al. (2010) proposed to identify a set of physical parameters such that the calculated gradient magnetic field data fit with the measurement data. The target parameter estimation, such as its unknown location and dimensions involves solving for a total of six unknown

quantities, three describing its location and three describing the target magnetic moments. A diagram of a gradiometer and a target is shown in Figure 20.

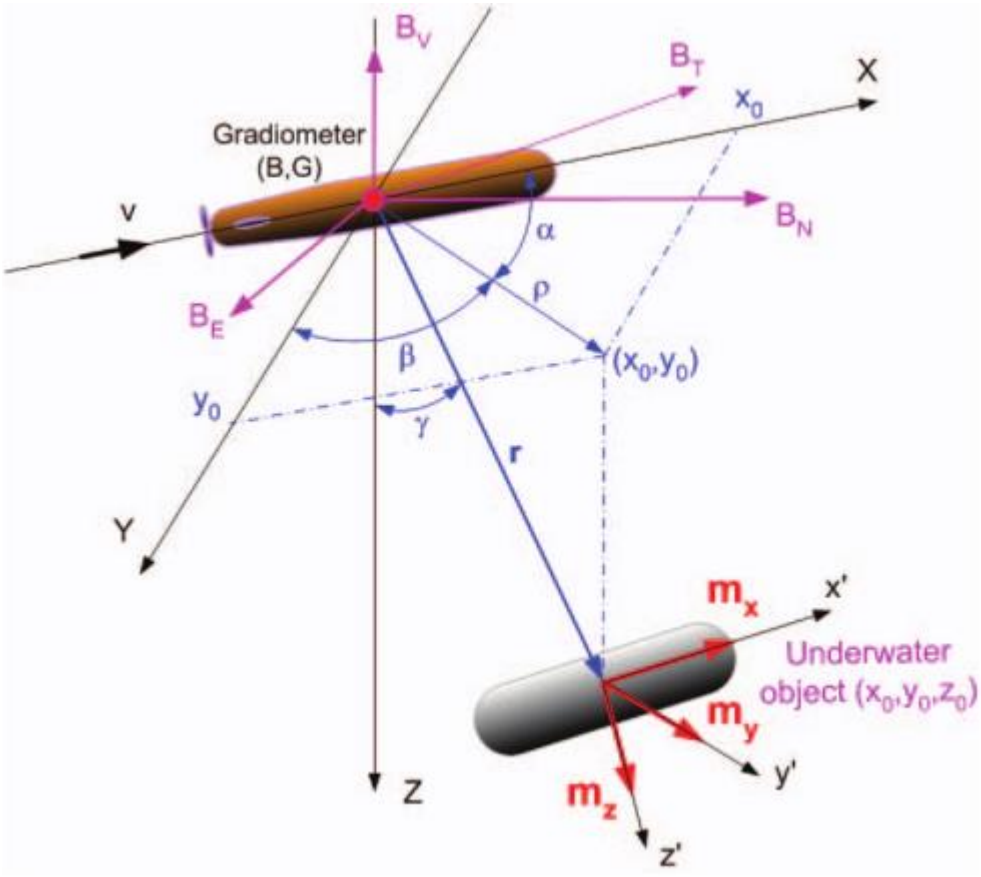

Figure 20 Schematic of magnetic gradiometer detection of a magnetic target (Pei & Yeo 2009)

Using an RTG setup, Pei et al. (2010) reduced some components of magnetic noise. They argued that gradiometers have the advantage of rejecting unwanted long-range environmental noise sources. However, they pointed out that the AUV's magnetic noise is one of the most critical technical problems for magnetic detection on board the AUV. Pei & Yeo (2009) classified an AUV's magnetic noise into two groups: as time constant components and time variable components. The first components are permanent and come from permanent magnetic sources, which are not difficult to predict or eliminate. The second, induced, components of the magnetic noise, change with time and come from sources such as magnet motors or untwisted power cables. Pei et al. (2010) proposed a mathematical compensation process to compensate for the time-constant magnetic field noise and an adequate calibration for reducing general noise.

Pei et al. (2010) reported successful simulation experiments but also sea trials with the use of AUV. They claimed they were able to detect long length objects from a distance of about nine metres (Pei et al. 2010).

3.4 Pulse induction

In practical applications of EMF detection, two kinds of approaches can be met. The first methods use active sensors, which calculate the backpropagation of the emitted signal. This sensing method uses an active approach. The magnetic field is emitted by on-board equipment. It induces electric current in ferromagnetic materials. After switching off the magnetic source, the MF produced by the remaining eddy current can be sensed.

The second method relies on inducing an AC current onto a transmission line and detecting the parameters of the MF in the near neighbourhood. This method often requires onshore access to the line as well as ensuring continuity of electric flow.

Although both approaches are similar in terms of sensing of MF, they require different hardware. Both of them will be described in the following chapter.

3.4.1 Searching coil localisation system.

In active sensor methods, coils emit an AC field and read the response from the utility. The obvious drawback is that the practical distance in which the MFs attenuate is doubled in comparison to the distance to the cable. To eliminate this problem, the tone can be actively induced into the utility.

This method was used on the land by Wang et al. (2010). The main purpose of the project conducted by them was to design a sensitive magnetic sensing tool equipped with appropriate algorithms for accurate localisation of 50Hz live power cables buried under a road in an industrial area.

They designed a frame of seven sensing coils as shown in Figure 21. The indication of the most likely location of the cable comes from the model which minimises the total square error in fitting the measured field data. The frame is placed at different locations where the position and measurement are recorded. By use of a Fourier analysis, they extract the 50Hz and harmonic signal components. A least square error method applied to the obtained data gives estimates of the cable currents, and the residual errors give an indication of the true position. They claimed that the searching coil method can be significantly improved. The main strength of this method is that it indicates the distance in both the horizontal and vertical directions.

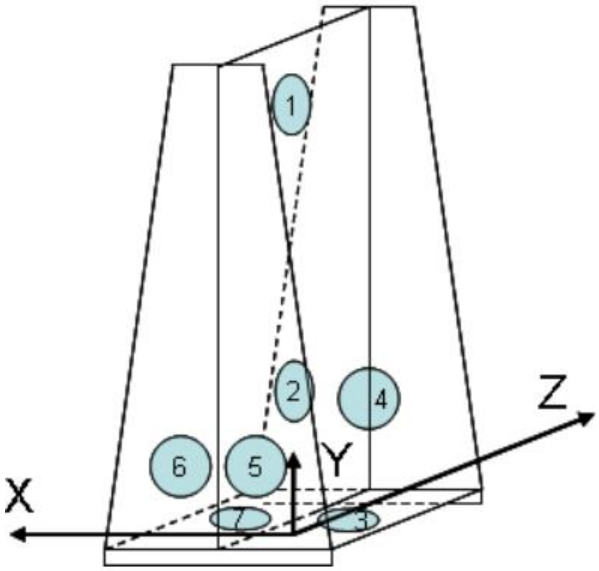

Figure 21 Expanded frame of searching coils (Wang et al. 2010)

The experiments by Wang et al. (2010) were conducted in an urban area where a large number of power cables exist in a relatively small neighbourhood. Wang et al. (2010) pointed out the over-fitting problem, where the model describes more noise instead of the underlying relationship. The number of simultaneous MF measurements needs to be significantly larger than the number of unknown currents. In practice, this limitation breaks down to the problem of the distance over which the obtained results are still independent.

For underwater detection over large distances, the problem is similar to the problem of obtaining a measure of the third side of a triangle, knowing that the other two are relatively very large. If the voltage difference between two coils is smaller than the value of the noise, the calculated location will result in a significant error, which could result in the impossibility of estimation of the location.

An extended setup allows estimation of the position of the cable in both the vertical and the horizontal directions. However, for underwater applications the influence of the signal propagation medium needs to be taken into account. In the experiments described by Wang et al. (2010), the soil has no effect on the propagation of low-frequency magnetic fields. The same does not necessarily apply to the subsea situation (Al-Shamma'a et al. 2004).

3.4.2 Autonomous Underwater Vehicle Implementation

AC MF detection of buried cables requires placing detection coils in close proximity to the cable. In practice, it can be achieved by using a diver or an unmanned underwater vehicle. The literature on this subject reports the successful use of underwater platforms.

From a historical perspective one of the first platforms with MF sensing methods was “AQUA EXPLORER” (AE). It was first launched in 1992 (Takagi et al., 1996; Kojima et al., 1997).The AE’s family included several platforms and were successfully commercialised. (Nautic Expo, 2012) Details of the optimisation methods used during the development of the AE can be found in Kato et al. (1998) and Kojima (2003).

Two “AE” AUVs were made for the purpose of inspection of underwater telecommunication cables. They were equipped with two tri-axial magnetometers, a video recorder and a high-bit-rate acoustic link for real-time video transmission and monitoring of the seafloor by an operator. The MF detection was compiled with the visual inspection. A traditional visual check and video recording was considered as good evidence of a cable and pipeline’s condition.

The AE decided that the cable has been found when the intensity of the AC MF exceeded a threshold limit of 5 nT. It means that the vehicle has reached a zone of 5m width on both sides of the cable (Kato et al. 1994).

After detecting the MF from the cable, the AE moved on to the second stage and tracks the cable. In a similar method to altitude-keeping, tracking is performed by a proportional-integral-derivative (PID) controller and fuzzy controllers. After finding the cable, the vehicle turned towards the direction of the cable. It advanced at an altitude between 1m and 2m. The description of the PID and fuzzy controllers can be found in Kato et al. (1994).

Detection of the cable performed by the AE was based on simple geometric and trigonometric rules. A horizontal and vertical distance from a cable was calculated from the angle between the direction of the cable and the direction of the vehicle, the outputs of each sensor and the distance between the two sensors. The procedure described in Ito et al. (1994) and Kojima et al. (1998) also incorporated the roll and pitch angles of the vehicle.

Experiments with the family of AE vehicles raised the issue of the magnetic noise. Typically the 50mA AC current in the subsea cable can produce the MF of 1nT at a point 10m distant from the cable. The noise level from the magnetometer was very low and normally did not exceed 0.02nT/Hz. However, the noise produced by a DC electric motor was about 5nT at a distance of 1m. The shielding of an AUV's electric motors can achieve some reduction but noise was still a big issue for the accuracy of the platform. Another onboard noise was produced by the current flow on the batteries and wiring to the thrusters and elevators.

Cancellation of the platform's noise can significantly improve the detection range. Some calculation for AE was carried out in Kojima (2003). It was claimed that if the noise level from the platform is reduced to 0.05nT, the SNR is 10dB, and assuming the AC current in the cable to be 50mA, the AE2 can find cables from 60m away.

In a similar fashion, if the SNR ratio is 20dB and the distance from the cable is 3 m, the required current for cable tracking is 4.5mA.

Electromagnetic detection is most suitable for detection of buried subsea cables but suffers from its own limitations. Attenuation of the MF in sea water makes the method difficult to use. For this reason, the sensors are often deployed in underwater platforms which result in the magnetic noise incorporated into the readings.

Although the sensing of MFs and EMFs is a demanding process it is often the only choice for detecting buried cables. In the next chapter, the commercially available tools will be presented as part of the market analysis. Knowledge of current techniques helps to develop a better solution but also helps to commercialise the methods and apply the research in real world applications.

Chapter 4. Market analysis Commercial cable detection methods

The first submarine cable was laid on the oceans floor as early as 1850. Since then subsea connections have become more important and are increasingly recognised as a substantial part of the international infrastructure. Submarine cables are the foundation of the world's telecommunication systems. Nearly all internet traffic from social media, business communication, to financial and bank transfers, relies on subsea connections.

Periodical maintenance and a quick response to cable faults are crucial in keeping these telecommunication channels alive. This chapter focuses on the importance of localisation methods and describes leading commercial tools used in cable detection.

4.1 Submarine Cables market

Nautical charts are marked with large numbers of subsea connections. Keeping this network operational involves an effort of many communities, nations and bodies up to governments on an international level. As Wargo & Davenport (2014) point out, in 2013 the economic costs of submarine cable faults in a country like Australia alone would amount to more than 3,000 million USD and the cost of a single repair in the United States can vary between one to three million USD. Constant cable usage is important for cable owners. With an estimated over 200 faults per year, it is crucial to have full knowledge about cable positions and their states.

Figure 22 shows the UK's submarine cables and pipelines chart from June 2015. The map shows only currently active cables which are protected and in constant operation. It is worth remembering that the first Atlantic cable was installed between 1854 and 1858 to connect Ireland and Newfoundland. From that point on, cable installations have rocketed and new cables are installed every year reaching a deployment of 50,000 km per year from the beginning of the twenty-first century. The life expectancy of a telecommunications cable is 25 years, thus the map in Figure 22 shows only a small part of all utility lines covering the ocean floor.

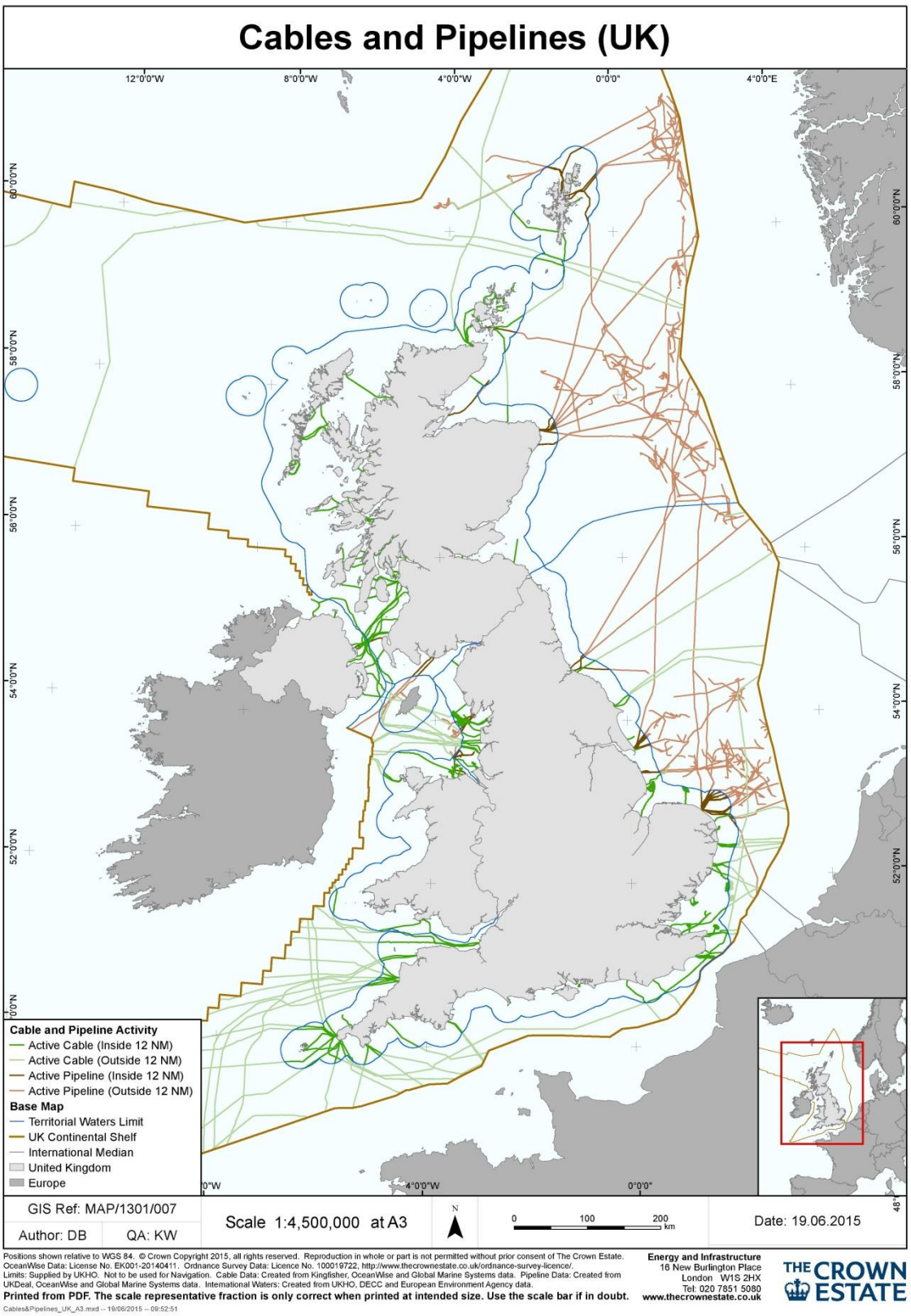

Figure 22 Submarine cables and pipelines around UK shore - summer 2015 (The Crown Estate, 2015)

The market of submarine cables has one of the most optimistic and stable perspectives in the marine industry. It was identified that in 2014 there were 160 new cable projects with a total value of 22.6 billion USD. (Terabit Consulting Inc., 2014).

The significance of submarine cables is difficult to overestimate. The International Cable Protection Committee (ICPC) compares submarine cables with satellite transmissions (International Cable Protection Committee, 2011b). They list advantages of the cable system, such as:

- High reliability, capacity and security
- Insignificant delay compared to satellite
- Most cost-effective on major routes hence rates cheaper than satellites
- Submarine cables carry more than 95% of transoceanic voice and data traffic.

Advantages of satellites are listed as:

- Suitable for regions that are vulnerable to disasters
- Provide wide broadcast coverage, e.g. for TV
- Suitable for minor routes such as links between small island nations
- Satellite traffic carry less than 5% of transoceanic voice and data traffic

In their documents, ICPC indicates that cables lying near the shore need protection from shipping, fishing and other activities. One of the protection measures is the identification of protection zones which are marked on nautical charts. In those areas, all activities harmful to the cables are banned. The protection zones do not always provide sufficient damage prevention and other measures need to be taken.

One of the most effective protections is prevention of direct access to the utility. In case of subsea cable such protection can be achieved by burying the utility in the seabed. ICPC clearly indicated cables burial in water depth up to 2000 metres as a key protective measure.

ICPC specify abrasive activity in shallow waters as the main cause of cable faults. They justify that:

- Around 70% of all cable faults are caused by fishing and anchoring activities
- Around 12% are caused by natural hazards, e.g. current abrasion or earthquakes
- Most faults are caused by human activities in less than 200 metres water depth

- Faults in more than 1000 metres water depth are mostly caused by natural events.

Data provided on the ICPC website suggest that the tendency for cable damage in shallow waters is growing in recent years and about 60% of all damage occurs in waters less than 100 metres deep (International Cable Protection Committee, 2011a).

In case of telecommunication lines, localisation of faults is often made by a cable station. Optical measurement of optic fibres gives a very good estimation of the distance to the break in the cable. The most precise method uses time domain reflectometry. The measurement sensors in the cables station send a light impulse into an optic fibre. When the impulse reaches the breaking point, a large portion of light energy is drained into the water but part of the energy is reflected back and caught by the sensor. The current methods can give the position of the break in the cable within one percentage of the total cable's length (Worzyk, 2009).

If the breaks are in depths where a cable ship can safely operate, the whole operation is conducted by a specialised vessel. Typically a ROV with a large sensing frame (usually TSS described in the following section) is deployed to crawl or fly within a short distance to the seabed. After the cable is localised the ship drags a grapnel, hooks the cable, lifts it out of the water and prepares a joint to connect working parts of the utility.

The problems are more difficult to solve if the cable is in shallow water where heavy machinery cannot be deployed. In shallow water, most operations are done from a small RHIB or a barge. ROVs are difficult to operate because of the lack of a support vessel and risk of damage. Operation in shallow water usually brings more challenges for all operations.

In shallow water, cable localisation and recovery are completed in a different manner than from a large cable ship. The operations require better planning and more precise localisation. Shallow water repairs often involve divers, hence carry more risk of injury or even loss of human life. Working underwater differs from carrying tasks on land. According to diving regulations, diving is a high hazard activity (Health and Safety Executive HSE, 2015). The working diving team requires support underwater but also on the surface. It is often difficult to provide specialise support vessel able to go into area of shallow waters. In such situations, different methods are preferred with more compact equipment designs for carrying out surveys from small boats.

Fault finding is not the only situation in which cables need to be precisely localised. Inspection, localisation and tracking of existing cables and transmission lines are important preparation steps before every new installation. A comprehensive survey reduces the risk of operation, its cost and improves its schedule. It also makes a substantial improvement for future link availability and repair costs (Worzyk, 2009).

The third situation for which cable tracking is required is regular maintenance. During installation, a cable is positioned and charted. However, as Li et al. (2013) point out, ocean floor currents and geological environment variations together with man-made berthing and anchoring of vessels etc, change the cable's position. Over time the laying depth and buried routeing changes gradually. In order to provide reliable technical data for the maintenance work of submarine cables, detection of the laying depth and buried routeing should be carried out on a regular basis. Li et al. (2013) suggest the process is an indispensable key link to maintaining a cable during its lifetime and assuring its quality. Unlike fault detection, maintenance detection is a long-term, daily work. The operational state of the cable cannot be interrupted; otherwise, it will cause a huge economic loss (Li et al., 2013).

Reliable methods of detection are still rare in the marine cables' market. Providing a good alternative to existing technology can fill the gap between the expectations and the market's offering. The next section describes the main techniques and tools used during cable operation, their localisation and tracking.

4.2 Industry standard for land cable localisation: Radiodetection locator RD

Cable and pipeline localisation systems manufactured by SPX-Radiodetection Limited from Bristol (SPX) are probably the most advanced locators available on the market. The company has 40 years of experience in providing a tracing service for underground utilities and manufactures equipment which has become a standard on construction sites. The company offers a wide range of locators from simple cable avoidance tools (CAT) to sophisticated radiodetection systems (RD) locating breaks or insulation deterioration. The equipment from higher range provides technological advances such as GPS functionality and Bluetooth communication between all parts of the system which increase precision and ease of use. (SPX Corporation, 2016).

The SPX offers products designed for different applications. The simplest version of the locator is the CAT system providing a visual and audio indication of a cable's proximity. The tool shown in Figure 23 (a)

senses the EMF of desired frequency induced in the utility. The EMF read by a searching coil is directly transferred into an audio or visual signal. Based on the intensity of the signal an operator can estimate the distance to the utility and by moving the CAT across the cable, can localise its position.

A similar product is offered for underwater tracking. A submersible double depth antenna is designed to be used by a diver or lowered into the seabed with a non-metallic boom. In a similar fashion to the CAT system, the antenna is equipped with searching coils sending the current induced by the EMF to a topsite unit and operator.

The submersible antenna shown in Figure 23 (b) is designed to respond only to one of two frequencies, 640 Hz and 8 kHz. It is factory calibrated and needs to be coupled with an RD system as a topside unit.

Figure 23 (a) Cable Avoidance Tool (CAT). (b) Submersible double depth antenna used for tracing underwater utility.

The CAT product is targeted at the construction market with the requirement of quick localisation of buried utility lines. It has only the simplest functionality with low precision. Some CAT products have the ability to estimate burial depth or distance to the cable. The measurement relies on a basic calculation taking the difference between two readings from coils placed in a fixed distance apart

Figure 24 shows the principle of a depth reading. The CAT system does not acquire measurements for estimating the cable's direction, the tool's offset or the angle to the cable. The depth measurement can be precise only if the tool's position is directly above the utility at the correct angle and without any tilt. In addition, the depth readings do not cope well with the situation when more lines or ferromagnetic objects are close to the cable of interest. To solve all of these problems SPX manufactures higher precision locators referred as RD detectors.

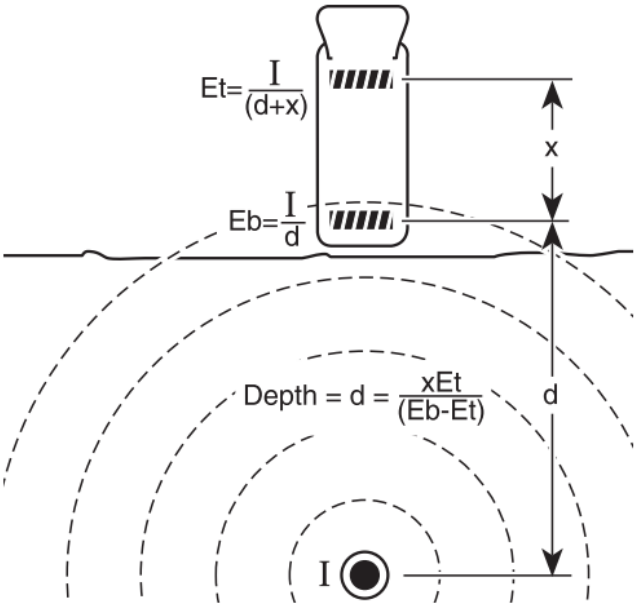

Figure 24 Depth measurement base on signal difference between top antenna (Et) and bottom antenna (Eb) (Radiodetecion Ltd, 2008)

The SPX holds several patents for tracking equipment and uses techniques based on multi-frequency detection. The locator tracks conductors carrying an alternating current with at least two distinctive frequencies. According to the patent, the receiver is equipped with at least one magnetic sensor converting EMF radiation to a digital reading of the signal strength of the isolated frequencies (Pearson et al., 2015). The multi-frequency detection provides additional advantages. An important feature of the system is its ability to single out a single conductor from a group of conductors in its close vicinity.

The system is composed of a receiver and transmitter inducing an EMF in the cable. The signal applied to the conductor comprises at least two components related to frequency and phase. The signals induced in neighbouring conductors may be of the same frequency but with a different phase. Comparing the phase of the signals the receiver determines the conductor to which the tone was applied. The method of differentiating the phase of the signals was patented more than twenty years ago. (Flowerdew & Regini, 1993).

The RD systems are able to detect faults in hidden electrical conductors. (Floweredew & Regini, 1990). Low and high frequency signals applied simultaneously tend to travel at different propagation. If there is a current leak to the Earth, the higher frequency tends to suffer more loss than the lower one. After the locator passes the fault, the higher frequency can be detected with phase reversal. In their patent Floweredew &

Regini (1990) proposed a system of detection based on the above postulates. They compare the phase and amplitude of the injected frequency and its harmonic. Irregularities in the measured signal allow them to inspect the state of the buried cable without its recovery.

The RD systems offered by SPX detect mainly higher frequencies. The main reason for this choice is in the compact design and size of the sensors. Depending on the configuration the locator can detect nearly twenty different frequencies. Interesting is the fact that the RD can also locate cables based on grid frequency (50 or 60 Hz) and radio frequencies. Long utility lines act as antennae. They resonate with frequencies common in their surroundings. In urban areas, the power grid emits large enough EMFs to induce eddy currents in long inductors. The secondary field from the conductors is strong enough to be detected by the RD system.

The RD detector is equipped with four custom-made core coils for precise location and distance measurements and one air coil to aid the estimation of the utility's direction. The RD receiver shown in Figure 25 contains a multifunctional display and its ergonomic design is patented (Ward & Harris, 2011) under international law.

Figure 25 RD receiver during locating existing lines before cable landing works in Italy (courtesy Subsea Cable Tracking Ltd)

The RD systems have strong competition from companies such as Vivax-Metrotech AUS from Australia manufacturing CAT systems, Leica Geosystems from Switzerland providing complete survey solutions or C.Scope from the UK specialising in metal detectors. Although the companies compete on prices and added functionalities and software, the principles of operations are the same.

The main disadvantage of these systems is their allocation to the construction market. The locators need to be used in close proximity to the buried utility. They are build with compact designs and casings using small searching coils which are designated to read radio frequencies usually with 512 Hz as the minimum frequency. The locators are not intended for use by a diver or even in harsh marine environments hence are not robust enough to be used in shallow water surveys.

The next sections describes locators built for the marine market. They often use the same principles as their land counterparts but their design is very different with more robust compositions, different functionalities and usage.

4.3 Teledyne-TSS

Subsea pipe and cable detection in deeper waters involve different tools to those used for a survey on land or surf zones. Almost in all cases, the survey vessel deploys an ROV equipped with TSS technologies. The first TSS system (TSS-340) was developed in 1991 and from this time it became the undisputed leader in deep sea cable tracking.

This marine industry standard for detecting magnetic materials is based on the technology of a searching coil inducing a magnetic field (Cowls & Jordan, 2002). The method is based on searching coils described earlier by Corbyn (1980). Traditional metal detectors were equipped with single coils emitting an EMF signal and after switching off, reading back the signal emitted from eddy currents in a target. Corbyn (1980) proposed to use two coaxial coils with different diameters. The coils are designed to maximise the primary MF at the target and the voltage induced in the receiving coil. The system was further developed into different configurations. Application of two receiving coils allows additional measurements of the input ratio, improving the detection ability of the system. In a simplified model, the ratio of the voltages induced in two different coils is a function of only geometrical parameters of the detector and does not depend on the parameters of the target. The depth of the object can be calculated based on the ratio and relative position of the coils (Das et al., 1985).

This concept used in TSS-340 and its application in subsea detection was described by Cowls and Jordan (2002). They pointed out that the system meets additional complications. The induced eddy currents flow in the target but also in surrounding water. The vehicle with the system flies a few metres above the seabed.

The returning waveform is further changed by interference between the seabed and salt water. The vehicle does not necessarily operate with all coils at the same distance from the target and the seabed hence contribution of sea water is not always constant for all used sensors. Lastly, the vehicle itself and its noise often contribute to the readings and the system needs to be precisely calibrated before the use.

Although it is difficult to find a description of how all these problems are solved, the TSS systems are the most popular in the marine market. The TSS-340 comprises three coils. The coils sample the reluctant signal on two places on the decay curve. The voltage on one of the coils provides the magnetic detection signal. The voltage on the second is the baseline. The distance of the coils from the source is determined by taking the difference between the baseline and the signal.

Around each coil, a changing magnetic field is generated by driving the coil with a maximum current of 20 A for a pulse duration of 1500 μs. In response, eddy currents are created in the conductive parts of the target such as a pipeline section, whereby a voltage is induced back into the search coils which affects the rate of decay of a back EMF voltage created in the coil on termination of the original 20 A drive pulse. The rate of decay is related to the conductivity, size and proximity of the pipeline.

The system is fully integrated with the vehicle. The decaying voltage in each coil is measured to determine two individual signal voltages which are supplied to the navigation computer where the relationship between the voltages is analysed to determine the position of the utility line relative to the coils. The navigation computer is in this context programmed to give priority to signals input from the search coils. (Bech et al., 1996)

The searching operation engages very costly equipment but also a specialised ROV operator and supervisor. During the search operation, most of the other activities on board the vessel are put on hold which results in a large amount of time and costs spent on the tracking activity.

Figure 26 shows an ROV on the deck of a specialised cable vessel during one of the cable repairs conducted in early 2016 near Sennen Cove in Cornwall.

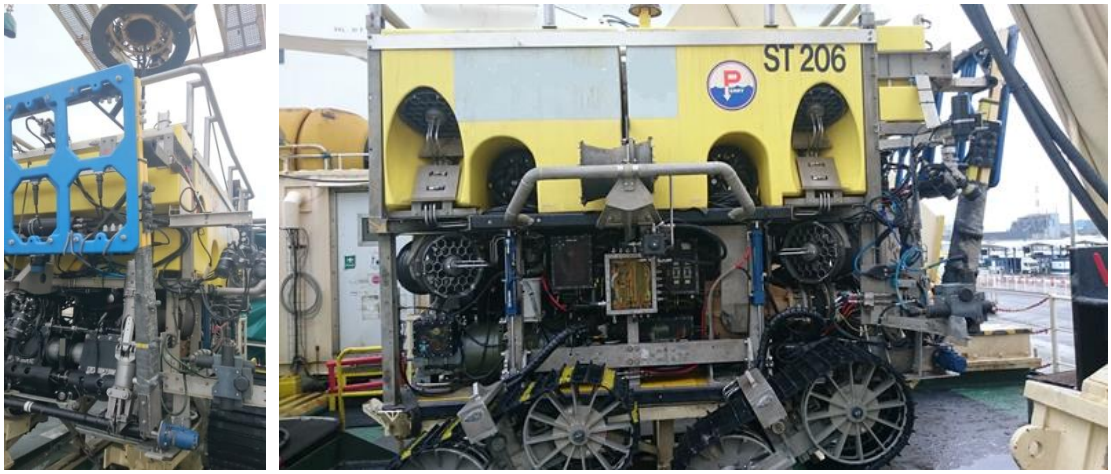

Figure 26 The TSS system mounted on the ROV used by one of the cable layer ship (courtesy Subsea Cable Tracking Ltd)

The cost of equipment, the ROV platform, the TSS sensors and its integration is beyond the scope of many companies offering shallow water surveys. The system requires on a highly skilled operator manoeuvring the vehicle above the seabed and specialised deployment and recovery arrangements. The vehicle can be used only if the weather conditions, sea state, current and other factors allow its safe usage.

Standby caused by the weather often occurs during marine operations. There are a big cost differences between the standby time of a cable ship and that of a shallow water survey crew. Figure 27 shows deployment of the vehicle equipped with a TSS sensor during a repair operation. The vehicle was mobilised and lowered into the water but the current was too strong and operation could not be conducted within the safety boundaries. After few minutes in the water, the ROV was raised on to the deck and the cable tracking operation was abandoned. The ship performed a grapnel pull to find the end of the sought after the cable.

Figure 27 Deployment of the ROV with TSS system during cable repair works near Cornish coast

Although practitioners comment on the limitations of TSS tracking, often this system is the only choice for tracking deep sea cables. It is well integrated with ROV platforms and vehicle operators are well trained and experienced in using the product.

Despite the above it would be difficult to use the system in a shallow water survey. The next section describes another tool designed to be used by a diver, hence in waters up to 30 metres depth.

4.4 Tinsley 5930

A simple method of cable localisation is adopted in the Submarine Cable Survey & Tracking System Model 5930 Mk II. The system uses the tone induction method and operates at extremely low frequencies from 10 to 110 Hz. It is designed to be used by a diver in areas where ROV operation may not be practical or even possible.

The system contains a probe connected to an amplifier and a computer's display (Tinsley Instrumentation Ltd., 2012). The Tinsley detection probe is a frame made of three separated searching coils. Two of the coils have the main axis in the horizontal direction, thus they sense the EMF perpendicular to the cable. The third coil has the main axis placed vertically and can help to pinpoint null spot measurement directly above the cable. Figure 28 shows a schematic diagram of underwater cable tracking performed by a diver.

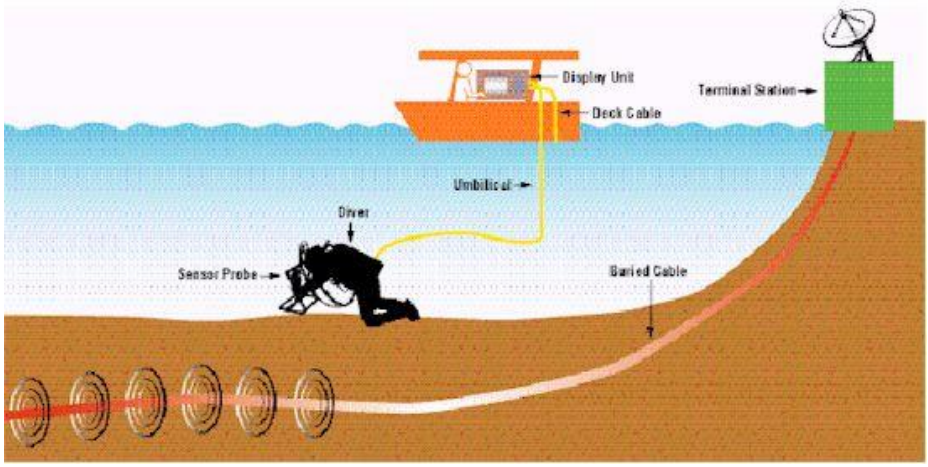

Figure 28 Diagram of underwater cable tracking by a diver (Tinsley.co.uk)

The horizontal coils are placed in the frame separated vertically by 0.5m. An induced voltage measured on the coils allows calculating the corresponding magnetic field from the AC current at the source. The measured voltages are sent to the amplifier and the software for signal processing. Fourier analysis extracts harmonic signal components related to the frequency of the induced current and allows extracting the amplitude of the induced signal. Two measurements sampled from separated coils, compared to tabulated values, allow the distance to the cable to be estimated.

The method of calculating the distance to the buried utility is very simple. According to magnetic field theory, the attenuation of the signal follows an exponential curve with decay inversely proportional to the cubed distance (Sun et al., 2002). In other words, the signal attenuates sharply in close proximity to the cable. Placing two coils at fixed distances gives two readings which can be related to the attenuation curve and the distance from the source.

The Tinsley manual advises performing a measurement calibration every time a new cable is going to be traced. The calibration process builds the tabulated values where the curves can be modelled based on appropriate readings. The procedure eliminates the need to incorporate current measurements or the response from the Earth's magnetic field at a particular location.

The Tinsley method has a very obvious drawback: it can operate only in close proximity to the source. The range of burial measurements is from 0.1m to 3m. In practice, this means engaging a diver who needs to place the frame on the seabed.

Precision and accuracy of the method may not be satisfactory. According to the manufacturer's website (Tinsley Instrumentation Ltd., 2012) burial depth accuracy is ±5%. For a maximum range of 3m, the position of the cable is estimated with an error of +/-15cm.

The measurement taken is based on the diver's subjective assessment. The diver needs to place the coil on the seabed and manoeuvre the frame to achieve the best possible strength of the signal. The position is monitored by the topside diver's supervisor who does not see the diver or the frame but only the readings on the computer. An experienced team can easy locate buried cables however, the overall error can be difficult to eliminate.

The Tinsley system is easy to use in shallow water surveys. Figure 29 shows the equipment during one of the cable works conducted in South America 2015 by the author of this thesis. The water visibility was less than 20 centimetres and the diver was fully relying on the supervisor's instruction. Even in low visibility and strong currents the diver was able to locate and confirm the burial depth at all measured locations.

(a) (b)

Figure 29 (a): equipment preparation for diver inspection during cable burial in South America 2015. (b): Burial depth confirmation by a diver

The Tinsley system is one of a few products available for shallow water surveys. Its compact design and ease of use allow it to be incorporated in many different survey configurations. It still has many limitations. The main constrain is the need for a diver. The burial depth check can be performed only in a limited number of locations. A commercial dive needs to be supported by a team of at least four people. Under UK law, most of commercial dives need to be carried with a breathing gas supplied from the surface which reduces the range of the survey. Although often it is the only alternative, cable localisation with Tinsley equipment is costly and time consuming.

4.5 Innovatum

An interesting approach is taken by engineers of magnetometer based tracking systems developed by Innovatum Ltd. The system was first presented in 1976 during the OCEANS ’76 conference (Cloutier et al., 1976). The company has many patents filed by Cloutier and is probably the only one which uses cable magnetisation to aid tracking ability. The company was bought in 2007 and moved to the UK where it continues marketing and support of their products in the marine industry.

The system is described in detail on the company’s website and manuals (Innovatum Ltd, 2016) but aside from the patents, there are not many scientific publications describing the approach.

The main difference between Innovatum and their competitors is their active approach to providing cables with a permanent magnetic signature. The cables are prepared before installation on the seabed. A patented magnetisation mechanism produces a set of magnetic properties in the cable, which are substantially greater than the natural magnetisation caused by the Earth’s magnetic field. The main claim of the patent is that the enhanced magnetic signature allows detecting cables and pipelines at much greater distances compared to traditional magnetometers (Cloutier et al., 2002).

The tracking system contains sensor arrays of fluxgate gradiometers with four axes of measurements and fluxgate triaxial sensors. The sensors are all placed in a precisely controlled plane and connected to an acquisition computer for data processing. The sensor array is depicted in Figure 30.

Figure 30 Innovatum sensor array mounted on small ROV and displayed during Marine Expo

The output from the gradiometers is calculated as a base signal in the centre line and its left and right offset. The cable's localisation is derived as a result of geometric relationships describing expected signals (Cloutier et al., 2008).

The main characteristic of fluxgate sensors used in the Innovatum system is their equal response to the magnetic field emitted by DC power cables, Low Frequency (up to 100 Hz) AC currents, the Earth's magnetic field and the magnetic field originated from magnetised components. Based on these properties Innovatum claims that their systems are able to sense any configuration of cables or pipelines.

The magnetisation of the cable done in the fabrication process is a specific feature of the Innovatum system but also their main marketing advantage. The company builds their market providing the ability to selectively track cables with unique magnetic signatures. The magnetisation process needs to be performed by the company's manufacture and is patented under USA law (Cloutier et al., 2002).

The inventors of the process claim that the magnetisation gives a greatly increased magnetic signature much larger than the ambient Earth's MF. They use a different wavelength which results in changing magnetic properties along the utility through multiple cycles of radial external MFs.

According to the claims of the patent, the properties of the magnetised cables allow to successfully track the utility. If there is a doubt or the cable was not magnetised prior to its installation the same equipment can track the cable using an induced AC current, or if there is no such possibility the same system can track ferromagnetic components of the cable's armour in the same manner as described before geomagnetic sensing.

4.6 Other sensing equipment

The main objective of the practical operation is to successfully localise subsea cables. Companies take all measures to prepare for the job and often deploy a whole range of equipment to cover every situation.

The subsea detection market offers a range of products that rely on basic detection principles. The company J.W Fisher is an example of a manufacturer of underwater metal detectors, pipes and cable trackers (Fisher, 2016).

The principles of operation are simple. The detector system is constituted from a diver's probe used by an operator performing the survey and a tone injector optionally connected to the utility on the shore. The diver probe shown in Figure 31 (a) is a compact, self-contained device designed to be easy operated by a diver. The display and control panel shown in Figure 31 (d) contains ten lighting diodes indicating signal strength, an ear plug connector allowing the output of an audio signal indicator, a five position frequency switch for changing the mode of operation, and a charger connector.

During cable tracking, the operator points the probe into the utility looking for the signal. The light and acoustic output indicate the strength of the emitted MF, and hence the direction and distance from the cable. The output originates from a vertically placed coil and becomes larger when the probe moves towards the utility, to disappear directly above, and then sharply rise and decrease when the probe moves away from the source. The divers can precisely pin-point the cable by looking for a null spot in the signal's output.

The company takes an interesting approach to burial depth estimation. At short distances the vertical coil's null spot is very sensitive to changes in position and coil alignment. It is used to indicate the distance to the utility. The null response of the coil, directly above the cable occurs only if the probe is verticaly aligned. Tilting the probe results in an increase of the signal measured. If the coil is aligned at 45 degrees to the floor, before it will show the null response, it needs to be moved sideways to pinpoint the utility again. Based on the properties of an isosceles Pythagorean triangle, the distance travelled to the side before the null response is reached is the same as the vertical distance directly above the cable. It is depicted in Figure 31 (c).

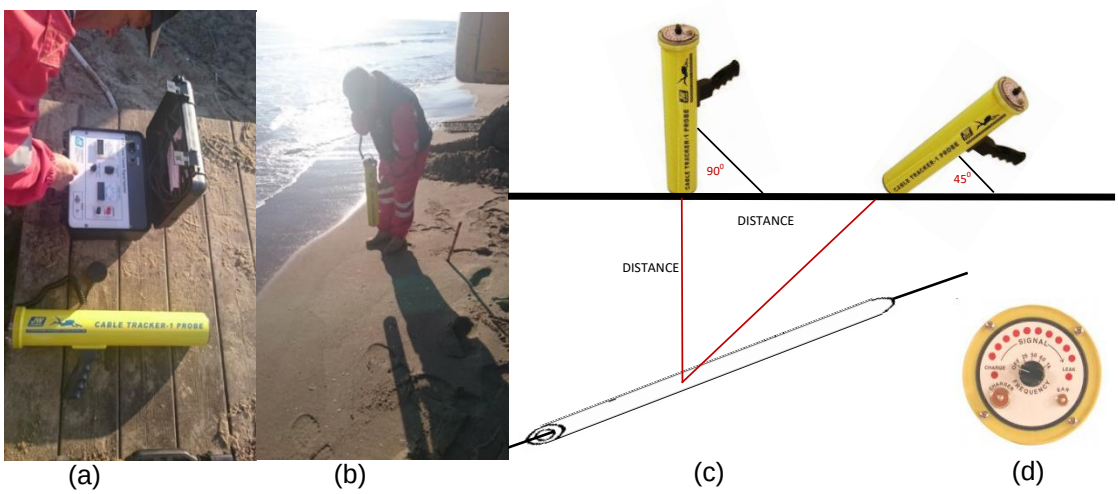

Figure 31 J.W. Fisher CT-1 Cable Tracker probe. (a): equipment setup during the cable work, (b): locating the cable in low water. (c): burial depth estimation principle, (d) CT-1 display (J.W. Fisher, 2016)

The probe was used during one of the cable landing operation in Italy. The cable was connected to the BMH on top of five already existing live cables. Before the new installation begun the route of the cable was planned and excavation works were conducted to prepare a trench for the new utility.

The operation was especially risky as the trench was excavated as close as two metres from live cables. Hitting the cable with an excavator's bucket would likely result in complications and possibly high costs. To avoid the problems the existing cables were monitored with the cable tracking probe.

The simplicity of the CT-1 system appeals to practitioners and performs well in the difficult conditions and requirements of shallow water surveys. Its design can serve as a good example for building a robust detector for underwater use.

4.7 Conclusion

The overview of the market and available equipment needs to be completed with an analysis of commercial aspects of the operations. It was already mentioned that cable installations, maintenance and repairs involve large costs. The same can be said about the equipment. The principles of localisation on land and at the sea do not differ to large extends. The same cannot be said about the costs of the equipment. Marking the product as designed for the subsea market increases the price tenfold. The sophisticated cable detector RD-8000 manufactured by SPX from Bristol and designed for land survey costs around £2000 (price accurate as of 2016). Its submarine counterpart CT-1 designed for the subsea market is advertised around the price of $15000.

This analogy is similar in all ranges of products from simple metal detectors to sophisticated sensing equipment. The price tag for a higher range of underwater localisation equipment is reaching hundreds of thousands of pounds and is available only on individual request.

Although the commercial prospects for manufacturers seem to be very promising it is not always the case. Most of the cable repairs are conducted by specialised cable layer ships. There are only a few vessels covering the whole world. The same applies for shallow water connections and repairs. There are only a handful of companies specialising in offering the service. These companies often can mobilise their crew and equipment in a few days flying sensors into the part of the world where it is needed the most.

From this point of view, there is no large demand for new equipment. The companies try to specialise in the service they offer, better understand cable operations, the risk involved, and to apply better procedures to guarantee a successful outcome. From this perspective, an experienced operator is more valued than complicated hardware without the insight and understanding of said operator.

All of this information and experience were taken into consideration during the planning and design of a new surveying method. The next chapter describes a prototype of the system. The objective of the proposed method was to aid a cable survey, work alongside other surveying tools and connect to the hydrographic system used by the surveyors.

Chapter 5. Overall system Design and Operating Environment

Most of the available methods for tracking and localisation of buried subsea cables either rely on analogue technology without the possibility of recording data samples or are equipped with a proprietary interface which does not allow custom algorithms to be applied.

The novel algorithm for localisation, the Batch Particle Filter (BPF) proposed in this work, requires the collection of multiple data points and sampling of the EMF on the surface of the sea. The BPF algorithm was developed mainly with data collected by the Tinsley 5930, but the Tinsley system is not suitable for further development and recording of all necessary information whilst maintaining the desired precision. For this reason, a new modular, digital concept of the acquisition unit was designed. The hardware prototype was tested on experimental trials and real cable tracking work. The concept proved to be adequate for the BPF requirements and it is planned to commercialise the unit into a standalone new subsea cable positioning system. In this chapter the main design ideas will be presented.

The hardware unit has a modular design with three major parts depicted in Figure 32 consisting of a sensor module, an acquisition box and a user interface unit (UI). The sensor module responds to an induced alternating EMF of known frequency with an analogue voltage output. The voltage fed into the acquisition box is amplified, converted from analogue to a digital signal (ADC) and filtered. The signal is translated into a sentence, in the form of NMEA 0183, describing the response of the sensor to the EMF's parameters along three physical axes. The sentence is forwarded to the UI module. The UI is configurable, and it can provide basic information about the EMF in the form of its values to being able to apply a searching algorithm to localise the submarine cable, or even connect to a navigation software suite for further processing.

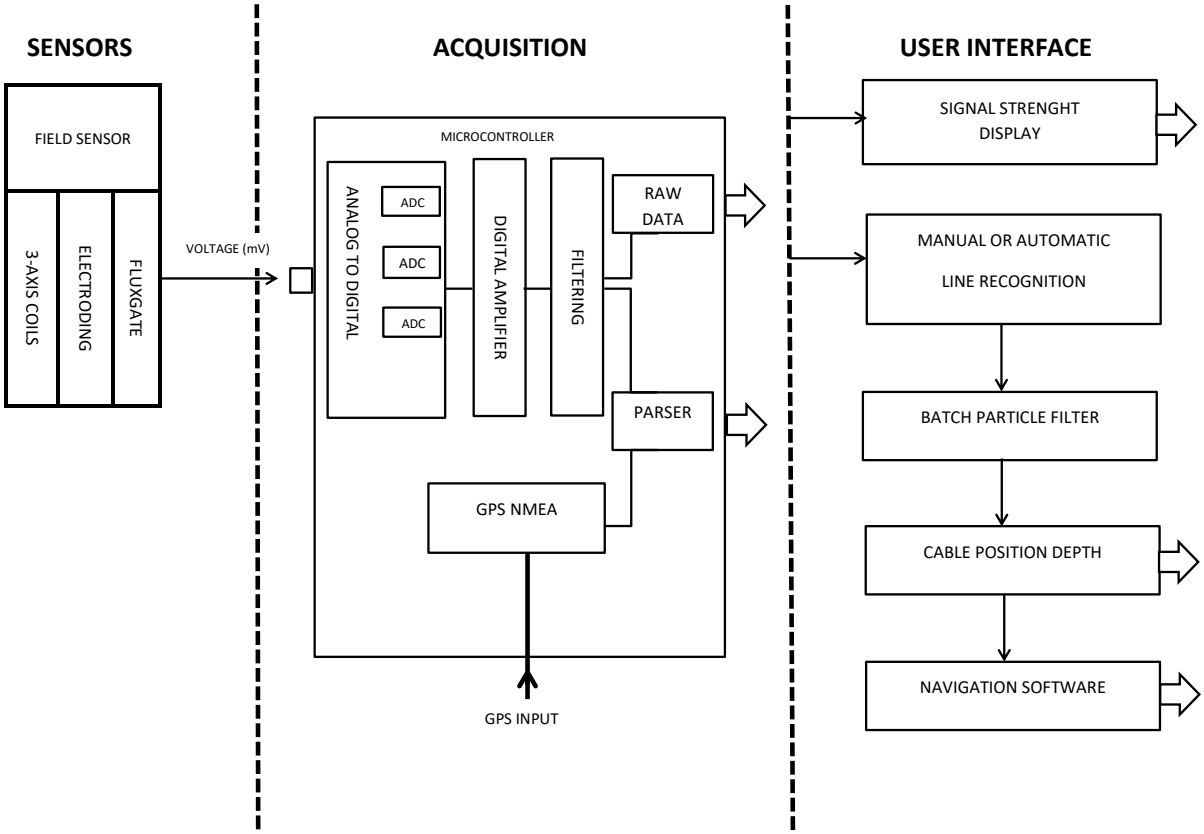

Figure 32 Prototype components diagram

All three major components will be described in the following sections.

5.1 Sensors

The primary function of the sensor module is to measure the EMF field induced by an alternating current flowing in the submarine cable. Traditionally the sensor is made up of searching coils with optimised parameters to give the best response to the EMF. For the purpose of developing the prototype different searching coils and fluxgate magnetometers were examined.

Many criteria need to be considered in good sensor design. The sensor should be sensitive enough to respond to the given signal strength but also adjusted for a specific frequency range. The coils should be robust and predictable, hence show a linear characteristic in their response to the EMF. Physical parameters of the sensor such as its weight and diameter need to be appropriate to its use. Although it is not the primary objective, the cheap build and possibility to replicate the sensors at low costs gives an advantage for their use in large arrays or in multiple locations simultaneously.

Equipment available on the market consists of proprietary sensor designs especially for subsea cable tracking surveys. The proprietary searching coils are manufactured as ferromagnetic core antennas. An example can be the coil used in the Tinsley 5930 which has a nickel-iron Mu-metal core. The sensors are difficult to purchase on their own. Manufacturing a Mu-metal coil requires specialised equipment for handling and requires special heat treatment – annealing in a magnetic field. Figure 33 shows the proprietary coils used with the prototype.

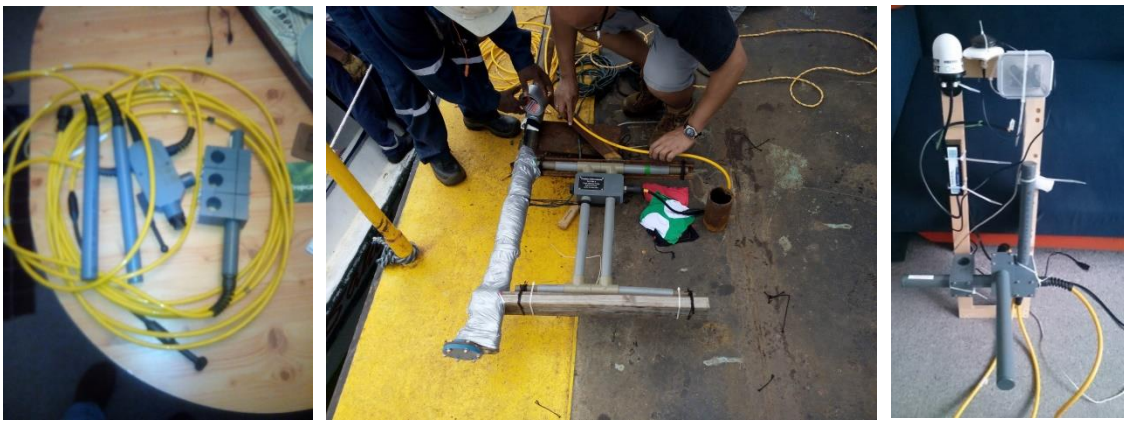

(a) (b) (c)

Figure 33 Proprietary searching coils. (a): Coils with an amplifier for three axis use. (b): Two horizontal and one vertical configuration for mounting on the side of the boat. (c): Three axis frame with GPS, Compass and fluxgate used during testing

To investigate the prototype, the proprietary coils were tested against air coils manufactured at the university's facility. Figure 34 shows the manufacturing process and the final three-axis sensor. The antennas are coiled on a non-ferromagnetic frame with 500 turns in each axis.

(a) (b)

Figure 34 Air coil with a diameter of 200 mm; (a): coils during production; (b): final sensor

The proprietary and the air coils were compared with a fluxgate magnetometer "Mag 690 MX -100" manufactured by Bartington Instruments Limited (Mag690). The sensor provides three-axis readings with a

resolution of 1nT, the flat frequency response between DC to 100Hz and the noise at the level of 20 pT (Bartington Instruments, 2014). The sensor was equipped with the same "Bulgin" connection as the proprietary coils. Figure 35 shows the instrument with the cable and connection prepared to work with the prototype acquisition box.

Figure 35 Fluxgate magnetometer Mag 690

The analogue output of the sensor is comprised of the induced current as the resulting signal. From a signal processing point of view, there is no fundamental difference between the output from the air searching coil, the ferromagnetic core antenna or the fluxgate magnetometer. All sensors provide two-point terminals with a voltage difference proportional to the strength of sensed EMF. The induced voltage creates a current that is proportional to the rate of change of the field. The sensitivity of the search-coil is dependent on the permeability of the core, and the area and a number of turns of the coil (Caruso et al., 1998).

The difference between sensors and their response to the EMF can be described by their transfer function. For the induction coil any change in the magnetic flux will cause an induced voltage (electromotive force) in the coil (Tumanski, 2007). The transfer function $V = f(\boldsymbol{B})$ resulting from the Faraday's law of induction:

$$V = -n\frac{d\boldsymbol{\phi}}{dt} \qquad (20)$$

In equation (20) $\boldsymbol{\phi}$ is the magnetic flux through a coil with n turns and area A. The signal from the coil V is proportional to the rate of change of flux density $\frac{d\boldsymbol{\phi}}{dt}$ which requires integration of the output signal.

The magnetic flux density depends on magnetic field strength H and vacuum permeability μ_0 but mainly on the distance r and current I induced in the cable. For the long straight wire the relation becomes:

$$\boldsymbol{\phi} = \mu_0 H = \mu_0 \frac{I}{2\pi r} \quad (21)$$

Equations (20) and (21) lead to

$$V = \mu_0 \pi f a^2 n \frac{I}{r} \quad (22)$$

Although fluxgate magnetometers can measure the MF produced from DC currents, its construction also depends on the searching coils. In this case there are two coils and a ferromagnetic core. One of the coils provides a varying field and saturates the ferromagnetic core. The pick-up coil senses the reluctance of the core to the external MF (Lenz & Edelstein, 2006). Similar to above, the transfer function depends on the strength of the MF and parameters of the sensor (Janosek , 2017):

$$V = -NS\,\mu_0 H \frac{d\mu_r}{dt} \frac{1-D}{[1+D(\mu_r-1)]^2} \quad (23)$$

where N is a number of turns of the pick-up coil and S is the area of the core cross-section, μ_r is the permeability of the core material and D is the dimension-less demagnetisation factor of the ferromagnetic body.

Wang et al. (2010) draw attention to the coil design. As Wang et al. (2010) suggest, it requires resolving conflicting interests. Small coils can be precisely located but they are less sensitive. An increase in the number of turns improves sensitivity, but it makes the position of the turns less precise. It is important to make a decision about coil's diameter in connection with desired spatial resolution. Wang et al. (2010) draw simple conclusions: in order to have a spatial precision of 100 mm they chose a coil with 100 mm diameter.

The cross-section of the coil plays a key role in the coil's sensitivity. For this reason the air searching coils become very large and difficult to use. The miniaturisation problem can be overcome by incorporating a ferromagnetic material as a coils core (Tumanski, 2007). The core concentrates the magnetic flux inside the coil. The relative permeability μ_r/μ_0 of modern ferromagnetic materials often exceeds the ratio of 10^5 and largely increases the coil's sensitivity. Adding a ferromagnetic core to the transfer function leads to:

$$V = -\mu_0 \mu_r n A \frac{dH}{dt} \quad (24)$$

Although the sensitivity of the coil can be increased, a ferromagnetic core does not always provide the best characteristics. Tumanski (2007) lists many disadvantages of this solution. He points out that the sensor loses linearity. Even the best materials introduce nonlinear factors to transfer function which depend on temperature, frequency, flux density, etc. Ferromagnets increase the magnetic noise known as the Barkhausen noise, hence decrease the resolution of the sensor. Altering the distribution of investigated MF results in difficulties of describing underlying phenomena.

The sensors were tested in the laboratory. The experimental setup included a drive coil. It was a large 1-metre radius coil with 100 turns coiled on a circular, half centimetre high wooden frame. The function generator induced a sinusoidal AC current with a given frequency. The current was measured with a multimeter. The magnetic flux $\boldsymbol{\phi}$ in the middle of the drive coil was calculated as $\boldsymbol{\phi} = \mu_0 I * n/l$ where $\mu_0 = 0.00000125663706\ [H/m]$, I stands for measured current, $n = 100$ is the number of turns and $l = 0.005\ [m]$ is the length of the coil.

The sensors were placed in the middle of the drive coil and the peak-to-peak voltage output of the sensor was recorded on the prototype acquisition box.

Figure 36 shows the sensors response for two frequencies, 20 Hz and 100 Hz.

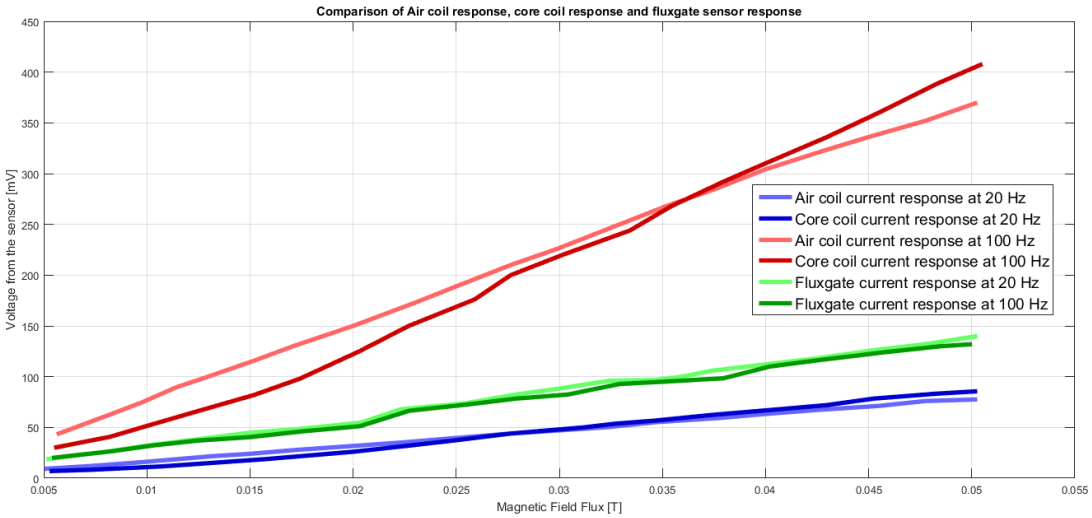

Figure 36 Comparison of sensor response for different signal strength at frequencies 20 Hz and 80 Hz

The outcome of the experiment shows important characteristics of the sensors.

As expected the fluxgate magnetometer has a similar response to different frequencies. Its output is comparable to the coil's response to a 20 Hz field. Analysis of results shows that the Fluxgate's readings are more noisy and unstable than the coil's response.

The proprietary, ferromagnetic core coil shows nonlinearities in response to a weak MF. The output of the coil is similar to that of the air coil. Nonlinearities in the response can result in unpredictable consequences. The depth measurement algorithm used by this tool relies on extrapolation of the response-distance function. The profile is produced during the on-land calibration process and is built only upon a small range of MF differences. Changing the MF characteristics, applying calibration data to a diver's search, weaker MF or different temperature can result in increased error. To fully justify the proprietary coil measurement more knowledge of the coil manufacturing would be required.

From the tested sensors, the air coil shows the most linear response with the output, at least as good as the expensive proprietary sensors. The linear characteristic is very important for application of the algorithms described in later chapters. The air coil sensor will constitute the final prototype.

In addition to laboratory experiments, the coils were tested in the field. Figure 37 shows the sensors at some distance from the test cable setup on Dartmoor in Devon, UK.

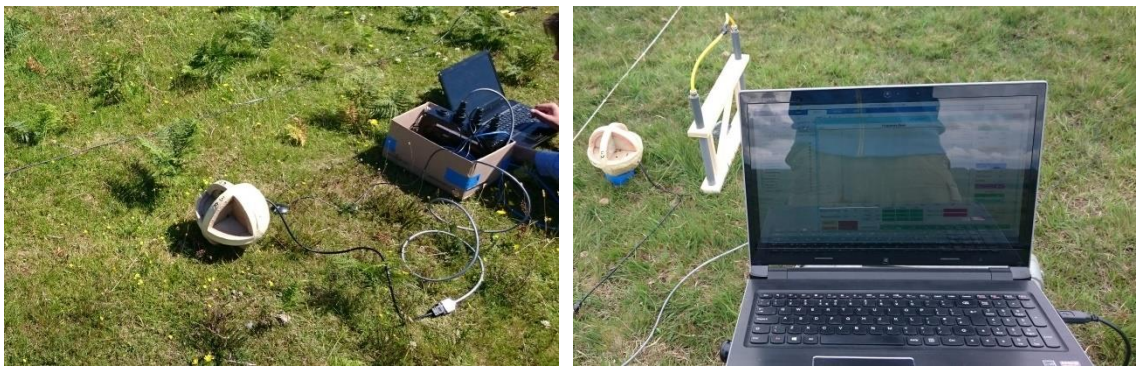

(a) (b)

Figure 37 Searching coils tested in the field; (a): Air coils and the acquisition box during field testing; (b): Frequency readings taken during field testing

The localisation was chosen to minimise the interference from the power grid. The 200 metres test cable was laid and connected to a portable tone generator. The readings were taken with the developed

acquisition box and user interface. Figure 38 and Figure 39 show the spectrum analyser from the sensors as the response to the ambient MF.

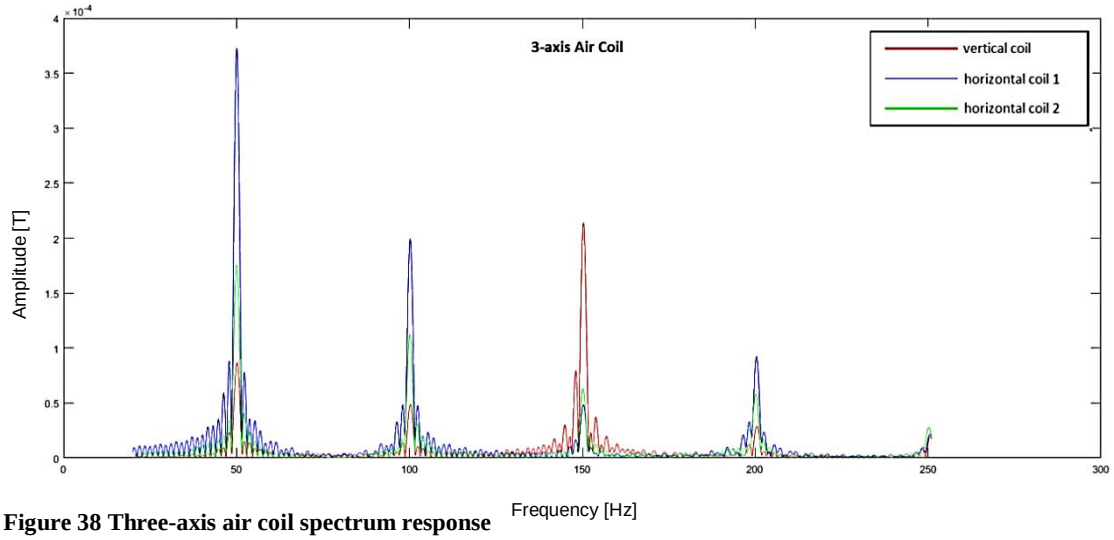

Figure 38 Three-axis air coil spectrum response

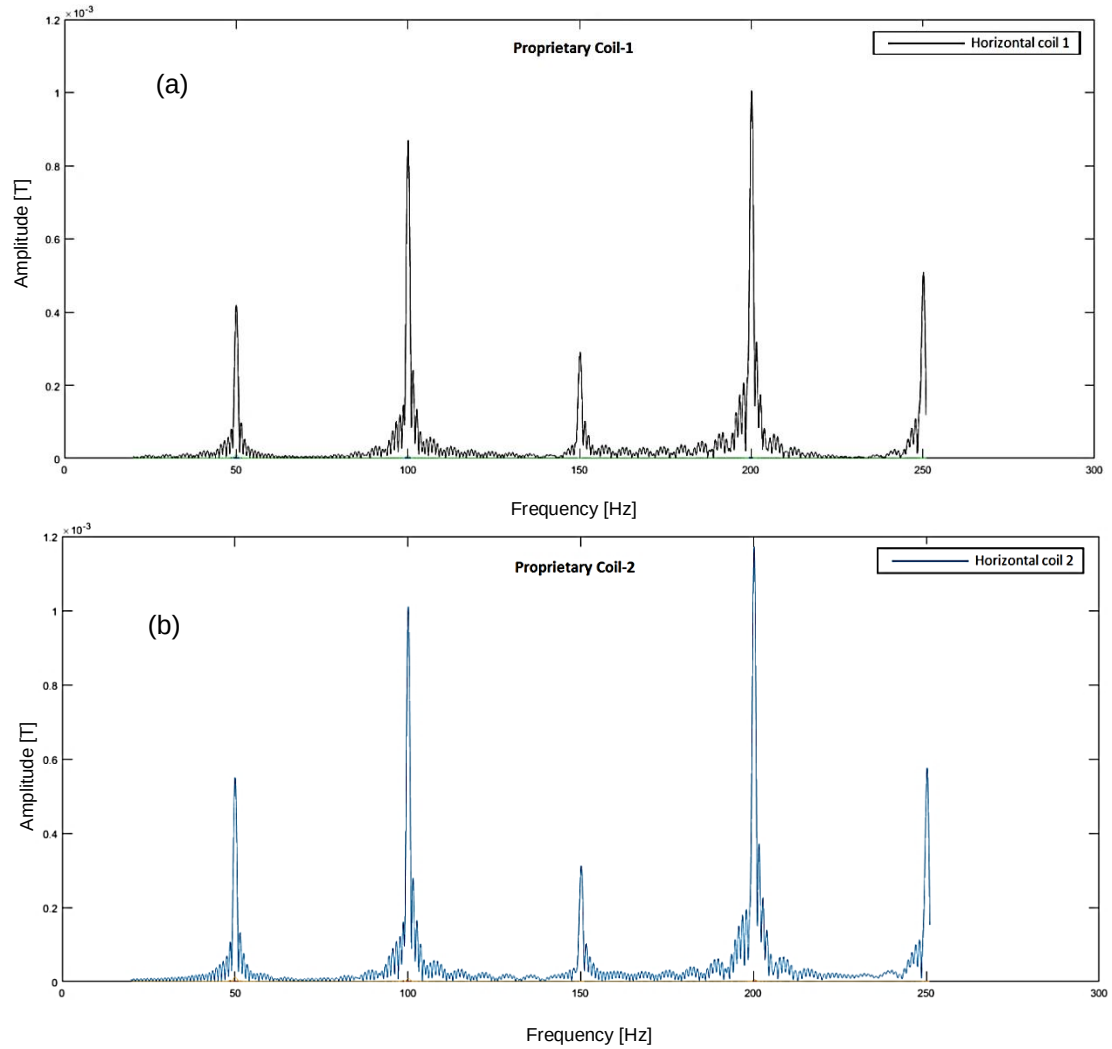

Figure 39 Proprietary coils spectrum response; (a): Propritary Coil-1; (b): Proprietary Coil-2

Conducted analysis and experiments show that the air magnetic coils have the best characteristics and least nonlinearity. They can be manufactured without specialised equipment with the material cost being less than £50. They are a good alternative to the proprietary sensors, which are more compact but have unwanted properties. The next section will focus on the conversion of the coil output into meaningful readings. It will describe the hardware acquisition box.

5.2 Prototype Description

The sensor output needs to be processed through an acquisition unit. The developed localisation algorithm requires EMF data collected on the field with a precise position of each sample. The available equipment does not provide easy mechanisms to acquire the necessary information. To overcome this limitation, a new, fully digitised design with recording and storage capabilities was proposed.

The main advantage of the new acquisition unit is its modular design with adjustable digital processing algorithms. The unit contains three input slots with the possibility to connect three-axis sensor such as a three-axis air coil, a fluxgate magnetometer or up to three individual channels in general representing different configurations of sensors.

The analogue voltage representing the information about the EMF provided from the sensors is converted into digital form. The oscillating EMF can be described by its frequency, amplitude and phase. All of these characteristics are encoded into numbers and passed to a processing unit for further calculation. The output is recorded as standard ASCII, comma separated sentences. The EMF data are integrated with a positioning system. Individual data points are processed into tracking algorithms for estimating the position and the burial depth of the submarine cable. Information is displayed as an aid to the survey and recorded on the memory card for later post-processing and mapping.

In many situations, AC currents induced in subsea cables need to travel hundreds of kilometres from one cable station to another or travel to the breaking point and come back on a return path through the sea or the beach. The supplied voltage might be very high but the resulting currents are low hence they often generate only a weak EMF around the utility. In addition, the low-frequency EMF used for subsea tracking attenuates with fast a rate resulting in the challenging task of sensing very weak signals.

Historically signal conditioning was done by analogue devices. The analogue technology required a high volume of amplifiers, filters and other electronic elements to support small frequency and amplitude ranges. (Mitola, 1995) Recent progress in ADCs allowed miniaturisation of receivers by applying ADC transformation in the first step and all subsequent processing is implemented digitally. ADCs can quantise wideband, different power signals with large SNR. They are essential components in modern receiver architectures (Araujo & Rui, 2007)

The current method is based on a proprietary system the Tinsley 5930. The acquisition hardware – display unit of the Tinsley system contains a series of analogue amplifiers and filters, 16-bits USB ADC module and a panel PC running a Windows XP operating system. The Tinsley instrument uses an ADC "NI USB-6221" (National Instruments, 2013). The module has 16 bits resolution with 250 kS/s sampling rate. The DAQ operates at a minimum of +-0.2V (National Instruments, 2014). The system is enclosed in a large 560 x 460 x 240 mm, 15kg waterproof pelicase.

The design of the prototype was focused on miniaturisation, high resolution and precision of the reading and robustness by elimination of a number of components. The prototype of the new sensing method relies on an acquisition system with digital signal processing. The central part is an ADC ADS1282 (Texas Instruments, 2007) described in detail further in this chapter. After the signal is converted from analogue to digital form, it is fed into and STM F4 ARM microcontroller for digital filtering. The digital signal is further sent to the computer and used in the cable tracking algorithm.

The basis of the prototype architecture is the ADC conversion. The performance of the ADC module can be summarised by a small number of parameters. The most important are stated resolution (number of bits per sample), sampling rate and SNR. The ADCs can be further characterised by spurious-free dynamic range and power dissipation (Walden, 1999). The ADC module chosen in the prototype's construction is an extremely high-performance instrument intended for applications requiring high precision and extremely low noise (Texas Instruments, 2007).

The ADS1282 is designed for demanding applications. Its 32-bit resolution is the highest publicly available on the market in the year 2014 with low cost. The resolution of the ADC determines the minimum strength of the signal compared to the reference voltage. The ADS1282 relies on the +5V reference voltage. In practice, the instrument measures the difference between the input voltage and provided base signal.

The 32-bit resolution allows for numerical precission of $5/2^{32}$ where 5 is a reference voltage of 5 volts and 2^{32} is a number of "zero-one" possibilities at this resolution. It means that the ADC can differentiate with a step of $1.2\ nV$. For comparison the 16-bit resolution of NI USB-6221 gives precision of $76.3\ \mu V$

The sampling rate (f_{samp}) is important in analysing different frequencies. Increase in sampling speed may give better processing capacity associated with the large number of elements. However, the high sampling rate carries also unwanted effects. Walden (1999) concludes that approximately one bit of resolution is lost for every doubling in rate. Sampling speed is limited by the ability of the comparator to make an unambiguous decision regarding the relative amplitude of the input voltage. Walden (1999) further suggested that the increase in sampling rate results in aperture jitter which is an error or deviation from true periodicity.

Walden (1999) conducted a comparison of available ADCs and reported that the SNR is a function of signal frequency. At low values of the frequency the SNR is constant. The value in which the SNR decrease to 3 dB is called the Effective Resolution Bandwidth (ERBW) and indicates the spectrum range over which the converter may be used. The aim of most manufacturers is to make Nyquist converters where ERBW $\geq$ $f_{samp}/2$. It means that the ADC can effectively measure all frequencies up to half of its sampling rate f_{samp}. Walden (1999) points out that the Nyquist frequencies are the edge of the instrument operation. He suggested that the best performance can be achieved by further reducing the frequencies by applying the criterion ERBW $\geq$ $f_{samp}/4$.

The ADS1282 sampling rate can be selected from a range of 250 samples per second (SPS) to 4000 SPS. Following safety rules and applying the ERBW suggested by Walden (1999), the instrument can efficiently sample signals up to 1 kHz. The ADS1282 has series of built-in filters for the incoming signal. With the fifth-order sinc filter, FIR low-pass filter and adjustable high-pass filter for DC removal, the ADC provides the signal of interest without additional interference.

The third most important characteristic of ADC is its SNR. The noise produced by the ADC includes the error coming from the quantisation process. It comes from the ADC resolution and it is the difference between the measured digital quantities and analogue values determined by the quantisation step. Other noise sources include circuit noise, aperture uncertainty and comparator ambiguity. The noise level

featuring in ADS1282 is of the order of $5nV/\ Hz^{1/2}$ where as the noise of the NI USB-6221 is stated by the manufacturer as an absolute accuracy of $3{,}100\ \mu V$.

The ADS1282 is equipped with a Programmable Gain Amplifier for dynamic gain control. It allows magnifying the signal with gains of 1 to 64. The gain of the amplifier is adjustable from the UI level and adequately compensates the absence of analogue amplifiers. The gain's level value is encoded in the final sentence output.

After the voltage from the sensor is digitised, its samples are processed with digital filtering for detailed frequency analysis. The frequencies of interest are separated from the signal. Traditionally analogue filters often gradually attenuate the signal from the passband to a stop band. The prototype design excludes the use of analogue filters. All frequency separation is conducted with digital methods. Digital processing also allows isolating very narrow passbands to read a specific phase and amplitude of the signal. The main algorithm used for signal analysis is based on the Fourier transform and Lock-in amplifier.

The Fourier analysis utilized in the prototype serves as a display of the sought after EMF. Its implementation is a simple Matlab function computing the discrete Fourier transform using the Fast Fourier (FFT) algorithm (Mathworks, 2014). The function takes a vector of samples and returns the Fourier coefficients of frequencies of the signal. The FFT is well understood and widely used in signal processing and many sources explaining the methods can be found in the literature.

The plot resulting from the FFT showing signal frequencies serves as an aid during the hydrographic survey. A Graphical User Interface (GUI) developed in Matlab provides a screen displaying the sensed frequencies. The surveyor can monitor the signal strength of the frequency induced in the cable in real time. When the boat approaches the utility the signal increases, to have its peak above the cable, and decrease when the boat departs from the utility.

In a traditional system, the signal is displayed as a single frequency indicator, often as a moving analogue needle. This solution does not provide full insight into the distribution of the EMF. Showing all frequencies allows ensuring there are no unwanted errors in the signal and allows to search for multiple cables with different frequencies.

The FFT serves only as a graphical representation of the EMF. For the localisation algorithm, a higher precision filter is used. For this purpose, a Lock-in amplifier filter was implemented.

A Lock-in amplifier is a technique to measure low-level periodic signals in the presence of noise. The device "locks-in" on a signal of a particular frequency and amplifies it, rejecting all other frequencies. It has a narrow bandpass, separating one Fourier component at a time. The underlying idea is to measure the amplitude and phase of the input signal in relation to the reference signal. Modern processing hardware such as microcontrollers and microcomputers allow high-performance implementation of the filter with minimal cost. In practice, the lock-in can measure voltage amplitude as small as a few nV while ignoring signals even thousands of times larger. The lock-in is capable of measuring multiple frequency sweeps simultaneously (Sonnaillon & Bonetto, 2005)

Although Lock-in is a popular and powerful digital processing technique, it originates from the analogue counterpart. The simplest device takes two inputs. One of the inputs is a reference signal coming from a voltage controlled oscillator able to synchronise with an external voltage trigger. The second signal is an amplified measured voltage. Both inputs are passed to a multiplier, called phase sensitive detector (PSD). The multiplication product is filtered by a low pass filter and finally, the DC is amplified and displayed on the instrument's meter (Scofield, 1994).

The same principles apply to digital lock-in implementation. The signal and reference are represented by a sequence of numbers. Multiplication and filtering are performed mathematically. Because digital reference signals can be computed as a pure sine wave over the same sampling range as the measured signal, the lock-in is insensitive to any other frequencies and harmonics.

The input signal for a given frequency $\omega_r = 2\pi f$ is represented by the voltage V_{sig} and can be described by a sine function $V_{sig}\sin(\omega_r t + \Theta_{sig})$ where Θ_{sig} is the phase of the signal. Similarly the reference signal V_L provided by lock-in is modelled by $V_L\sin(\omega_L t + \Theta_{ref})$. The output of the PSD multiplier becomes:

$$V_{PSD} = V_{sig}V_L\sin(\omega_r t + \Theta_{sig})\sin(\omega_L t + \Theta_{ref}). \quad (25)$$

Using the trigonometric identities $\cos(a)\cos(b) = 1/2[\cos(a+b) - \cos(a-b)]$ and $\cos(2a) = (\cos(a) + \sin(a))(\cos(a) - \sin(A))$ it can be proven that equation (25) becomes a DC signal if $\omega_r = \omega_L$

$$V_{PSD} = \frac{1}{2} V_{sig} V_L \cos(\Theta_{sig} - \Theta_{ref}). \quad (26)$$

To avoid problems with phase synchronisation, modern lock-ins reference two signals where the second has a phase shift of 90^o. The double-phase lock-in compares the input signal with the cosine and sine functions. It results in two values $X = V_{sig} \cos\Theta$ and $Y = V_{sig} \sin\Theta$. The magnitude A and phase Θ can be calculated as

$$R = \sqrt{X^2 + Y^2} = V_{sig} \quad (27)$$

$$\Theta = tan^{-1}(\frac{Y}{X})$$

The lock-in amplifier is easy to implement. The filter can be run on a simple microcontroller (Dorrington & Kunnemeyer, 2002) and can be used to sweep through all frequencies simultaneously (Sonnaillon & Bonetto, 2005).

In the prototype tool the signal from the ADC goes to microcontroller for parsing all information into values from three channels. The data are also filtered for a frequency of interest. The implementation of the lock-in amplifier written in the Python programming language can be found in Appendix F

The amplitude and phase of the signal are parsed into the sentence with GPS data. Figure 40 shows the acquisition box and sensors prepared for trials.

The filtered information is processed to the BPF algorithm described in later chapters. The algorithm is programmed on a Raspberry Pi microcomputer. The BPF requires the positions of sample points where the EMF was measured and the amplitude of the field. Based on this information it is able to estimate the position of the source, which is recorded on a flash memory stick and displayed on the screen of the GUI.

In parallel the real-time spectrum analysis can be displayed on the computer screen. The external computer can connect to the Raspberry Pi via an Ethernet TCP/IP connection or Serial Port COM.

The acquisition box can work independently of an external computer. In this case it records all the data. The information about the EMF at the sample points and estimated cable's position can be later copied from the memory stick and used in post-processing.

(a) (b)

(c) (d)

Figure 40 (a): Three ADC converted mounted on a board ready for connection. (b): ARM microcontroller connected to ADC ready for testing. (c): acquisition box with three ADC connections, STM microcontroller and Raspbery Pi for BPF algroithm and data recording. (d): Prototype box with coils sensor, GPS, compass, Fluxgate magnetometer, prepared for trials

For the purpose of the prototype the GUI software was proposed. The UI and graphical display GUI is described in next section.

5.3 Computer interface

Filtered information from the sensors is passed to the UI for processing data with positioning algorithms. The final output is a formalised sentence parsed into the tracking algorithm or navigation software. The system records raw data from each sensor channel, data about a single frequency of interest and GPS positioning. The data are passed to the localisation algorithm which gives the final cable location in terms of longitude, latitude and distance from the water surface.

The connection between the acquisition box and the UI module is optically isolated based on COM and USB technology. The system can be controlled through the Ethernet connection. For the survey it is advised to use the COM port as it is more robust.

The user interface allows seeing a tracked cable in real time during the survey. The user can view the past survey path and prediction of the cable route for navigational adjustments by feeding data from the csv record into a navigation software or Geographic Information System (GIS).

Information about the observed cable can be fed directly into third party software through a standard USB data connection. The normalised data is parsed into a sentence with the cable geographical position points and its burial depth.

If the computer utilising information is a navigation PC it needs to have designated connections for a positioning system, normally: GPS, Compass and water depth measurement – transducer. In this case a custom parser needs to be written for the particular application.

The main screen of the GUI for the prototype is shown in Figure 41. It aids the survey and displays basic information about the EMF signal.

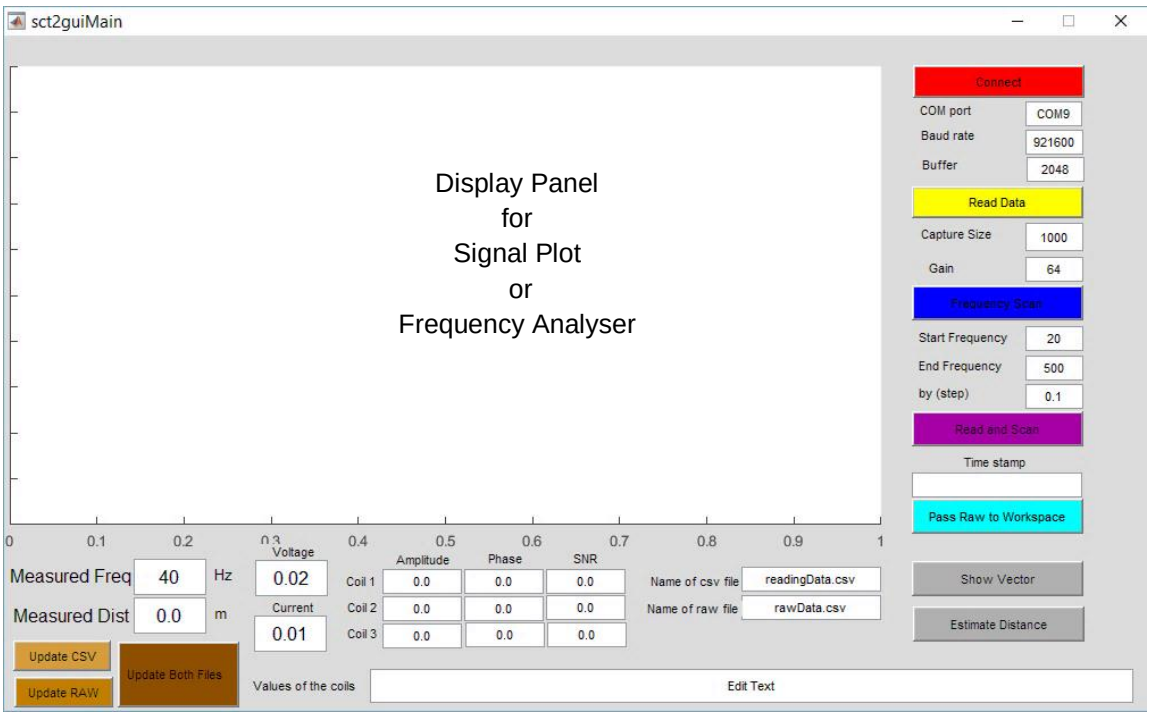

Figure 41 Graphical User Interface GUI

After the computer running the GUI is connected to the USB port of the acquisition box, it can establish a TCP/IP connection with the microcomputer and read EMF information from the sensors. Most operating systems automatically discover connected USB devices. Some of the connection parameters such as serial port number need to be manually adjusted based on the local computer information. The right hand top panel gives the possibility to set the serial port number, speed of transfer – Baud rate and Buffer size responsible for allocating internal memory for data communication. After pressing the "Connect" push button (BTN) the computer starts to listen on the serial port.

The data coming to the interface are primarily filtered and amplified. The "Capture Size" editable Text Box (TXT) allows to specify the size of the data processed in cycle. The sampling rate of the system is 4000 SPS thus the value of 1000 gives a filtered reading with a rate of 4 hertc. The following "Gain" TXT allows changing the ADC gain and input signal amplification. "Read Data" BTN sends information to the microcontroller to indirectly change ADC parameters.

The next BTN "Frequency Scan" triggers the spectrum analyser. The spectrum analyser is produced by Lock-In amplifier sweep with given step, between two frequencies. The parameters can be adjusted by three TXT positions. The frequency can also be displayed in real time with Fourier analysis. The "Read and Scan" BTN conducts a FFT and real time display.

The Time stamp section carries out two tasks. Every time when a new data point is fed into the system, it receives a unique time stamp. The time stamp display flashes green with the new data point. It indicates the system is working and data are fed into the parsing algorithm. Without such indicators, the operator or surveyor tends to periodically check if the system is in good working order.

The next "Pass Raw to Workspace" BTN manual triggers the finish of the tracking line. The data are sent to the BPF algorithm for the cable's position estimation.

The following two BTNs are not implemented in the prototype interface. They can be implemented in a future interface as aids to a real time survey. The first BTN "Show Vector" will implement a three dimensional arrow pointing to the cable. The second "Estimate Distance" can serve as a traditional inversion distance measurement. Implementing these facilities requires more testing and collecting more experimental data.

The system focuses on one frequency filtered from the sensed EMF signal. The first field from the left on the bottom of the interface is designated for manual choice of the frequency. The next positions allows to input the voltage and current fed into the cable. The middle section of the GUI displays the amplitude, phase and SNR of the signal coming from all different sensors. The bottom TXT field displays the sentence with all parsed data points, which is recorded on the comma separated values file (CSV). When the system is running and the data are read from the sensors, the displays change their colour to green to indicate the system is in operation.

The sentences are kept in a buffer and are appended to the end of the file manually. The files are stored with names provided in the fields “Name of csv file” and “Name of raw file”. The toggles in the left bottom corners allow clearing the buffer and appending all sentences onto the end of active files.

Lastly the field “Measured Dist” provides the vertical distance to the last calculated point. The measurement comes as the last data vector processed by the localisation algorithm and BPF.

Figure 42 shows a computer screen with active GUI, data fed into the interface and spectrum analyser displayed on the screen.

Figure 42 Computer with GUI display during trials in Dartmoor

The acquisition box was tested in an experimental setup in Hooe Lake in Plymouth. To test the data collection, a 200m cable shown on Figure 43(a) was laid down on the seabed. The acquisition box was placed on board of the remotely operated platform shown in Figure 43(b). Two searching coils with the GPS antenna shown in Figure 43(c) were attached to the platform and connected with the acquisition box.

(a) (b) (c)

Figure 43 Wet trials conducted on Hooe Lake in Plymouth; (a): testing cable; (b): Remotely operated platform; (c): Searching coils in mounting bracket

The system was set-up to track a 90 Hz tone induced in the cable. Before the boat conducted the survey a frequency sweep revealed large noise on 50 Hz and its harmonics. The 90 Hz frequency was arbitrarily chosen as the least noisy frequency.

The tone was induced into the cable by a proprietary tone generator. The current was set to 0.2 mA with 2.2 V connected to the cable. The test cable was constituted of two wires. One of the wires was 200 m long. It was laid straight on the seabed with four 2kg weights and buoys showing the position of the cable. The second wire was short of 10m long and is used only to connect the tone generator to the water. The ends of the wire on the shore were connected to the tone generator's terminal. The other ends were open with full contact with the water. The current fed on the shore end has the return path through the sea water.

The survey platform was steered to criss-cross the cable's path. Criss-crossing lines separated from collected data are shown in Figure 44. During the marine survey, the information collected during data acquisition was processed in various software components. For the purpose of the experiments and prototype, Quantum GIS (Q-Gis) was used as a primary tool. The choice of the Q-Gis is dictated mostly by the fact that it is free, open source software with a good interface to external programs or programming languages such as Python.

Figure 44 Crossing lines mapped in GIS software Q-Gis

During the trials, the acquisition box collected and recorded data in real time but all data were processed after the trials. Two files were created. The first one, with the snapshot shown in Figure 45 gives data from the acquisition box together with the data from the GPS in a NMEA standard.

The line containing information from the EMF sensor includes name of the line, Channel one out of Four, Socket A or B, Frequency, number of samples processed from the previous line, number of errors, amplitude of the frequency of interest, root mean square (RMS) value of the input, SNR, phase of the frequency of interest, gain set on the ADC and control number.

The line containing GPS information was the standard "NMEA 0183" sentence. It included time, latitude, longitude, fix quality, number of satellites, horizontal dilution, altitude, height of geoid, time since last update, reference ID and checksum. The format of this information should be the same for all GPS devices.

```
'Name','Chan','Sock','Freq','Samps','ErrLines','FreqAmp','InputAmpRMS','SNR','Phase','Gain','Count'
$BOX,1,A,90,250,0,0.0000001061,0.0000061359,-35.091,1.920,8,*FF
$BOX,2,A,90,250,0,0.0000002885,0.0000167966,-35.151,1.701,8,*FF
$BOX,3,A,90,249,0,0.0000002563,0.0000123958,-33.510,1.487,8,*FF
$GPGGA,220354.000,5022.2806,N,00409.3707,W,1,04,8.6,15.0,M,51.5,M,,0000*74
$BOX,1,A,90,250,0,0.0000001300,0.0000062191,-33.411,1.781,8,*FF
$BOX,2,A,90,250,0,0.0000002919,0.0000166524,-34.970,1.899,8,*FF
$BOX,3,A,90,251,0,0.0000001915,0.0000124091,-36.098,2.065,8,*FF
$GPGGA,220355.000,5022.2613,N,00409.3776,W,1,04,8.6,9.9,M,51.4,M,,0000*4C
$BOX,1,A,90,250,0,0.0000001296,0.0000062125,-33.429,1.502,8,*FF
$BOX,2,A,90,250,0,0.0000003214,0.0000167359,-34.163,1.970,8,*FF
$BOX,3,A,90,249,0,0.0000001957,0.0000124175,-35.912,1.479,8,*FF
```

Figure 45 Snapshot of parsed data with values for three channel on socket A of the box and NMEA sentence from the GPS

The second CSV file shown in Figure 46 recorded all raw data coming from the ADC. The file served only as a back-up file or as additional information for further development. The file contained digitised information about the voltage read in each channel. The data were presented in packages of four hexadecimal values. Each line of the file contained "$" sign, "B" marking that the data comes from the box, number of samples, channel one out of three, socket A or B, gain set on the ADC, four values representing the voltage.

```
$,B,000AFC5A,3,A,8,03EA1040,06F50AC2,06755728,06A12514
$,B,000AFC83,1,A,8,FFFFF80F,FFFFDCF7,FFFFD11D,FFFFD4BB
$,B,000AFC6F,2,A,8,000037F0,00002FD4,000040BC,0000546A
$,B,000AFC5B,3,A,8,0555D142,021960F4,054FA24A,06E8442C
$,B,000AFC84,1,A,8,FFFFA6ED,FFFFBD3B,FFFFB54B,FFFFE435
$,B,000AFC70,2,A,8,0000553C,00005C94,00001956,00001A6C
$,B,000AFC5C,3,A,8,06C45CC0,08504530,071BA7AA,0512AB42
```

Figure 46 Snapshot of raw data read from the ADC.

Information from the acquisition box can be parsed into a CSV file including data required by a surveyor. The equipment and software used on different surveys vary hence the output information might be different. Figure 47 shows a snapshot example of the data prepared as a final survey report. The file included positioning data where the sample was taken, and information from the EMF channel. The structure of this file might be different for other requirements.

```
index,time,GPSout,Lat,Long,Easting,Northing,Freq,Amplitude,ADCinput,SNR,Phase,Gain,NormAmp
15743,103652.8,"5021.413434,N 00406.387154,W",50.35689057,
-4.10645257,421293.241,5578897.884,90,0.062019075,0.130164476,-0.818,1.394,8,0.006891
15744,103653.0,"5021.413516,N 00406.387250,W",50.35689193,
-4.10645417,421293.1289,5578898.037,90,0.061241752,0.128660516,-0.835,-2.057,8,0.006804639
15745,103653.4,"5021.413690,N 00406.387441,W",50.35689483,
-4.10645735,421292.908,5578898.363,90,0.061241752,0.128660516,-0.835,-2.057,8,0.006804639
15746,103653.6,"5021.413771,N 00406.387541,W",50.35689618,
-4.10645902,421292.791,5578898.515,90,0.061631988,0.128570698,-0.7170,-2.061,8,0.0068479
15747,103653.8,"5021.413858,N 00406.387633,W",50.35689763,
-4.10646055,421292.685,5578898.6779,90,0.061605957,0.128784178,-0.752,2.8369,8,0.006845106
```

Figure 47 Snapshot of final file containing all information

Information from the acquisition box were processed with the cable localisation algorithm described further in this work. The algorithm separated the lines of cable crossing and applies the BPF to estimate the position of the utility.

The final position for the five lines from the trials is presented in Figure 48. The position is shown as geographical data and the depth as a distance from the water surface. For estimating burial depth of the

utility, additional information about water column depth is required. Usually this data are taken from a SSS or echo sounder. Subtraction of the water column depth and depth to the cable gives a burial depth of the utility. The SSS is an expensive item of equipment and it was not feasible to hire the sounding equipment for these trials

Lat	Long	Easting	Northing	Depth
50.357133	-4.10673075421273.854	5578925.134	1.31	
50.35709302	-4.10684025421265.999	5578920.805	1.29	
50.35705987	-4.10696725421256.91	5578917.253	1.34	
50.35706037	-4.10694625421258.405	5578917.286	1.31	
50.35704887	-4.10702225421252.98	5578916.088	1.36	

Figure 48 Positioning data for each line including cables position and depth

Finally the data can be presented for the reporting purpose. It is a decision of surveyor what software will be used for final reporting. Figure 49 shows a simple implementation of a graphical output in the Python programming language.

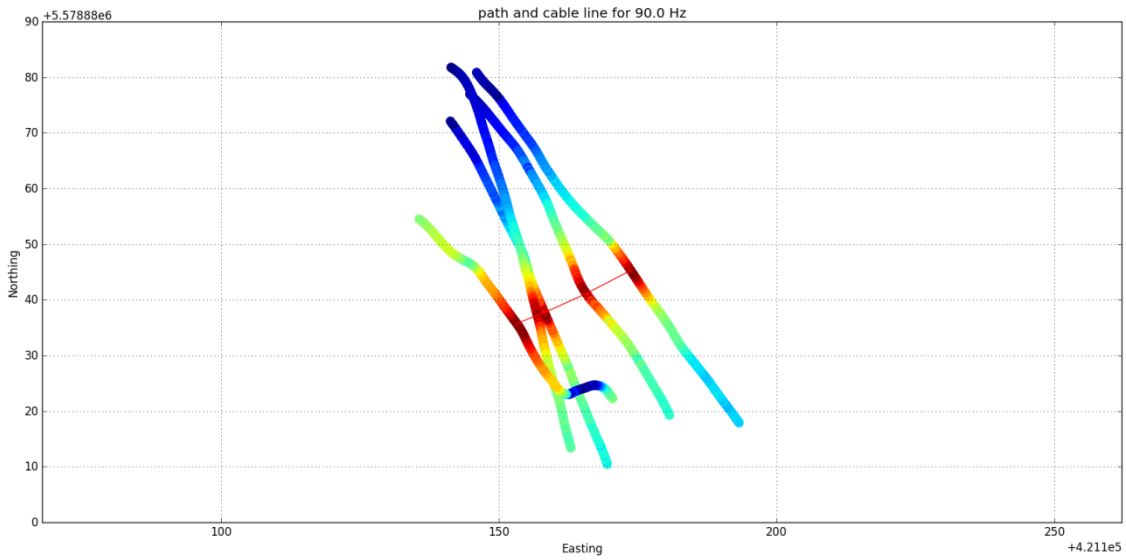

Figure 49 Crossing lines with EMF from one of magnetic coils and cable position

The horizontal coil readings were used to present the strength of the signal and represent the survey path on the geographical grid with easting as the x-axis and northing as the y-axis. The cable line was presented as simple connection of the positions estimated by the localisation algorithm.

The main output form the acquisition box was the file including information about the cable, its position, depth and the EMF read by the sensor. The information analysed in the software was available to the

surveyor and was customised to personal or company's preferences. Figure 50 shows pictures taken during a survey in South America in 2015 where the set-up was different to those from the experiments. The surveyor used Hypack navigation software for data display and AutoCad software for mapping. Most of the software is able to process CSV files with custom information. The real time data collection can be read in navigation software as a generic device. The requirements of the survey also depend upon the hardware used. All of this information needs to be considered during the survey planning stage or if the equipment is to be commercialised.

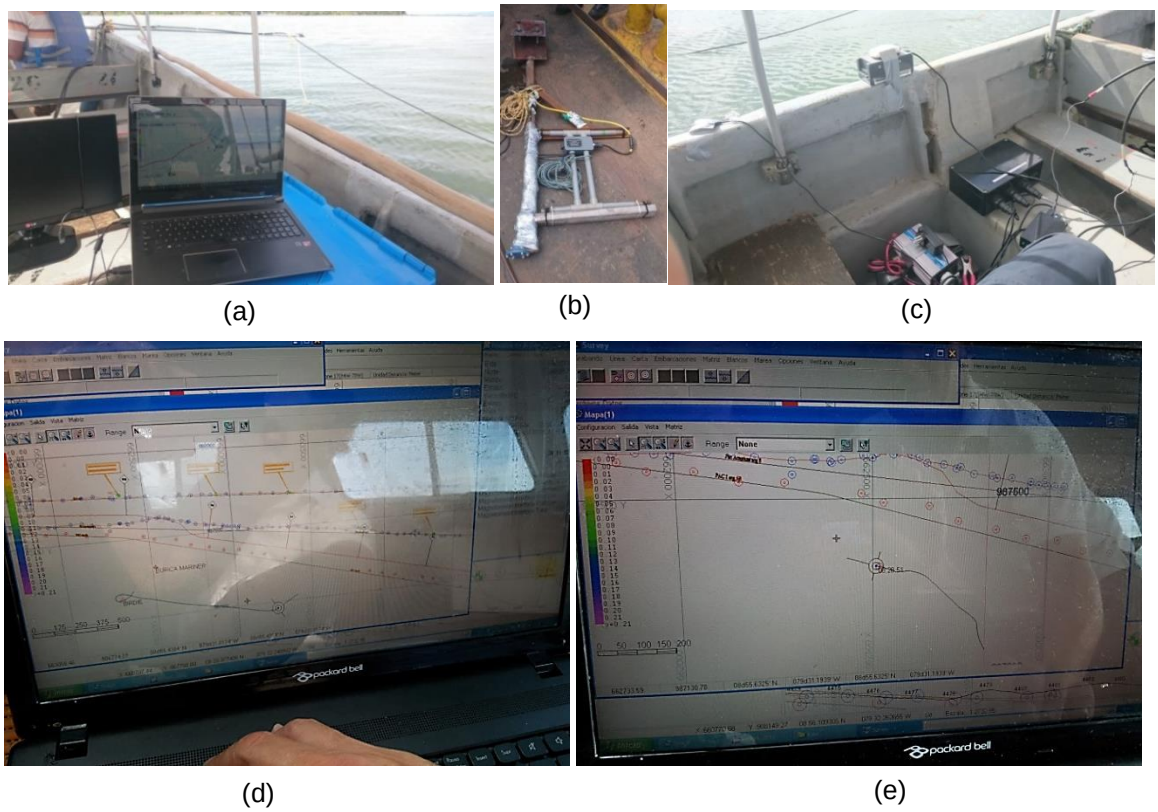

Figure 50 Trials conducted in South America 2014. (a): Hypack navigation system. (b): Searching coil sensors with bracket. (c): Acquisition box setup (d,e): Cable positioning in Hypack Navigation Software

Development of the new tool for subsea cable tracking requires a modular and flexible design. To address all the requirements of the market the system needs to be adaptable and have the possibility to connect to different survey equipment.

In this chapter, the main ideas behind the design of the system were presented. The system constitutes different sensors suites, which can be adjusted to different requirements, the acquisition hardware and the user interface. All of these elements can accommodate demands from particular survey needs.

The main purpose of the system is for subsea cable detection. The acquisition of the EMF induced in the cable allows applying a novel algorithm for estimation of the cable position and burial depth. The algorithm will be described in the following chapters.

Chapter 6. Investigation of Novel Approaches to Cable Location Detection

Traditionally the detection of a cable's burial depth relies on the magnetic signal and its attenuation function. The function relates the level of the electromagnetic field at some distance from its source to its decay curve. This method works only in close proximity of the cable. As the signal decays exponentially, the difference can be read only if the signal is relatively strong, higher than the noise incorporated into the measurement. In close proximity with strong signal the decay curve is relatively steep making it possible to assess the distance to the source. Current methods effectively estimate the distance only up to three metres range.

Short distance limitation means that in a practical survey, inspection must be completed by a diver. To perform cable localisation from a larger distance, various methods were investigated. In this chapter different attempts of improvements will be described.

The methods were tested both in simulated data, real word experiments and data collected during cable tracking jobs. The majority of samples were collected during a survey performed in 2011 near the Danish coast. To confirm the initial findings and to develop a better understanding of the system, additional experiments were performed at various locations.

In the spring of 2013 a tracking experiment was completed at Sennen Cove near Penzance. Several cable landing points and a historic first cross-Atlantic cable are situated at this location. For the experiment a tone was induced into one of the Atlantic Crossing cables, AC1.

In years between 2013 and 2016 additional experiments were performed at Hooe Lake in Plymouth with a laid wire connected to a tone generator and through a water return path. The electromagnetic field was acquired with experimental tools and different sensors. These trials allowed testing different sensors, acquisition methods and survey platform paths.

In addition to the above experiments, cable tracking using various methods, tools and equipment was completed during new cable installations in Panama in 2014, Columbia in 2015 and Italy in 2015. The

experiments allowed the collection of data with different parameters, such a water salinity or tone frequency and voltage.

Most of the surveys are constrained by their cost and need to meet specific criteria. It is often difficult to have a full suite on board of the vessel. From all conducted cable surveys, the inspection in Denmark 2011 was the most comprehensive. The boat was equipped with a full sensor suite and after the initial survey the position of the cable was checked and confirmed by a diver.

The data shown in Figure 51 illustrates the electromagnetic readings collected during the first set of experiments in Denmark 2011. The survey boat made multiple crossings of two cables with applied very low frequency alternating current. The survey purpose was to perform the Side Scan Sonar (SSS) in the area where the cables needed to be localised for later repair. The boat was equipped with a SSS, a high precision GPS positioning system and navigation computer running survey software.

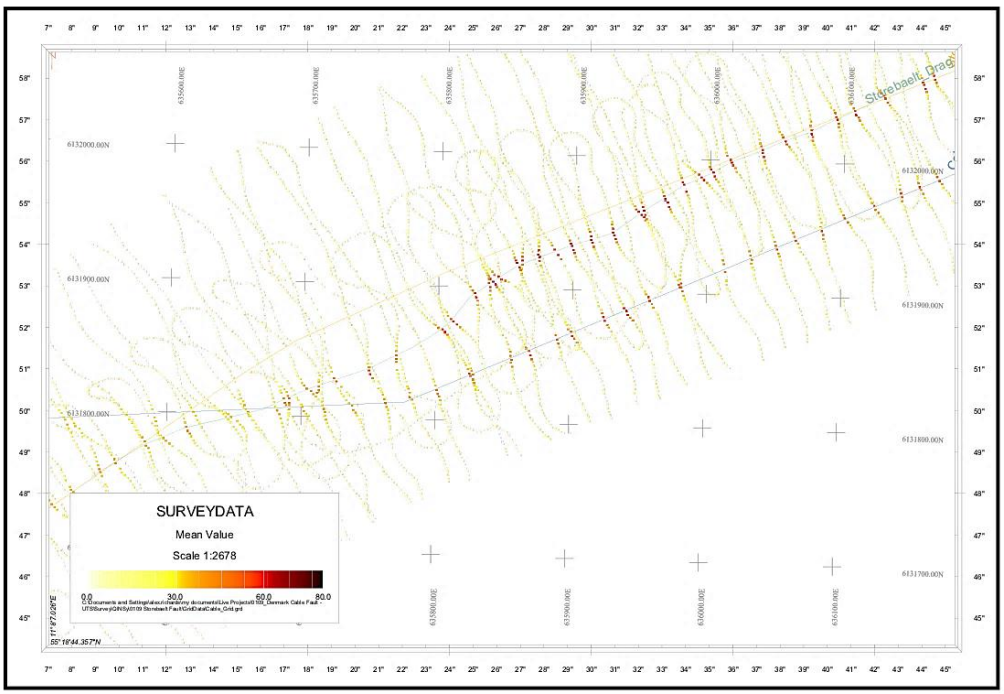

Figure 51 Survey chart of collected samples

In addition to standard surveying equipment, two searching coils were mounted on the side of the boat. The coils were connected to acquisition instruments “Tinsley 5930”. This set-up allowed collecting

electromagnetic data sampled by the coils. The set-up is shown in Figure 52. A similar set-up was replicated during later trials near Penzance and in Panama City although the survey did not collect water depth measurements.

(a) (b) (c)

Figure 52 Survey boat set-up with searching coils mounted on the side of the RHIB; (a): Mounted coils on the RHIB side view; (b): coils bracket; (c): RHIB prepared for survey

The samples collected by searching coils allowed positioning of both cables. The measurements were taken with a sampling rate of 1 Hz constrained by the GPS and acquisition software. Figure 53 shows the sample points and the level of EMF sampled directly with horizontal coils.

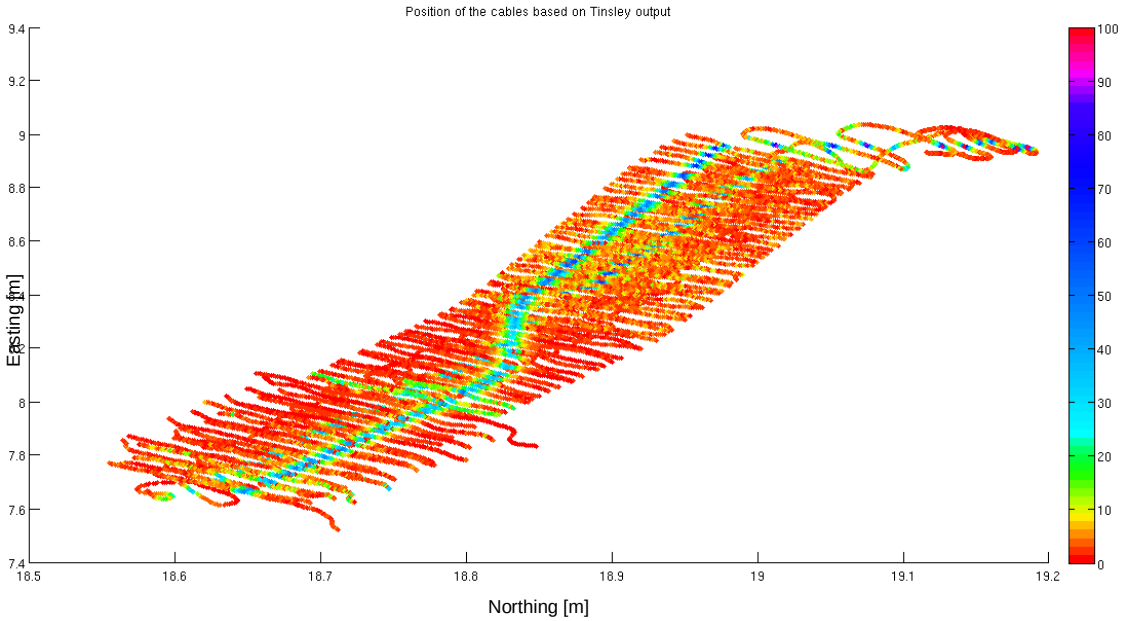

Figure 53 Cable's position based on intensity of induced EMF

Even a quick look at the EMF level shows that the cable's positions can be drawn from the collected samples. In most cases, a crossing line has a horizontal coil's peak over the cable. The position of the cable

can be assumed in the space between three consecutive samples where the middle point shows the highest EMF level for the line. The horizontal coil's peaks are shown in Figure 54.

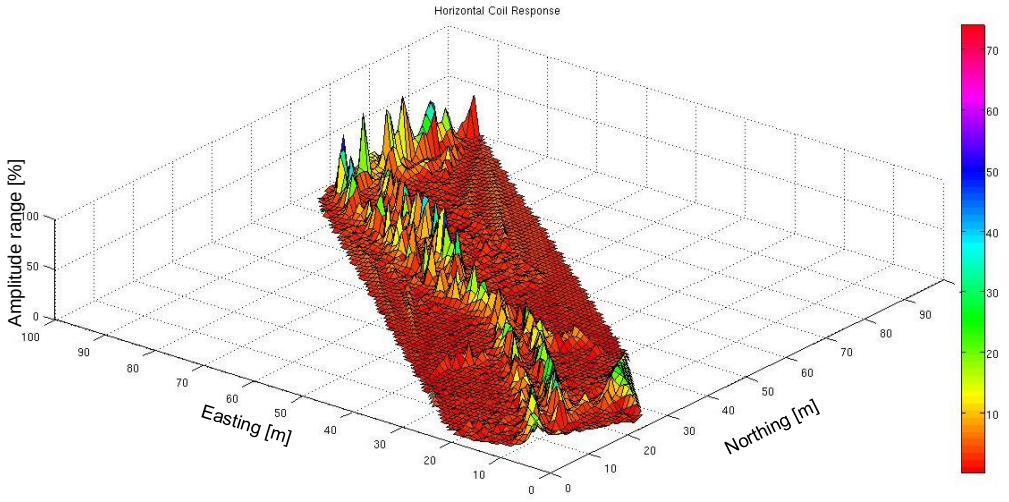

Figure 54 Horizontal coil's readings

Similarly to horizontal coil readings, the vertical coil has null response directly above the cable. Figure 55 shows the EMF readings of the vertical coil. The EMF increases when the survey boat approaches the cable, sharply drops in close vicinity to the cable, increases again and slowly decreases as the boat departs from the cable's vicinity.

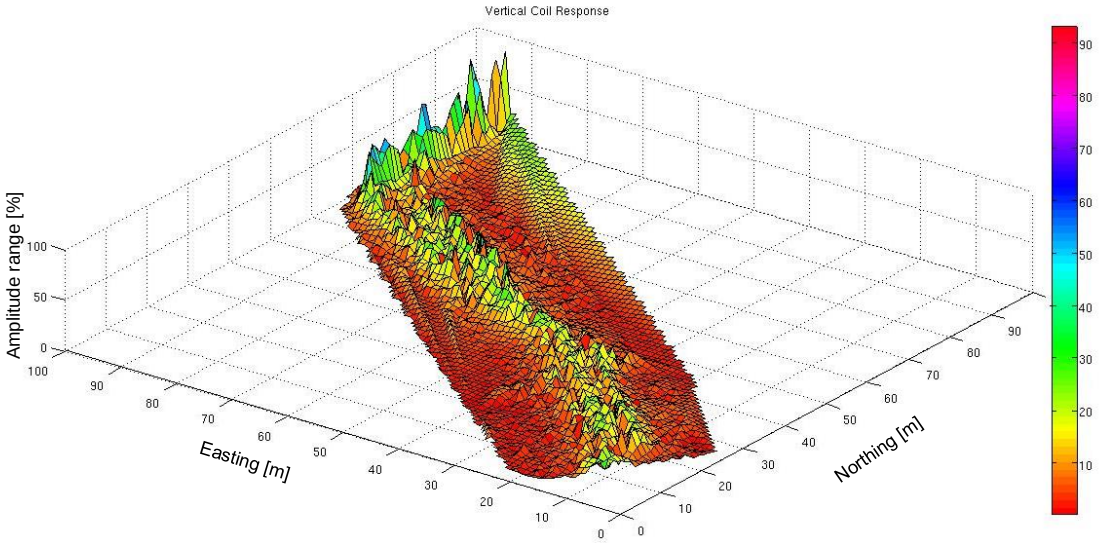

Figure 55 Vertical coil's readings

The behaviours of the horizontal and vertical coils can be used to indicate the position of buried utilities. It will be used in further investigation of precise positioning techniques and estimation of the burial depth.

6.1 Inverse method

In the magnetic inverse based method the localisation of the source is calculated on the assumption that the strength of the magnetic field at a known distance from the source can be characterised.

The magnetic field density $d\boldsymbol{B}$ at a point in space induced by the current i flowing through a straight section of conductor with length $d\boldsymbol{l}$ follows Biot-Savart's law (28) (Dezelak et al., 2010)

$$d\boldsymbol{B} = \frac{\mu_0 i}{4\pi R^3}(d\boldsymbol{l} \times \boldsymbol{R}) \quad (28)$$

where μ_0 is the permeability of the free space and $\boldsymbol{R}$ denotes a vector from the element $d\boldsymbol{l}$ to the observation point.

The magnitude of the magnetic flux density $\boldsymbol{B}$ in root mean square (rms) value can be described in terms of its components in Cartesian coordinates according to equation (29)

$$\boldsymbol{B} = \mu_0 \sqrt{H_x^2 + H_y^2 + H_z^2} \quad (29)$$

Dahab et al. (2005) suggest that for calculation of MF from transmission lines the terms in the equation can be reduced to the x and y components, considered to be in two dimensional space.

The MF decay can be related to the initial strength of MF at the source, distance to the sample point, attenuation rate r and attenuation parameter α. The proportion of the signal strength $H(s)$ at sample point s can be calculated as:

$$H(s) = \alpha \frac{H_0}{d(s)^r} \quad (30)$$

where H_0 is the initial strength of the Magnetic Field as can be read on the cable, $d(s)$ is the distance between the sample point and the source.

The decay of electromagnetic signals is considered by Al-Shamma'a et al. (2004). They proposed that conductivity of the sea water was the main reason for EMF attenuation. In their work they focused on transmission of linearly polarised plane EM waves propagating in one direction. It can be described by the strength of the electric field E_x following equation (31) and strength of its magnetic component H_x following equation (32).

$$E_x = E_x exp^{(j\omega t - \gamma z)} \quad (31)$$

$$H_x = H_x exp^{(j\omega t - \gamma z)} \quad (32)$$

where j is the imaginary unit, ω is the angular frequency and t describes time. The propagation constant γ can be expressed in terms of the permittivity ε, permeability μ and conductivity σ and reduces to equation (33)

$$\gamma = \alpha + j\beta \quad (33)$$

where β is a phase factor.

Al-Shamma'a et al. (2004) suggested that the basic attenuation equations can be derived. The attenuation is given by:

$$\alpha = \left(35\sqrt{\frac{cf}{4}}\right) \quad (34)$$

where c is the conductivity of the sea water in Siemens per metre S/m and f is the frequency of the signal in MHz.

Following the above, the attenuation of the electric signal strength E and magnetic signal strength H increases with the distance and follows Maxwell's equation. The same applies to the strength of the magnetic field decay and relates it to the initial frequency of alternating current and conductivity of the surrounding water.

In the above equations, the value of the conductivity of sea water is difficult to estimate exactly. It depends on the water's temperature, depth and other factors such relative conductivity. Following Feistel et al. (2009) the conductivity of the Baltic Sea may be given as 2.3 Sm^{-1} but this value can vary with the region, temperature and other environmental aspects.

Taking the above figure and frequency of 25 Hz the value of attenuation becomes $\alpha = 0.1327$.

The second parameter in equation (30) is the attenuation rate r. This parameter was considered by Cowls & Jordan (2002). They used a linearisation algorithm to calculate the signal strength decay in relation to the distance x from the source. Cowls & Jordan (2002) suggested that signal strength decays with a relation of x^{-3}. Although they have satisfactory results, they have already pointed out that this assumption is not always true.

In a survey environment the initial magnetic field H_0 emitted from the cable is often unknown. In most situations the pulse current is fed from the cable stations at a large distance from the survey field and the return path is through the sea water. For broken cables the current is fed into the armour of the cable and every contact with the water changes its properties. For this reason the initial H_0 together with the attenuation α can be described as one constant a.

For the purpose of simulation the MF emitted from the cable is described in terms of the percentage of its initial value. The output of the simulation is shown in Figure 56

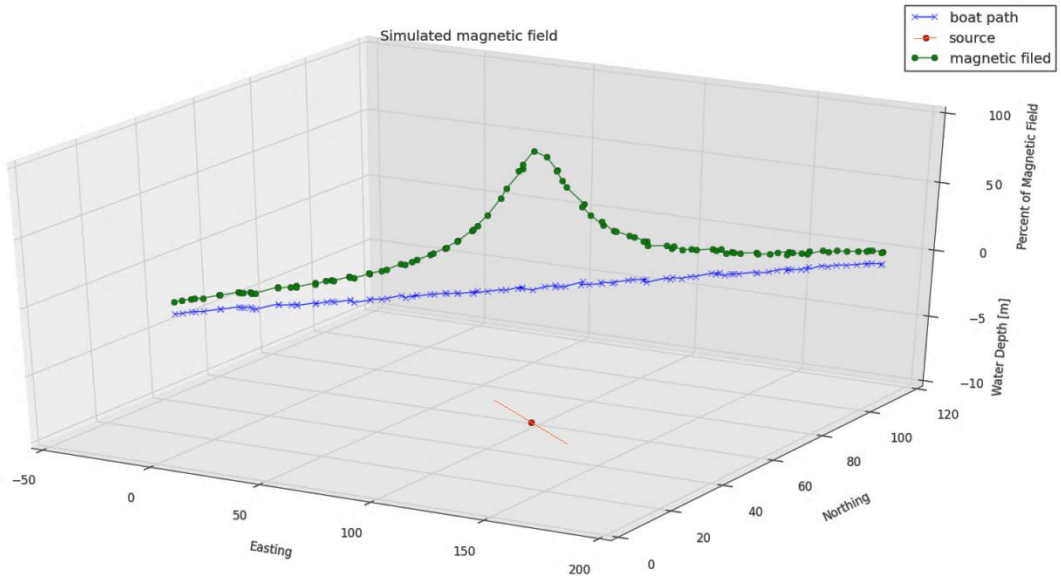

Figure 56 Simulation of MF along the crossing path with incorporated position's noise

In most marine surveys some assumptions about the cable's position are already made based on historical data. Most surveys are planned to have their surveying lines at equal intervals, as straight as possible and crossing the cable perpendicularly.

The direction of the cable allows calculating the vector of MF $\boldsymbol{B}$ at a given distance from the moving charge. The direction of vector $\boldsymbol{B}$ can be deduced from the cross product of the vector in direction of the moving charge and the vector pointing to the sample point. The magnitude of the vector $\boldsymbol{B}$ depends on the initial signal strength and attenuation of this signal along the distance from the source.

The MF vector $\boldsymbol{B}$ can be broken into its Cartesian components as shown in Figure 57. During the survey, the positive measurements of the angle $\propto$ between the vector and the horizontal plane take values from zero to ninety degrees. At large distances from the cable the angle is close to a right angle. It reduces when the survey platform approaches the cable. Directly above the cable the vector of MF is parallel to the water surface with angle $\propto = 0$ and the biggest magnitude. The positive measurement of the angle $\propto$ grows again when the survey platform departs from the cable

The vector $\boldsymbol{B}$ at the sample point is measured by searching coils that provide the projections of the magnitude of the MF $\boldsymbol{B}$ along the direction of the coils.

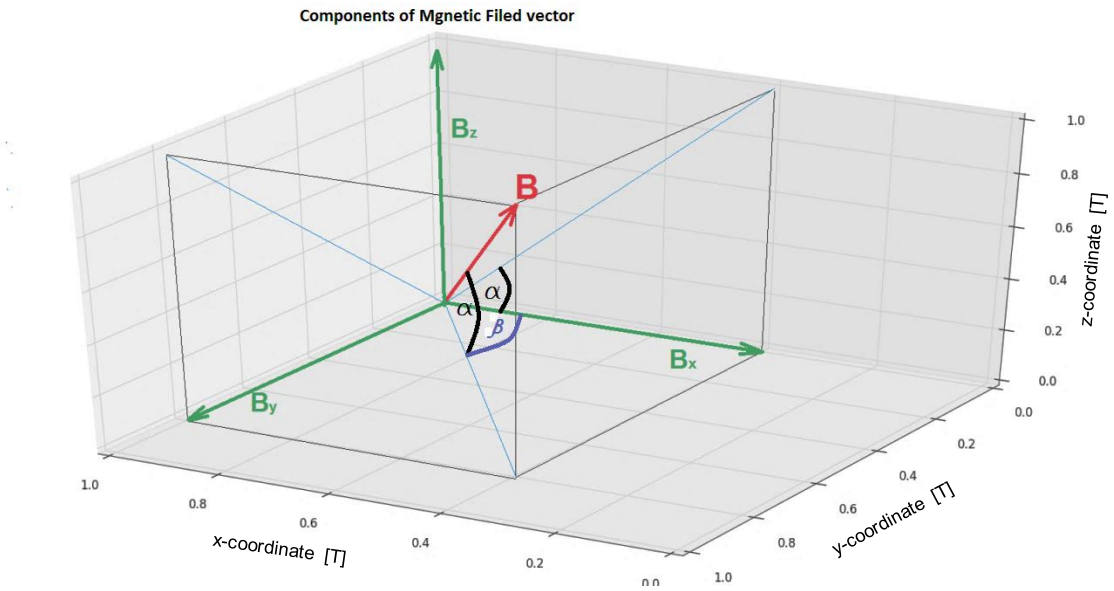

Figure 57 Magnetic field vector and its projection to the axis

In the case of submarine cable tracking with criss-crossing survey lines, the vector of the MF is perpendicular to the cable's direction and to the vector pointing from the nearest source position to the sample point. The angle β between the boat's path and direction of MF vector should become zero. Any offset of the coil's direction from the direction perpendicular to the cable path reduces the magnitude of the coil output voltage.

The main reason for this reduction is a change in the survey platform direction. The change of the boat path can be expressed in the measurement model where the searching coil readings C depend on the magnitude of the vector $\boldsymbol{B}$, the angle between the boat path and the cable's direction and the angle $\propto$.

Another contribution to the reduction in the searching coil's output is the platform's yaw, pitch and roll depicted in Figure 58. To some extent it can be controlled by measurement of the yaw, pitch and roll angles and incorporating a compensation algorithm (Sabatini, 2006; Pei & Yeo, 2009). In small surveys in shallow waters the compensation instruments are often absent and yaw, pitch and roll will contribute to measurement noise.

The yaw and pitch angle will contribute positively to the output voltage if the change is towards the direction of the MF vector and reduce the voltage output if the change is in opposite direction.

For the horizontally placed coil only pitch and yaw contribute to the readings. The same analysis can be performed for a vertical coil. The main difference would be the noise source, which in that case will come from roll and pitch, whereas the yaw will not contribute to the vertical coil's reading.

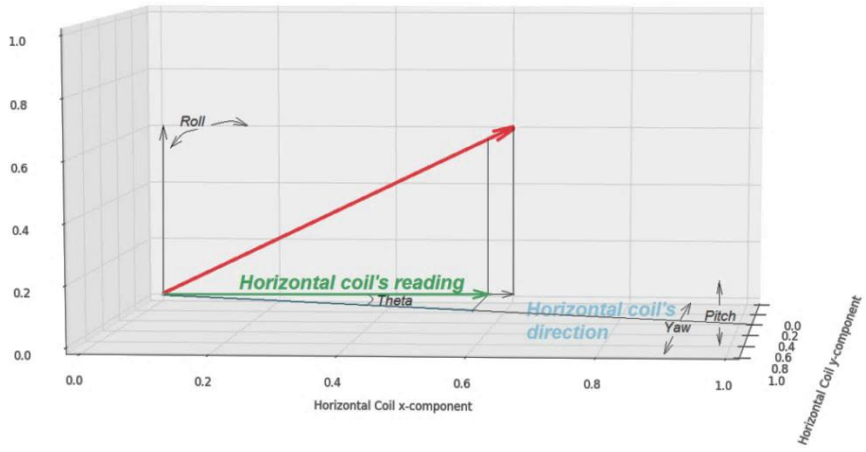

Figure 58 Magnetic field with zero y-component and its reading by horizontal coil

The direction and magnitude of the MF vector along with the position of the searching coils leads to a set of measurement equations. For the two dimensional case, the horizontal coil's output follows equation (35)

$$C_H = |\boldsymbol{B}| \cos \propto \cos \beta + v \qquad (35)$$

The vertical coil's output follows equation (36)

$$C_V = |\boldsymbol{B}| \sin \propto + v \qquad (36)$$

where C_H and C_V are the horizontal and vertical coils output and v is the measurement noise. In the criss-cross survey situation it is assumed $\cos \beta = 1$ and can be omitted or incorporated into the noise v.

In a practical environment, the coil's output depends on the acquisition tools' settings. The analogue voltage produced by the coil is amplified and converted into its digital representation. The amplification and digitalisation are only possible if the voltage falls into a previously assumed range. If the output exceeds the range limits or is too small compared to the digitisation resolution, the range is changed to one better fitting

the voltage read on the coils. For this reason, the coil's output is often given as a percentage of the acquisition range instead of real voltage values.

In the inverse method information about the MF at the sample point with known position is used to calculate the position of the source of the MF. To simplify the setup some assumptions are made.

It is assumed that the survey path follows straight lines crossing the cable perpendicularly. The origin of the coordinate system is located at the first sample point. In this setup, the coordinate system is reduced to two dimensions with the boat's path being the x-axis and depth to the cable the y-axis. The setup is shown in Figure 59.

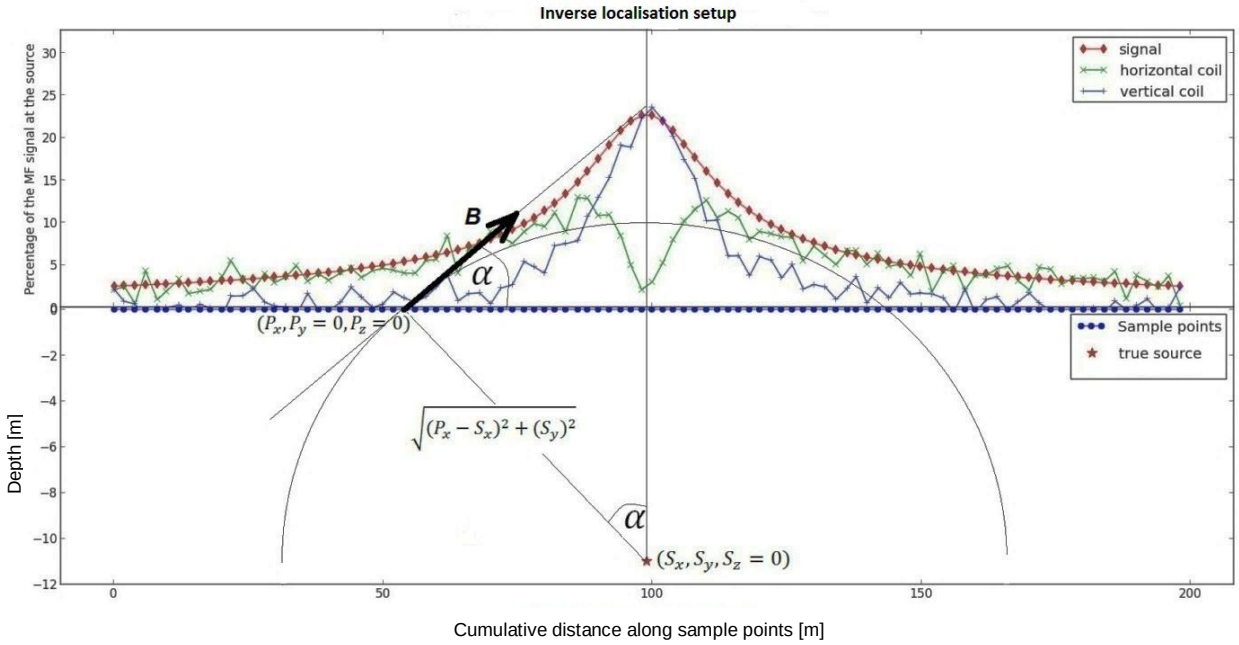

Figure 59 Magnetic Field measurement setup

The above leads to equations (37), (38), (39) and the resulting system of equations (40) with two unknowns S_x and S_y.

$$H = \frac{a * H_0}{\left(\sqrt{(P_x - S_x)^2 + (S_y)^2}\right)^3} 100\% \qquad (37)$$

$$\sin \propto = \frac{|(S_x - P_x)|}{\sqrt{(P_x - S_x)^2 + \left(S_y\right)^2}} \quad (38)$$

$$\cos \propto = \frac{|S_y|}{\sqrt{(P_x - S_x)^2 + \left(S_y\right)^2}} \quad (39)$$

$$\begin{cases} C_H = H \cos \propto + v = \dfrac{a\, H_0 S_y}{\left((P_x - S_x)^2 + \left(S_y\right)^2\right)^2} + v \\ C_V = H \sin \propto + v = \dfrac{a\, H_0 (S_x - P_x)}{\left((P_x - S_x)^2 + \left(S_y\right)^2\right)^2} + v \end{cases} \quad (40)$$

To obtain an analytic solution the noise term v is omitted. Solutions to the system (40) is presented in equations (41). The solution was obtained in Matlab programming language by solving system of equations (40)

$$\begin{pmatrix} S_x \\ S_y \end{pmatrix} \in \begin{cases} if\ C_h = 0 \wedge C_v \neq 0 \wedge H_0 \neq 0 \wedge a \neq 0: \\ \quad \left\{ \begin{pmatrix} z1 \\ 0 \end{pmatrix} \middle| given\ that: \begin{array}{c} z1\ is\ solution\ to\ equation: \\ (C_v z^3 - 3C_v P_x z^2 + 3C_v P_x^2 z - C_v P_x^3 - H_0 a, z) \end{array} \right\} \\ if\ C_v = 0 \wedge C_h \neq 0 \wedge H_0 \neq 0 \wedge a \neq 0: \\ \quad \left\{ \begin{pmatrix} P_x \\ \left(-\frac{1}{2} + \sigma_3\right)\sigma_2 \end{pmatrix} * \begin{pmatrix} P_x \\ -\left(\frac{1}{2} + \sigma_3\right)\sigma_2 \end{pmatrix} * \begin{pmatrix} P_x \\ \sigma_2 \end{pmatrix} \right\} \\ if\ C_h = 0 \wedge C_v = 0 \wedge (H_0 = 0 \vee a = 0): \\ \quad C^2 \\ if\ C_h = 0 \wedge C_v = 0 \wedge (H_0 = 0 \vee a = 0): \\ \quad \left\{ \begin{pmatrix} \dfrac{C_h P_x + C_v\left(-\frac{1}{2} + \sigma_3\right)\sigma_1}{C_h} \\ \left(-\frac{1}{2} + \sigma_3\right)\sigma_1 \end{pmatrix} * \begin{pmatrix} \dfrac{C_h P_x - C_v\left(\frac{1}{2} + \sigma_3\right)\sigma_1}{C_h} \\ -\left(\frac{1}{2} + \sigma_3\right)\sigma_1 \end{pmatrix} * \begin{pmatrix} \dfrac{C_v\sigma_1 + C_h P_x}{C_h} \\ \sigma_1 \end{pmatrix} \right\} \\ otherwise: \\ \quad \emptyset \end{cases} \quad (41)$$

where

$$\sigma_1 = \left(\frac{C_h^3 H_0 a}{C_h^4 + 2C_h^2 C_v^2 + C_v^4}\right)^{1/3}$$

$$\sigma_2 = \left(\frac{H_0 a}{C_h}\right)^{1/3}$$

$$\sigma_3 = \frac{\sqrt{3}i}{2}$$

From the solutions only one, real solution is valid in an experimental scenario. It leads to the system of equations for S_x and S_y presented in equation (42).

$$S_x = \frac{C_v\left(\frac{C_h^3 H_0 a}{C_h^4 + 2C_h^2 C_v^2 + C_v^4}\right)^{1/3} + C_h P_x}{C_h} \qquad (42)$$

$$S_y = \left(\frac{C_h^3 H_0 a}{C_h^4 + 2C_h^2 C_v^2 + C_v^4}\right)^{1/3}$$

To apply solution (42) to collected data the attenuation a and initial field strength H_0 must be established. Values for these parameters were calculated experimentally. To obtain the attenuation the MF from a known source was calculated according to equation (37). The parameter a was chosen to minimise the least square fit between the theoretical readings for the horizontal coil and collected data for 19 samples closest to the source. This procedure led to calculate the attenuation rate and water conductivity according to equation (34) as 1.67.

The inverse method was tested on different survey lines collected in Denmark 2011. Figure 60 shows data for the line number two, which was the first survey line for one of the cables. The true location of the cable was established by a diver. The figure shows the theoretical magnetic field and theoretical coil readings and its measured counterpart for each sample. For each sample the position of the sample and the coil readings were fed into equations (42). The resulting position of the calculated source is represented by a blue dot.

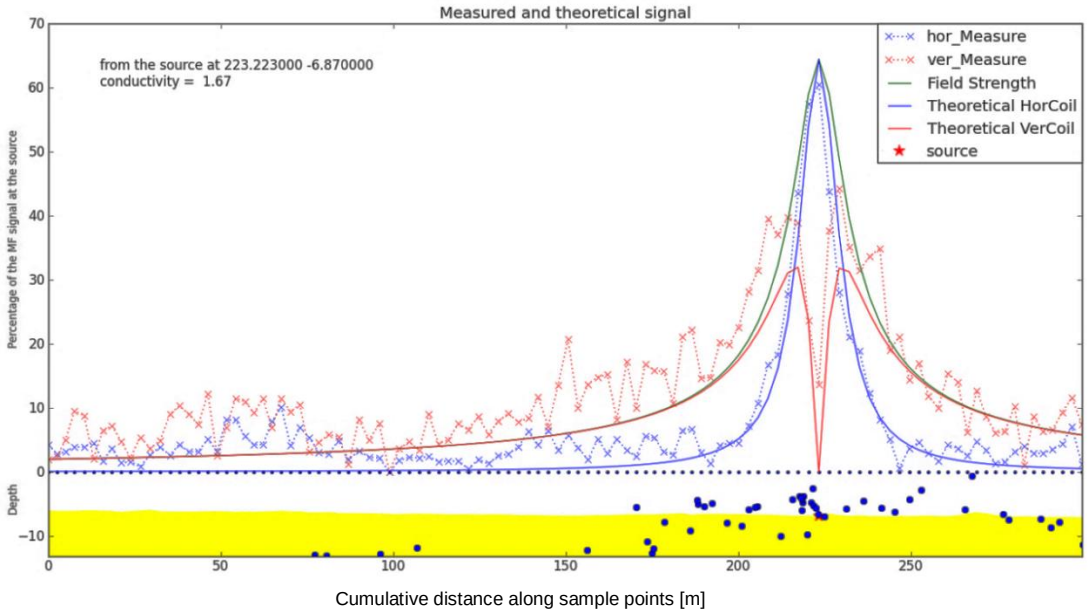

Figure 60 Inverse method fit to line 6

The inverse method performance is not satisfactory by any standard. The position of the calculated source is far from the true position. The calculated theoretical source positions are close to true source only when the data points were taken directly above the cable but the precision of the calculations are difficult to predict in a real work environment.

The method was tested on different data from different lanes and cables. Figure 61 shows the same calculations performed on lane 70 for the same cable. The calculated source positions diverge from the true location.

It can be noted that parameters of the MF calculations do not give an appropriate fit to the collected readings.

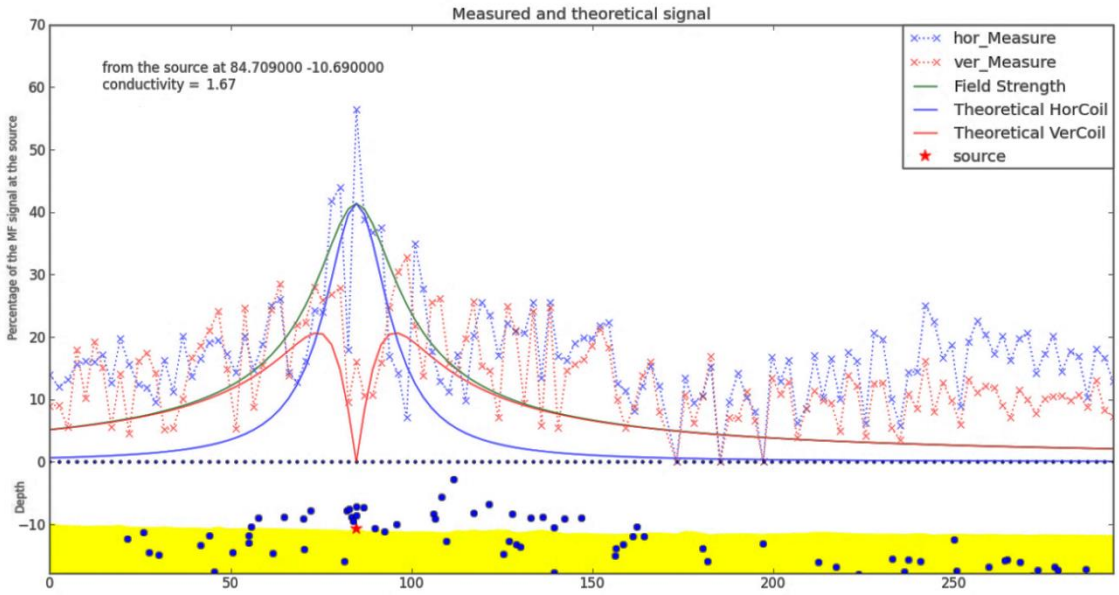

Figure 61 Inverse method fit line 54

The poor performance of the method was expected but is difficult to improve. The main problem is the difficulty to incorporate measurement noise into calculations. To perform source localisation from a single point, the noise needs to be reduced. In the point diver localisation, the sensor frame is kept still on the bottom of the sea. It allows the noise component to be reduced, most often by readings averaging. It is impossible on a moving boat.

In addition to the failure of convergence to the true source, the calculations require estimating the attenuation and initial MF values. In practice this is possible only if the true source is known beforehand. This requirement makes the method inefficient for localisation of the cable from the sea surface.

6.2 Inverse method improvements with neural networks

To investigate the inverse method further, the data were processed with various Neural Network (NN) models. The main problem set for this procedure was to deduce the position of the cable based on known sample points and estimated distances.

Similar procedures can be found in the literature. Neural Networks (NN) are used in determination of various signal sources for example in acoustic or in testing source of an odour.

Colnet & Di Martino (1996) used NN to determine the source of an acoustic signal sampled by the sensor's array. They measured delay time of the sound on each sensor at different localisations. The advantage of using an NN approach is that they learn to link features of the signal with the distance to the array. The procedure eliminated requirements of prior knowledge about parameters of the signal.

The method of NN in source detection has many practical applications. For example Geng & Jung (2008) used NN for detecting the angle of incoming sound in robotics. They trained a humanoid robot equipped with two microphones to track a human's voice. They used feed-forward back propagation NN to learn to localise the source based on the amplitude of a single wave separated from the incoming signal. They pointed out that although they reached high precision the system still suffered some limitations. Aside from the problem of obtaining an adequate signal direction (directly facing the microphone array) the NNs require large sets of good quality training data, is computationally intensive and difficult to perform in real time.

The computational complexity problem was noticed by other authors. To overcome some of the limitations, Dehkordi et al (2011) proposed to use NNs for pattern recognition in carefully extracted features of the signal. By using the most effective features of the acoustic signal emitted from the source, Dehkordi et al. (2011) were able to achieve fast convergence with good accuracy.

An interesting application of source localisation by NNs is presented by Cui et al. (2011). They used a NN model inspired by wasps to search the source of an odour. The chemical plume tracing was done by using

an ion detector providing concentration data to a robot. In addition the robot was equipped with a wind sensor. All the information was fed to a NN algorithm which predicted the direction to follow. Although all the work was done in simulation, by Cui et al. (2011) claim good results and that they were able to mimic a wasp's swarm.

Following examples found in the literature (Geng & Jung, 2008; Cui et al., 2011) where a feed-forward back propagation model was used to predict the distance to the cable based on the collected MF samples. The NN algorithm was trained on randomly selected data points with the known distance to the utility and later was tested with part of the remaining data. The model of the NN was used to extrapolate results and predict the distance to the cable in the first and the last line from the survey.

Although different configurations were considered, only selected, representative examples are presented. The NN models presented have one input (horizontal coil readings) and one output (distance to the cable), and two inputs (horizontal and vertical coil readings) and one output, respectively. In addition to the presented models other configurations like those with two inputs and two outputs (distance and angle to the source) were investigated.

Methods to measure burial depth are based on measurements of the distance between the cable and sample point taken. The underlying principle is a difference in amplitude of MF read by the horizontal coil and its comparison with an attenuation curve. In a similar way, the problem was set for NN training. It was assumed that the readings from the horizontal coil can be directly translated to measured distance.

The novelty of this approach is in the scale of the experiment. In normal situations, the readings are taken in close proximity of the source. The MF is read by a diver up to three metres from the cable or by flying autonomous or remotely operated vehicles kept in close proximity of the seabed.

For NN training the data come from the samples taken at a distance between 7 m and 50 m to the cable. Different NN models were tested but none was found which would perform with satisfactory results. The calculations were done with the use of Matlab and Python programming language utilising the PyBrain library (Schaul et al., 2010).

First, the training set was used to build a NN model and to calculate the parameters. From the available data only those sample points within 30 metres of the source were considered. This made a set of 2046 data

points. One quarter of the points (510) were chosen randomly and used to train the NN model. From the rest of the data points, 100 points were chosen to test and validate the fit. The detailed parameters and output fit can be found in Appendix 1

The validation test in red and training data points are shown in Figure 62. The horizontal axis of the plot shows the distance from the cable to the sample point. The vertical axis shows the output of the horizontal magnetic coil as a percentage of its range.

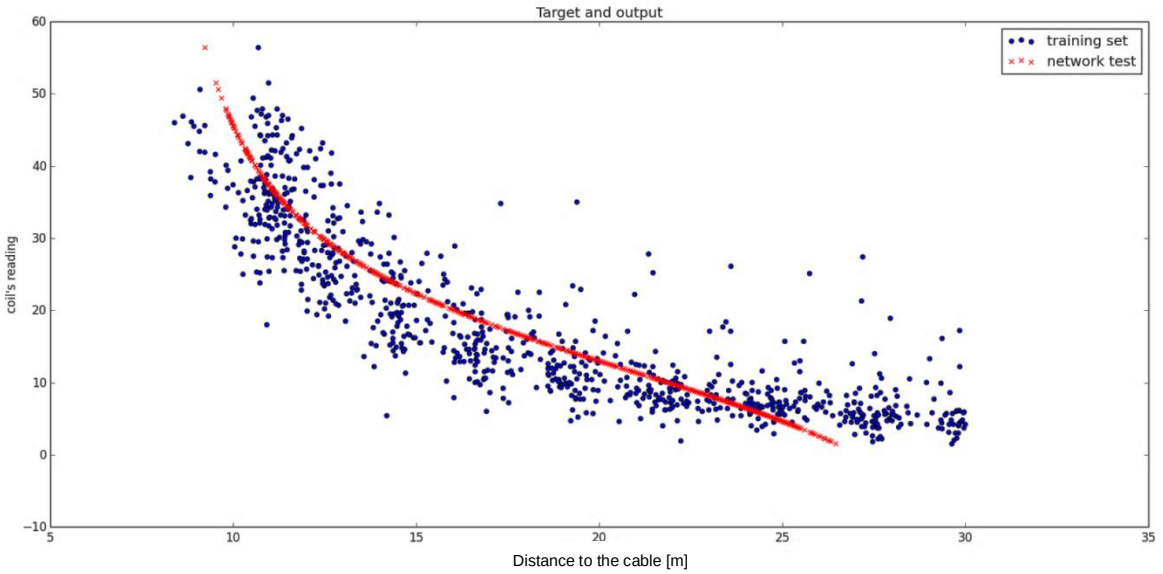

Figure 62 Samples used for training set and the output of the coil predicted by the NN

It can be seen that the model of magnetic readings corresponds to the exponential curve of MF attenuation. As was expected the amplitude of MF attenuates quickly but it can differentiate the readings in a range of up to 25 m.

To check the possibility and precision of the distance prediction, the NN model was used to extrapolate data. The first survey line was not included in the data set for training the NN. Thus the data were new to the NN model. From line 35, data points were fed into the NN and for each data sample, the NN model predicted the distance to the utility. That distance was compared with that reported by a diver.

Figure 63 shows the difference between the true distance and distance predicted. It can be seen that the NN model does not provide a satisfactory estimation.

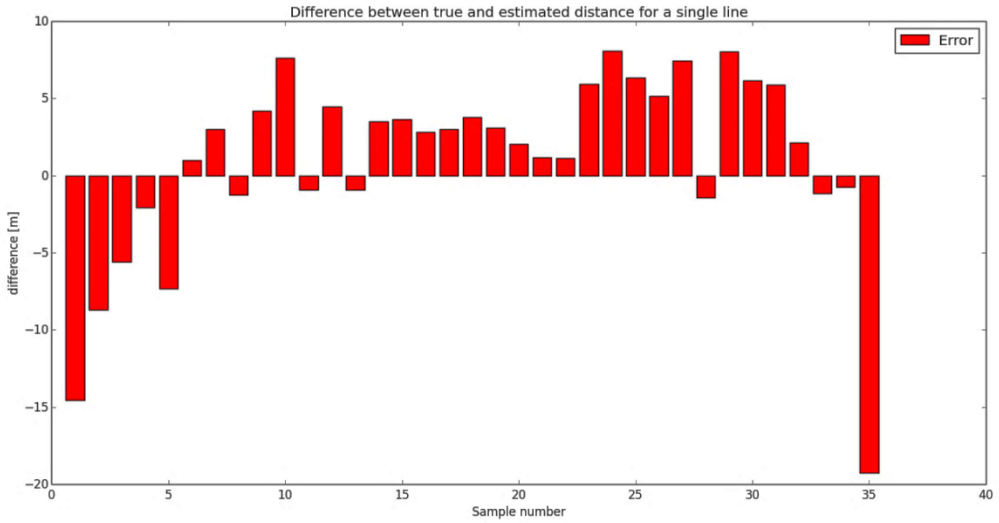

Figure 63 Difference between the true distance and the distance to the cable predicted by NN

To improve the quality of the prediction, a similar approach was taken with two inputs to the system, namely the horizontal coil reading and the vertical coil reading for the same sample point. This "two input one output" model was built in a similar fashion to the previous one. The trial and error method was used to select parameters for the best fit model. The detailed parameters of the model can be found in Appendix 1.

For practical applications, it is worth noting that on a 4 Core 2GHz computer, the time of the script execution was as much as 464.96 seconds. The procedure was not optimised for speed but for a real time tracking application it would require much improvement. Apart from the code optimisation, the NN specific parameters like number of recursions and error shown in Figure 64 would require modifications.

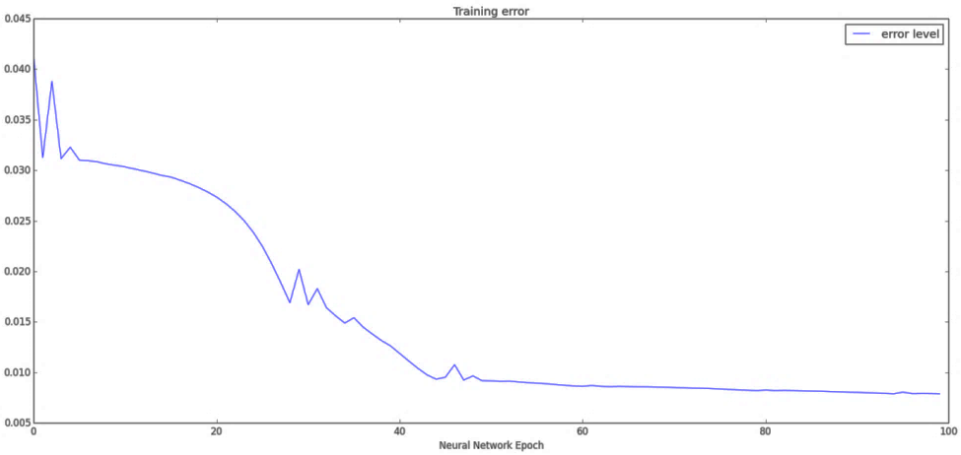

Figure 64 Training error of Neural Network after 100 recursions

The training and validation of the model are shown in Figure 65 and Figure 66. In a similar fashion to a one dimensional data input, the vertical axis corresponds to the coil reading and the horizontal axis to the distance to the cable.

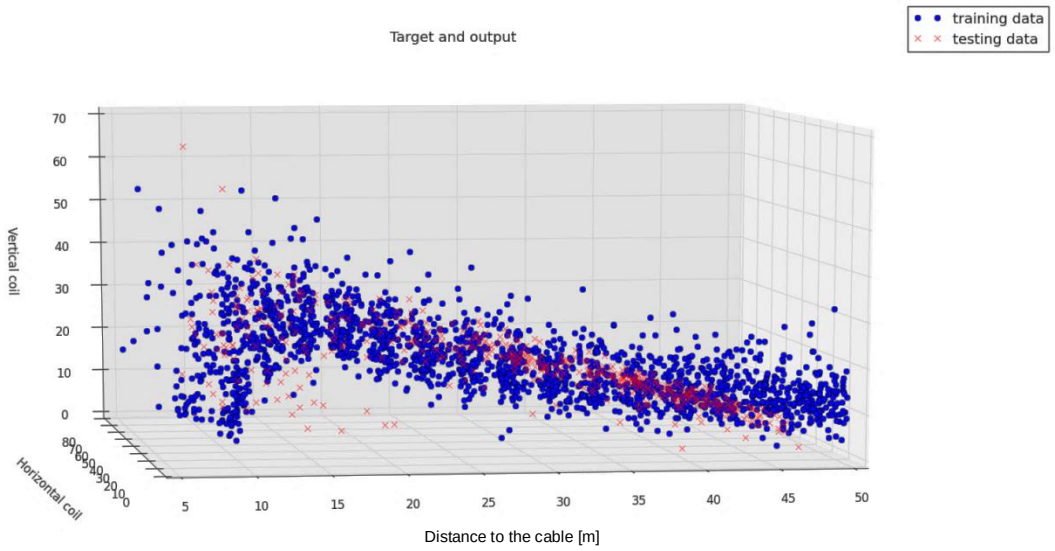

Figure 65 Vertical coil output vs distance

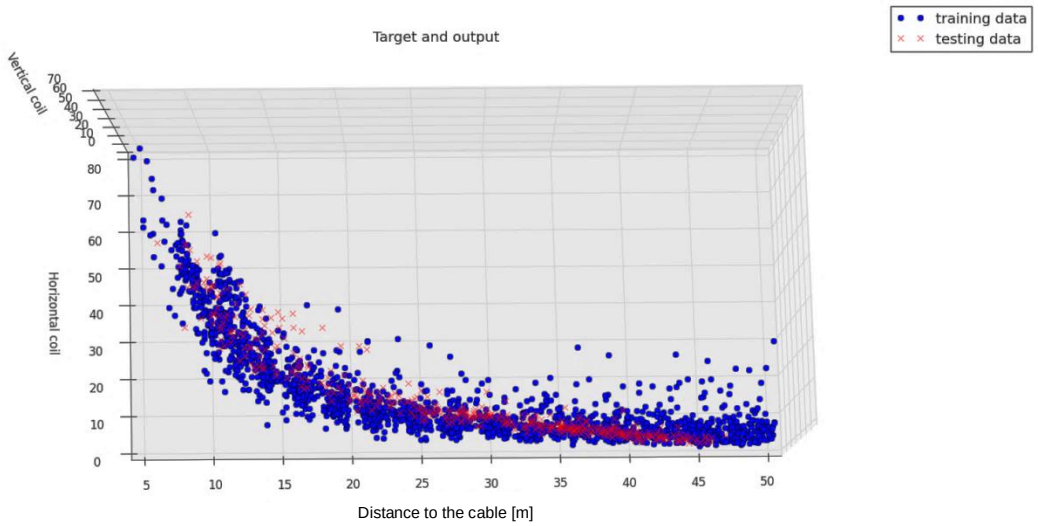

Figure 66 Horizontal coil output vs distance

It can be noticed that the model follows expectation.

To validate the prediction, the model was used to estimate the distance on the first survey line. Figure 67 shows the difference between the true distance and that estimated by the NN. The prediction of the distance is unsatisfactory.

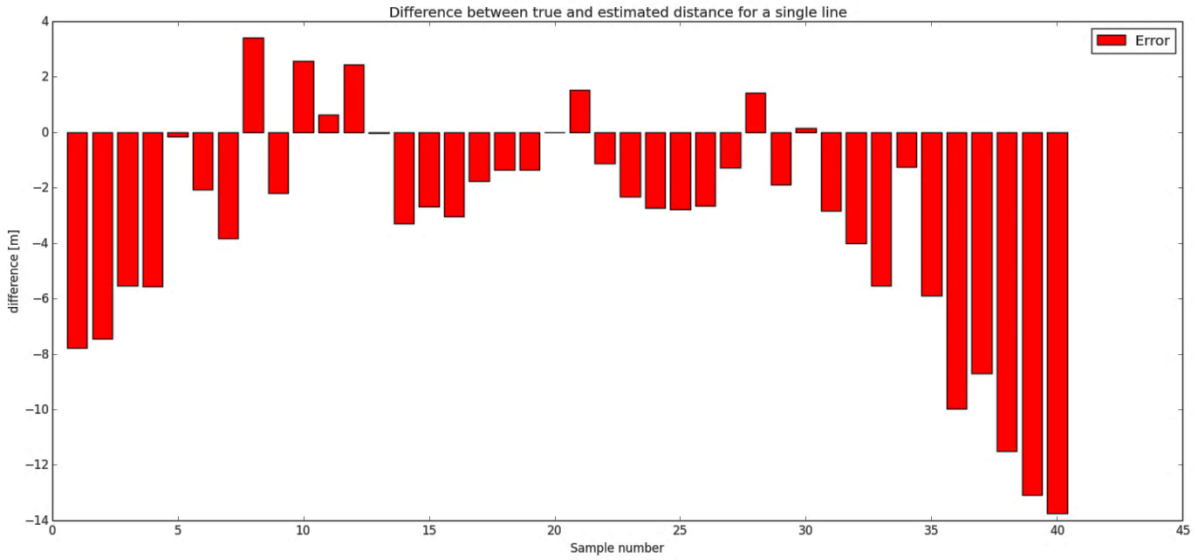

Figure 67 Difference between true distance and that predicted by a NN - first survey line

To confirm that the lack of precision is not associated with unknown anomalies on the first survey line, the same procedure was completed with the last survey line. The line was excluded from the NN data set and the model was checked against the distance. Figure 68 shows the difference between the true and predicted distances applied to the last survey line.

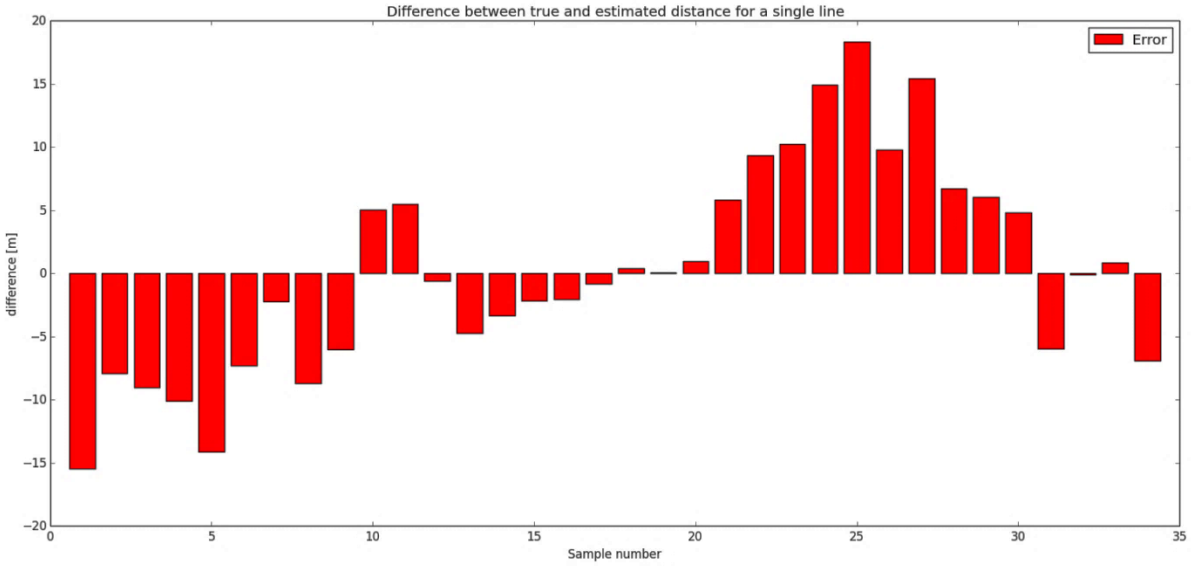

Figure 68 Difference between true and predicted distances by the NN - last survey line

The NN modelling was investigated with different parameters, size of training sets and configuration. The results led to the conclusion that the NN procedure might be difficult to apply to this particular problem to accurately predict the distance to the cable hence the burial depth.

Although it would be interesting to further investigate this method, the NN has a very important and difficult to overcome drawback. The algorithm requires a good data set as a training input. In real survey environments, the position of the cable, its burial depth and distance to the sample point are unknown. It would be difficult to collect enough, good quality data samples to build a reliable NN model.

The inverse method used in traditional cable tracking tools does not yield accurate results in detection from larger distances. Reading the distance to the utility based on exponential attenuation decay curves cannot be used except when in close proximity to the cable. In next chapter variations in the readings will be modelled with a different approach. Kalman filtering methods will be investigated to check the possibility of estimating cable positions from distances larger than those possible with the inverse methods.

Chapter 7.Cable localisation based on a family of Kalman Filter algorithms

One of the methods which was tested for improvements in the localisation of the source from noisy readings is based on the family of algorithms called Kalman filters (KF)

KF algorithms were often used for acoustic source localisation. The noisy measurements were taken by an array of sensors and the position of the source was estimated based on signal characteristics. Sturim et al. (1997) proposed to estimate the position of a sound source based on the measured time of arrival. The raw data from a sensor array was enhanced with a simple, linear KF algorithm. First, a model of the talker's motion was established. Data received by two microphone arrays gave a raw estimate of the talker's position. The position was later enhanced with a KF algorithm giving a good approximation of the source's location.

Rullan-Lara et al. (2013) used a KF algorithm to estimate the position of a terrestrial robot based on measured radio signals. The procedure was applied to the problem where the array of radio transmitter emitted a signal read by a moving sensor. Different signal characteristics such as its received signal strength or its time or angle of arrival gave an initial estimate of the position. KF algorithms were used to filter noise from the data and use sensor fusion to achieve a better estimation. Rullan-Lara et al. (2013) pointed out that the motion and observation models were not always linear and their errors not always Gaussian. In such case extended or unscented KFs can be used.

Another example of the use of KF algorithms can be found in underwater navigation. Batista et al. (2011) measured the range to a single source and the relative velocity readings of a moving agent to estimate its location. They focused on the estimation of linear motion quantities to describe precisely the moving agent's position. The derivation of a linear time varying system provided a way to use a standard KF to improve the location estimate.

In those examples, the KF algorithm was used to filter the noise and enhance prediction in the next step. The state was estimated by forward projection and its correction was based on feedback from the current measurement. It received only an input coming from a measurement z at time step k and it outputs an

estimate of the state variable x as $\hat{x}_k$. A flow diagram describing all the steps in a simple KF computation is shown in Figure 69.

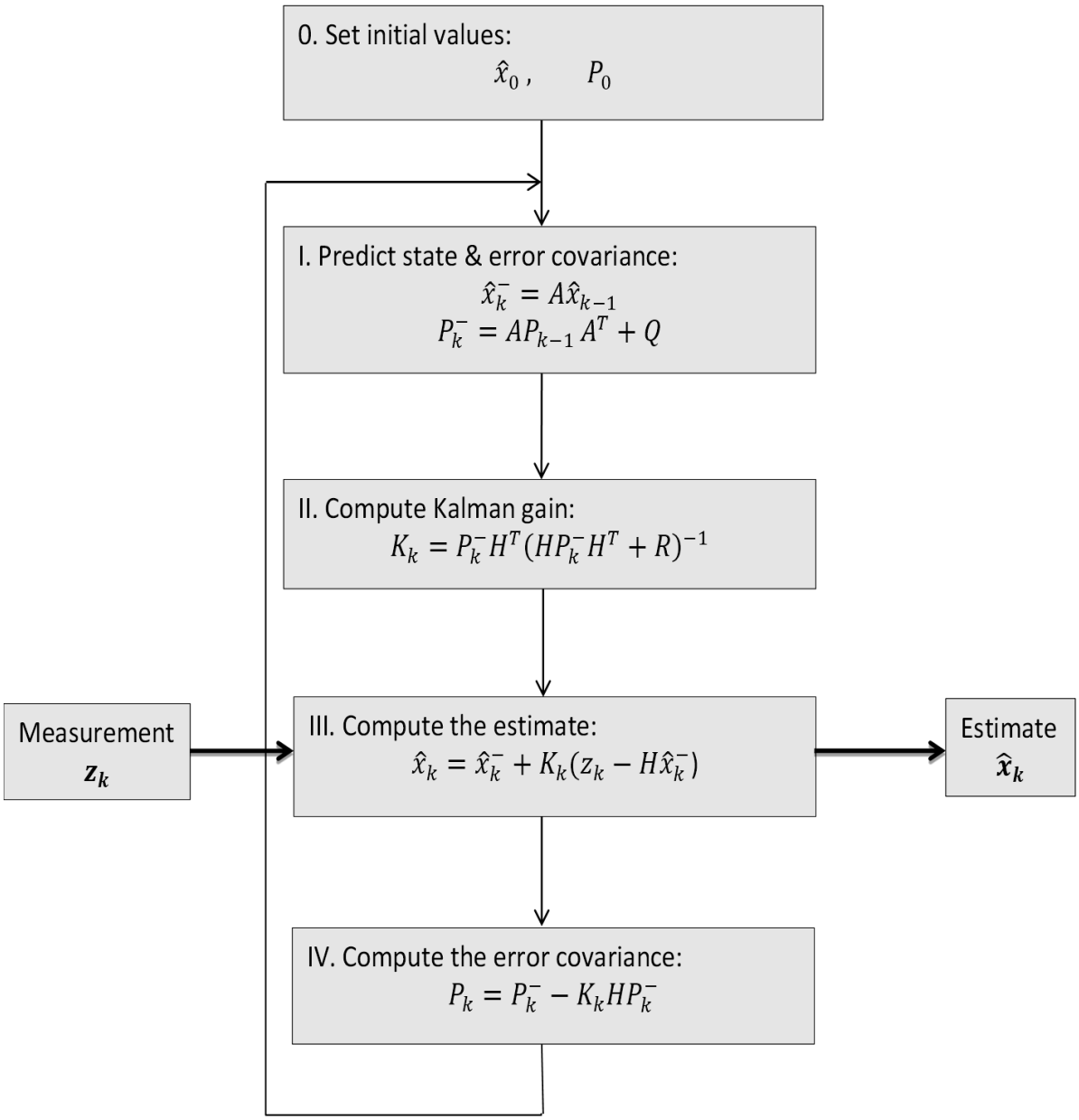

Figure 69 Kalman Filter Algorithm (Kim, 2011)

where $\hat{x}_0$ and P_0 are the initial state and error covariance, $\hat{x}_k^-$ and P_k^- are predicted values of the state variable and error covariance at time step k, and P_k is a computed error covariance. The matrices A, Q, H and R are the system model parameters. The matrix A is a transition model of the system and Q is a model of the error covariance. The matrix H desribes the measurement function and R is the measurement‘s error

covariance. The variable K_k is the Kalman gain corresponding to the relative importance of the estimate's error with respect to the prior estimate (Kim, 2011).

Implementation of the KF is based on the correct identification of the system model. Two main elements of the model describe the way in which the model evolves in time and how the measurements from the sensors relate to the actual system state.

In real world applications building linear system models proved to be difficult. The family of KF algorithms provides versions which can be used in such situations.

The simplest solution is to linearise the system model and use the procedure called linearized KF (LKF) (Kim, 2011). LKF uses the same filtering algorithm as the standard KF but instead it focuses on linearisation of the model. The problem with this solution is that the linearised system is close to its non-linear counterpart only around the point at which it was linearised.

Another possibility to deal with nonlinear transfer functions is to use the extended KF (EKF). It also derives a linear model by linearising the nonlinear model but it uses the state estimate as a reference point. The EKF gradually expands the linear algorithm. The linearisation is provided by partial differentiation of the system functions in the proximity of the current state by use of the previous estimate.

Linearisation can be difficult and give undesired results. The procedure that helps to eliminate this problem is to use the unscented KF (UKF). Instead of manipulating a nonlinear transfer function, it uses an unscented transformation where a set of carefully chosen points (Sigma Points) are projected through an unchanged system model.

The unscented transformation has the ability to propagate the mean and covariance information through nonlinear transformations (Julier & Uhlmann, 2004). The probability distribution is easier to approximate than an arbitrary nonlinear function or transformation. The set of sigma points is chosen to have a known mean and covariance. The nonlinear function is applied to each point transforming them to a cloud of new points. The new mean and covariance can be calculated again from the transformed set of points.

The algorithm of the UKF is presented in Figure 70. The algorithm is similar to the standard KF described before as it has three major parts: prediction, computing the Kalman Gain, and estimation. The only

difference is that it accepts nonlinear transfer functions and uses Sigma Points to compute the prediction and error covariance.

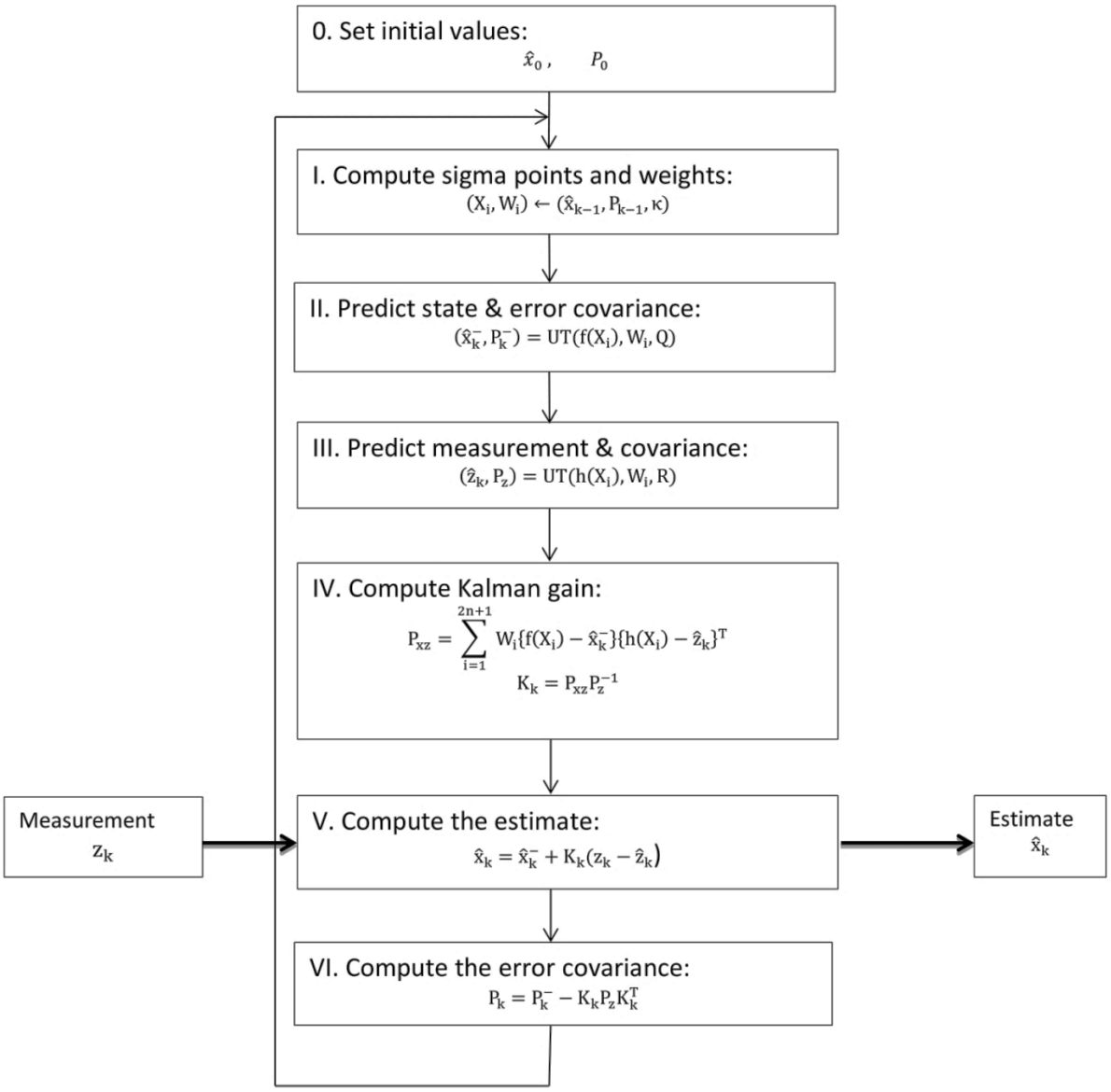

Figure 70 Unscented Kalman Filter Algorithm (Kim, 2011)

After initialisation, the sigma points X_i and their weights W_i are computed based on the previous estimate, where κ is an arbitrary constant. In the next step the state and error covariance are predicted by means of the UT. The same procedure is applied to the measurement function. Given all the information the covariance matrix P_{xz} of the state vector x_k, measurement z_k and Kalman gain K_k are computed. In the last two steps the new estimate and error covariance are calculated.

Both the standard and unscented KF algorithms will be used to investigate possible application to the problem of cable localisation.

7.1 Kalman Filter two-dimensional prediction based on theoretical model

During marine surveys the electromagnetic cable tracking is combined with the use of other sensors to effectively use the available resources and boat's offshore time. Often in such cases, the boat or other survey platform is kept perpendicular to the utility line and crosses the cable path. The sample points are taken along the line. In such a setup the cable tracking can be considered in two dimensions.

For a simplified two dimensional model it can be assumed that the next source estimation depends only on the distance travelled by the sensors and the noise coming from the reading of the position readings.

Sensors' readings depend on the distance from the source and angle to the source. The trigonometric relations of the angle correspond to coils' readings. The cosine of the angle relates to horizontal readings and sine of the angle relates to vertical readings. The readings are corrupted by the sensors' noise as well as the roll, pitch and yaw of the vehicle.

For a two-dimensional model, every data point measures the MF from the same source. The initial estimation of the source position is corrected with every data point fed into the system.

In this case, the coordinate system can be defined as follows: the x-coordinate along the survey platform path, and the y-coordinate as the depth, the vertical distance to the source. The z-coordinate is equal to zero and can be omitted. The starting point for the platform movement is taken as the origin of the coordinate system.

Following Biot and Savart's law, the MF from the source point ($S_x,\ S_y,\ S_z = 0$) is calculated as a function of the electric current and the distance. In addition, the attenuation depends on the attenuation factor (A).

The MF H for each sample point ($P_x,\ P_y = 0,\ P_z = 0$) is given by:

$$H = \frac{A * I}{\left(\sqrt{(P_x - S_x)^2 + (S_y)^2}\right)^3}\ 100\% \qquad (43)$$

where *I* stands for the electric current induced in the cable and *A* is the attenuation factor. The signal is expressed as a percentage of the strength of the field at the source point.

The MF is read by a horizontal coil C_H and vertical coil C_V.

$$C_H = H * \cos\alpha \quad (44)$$

$$C_V = H * \sin\alpha \quad (45)$$

where α is the angle between the water surface $y = 0$ and the tangent of the circle with radius equal to the vector pointing from the source to the sample point. The simulation setup was previously shown in Figure 59.

The first requirement for KF implementation is to describe the system in terms of a mathematical model. Physical knowledge of some facts about the system can be built into a Grey-Box model. It describes a physical phenomenon but certain parameters are still unknown (Ljung, 2013). Following this advice, a simple mathematical model was built based on physical properties of the problem.

The MF in the two-dimensional case comes from a single source. The position of the source is the underlying cause of the MF and the signal measured by sensors. The position of the source can be regarded as a state variable and can be expressed as:

$$x_k = \begin{bmatrix} S_x \\ S_y \end{bmatrix} \quad (46)$$

When the survey platform moves perpendicularly to the cable, the MF source does not change its location. The state transition matrix for this case is

$$A = \begin{bmatrix} 1 & 0 \\ 0 & 1 \end{bmatrix} \quad (47)$$

Thus the next source location should be the same as in the previous step.

$$x_{k+1} = Ax_k + w_k = \begin{bmatrix} 1 & 0 \\ 0 & 1 \end{bmatrix} \begin{bmatrix} S_x \\ S_y \end{bmatrix} + w_k = \begin{bmatrix} S_x \\ S_y \end{bmatrix} + w_k \quad (48)$$

The measurement is taken by two coils where one coil is placed vertically and the second coil horizontally to the vector of the MF $\boldsymbol{B}$. The measurement z_k is given by the signal strength and the function of the angle between the direction of the coil and vector B

$$z_k = h(x_k) + v_k = \begin{bmatrix} H * \cos(\alpha) \\ H * \sin(\alpha) \end{bmatrix} + v_k \quad (49)$$

where H follows equation (43) and the trigonometric functions are defined as follows:

$$\cos(\alpha) = \frac{P_x - S_x}{\sqrt{(P_x - S_x)^2 + (S_y)^2}} \quad (50)$$

$$\sin(\alpha) = \frac{S_y}{\sqrt{(P_x - S_x)^2 + (S_y)^2}}$$

The above equations were adapted to the KF algorithm. First, the algorithm was initiated with some arbitrary values of initial state x_0 and the error covariance P_0. After initialisation the algorithm was iterated over the data points. In the iteration process each prediction and Kalman gain in the current step were computed based on the source position and parameters from the previous step. After applying the measurement's correction, the current iteration loop gave a new estimate and led to computing new error covariance. This information was fed to a new iteration loop and a new data point is processed in the iteration.

The system was tested in simulation and on empirical data from Denmark's experiments. The algorithms were verified with different parameters and trial and error investigation. The procedure led to the following conclusions.

The system is very sensitive to the initial data. Even a careful choice of initial matrices does not guarantee acceptable performance. Figure 71 and Figure 72 show the performance of the same algorithm tested in

simulation on two different sets of random noise incorporated in the position and the horizontal and vertical readings.

The parameters of the system model for the KF algorithm are presented in (51)

$$A = \begin{bmatrix} 1 & 0 \\ 0 & 1 \end{bmatrix}, \quad P_0 = \begin{bmatrix} 1 & 0 \\ 0 & 1 \end{bmatrix}, \quad Q = \begin{bmatrix} 0.13 & 0 \\ 0 & 0.001 \end{bmatrix}, \quad R = \begin{bmatrix} 5 & 0 \\ 0 & 1 \end{bmatrix} \qquad (51)$$

The true source position is at the point $[100, -10]$, the starting point is one-third of the way along the line and 2 metres deeper at $\hat{x}_0 = [65.934850, -12.000000]$. In the first presented figure the estimation is inaccurate by 0.13 m along the platform's path and 0.03 m along the depth measurement. Such an error would be perfectly satisfactory in a real world application.

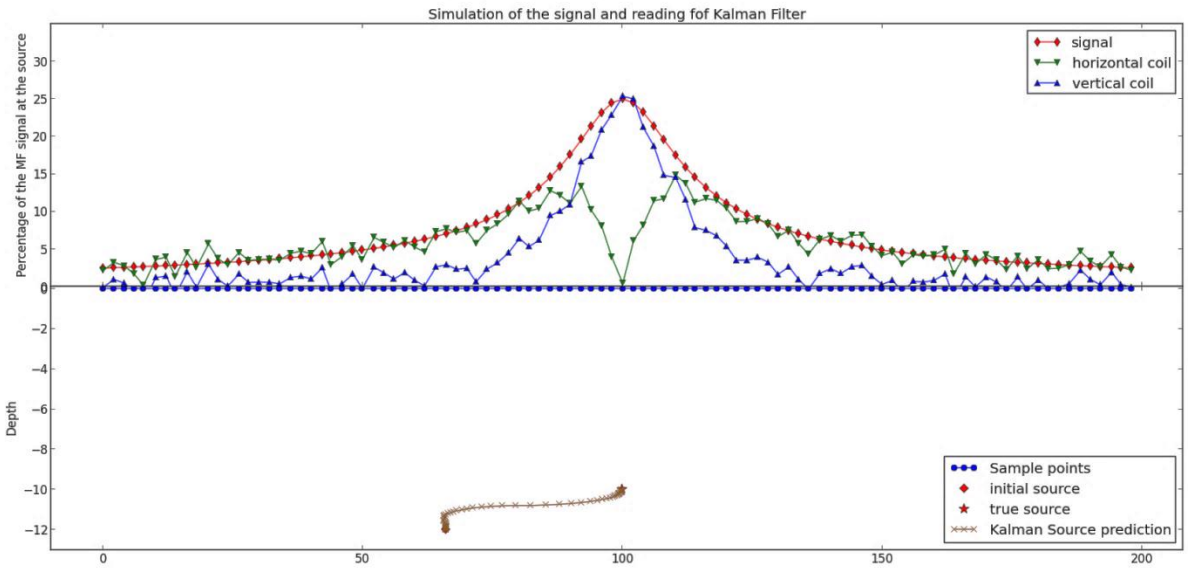

Figure 71 Kalman filter for salinity 1.5

The final estimate is presented in equation (52) as the algorithm's output for the state variable and error covariance.

Kalman starting point x=65.934850 y=-12.000000 (52)

X=
[[99.82924738]
 [-10.02952874]],

with P=
[[12.94187727 0.   ]
 [0.   1.09382416]]

The same parameters were applied to slightly changed data. Figure 72 presents different random numbers incorporated into the measurement noise and change in salinity which often occurs in a real environment in shallow water. The estimate misses the true location by 3.7 m horizontally and 0.2 m along the depth. The final estimate is presented in equation (53).

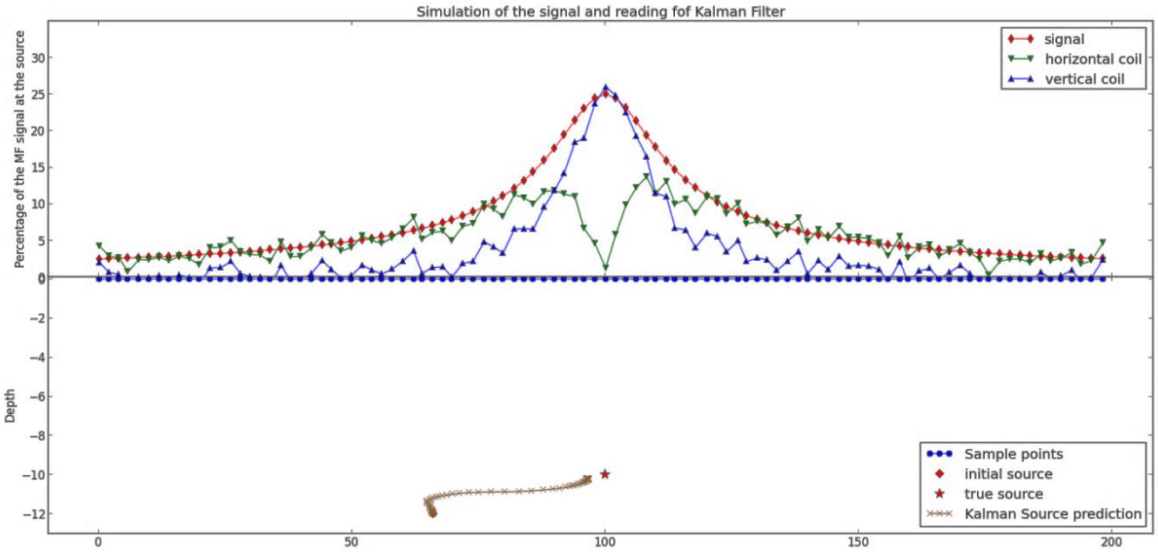

Figure 72 Kalman filter for random noise with attenuation for salinity 5

Kalman starting point x=65.934850 y=-12.000000 (53)

X= with P=
[[96.30423339] [[13.01795819 0.]
[-10.18141616]], [0. 1.0941064]]

The application of a different random noise and attenuation factor in the simulation led to a poor performance of the algorithm. Similar changes can be seen in real world tracking. To confirm such differences, a similar procedure was applied to the empirical data. For this purpose one of the lines was chosen and the model's parameters were adjusted to best fit the data. It was then applied to a different surveying line to confirm the algorithm's performance.

Although a large set of different values was tested, none led to satisfactory results and good performance for multiple lines.

The first implementation of the standard, linear KF illustrated in Figure 73 shows that the algorithm can perform source localisation.

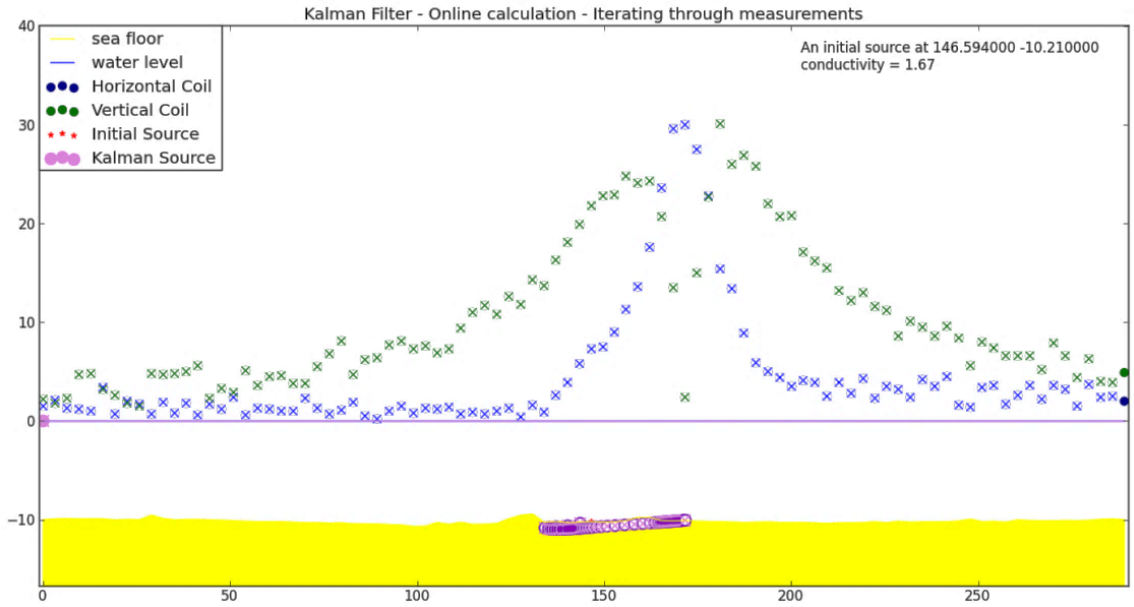

Figure 73 Computation of Kalman Filter

The algorithm was adjusted to the data obtained on line 27 in such way that the parameters were chosen to obtain the best localisation. The estimated source was in the range of 7 cm from the location reported by a diver.

The same parameters of the system model and the same attenuation were applied to line six. The output of the algorithm differed from the localisation reported by a diver by 31.25 metres.

Figure 74 shows the performance of the algorithm when the water depth was different to the previous case. In the case of different situations, the algorithm miscalculates the location of the source.

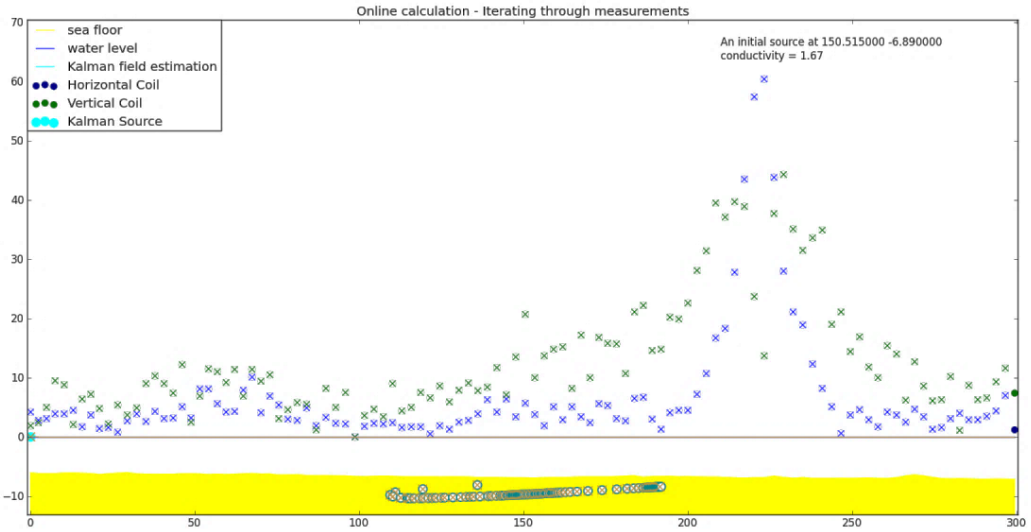

Figure 74 Computation of Kalman Filter - bad performance

The investigation shows how challenging it can be to track a cable by modelling the parameters and applying the KF algorithm. The localisation is possible only with well-chosen parameters and is very sensitive to the model.

In the following section, the family of KF algorithms will be further investigated. To start with, the underlying model will be developed as a set of linear equations with a single input and a single output and the KF algorithm will be exercised to improve model prediction. Further, the model will extend to a nonlinear description with multiple inputs and outputs and a UKF will be adopted to improve cable tracking.

7.2 Implementation of the Kalman filtering algorithm with Black Box modelling

Physical modelling of the system is not the only option to describe relationships between cause and effect. Mathematical models of dynamical systems can be deduced from observed input and output signals. In Black Box modelling there is no physical insight or interpretation (Ljung, 2013; Ljung & Chen, 2013). The model can be built from a parameterized collection of models describing relations in input and output signals. It allows predicting the output at time t based on observations of previous input-output data up to time $(t-1)$.

Linear systems can be modelled by a transfer function $\boldsymbol{G}$ relating the input and output, and a transfer function $\boldsymbol{H}$ modelling the relationship between a white noise source e and the output disturbances. The model $M(\Theta)$, where Θ are particular parameters, can be described by equation (54). It provides a rule to predict the one step ahead output $y(t)$.

$$y(t) = \boldsymbol{G}(q, \Theta)u(t) + \boldsymbol{H}(q, \Theta)e(t) \quad (54)$$

where $u(t)$ and $e(t)$ are the input signal and its corresponding white noise respectively, Θ is a set of parameters and $\boldsymbol{G}$ and $\boldsymbol{H}$ are transfer functions described in following equation:

$$\boldsymbol{G}(q, \Theta) = \frac{B(q)}{F(q)}; \quad \boldsymbol{H}(q, \Theta) = \frac{C(q)}{D(q)} \quad (55)$$

For a linear autoregressive model with exogenous inputs (ARX), polynomials F and D are equal ($F = D = A$) and $C = 1$. The model becomes:

$$A(g)y(t) = B(q)u(t) + e(t) \quad (56)$$

For the purpose of estimation of the distance to the cable, the model of the system was built based on existing data. With the cable's magnetic field sampled with a period of 1Hz, the relationship between successive readings and the distance to the cable was modelled as a discrete-time dynamic system. A linear ARX model was fitted to the data leading to the following state-space description

$$x_{k+1} = \mathrm{A}x_k + Bu_k \quad (57)$$

$$y_k = \mathrm{C}x_k + Du_k + v_k$$

where x_k is the state vector of the system at time step k. The state x_{k+1} at time step $k + 1$ depends on the previous state and the input to the system u_k which are the readings from the horizontal coil. The term v_k stands for noise related to the input and it is assumed to be white.

The variable y_k is the output of the system. The output represents the distance to the cable in metres. The output y_k depends on the state of the system and its input.

For the KF the input to the system follows equation (30). The horizontal coil reading can be related to the output via

$$H_C = f(d) = a/d^3 \quad (58)$$

where d is the distance to cable and a is some constant of attenuation rate. Equation (58) leads to the measurement function:

$$d = f^{-1}(H_C) = \sqrt[3]{a/H_C} \quad (59)$$

The above equations (57) are used for the KF algorithm and equation (59) to simulate the distance based on known H_C. The data with known cable position was split into two parts. The first part was used to obtain the model and the second part was used to validate the KF results.

Three different cases were analysed and three different models were obtained. All of them are based on a single input, single output (SISO) model and enhanced with the standard KF algorithm. The first case is when the surveying boat crosses the known cable points. The second case is when the surveying boat crosses the known cable's line and only samples due to the cable's presence are analysed. The third case is when the surveying boat moves along the cable, sampling directly above the cable.

7.2.1 Case 1: Single Line

Data from one of the lines were fed to the system as the training line for the system parameters. Based on the horizontal coil's reading and known distance to the cable the best ARX model was one with three poles, one zero and one step delay:

$$A(z) = 1 - 1.584\,z^{-1} + 0.2434\,z^{-2} + 0.3399\,z^{-3}$$

$$B(z) = 1.789\,z^{-25} \qquad (60)$$

The ARX model leads to a state-space model, which in this case gives:

$$A = \begin{vmatrix} 1.584 & -0.2434 & -0.6798 \\ 1 & 0 & 0 \\ 0 & 0.5 & 0 \end{vmatrix}$$

$$B = \begin{vmatrix} 1 \\ 0 \\ 0 \end{vmatrix} \qquad (61)$$

$$C = |1.789 \quad 0 \quad 0|$$

$$D = |0|$$

The one step ahead prediction from the model is shown in Figure 75. The right side of the figure shows the overall distance to the cable and the left side shows the difference between the model prediction and true distance to the cable.

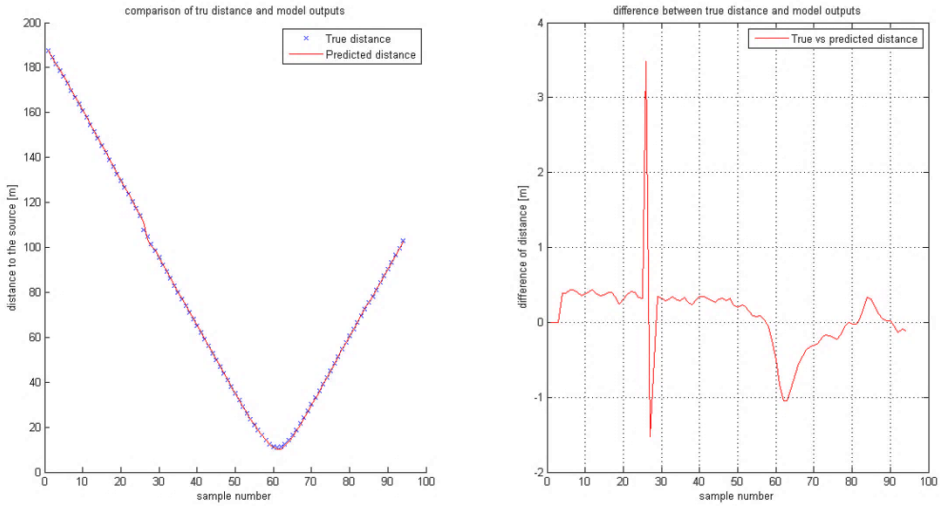

Figure 75 One step ahead prediction with ARX model

The measurement equation requires an attenuation factor a. To obtain the attenuation the output of the coil was compared with the theoretical output with a different attenuation rate. Least squares was performed only on the outputs exceeding a value of 0.1 mV, which in practice discriminates the voltages caused by the cable from voltage caused by noise. After this calculation the attenuation rate was set to 256 for this particular line.

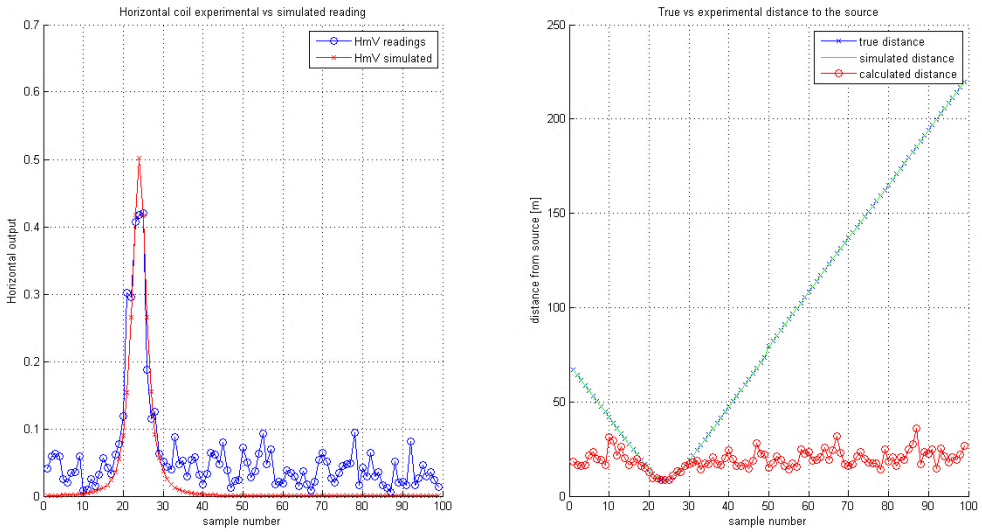

Figure 76 Experimental and theoretical coil's output and inverse distance calculation

The left side of Figure 76 shows an inverse calculation by means of equation (59). The inverse method shows a good fit to the distance to the cable in the area between the 10th and 32nd sample. This range of samples corresponds to a 50 metres section of the survey path. It suggests that the response of the coil is caused by the cable's presence. The rest of the readings are caused by noise only.

The attenuation rate for different lines is not a constant value. It depends on two major components. One is water salinity related to its density, temperature and other difficult to control factors. The second is the initial magnetic field at the sampling source.

To illustrate this dependency two other lines were plotted in Figure 77. The attenuation factor is rarely known beforehand and it can be obtained after the distance to the source has been calculated.

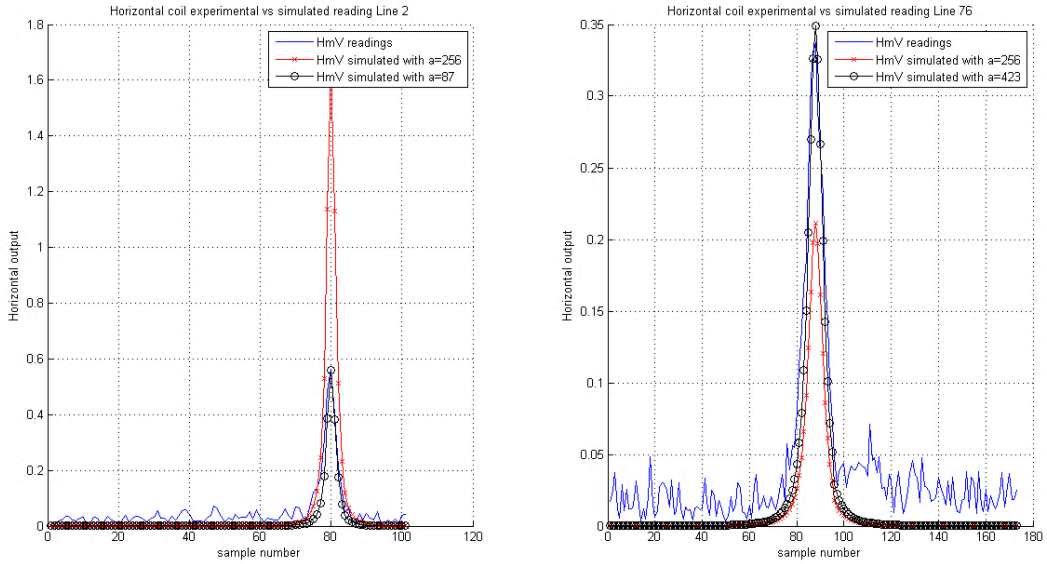

Figure 77 Comparison of attenuation for Line 2 with a = 87 and Line 76 with a =423

Information obtained from the training line was validated on a different survey line. To improve the distance estimation the KF was implemented on the ARX model (60). For the algorithm the state-space model (61) was used. In the survey situation, the precise attenuation is unknown, thus the attenuation of 256 was used, the same as was obtained from the training line.

The output is shown in Figure 78. It can be noticed that the KF does not perform better than the ARX system modelling method used in prediction.

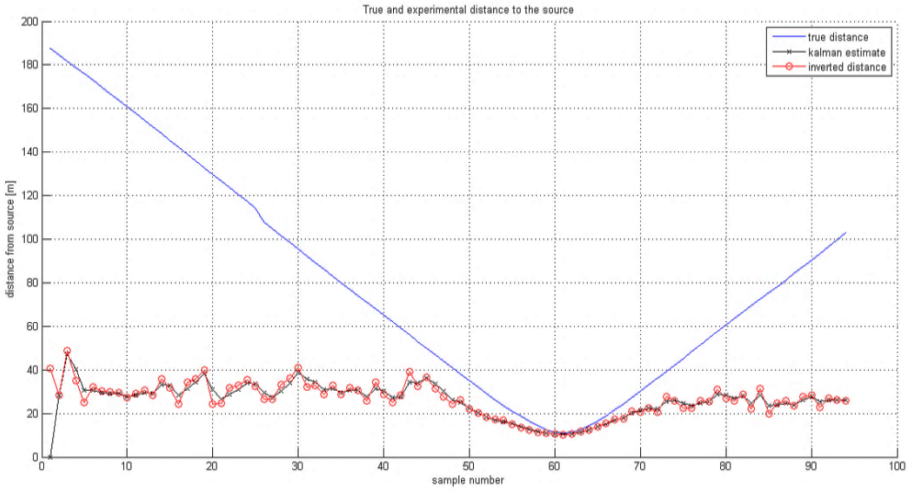

Figure 78 Kalman Filter output in comparison with inverse method and true distance

The comparison of performance between the KF and the inverse method shows no significant improvement between the two methods. Figure 79 shows the difference between the true distance and the distance estimated by both methods. The KF yields a very similar estimate as that given by the inverse method.

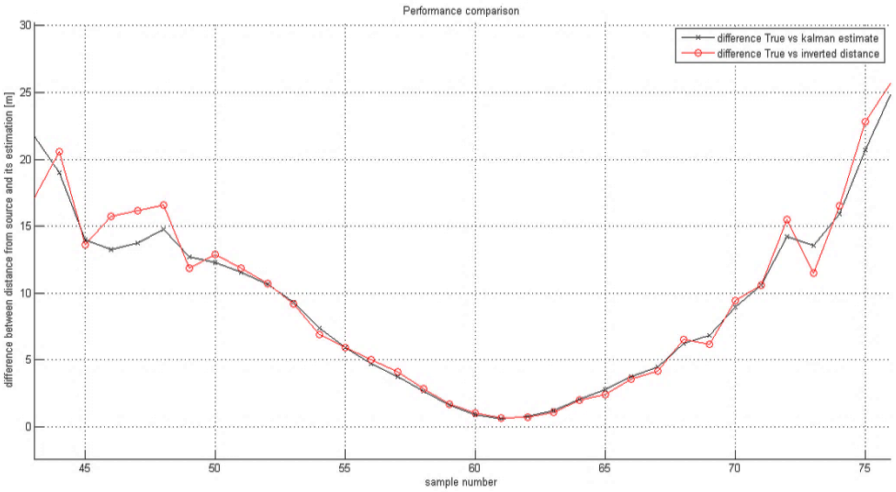

Figure 79 Difference between true distance and its estimation

7.2.2 Case 2: Multiple crossings

Modelling for a single line yields unsatisfactory results. To overcome this limitation, the input and output to the model was extended to multiple lines and the samples were reduced only to samples whose responses are caused by the cable's presence and not only to the coil's noise.

The presented model was built with six consecutive lines and validated on the 14 lines that followed. The motivation behind this procedure is that the cable would be first localised by a diver and later followed by a survey platform from the surface. In the real world on one dive a diver can perform localisation of a cable section about 100 m long. This value roughly corresponds to six survey lines.

The best ARX obtained model is given by:

$$\mathrm{A(z)} = 1 - 1.413\,\mathrm{z}^{-1} + 0.7662\,\mathrm{z}^{-2} - 0.2144\,\mathrm{z}^{-3}$$
$$\mathrm{B(z)} = -9.397\,\mathrm{z}^{-3} + 25.56\,\mathrm{z}^{-4} \qquad (62)$$

The ARX model in equation (62) leads to state space model for the KF:

$$\mathrm{A} = \begin{vmatrix} 1.413 & -0.7662 & 0.4288 \\ 1 & 0 & 0 \\ 0 & 0.5 & 0 \end{vmatrix}$$

$$\mathrm{B} = \begin{vmatrix} 8 \\ 0 \\ 0 \end{vmatrix} \qquad (63)$$

$$\mathrm{C} = |-1.175 \quad 3.195 \quad 0|$$

$$\mathrm{D} = |0|$$

The model's one step prediction and validation is shown in Figure 80. The difference between the true distance and estimated distance is as large as four metres.

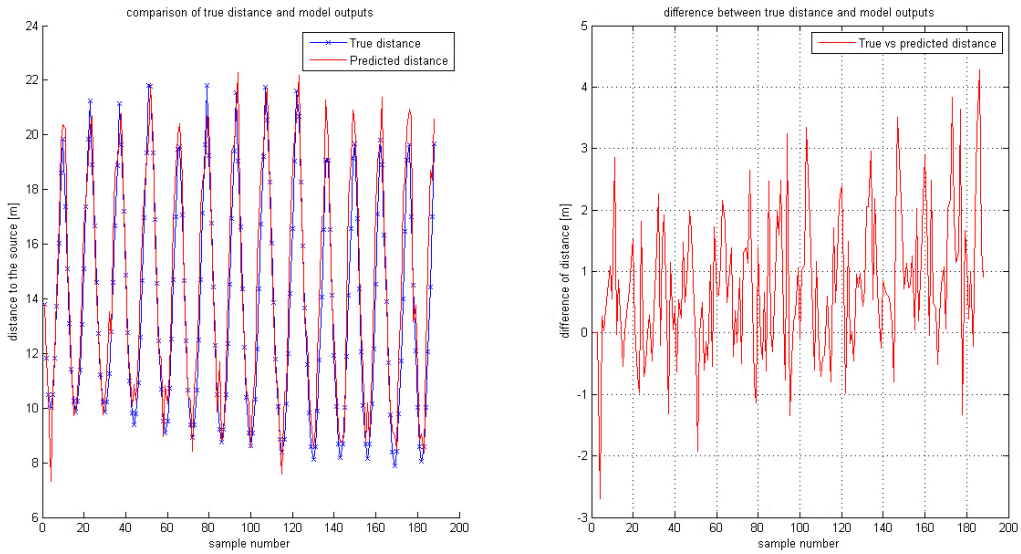

Figure 80 One step model's prediction for multiple lines

The left side of Figure 80 shows the output of the system, true distance to the cable and the distance extrapolated by the model. The right side of Figure 80 shows the difference between the true and predicted distance. It can be noticed that the model's prediction misses the distance to the cable by as much as four metres.

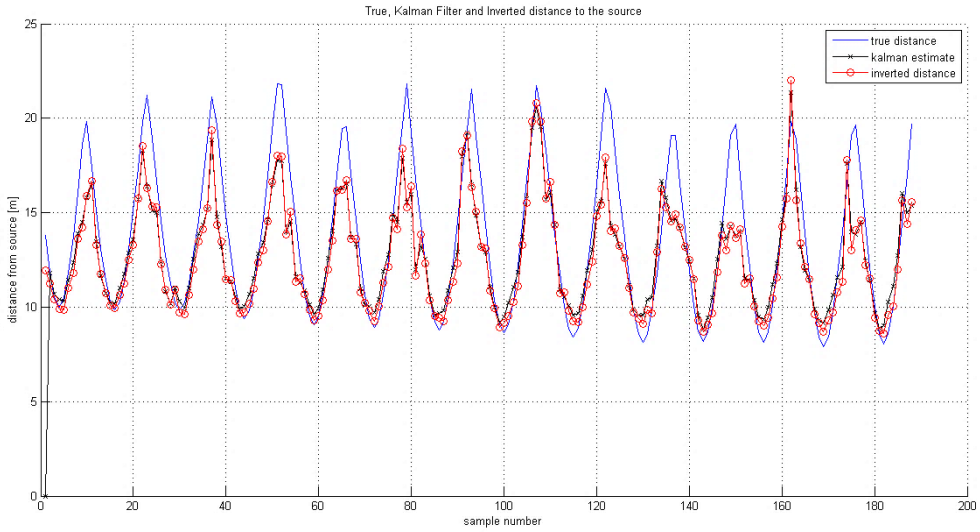

Figure 81 Kalman Filter output in comparison with inverse method and true distance for multiple lines

The model (63) was used for the KF algorithm. The output is shown in Figure 81. The estimation of the KF is very similar to that made by the ARX method.

The differences between estimation outputs from both methods and the true distance are shown in Figure 82. The KF algorithm does not perform any better than the inverse method.

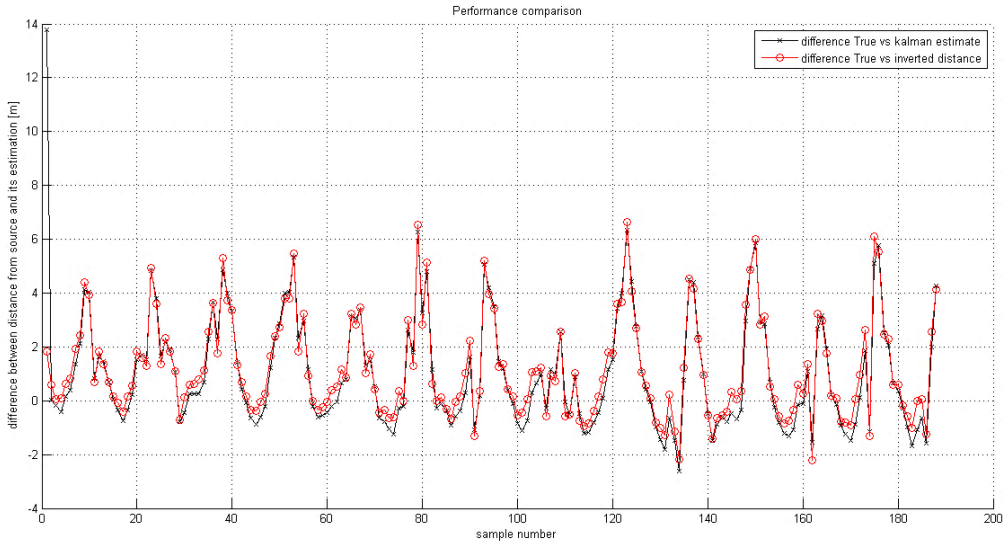

Figure 82 The difference between true distance and Kalman Filter vs Inverse method

7.2.3 Case 3: Sampling directly above the cable

In some applications tracking of the cable or pipeline is always performed by flying a surveying platform directly above the utility. The existing methods take measurements right above the cable. First, the position of the cable is assumed from the output of the coils and the burial depth measurement is taken with stationary readings straight above. A similar situation was analysed as a third case. From 76 crossing lines only the closest to the cable points were taken as inputs and outputs to the system. The model was calculated based on the first one third of the points and validated on the remaining samples.

The best ARX model obtained for the samples taken directly above the cable is given by:

$$A(z) = 1 - 0.8418\,z^{-1} - 0.2185\,z^{-2} + 0.05848\,z^{-3}$$

$$B(z) = -0.6935 + 0.5994\,z^{-1} \qquad (64)$$

The ARX model (64) gives state space model:

$$A = \begin{vmatrix} 0.8418 & 0.2185 & -0.2339 \\ 1 & 0 & 0 \\ 0 & 0.25 & 0 \end{vmatrix}$$

$$B = \begin{vmatrix} 0.5 \\ 0 \\ 0 \end{vmatrix} \qquad (65)$$

$$C = |0.03125 \quad -0.3031 \quad 0.3244|$$

$$D = |-0.6935|$$

The one step ahead prediction performance of the model is shown in Figure 83. The difference between the true distance and that predicted by the model is as large as 0.8 metres.

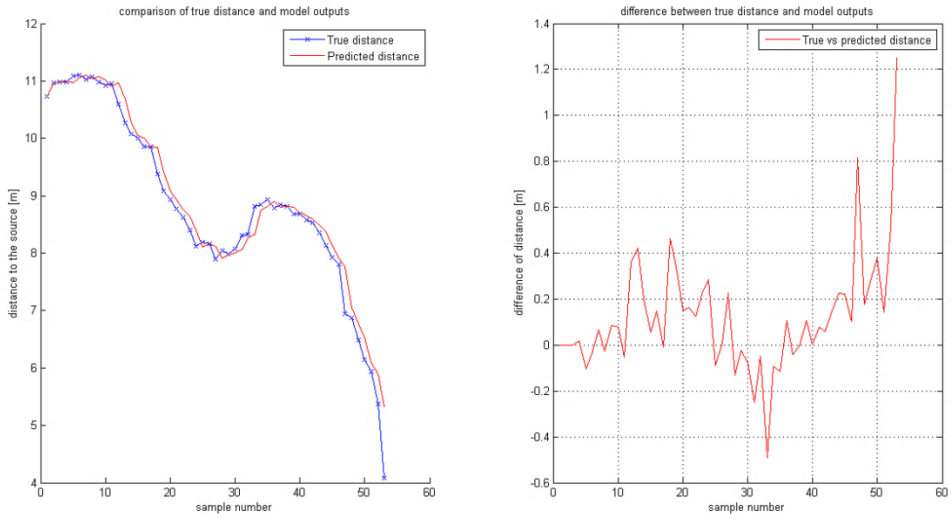

Figure 83 One step ahead model's prediction for samples above the cable

The model was used for the KF estimation. The output from the KF and the inverse method is shown in Figure 84 and the differences between two methods and the true distance are shown in Figure 85. The KF estimates converge to some distance but do not incorporate variation of the readings.

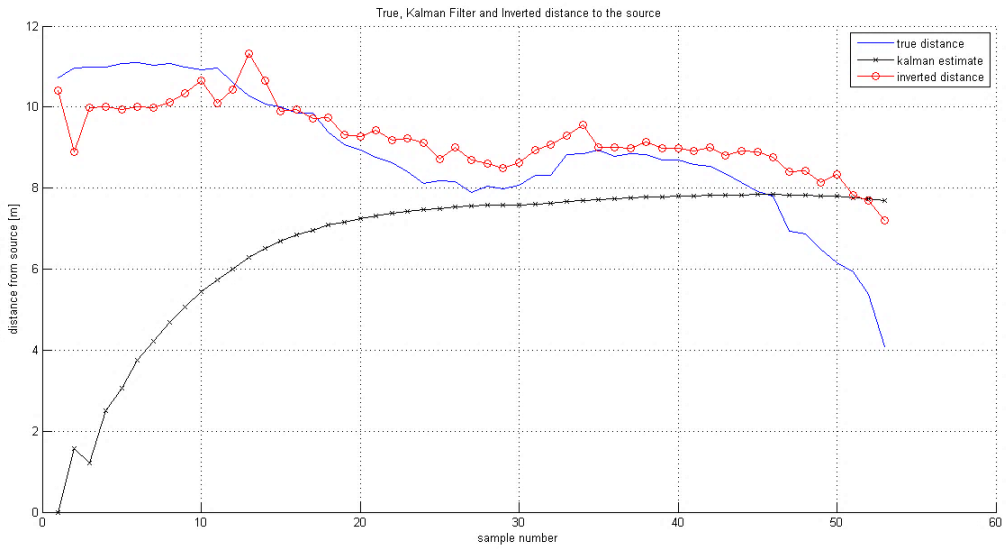

Figure 84 Kalman Filter output in comparison with inverse method and true distance for samples above the cable

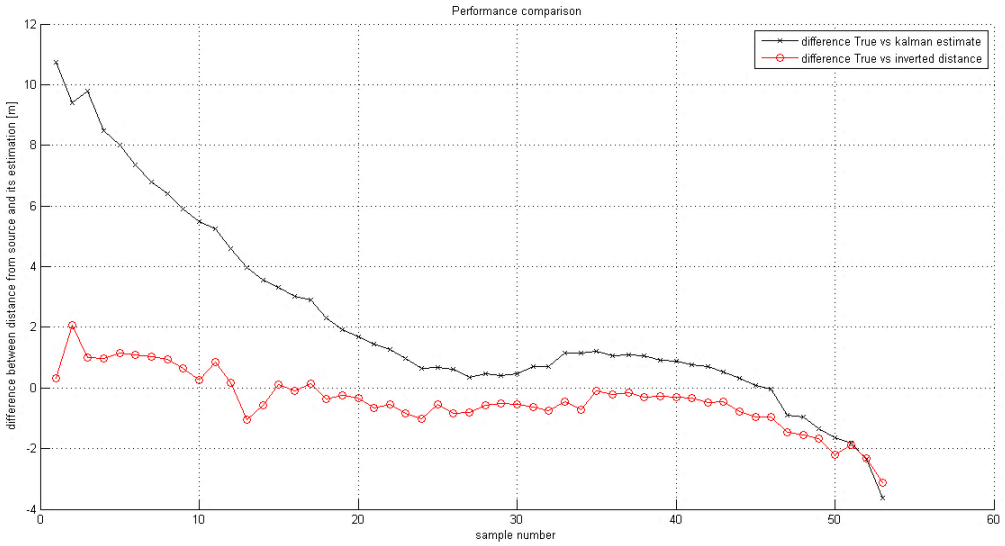

Figure 85 The difference between true distance and Kalman Filter vs Inverse method for samples above the cable

A single output, single input modelling of the system and an attempt to improve prediction by Kalman Filtering did not yield satisfactory results. In the next section, the model is extended to multiple inputs and multiple output one and includes nonlinearity in the system. For this purpose, an Unscented Kalman Filter is used.

7.3 Unscented Kalman Filter application

To further investigate KF estimation, the procedure used in the previous section was adapted to multiple inputs, multiple outputs (MIMO) systems with nonlinear measurement functions. This change required the implementation of an unscented KF with sigma points

In tracking applications, where a KF algorithm is used, the model represents one of two situations. The first one is when the observer is stationary and the object moves according to the observer's coordinate system (Sturim et al., 1997). The second situation is when the observer is moving and the parameters related to his position are updated according to the stationary coordinate system (Batista et al., 2011).

The typical, first situation is when the moving object is tracked. Examples can include tracking a moving object on the computer screen, tracking an aeroplane with the prediction of its future direction or multiple tracking of players on the football pitch.

The second situation often relates to the problem of correcting the position when the object moves but reads the location with a reference to an outside system. It can include an update of the output from the GPS positioning system or the reading from the underwater network sensors. The readings are often corrected with the output from internal sensors like gyro-compass or accelerometer.

In the first case for cable tracking applications, the input to the system was generated from combined horizontal and vertical coils output. The outputs of the system are the distance to the source, the attenuation rate and the horizontal deviation from the cable line, in other words how far from the cable's projection to the water surface, the sample was taken.

The three outputs of the system allow identifying the source of the magnetic field (MF) and resulting current in the searching coil.

In the second analysed case, the platform movement was taken as the input to the system and the coils readings were used as the measurement. In both cases to improve the estimation of the source localisation from the model, the UKF algorithm was applied to the empirical data from Denmark's experiments.

The UKF was applied to the model's prediction. During the output estimation, the state prediction (66) was compared with the measurement function relating the state to the current induced in the searching coils.

$$x_k = \begin{bmatrix} distance_k \\ attenuation_k \\ deviation_k \end{bmatrix} \quad (66)$$

The induced current read by a horizontal coil C_H and vertical coil C_V depends upon the magnetic field B and the angle between the vector of MF and the direction vector of the coil. The relations for horizontal and vertical coil readings are described in (67) and (68) respectively

$$C_H = B * \cos\alpha \quad (67)$$

$$C_V = B * \sin\alpha \quad (68)$$

where the angle α is the angle between the water surface and the tangent of the circle of radius equal to a vector pointing from the source to the sample point. The setup for the measurement function is very similar to the one used before, and is shown in Figure 86

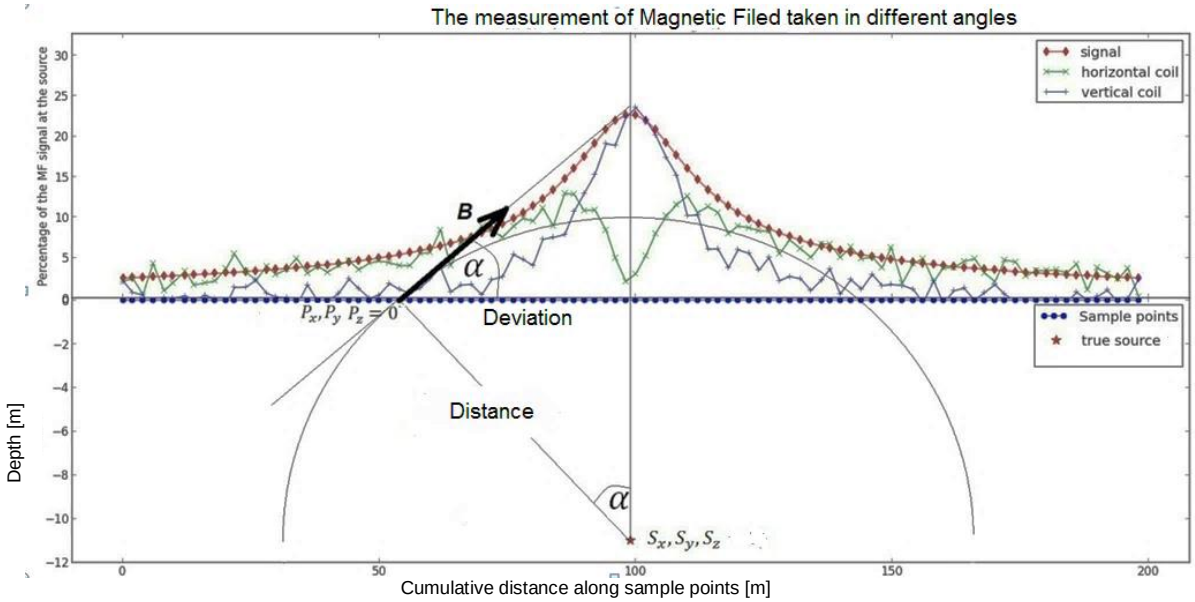

Figure 86 The measurement function setup

The measurement z_k is given by the signal strength and is a function of the angle between the direction of the coil and the vector $\boldsymbol{B}$ as in equation (69), where v_k is the measurement noise

$$z_k = h(x_k) + v_k = \begin{bmatrix} B * \cos(\alpha) \\ B * \sin(\alpha) \end{bmatrix} + v_k \quad (69)$$

The angle and its trigonometric functions are defined as follows:

$$\cos(\alpha) = \frac{\sqrt{Distance^2 - Deviation^2}}{Distance} \quad (70)$$

$$\sin(\alpha) = \frac{Deviation}{Distance}$$

The trigonometric functions give nonlinear relations and together with the nonlinear model of the system they require use of a nonlinear Kalman Filter.

7.3.1 Modelling a cable in relation to the magnetic field read by searching coils

For the purpose of testing the relation between cable position and magnetic readings, a MIMO ARX model was built. Empirical data from Denmark's survey were filtered to have only data points for which the distance to the cable projected on the water surface, i.e. "deviation", was less than 10 metres. From the filtered data, first one third of the data points were used to build a Black-Box model and the remaining lines were used to validate the model and test the UKF estimation. The estimated data were extrapolated.

With horizontal and vertical coil readings as inputs to the system the best Discrete-time ARX model obtained is given by a set of equations describing the relation between the input and the output. Equation (71) describes the dependency between the coils readings as the input and the Vertical Distance as the output. Equation (73) for input and the attenuation as the output and equation (75) for relating the input with to the deviation from the cable. Each relation requires a set of polynomials, which are presented in equations (72), (74) and (76).

Output "Vertical Distance"

$$\mathrm{A(z)}y_1(\mathrm{t}) = \mathrm{B(z)u(t)} + e_1(\mathrm{t}) \qquad (71)$$

$$\begin{aligned} \mathrm{A(z)} &= 1 - 1.274\,\mathrm{z}^{-1} + 0.4084\mathrm{z}^{-2} \\ \mathrm{B1(z)} &= 3.247\,\mathrm{z}^{-1} + 5.312\,\mathrm{z}^{-2} \\ \mathrm{B2(z)} &= 1.226\,\mathrm{z}^{-1} - 4.055\,\mathrm{z}^{-2} \end{aligned} \qquad (72)$$

Output "Attenuation":

$$y_2(\mathrm{t}) = -A_i(\mathrm{z})y_i(\mathrm{t}) + \mathrm{B(z)u(t)} + e_2(\mathrm{t}) \qquad (73)$$

$$A_1(z) = -8.646\, z^{-1} - 5.953 z^{-2}$$

$$B1(z) = 446.8\, z^{-1} + 367.8\, z^{-2} \quad (74)$$

$$B2(z) = 133.1\, z^{-1} + 167.2\, z^{-2}$$

Output "Deviation":

$$y_3(t) = -A_i(z) y_i(t) + B(z) u(t) + e_3(t) \quad (75)$$

$$A_1(z) = -2.186\, z^{-1} + 1.709\, z^{-2}$$

$$B1(z) = -4.321\, z^{-1} - 0.4342\, z^{-2} \quad (76)$$

$$B2(z) = 9.924\, z^{-1} - 8.01\, z^{-2}$$

In above equations $y_i(t)$ is the output of the system and $u(t)$ is its input. Polynomials $A_i(z)$ and $Bi(z)$ are polynomials in the delay operator z^{-i}, where i corresponds to previous data in step i.

The ARX model described by equations (71) to (76) leads to a state space model for use in the UKH. As the state-space model is only a different representation of the system, it can be found in Appendix B.1 together with a more detailed output and numerical data.

The model was tested on the remaining data. Figure 87 shows the one step ahead prediction of the model. The left side of the figure shows the true distance to the source and the distance estimated by the ARX model. The middle part depicts the attenuation factor as calculated for each single line by the least square method used before. The right part of the figure shows the true horizontal deviation from the cable and its estimation by the ARX model.

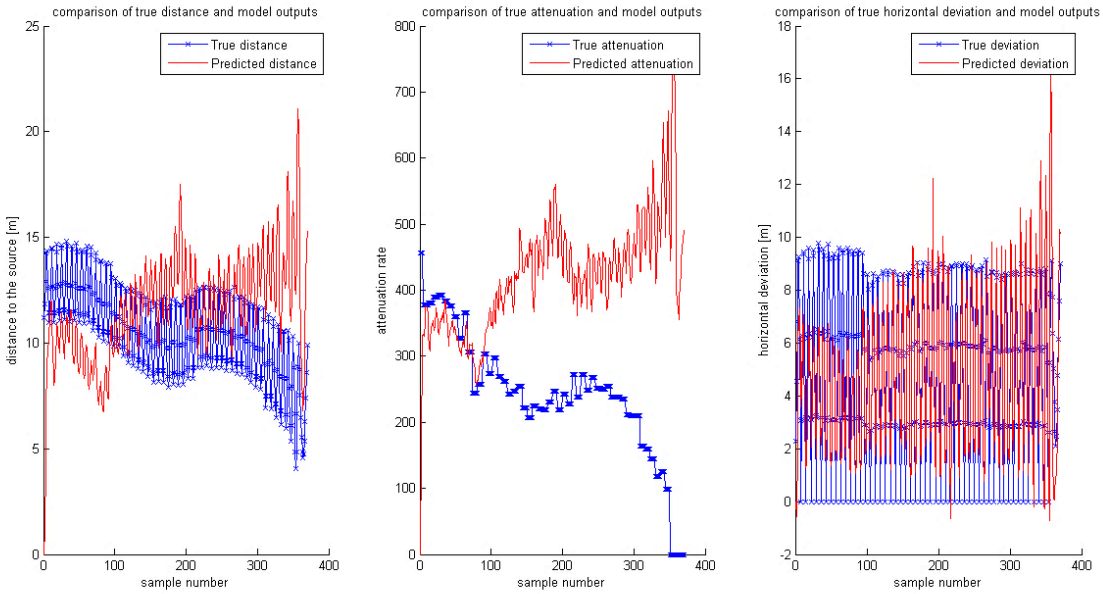

Figure 87 Simulation from the model

The estimation did not yield satisfactory results. To improve the model's output the UKF was applied, Each state estimation x_k corresponds to the distance, attenuation and deviation as result of the input to the system, horizontal coil and vertical coil readings at step $k-1$ and previous states. For each coil readings sigma points were created and transformed through the model. After transformation the Kalman gain was obtained and values of state variables were corrected accordingly.

The output from the UKF for distance, attenuation and horizontal deviation is shown in Figure 88 to Figure 90.

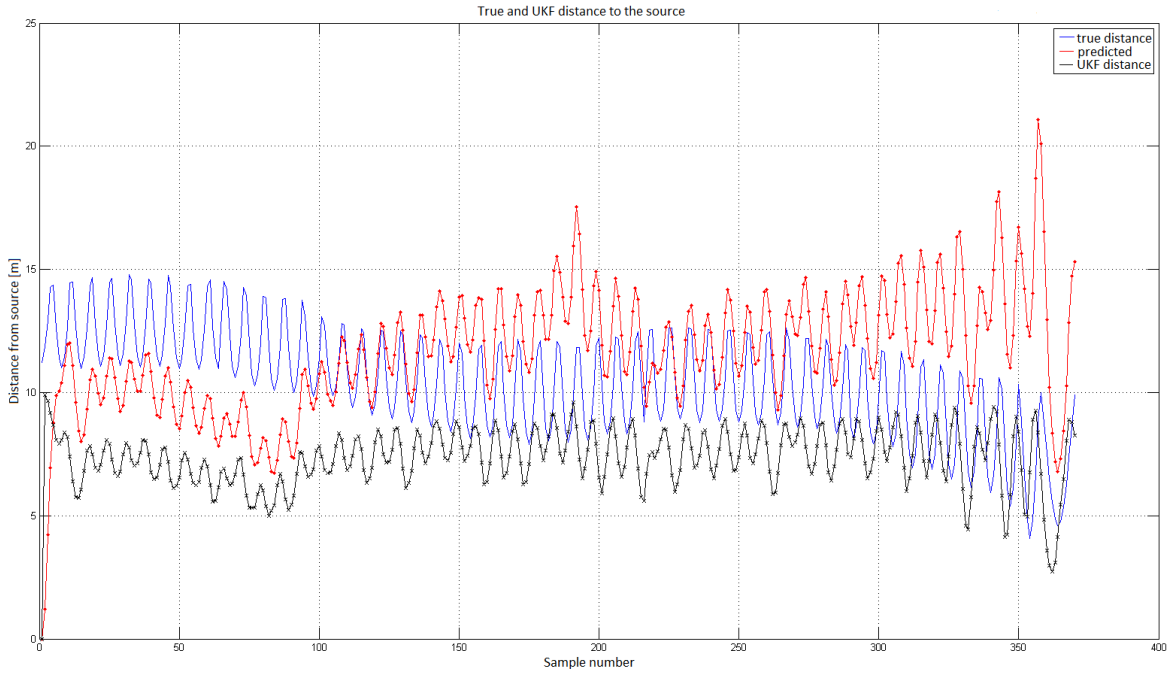

Figure 88 UKF estimation the distance to the cable

The UKF estimation does not approximate the distance to the cable better than the model prediction alone. It can be noticed that the UKF follows both the platform movement pattern and the variation of the water depth. However, comparison for the single sample points shows that the difference between the estimated distance and its true value is still much bigger than required.

The same can be said about the estimation of the attenuation rate as the output from the system. A comparison is shown in Figure 89.

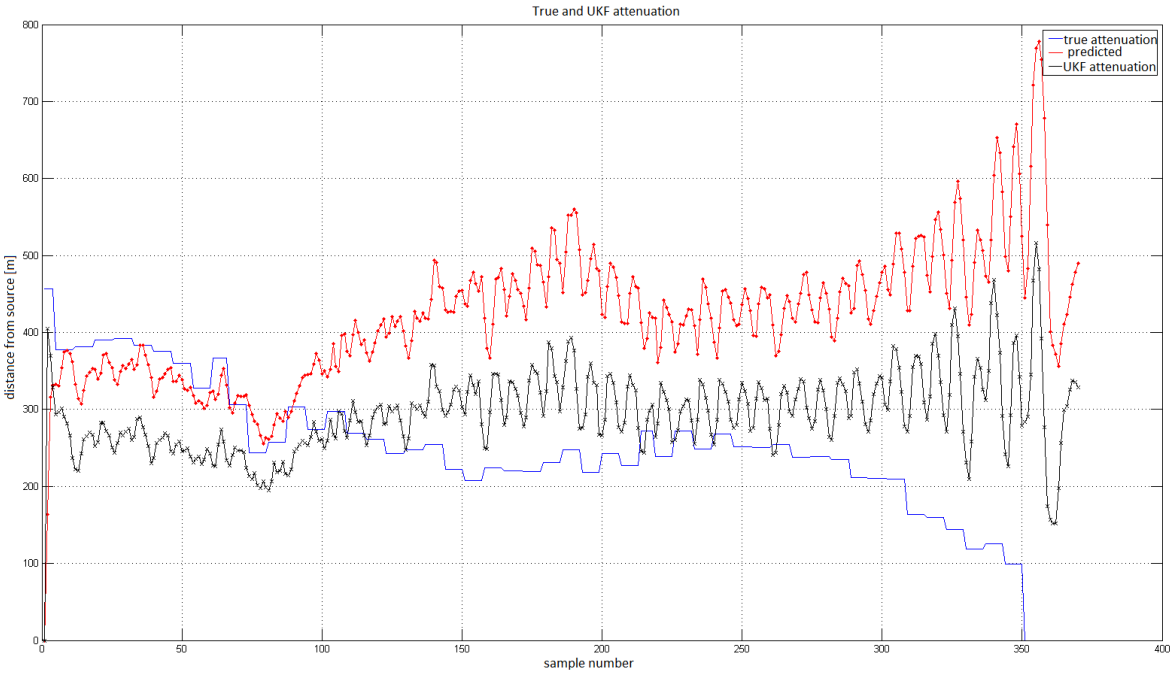

Figure 89 UKF estimation of the attenuation rate

The UKF prediction of the attenuation rate shows that UKF diverges from the true attenuation rate.

Similarly, the true deviation was compared with the ARX output and UKF estimation. The outcome is shown in Figure 90.

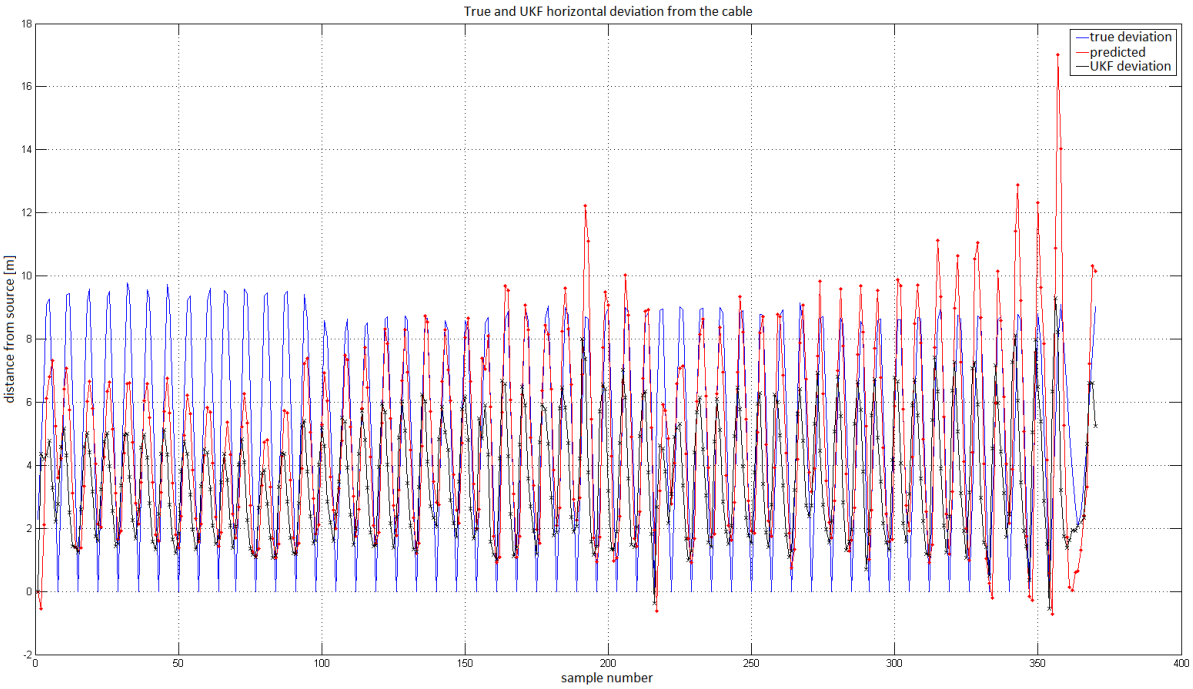

Figure 90 UKF estimation of the horizontal deviation

The UKF estimation of the horizontal deviation from the projection of the cable follows the true pattern better than the model alone. Again it is worth noticing that for a single sample point the estimation rarely gives the value close to the true deviation.

Although some improvements can be noticed, the UKF algorithm did not perform cable localisation with satisfactory results. To fully investigate cable tracking in the next section the model will be built with different assumptions.

7.3.2 Modelling a cable in relation to a platform's position

Modelling of the cable position in relation to magnetic field sampled by the coils does not yield satisfactory results. In this section the path of the platform, distance moved between sample points and direction of the platform are taken into account.

In tracking the submarine cable, the surveyor's boat is moving along the assumed path of the cable. The MF read at every sample point is a result of the moving charges, where the dominant component of MF vector comes from the point on the cable, closest to the sample point on the surface.

The MF at every sample point originates from a different point along the cable. The model of tracking investigated in this section incorporates both the movement of the survey platform from where the reading is taken and the change in the source position as the platform moves along the cable.

The movement of the boat is taken through GPS readings, which is a standard practice during marine survey procedures. Before the survey is undertaken the survey plans contain a grid and some assumption of the position of the surveyed utility. The movement of the boat can be described in terms of the spatial components of the vector pointing from one sample point to the next one.

Describing the survey platform and the position of the cable in one coordinate system allows projecting the platform's movement vector on the direction of the cable. This projection can give an *a priori* estimation of the next source point for the sample and thus, it gives an *a priori* position of the cable.

For the purpose of modelling, the boat movement was characterised by the distance travelled between sample point P_{k-1} and point P_k.In addition to the distance the, heading of the boat as the angle with respect

to magnetic North was calculated. Such characterisation allows fully reproducing the boat's path and representing its movement.

The underlying motivation for this procedure relies on the assumption that the MF read by the sensor depends on the distance from the cable line and the angle between the cable's direction and direction of the heading, hence searching coil. Modelling of data based on a large set of samples gives the possibility to build a well-fitted model and predict the source position at the current time step knowing the distance travelled and the change in heading from the previous time step.

The information about the boat path and heading were fed to the MIMO ARX modelling algorithm as inputs. Similar to before the outputs of the system are the Distance, Deviation and Attenuation. The underlying functions and corresponding polynomials are presented in equations (77) to (82).

Output "Distance"

$$\mathrm{A(z)}y_1(\mathrm{t}) = \mathrm{B(z)u(t)} + e_1(\mathrm{t}) \qquad (77)$$

$$\begin{aligned} \mathrm{A(z)} &= 1 - 1.318\,\mathrm{z}^{-1} + 05792\,\mathrm{z}^{-2} \\ \mathrm{B1(z)} &= 0.09624\,\mathrm{z}^{-1} + 0.1272\,\mathrm{z}^{-2} \\ \mathrm{B2(z)} &= 1.659\,\mathrm{z}^{-1} - 0.05871\,\mathrm{z}^{-2} \end{aligned} \qquad (78)$$

Output "Attenuation":

$$y_2(\mathrm{t}) = -A_i(\mathrm{z})y_i(\mathrm{t}) + \mathrm{B(z)u(t)} + e_2(\mathrm{t}) \qquad (79)$$

$$A_1(z) = -0.568\,z^{-1} - 12.29\,z^{-2}$$

$$B1(z) = 2.039\,z^{-1} + 2.835\,z^{-2} \quad (80)$$

$$B2(z) = 56.37\,z^{-1} + 24.93\,z^{-2}$$

Output "Deviation":

$$y_3(t) = -A_i(z)y_i(t) + B(z)u(t) + e_3(t) \quad (81)$$

$$A_1(z) = -2.599\,z^{-1} + 2.068\,z^{-2}$$

$$B1(z) = -0.04084\,z^{-1} - 0.072\,z^{-2} \quad (82)$$

$$B2(z) = 0.2589\,z^{-1} - 1.009\,z^{-2}$$

Similar to the previous problem, the state space model with more information about the outputs is presented in Appendix B.2.

The system allows validating the model on the remaining data points. Figure 91 shows a comparison of true values and those simulated by the model.

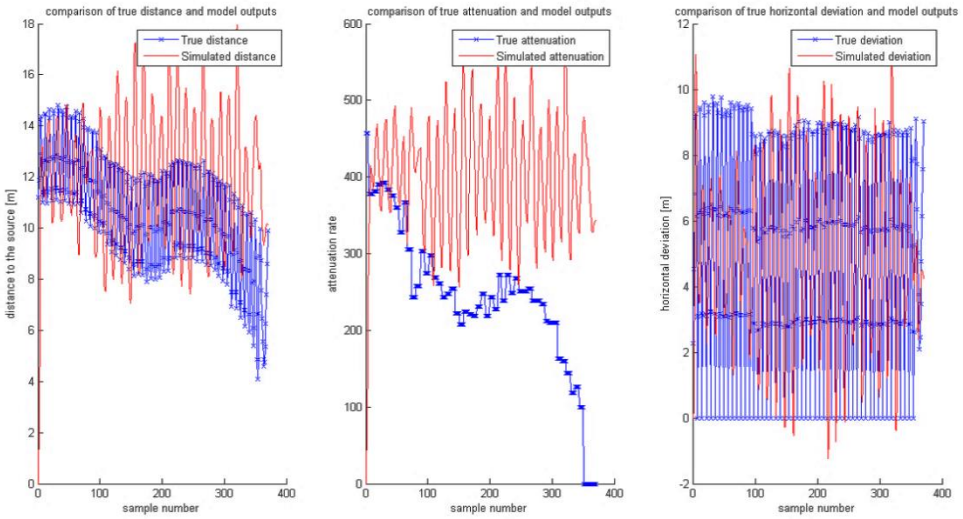

Figure 91 Simulation from the model

From above it can be seen that the model does not extrapolate data correctly. Although the calculated data agree to a greater degree than that calculated by the preceding model, the error is still unacceptable.

To enhance the output estimation, the UKF algorithm was applied to the system. Similar to before the measurement of the MF is obtained by the searching coils. The sigma points for the UKF procedure were transformed through the system transfer function and through the measurement function.

The output of this investigation is shown in Figure 92, Figure 93 and Figure 94.

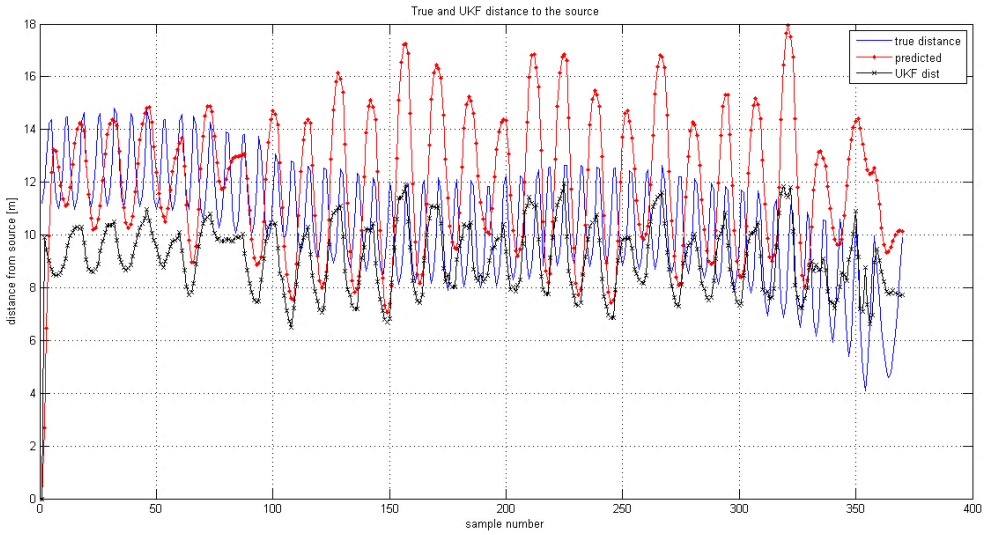

Figure 92 UKF for boat path as the input and vertical distance to the cable as the output

The estimation of vertical distance, hence depth to the cable was not improved by the UKF. Both the model's output and the UKF output yield unsatisfactory results.

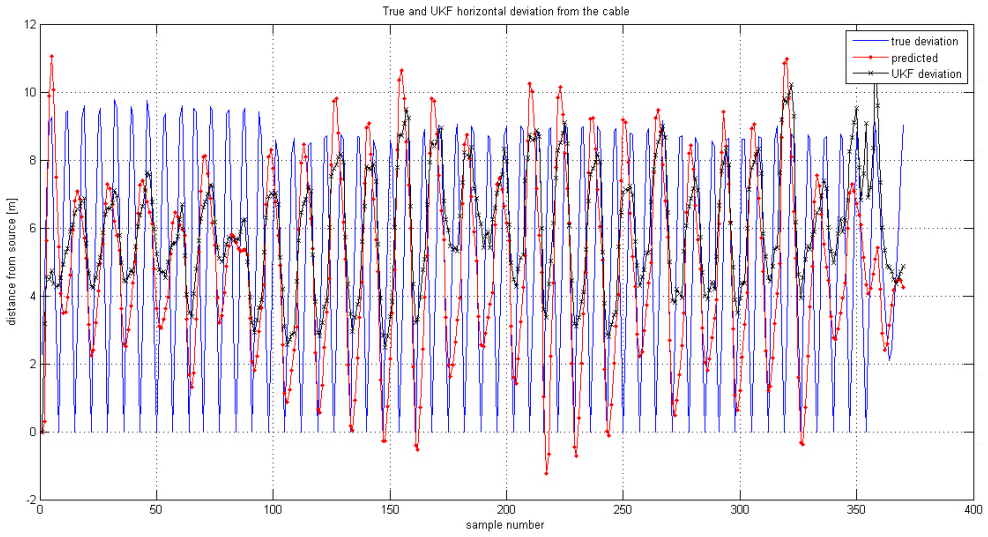

Figure 93 UKF for boat path as the input and horizontal distance (deviation) to the cable as the output

Similarly to depth to the cable, the horizontal deviation estimated by the UKF does not improve cable's tracking.

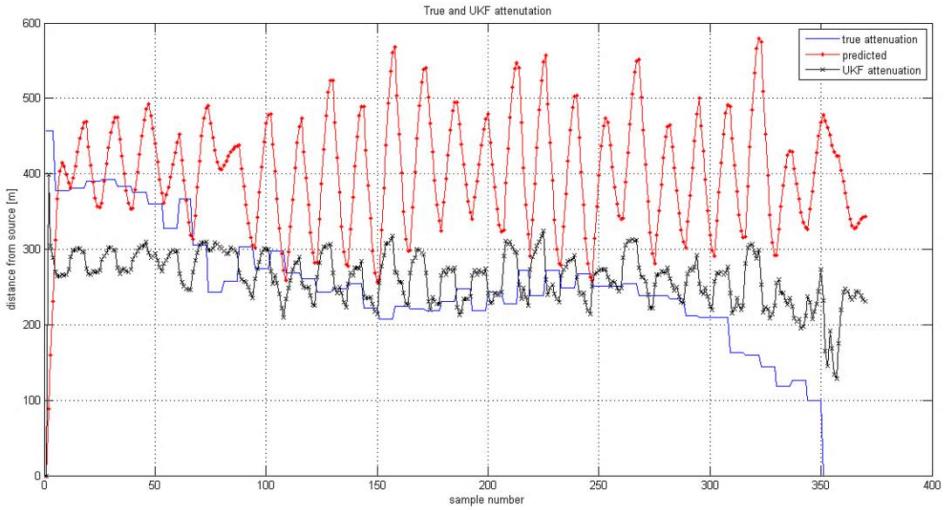

Figure 94 UKF for boat path as the input and the attenuation as the output

The validation of the Attenuation Factor shows that the UKF does not increase the quality of the estimation substantially.

The modelling and KF methods do not yield good results for estimating the distance from the cable. These methods are prone to errors related to the unknown change of attenuation rate. The attenuation is difficult to measure and control in situations when the distance to the cable is not known beforehand.

The analysis of the UKF estimation for cable localisation shows that it is difficult to describe the cable tracking as a dynamical system where the KF can be applied. The unknown future direction of the cable and variations in the survey platform path result in a problem which should rather be viewed from a different perspective. The investigation can conclude that the results from the KF do not yield a satisfactory improvement.

To improve this limitation, model-less estimation with multiple sampling points will be proposed. This different approach based on batch sample particle filters will be proposed in next chapter.

Chapter 8.Particle Filter Approach to Cable Location Detection

Particle Filters (PF) were introduced by Gordon et al (1993) as a robust Bayesian approach to estimate dynamical state probability density functions (PDF) (Crisan & Obanubi, 2012; Fallon & Godsill, 2010). The need to construct this filter arose from the consideration of nonlinear or non-Gaussian problems without general analytic expression for the required PDF. The main idea behind PFs is to recursively approximate a PDF by a set of random samples called particles. The particles tend to concentrate in high probability density regions, and hence give an approximation of the true PDF value.

PFs can be applied in areas where other methods such as Kalman filtering cannot be used (Chen, 2003). The only requirement is the ability to the sample state vector PDF $p(x_k)$ and the functional form of the likelihood of a measurement given a state $p(y_k|x_k)$. In their original paper, Gordon et al. (1993) point out that the PF algorithm relaxes the restrictions placed not only on the transition function f_k and measurement function h_k but also on the distribution of the corresponding noise.

Similarly to the KF approach, the PF method assumes that the state vector $x_k \in \mathbb{R}^n$ evolves according to the system model:

$$x_{k+1} = f_k(x_k, w_k) \quad (83)$$

where $f_k \in \mathbb{R}^n \times \mathbb{R}^m \to \mathbb{R}^n$ is the system transition function, with $w_k \in \mathbb{R}^m$ independent, zero-mean white noise.

The state vector is often unobserved and only the measurement vector $y_k \in \mathbb{R}^p$ is available.

$$y_k = h_k(x_k, v_k) \quad (84)$$

The observation equation (84) relates the measurement of the state through the measurement function $h_k \in \mathbb{R}^n \times \mathbb{R}^r \to \mathbb{R}^p$ with $v_k \in \mathbb{R}^r$ a zero-mean white noise independent of the previous and current states and the system noise w_k.

The aim is to construct the PDF $p(x_k|D_k)$ of the current state x_k given all available information at time step k which is the set of measurements $D_k = \{y_i : i = 1, \dots, k\}$. The PDF can be found using an algorithm based on two stages: prediction and update. In prediction step the prior PDF of the state is constructed based on all information up to step $k-1$. The prior PDF is described in equation (85)

$$p(x_k|D_{k-1}) = \int p(x_k|x_{k-1})p(x_{k-1}|D_{k-1})dx_{k-1} \qquad (85)$$

The probabilistic state evolution follows a Markov model which says that the state at time step k depends only on the previous state $k-1$ and not on the events that occurred before it. It is described by the system model (83) and some known statistics of w_{k-1}. Gordon et al (1993) describe the probabilistic state evolution model by equation (86).

$$p(x_k|x_{k-1}) = \int p(x_k|x_{k-1}, w_{k-1})p(w_{k-1}|x_{k-1})dw_{k-1} \qquad (86)$$

The property of the independence of the white noise w_{k-1} can be used to reduce $p(w_{k-1}|x_{k-1}) = p(w_{k-1})$ hence:

$$p(x_k|x_{k-1}) = \int \delta\{x_k - f_{k-1}(x_{k-1}, w_{k-1})\}\, p(w_{k-1})dw_{k-1} \qquad (87)$$

where $\delta\{\,\}$ is the Dirac delta function and we can use this function in the case when x_{k-1} and w_{k-1} are known and lead to x_k by a deterministic relationship.

The measurement y_k at time step k becomes available by the use of Bayes's rule

$$p(x_k|D_k) = \frac{p(y_k|x_k)p(x_k|D_{k-1})}{p(y_k|D_{k-1})} \qquad (88)$$

The normalising factor in the denominator of (88) is given by:

$$p(y_k|D_{k-1}) = \int p(y_k|x_k)p(x_k|D_{k-1})dx_k \quad (89)$$

The measurement model (84) defines the conditional PDF of y_k given x_k as

$$p(y_k|x_k) = \int \delta(y_k - h_k(x_k, v_k)) \times p(v_k)dv_k \quad (90)$$

An analytic solution for this Bayesian relation is possible only if both f_k and h_k are linear or can be linearized and both w_k and v_k are additive Gaussian noises with known variances. In such a case the Kalman filter is the most commonly used approach (Gordon et al., 1993). Although the KF and its nonlinear forms, extended and unscented KF, give approximations for nonlinear systems, they assume the Gaussian character of the PDF. In the case of high nonlinearity or non-Gaussian system dynamics the KF algorithms give poor results (Salih & Malik, 2011).

In the case when KF algorithm fails, Sequential Monte Carlo techniques (SMC) can prove to be good alternatives to solve the problem. In particular, the PF algorithm can perform well even when the dynamics of the problem is difficult to capture by the use of the Kalman filter (Chen, 2003).

The PF algorithm propagates and updates a set of random samples $\{x_{k-1}(i): i = 1, \dots, N\}$ from the PDF $p(x_{k-1}|D_{k-1})$ to obtain a set of values $\{x_k(i): i = 1, \dots, N\}$ with a distribution close to $p(x_k|D_k)$.

One of the advantages of the proposed method is its easy structure and implementation. It is based on an iteration method and resampling (Gordon, 1997).

The algorithm can be presented in three steps:

1. Initialisation, $k = 0$
    - For $i = 1, \dots, N$ sample $x_0^{(i)} \sim p(x_0)$ and set k= 1
2. Importance sampling step

- For $i = 1, \dots, N$ sample $\tilde{x}_k^{(i)} \sim p(x_k | x_{k-1}^{(i)})$ and set $\tilde{x}_{0:k}^{(i)} = (\tilde{x}_{0:k-1}^{(i)}, \tilde{x}_k^{(i)})$
- For $i = 1, \dots, N$ evaluate the importance weight $\tilde{w}_k^{(i)} \sim p(y_k | x_k^{(i)})$
- Normalise the importance weights

3. Selection step
    - Resample with replacement N particles $(x_{0:k}^{(i)}; i = 1, \dots, N)$ from the set $(\tilde{x}_{0:k}^{(i)}; i = 1, \dots, N)$ according to the importance weights
    - Set $k \leftarrow k + 1$ and go to step 2

The algorithm has been considered and implemented by many authors. It is often compared to a genetic algorithm (GA). Both follow a similar initialization step, iteration and selection but the GA approach includes the additional mutation between the GA's chromosomes while the PF computes weights for each particle (Kwok & Zhou, 2005).

The PF is used in different estimation problems including source localisation. If it is used for source tracking, some prior location is assumed in the initialisation step. Based on this initial location and its possible range, hypothetical locations are drawn from uniformly distributed random samples. In the next step each sample has a calculated weight based on a given measurement. After normalisation of all weights, particles are resampled and a new estimate and uncertainty of covariance are calculated.

The initialisation and importance weights depend on the system and measurement model. The resampling procedure needs to be carefully considered and implemented.

The problem of resampling was investigated by Hol et al., (2006). They proposed different resampling methods. The general procedure of resampling is as follows:

1. First particles are drawn uniformly from the discrete set of choices.
2. Construct the function of β initialised to 0

Index $i = U[1 \dots N]$, and $\beta = 0$

3. Draw next index

For $i = 1 \dots N$

The function β adds a new random value between 0 and twice the largest weight in the importance set

$$\beta \leftarrow \beta + U\{\, 0 \ldots 2 * w_{max} \,\}$$

If $w_{index} < \beta$ if the importance weight is smaller than the β value (does not survive), move index to the current one and remove the amount of weight form the previous

$$\beta \leftarrow \beta - w_{index}$$

$$index \leftarrow index + 1$$

Else if the weight of the particle is bigger than the β the particle is pcked

Pick p_{index}

Each particle is picked in proportion to the weight it has in the total weights

A schematic representation of the PF algorithm is represented in Figure 95.

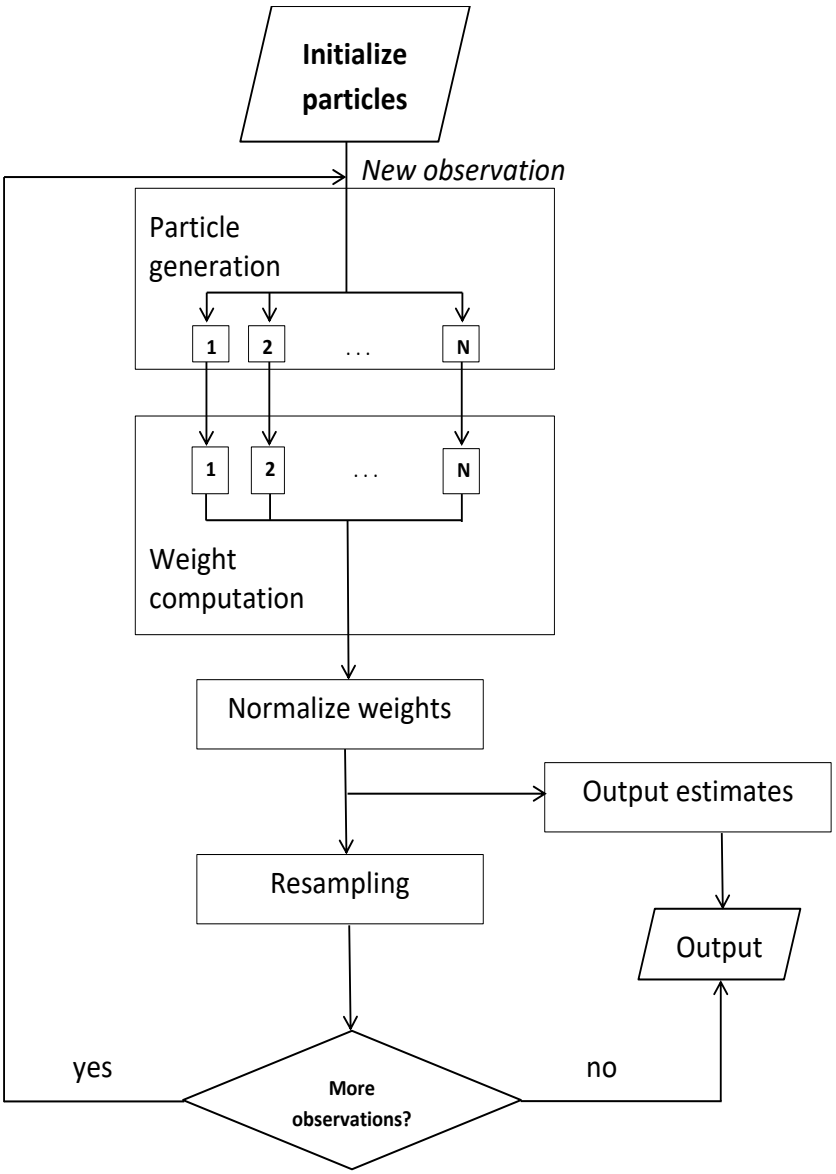

Figure 95 Particle Filter algorithm

8.1 Particle filter for source localisation, system description

Source localisation by means of PF is used in the determination of the origin of events in many fields including robotics, computer vision (Said et al., 2004), sonar, seismology or acoustics (Ward et al., 2003).

The PF has already been used in cable tracking by Ortiz and coworkers. (Wirth et al., 2008; Ortiz & Antich, 2009b; Ortiz et al., 2009a; Ortiz et al., 2011). The group used PF in computer vision to recognise a cable segment exposed to a video camera onboard an unmanned platform. Each video frame was fed into the PF algorithm which successfully estimated the best cable location based on the distribution of the frame's

pixels. The estimated cable's position and its direction were used to steer an unmanned underwater vehicle following the cable.

Although the work presented by Ortiz et al. (2009a) and his group is very inspirational, it cannot be used in tracking buried utilities. For cables trenched into the sea bottom other, non-visual, sensing techniques are applied in which signal can be emitted regardless of the accessibility.

Vallivaara et al. (2011) proposed to use magnetic field anomalies as for a means for self-localisation of a moving robot. In this approach, the robot builds a map of the area using low-cost magnetic sensors. Based on the distribution of the MF the robot can extract the features of the area and define its position.

This approach, often used in robotics, is referred as Simultaneous Localisation and Mapping (SLAM). A robot needs to find its location and map the environment at the same time. In a SLAM approach the process estimates a probability distribution of the state x of a system based on given observations z and control signals u.

$$p(x_t, m \,|z_{1:t}, u_{1:t}) \tag{91}$$

where in equation (91) x_t is the position if the robot, m is a representation of the environment, z_t is a measurement and u_t is a control signal that drives the robot's movement.

The SLAM approach is represented in Figure 96 where the shaded elements are considered to be estimated but only outlined part as the online SLAM.

In the algorithm, the platform moves to a position x in some given time t. From position x_t the measurement z_t is taken. The measurement z_t depends on the features of environment which solely depend upon the position of the sensor and can be built into the environment's map. The control input u_{t+1} then moves the robot into position x_{t+1} to perform a new measurement z_{t+1} and build a more precise map of the environment.

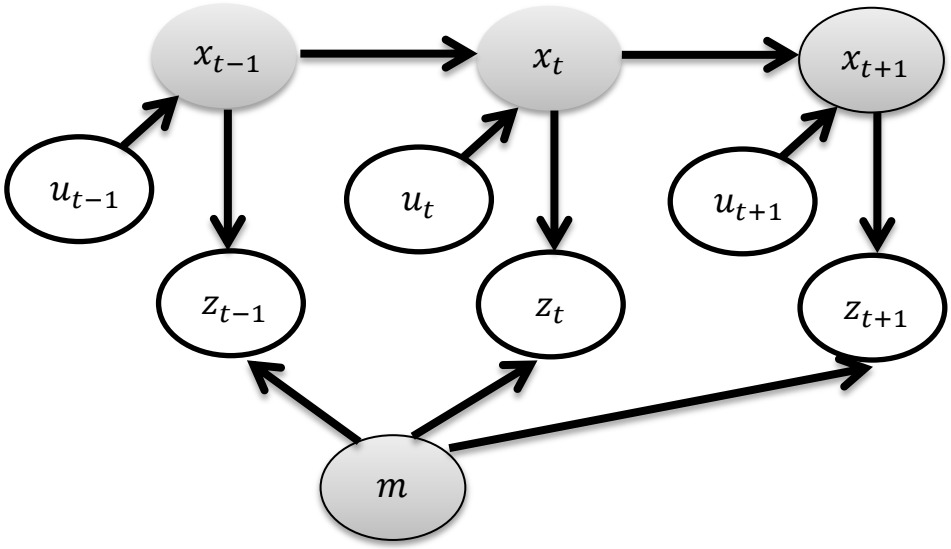

Figure 96 Simultaneous Localisation and Mapping

For the online SLAM the estimation is made in an iterative process

$$\int_{x_0} \dots \int_{x_{t-1}} p(x_{0:t}, m \,|z_{1:t}, u_{1:t})\, dx_{t-1} \dots dx_0 \qquad (92)$$

The system evolves in two steps. The prediction step or motion model where the next reading is a predicted and a correction step or observation model where based on the measurement at time t the system's state is evaluated.

$$\overline{believe}(x_t) = \int p(x_t \,|u_t, x_{t-1})\ believe(x_{t-1})\, dx_{t-1} \qquad (93)$$

Correction

$$believe(x_t) = \eta\, p(z_t \mid x_t)\, \overline{believe}(x_{t-1}) \qquad (94)$$

Where η is a normalizing factor $p(z_t)$

Individual measurements $z_t = \{z_t^1, \dots, z_t^k\}$ are independent given the robot position

$$p(z_t \mid x_t, m) = \prod_{i=1}^{k} p\left(z_t^i \mid x_t, m\right) \quad (95)$$

In the case of cable tracking by a survey boat, the map m can be related to the cable's topography in relation to the readings z_t taken by the sensors placed on the boat. In each sampled position x_t the boat's location is known from precise GPS readings. The boat moves from position x_t to position x_{t+1} by means of the control input u_{t+1} which in most cases is independent of the readings and in practice steering is performed by the boat's crew.

The approach based on SLAM was tested on Denmark data and is presented in later parts of this work. An implementation of the algorithm is described in section 8.1.2. The data from the survey line were fed into the PF algorithm in an online iterative process. Based on the coils measurement the localisation of underlying feature – the cable position was estimated. This approach did not bring satisfactory results caused by a large number of sample points collected far from the source where the signal was too low to be detected.

SLAM is not the only methodology based on PFs. Although in the literature there is a lack of PF methods used in the electromagnetic detection of cables, there exist other fields where source localisation has been performed successfully.

Principles of the magnetic source localisation do not significantly differ from the localisation of a source in other domains. The medium is sampled at different points in space. Based on the readings, the relation between the characteristics of sampled values and source, typically a distance and an angle to the source can be established. The similarities between the localisations techniques can be drawn from domains like acoustics or optics (Brandstein & Silverman, 1997).

Localisation of a sound's source was proposed by Brandstein and Silverman (1997). They introduced a locator steering microphone array in different directions in search for the point at which the signal has its maximum value. In practice the problem is based on an optimisation algorithm such as steepest decent or the Newton-Raphson method for finding the maximum of the underlying signal function.

The measurement techniques are based on time difference of arrival (TDOA). Brandstein and Silverman (1997) proposed to separate the algorithm into two stages. In the first stage, the relative time delay of the signal is measured in distinct locations of the sensors. The second stage estimates the source position based on sensor-source geometry.

This approach can be compared to EMF measurement by an array of sensing coils in which case TDOA will have the same analogy as an amplitude on MF.

Because of the time varying nature of an acoustic signal, calculation of the difference between the arrival times of the wavefront is a complex task. Brandstein and Silverman (1997) proposed to separate the signal into 20-30 msec windows and independently calculate the arrival time for each receiver. In a uniform medium, the signal propagates with constant speed. The propagation times are directly related to the distance between the source and the specific sensor. However in practice, the absolute propagation time is not known and can be measured only in relation to the sensor pair. In real world applications the arrival time of the signal is corrupted by noise.

The method of TDOA was improved by Vermaak and Blake (2001). They noticed that approximation of the true solution with a set of samples does not require difficult triangulation and is less intensive computationally. The system based on SMC method has an ability to operate robustly even in moderate reverberant conditions. In their later work Vermaak et al. (2002) propose the use of several SMC methods modified mainly to reduce computational requirements.

A similar approach was investigated by other researchers. Ward et al. (2003) pointed out that the PF algorithm can perform localisation when the KF cannot be used directly. It is suitable for nonlinear functions and non-Gaussian noise. The tracking algorithm proposed by Ward et al. (2003) is as follows:

Procedure an initial set of particles with uniform weights. When the new data frame is received:

1. Resample particles from the previous frame according to their weight and form a resampled set.
2. Predict the new set of particles by propagating the resampled set according to the source model
3. Transform the raw data into localisation measurement through the application of the measurement function.
4. Form the likelihood function.

5. Weigh the new particles according to the likelihood function
6. Compute the current source localisation.
7. Store the particles and their respective weights.

In their work, Ward et al. (2003) focused on different forms of the likelihood function. They proposed three methods to obtain a likelihood that a single particle will manifest the true source location after transformation through the state's dynamic equation. The likelihood can be calculated based on obtained data and the estimation from a particle.

Apart from the Mean Standard Method and Frame Convergence Ration as likelihood functions Ward et al. (2003) used the Root Mean Square Error (RMSE). The RMSE is the most versatile and can be used in traditional localisation methods. In this method for each estimate of the current source location $\widehat{\ell_s} = \widehat{\ell_s}(t)$ the square error ε_t following (96) is computed for time frame t in accordance to data received from the sensor.

$$\varepsilon_t = \left\| \ell_s - \widehat{\ell_s} \right\| \qquad (96)$$

The above algorithm used in a reverberant environment can deal with a noise level two to three time higher than classical localisation methods (Ward et al., 2003).

Lehman and Williamson (2006) improved the tracking algorithm by tuning its importance function. They relocated particles in state space taking the current observation into account. Among other innovations, they added a re-initialisation step and additional iterations

They reported that the proposed incorporation of importance sampling algorithm leads to more robust method during particle filter detection.

The method of PF for source localisation and tracking is widely used in Acoustic Source Tracking or Localisation. The method attracts the interest of researchers, being a robust method of solving different problems. It can be applied not only to single source tracking but also in problems when the source emanates from many points. Fallon & Godsill (2010) extended use of the method to localisation of speech coming from multiple speakers. They worked on tracking the position of the speakers in different scenarios,

where multiple chatters were speaking at once. They also introduced a null particle which represents no target states at all.

Acoustic source tracking used in speech applications is not the only application that uses a Bayesian approach. Yardim et al (2011) conducted work on sonar based tracking during shallow water AUV operation. They noticed that the PF can be computationally more intensive than the KF but makes fewer assumptions. PF can solve more complex problems and is easy to implement. The SMC methods track evolving state parameters as new data become available. The algorithm can be implemented based on two equations. The first describes the state and dynamical transition between them, whilst the second equation characterises the relation between data and state for a particular measurement.

The PF algorithm for cable tracking will be investigated in following sections.

8.1.1 Model description

To investigate the ability of PF cable tracking based on MF sensing from a cable buried in the seabed, a theoretical representation of the problem was constructed. For the purpose of the PF searching algorithm, a descriptive model is implemented.

A model of the cable for simulation purposes is considered to be a line that follows some given equation. In the real world, the cable can be modelled by splines connecting discrete points along its length (Asif & Arshad, 2006). The induced MF on the water surface is represented by a vector field in the plane $z = 0$. The MF from the cable is approximated as a function of the intensity of the electric current within the shortest distance from the cable, a single attenuation parameter and a flux vector defined as the cross product of the cable's tangent vector and the shortest distance vector. The setup is presented in Figure 97.

The MF is sampled along the path covered by a survey platform with mounted magnetic sensors. The samples are taken at equal time intervals with the platform moving at a constant speed and along lines perpendicular to the cable's direction. The path of the platform can be modelled by a sinusoidal function and can be called the sensor's path. The MF on the water level constitutes a surface which can be interpolated to any point along the sensor's path. The mesh is constructed from a finite number of points and the shortest distance to the cable is calculated from each point. The direction of the MF is given by the

direction of the unit vector, which is the cross product of the direction of the cable and that of the shortest distance. The magnitude of the MF is calculated from the distance and the attenuation factor.

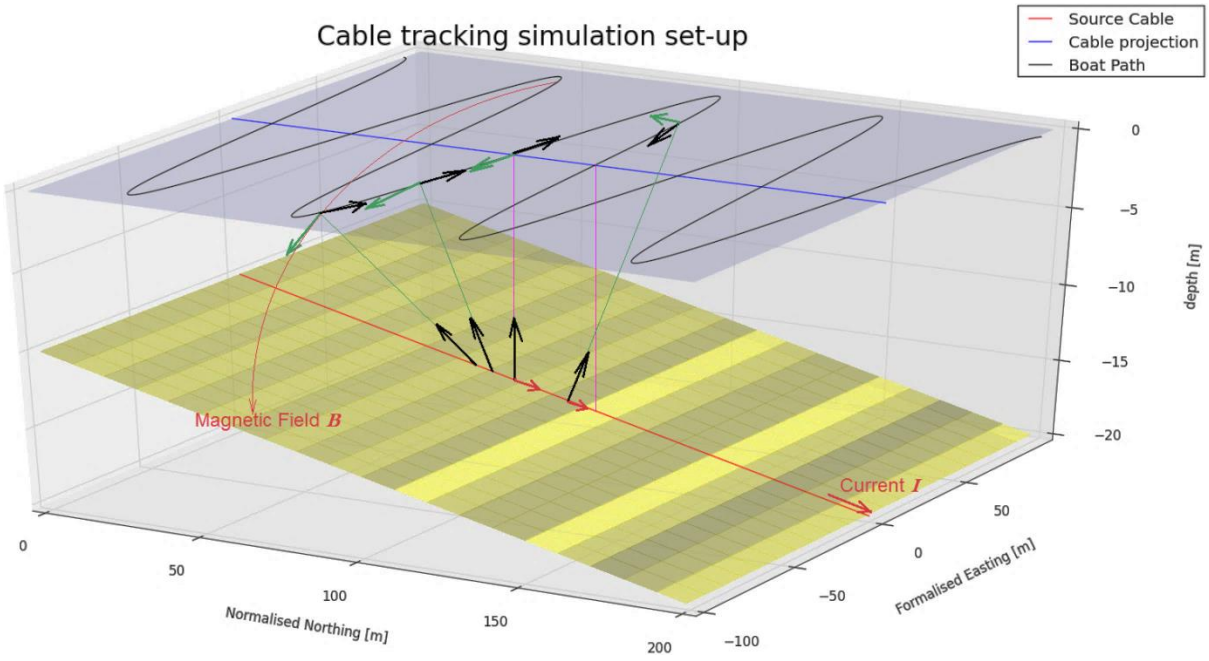

Figure 97 Cable tracking set-up

The MF resulting from the current in the cable can be read by any appropriate sensors. In case of experimental data, it is sampled with searching coils producing a voltage treated as a response signal.

The distribution of MF above the cable is depicted in Figure 98

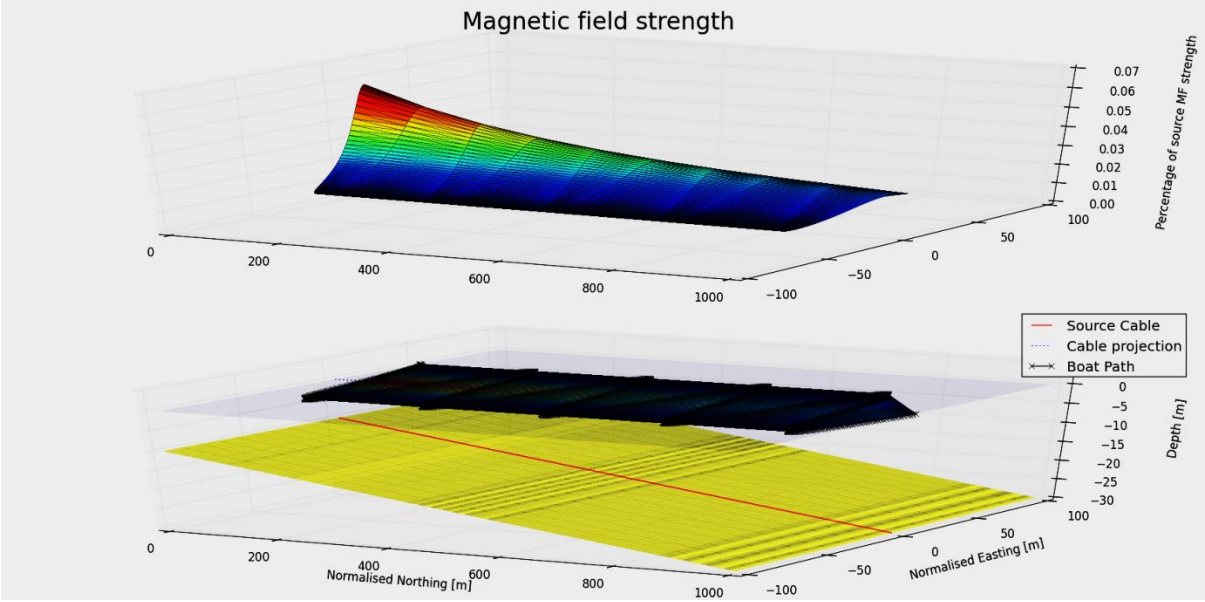

Figure 98 Strength of magnetic field above the cable

A good description of sensors based on inductance coil can be found in Tumanski (2007). The transfer function $V = f(\boldsymbol{B})$ describes a coil's output voltage V as a signal related to a changing magnetic field B and is defined by Faraday's law of induction:

$$V = -n\,\frac{d\boldsymbol{\phi}}{dt} = -n\,A\,\frac{d\boldsymbol{B}}{dt} = \mu_0\,n\,A\,\frac{dH}{dt} \qquad (97)$$

In equation (97), $\boldsymbol{\phi}$ is the magnetic flux through a coil with n turns and area A. The voltage signal from the coil V is proportional to the rate of change of flux density $\frac{d\boldsymbol{B}}{dt}$.

To verify the theoretical aspects of this work, data were collected during a real survey in the Baltic Sea. The searching coils were on board the survey platform which consisted of an eight metres long boat. The horizontal coil was placed aligned with the boat heading and the vertical coil was placed in the direction of the vector with zero horizontal components and the unit vertical component [0,0,1].

During the survey, the position of the survey boat is read by a precise global positioning system (GPS) reading and a tidal height variations control system was used to correct the measurement of the water column depth.

The strength of the MF above the cable can be described as a distribution with a given shape as is shown in Figure 98. Each sample point can be represented as the column vector of the position's components $\boldsymbol{P_k}$ but it also needs to incorporate the vector direction of the cable $\boldsymbol{d_k}$ at the time step k and a vector of platform heading $\widehat{\boldsymbol{h}}_{\boldsymbol{k}}$, which in practice gives the orientation of the sensors. As the future direction of the cable can be assumed based on the past data, the direction of the cable at the source point S_k can be estimated as $\hat{d}_k$ where the hat notation represents the unit vector.

When the survey platform moves along a non-perpendicular path, all three components of the MF source change together with the platform's movement. As the platform moves from point P_{k-1} to P_k by a vector $\boldsymbol{p_k}(p_k^{(x)}, p_k^{(y)}, p_k^{(z)} = 0)$, the dominating source of MF moves by the projection of the vector $\boldsymbol{p_k}$ onto the vector of the direction of the cable $\boldsymbol{d_k}(d_k^{(x)}, d_k^{(y)}, d_k^{(z)})$. The vector $\boldsymbol{d_k}$ is the vector of the cable at the source S_k. A moving charge of electric current moves on the same path, thus the vector $\boldsymbol{d_k}$ is also direction of the moving charge.

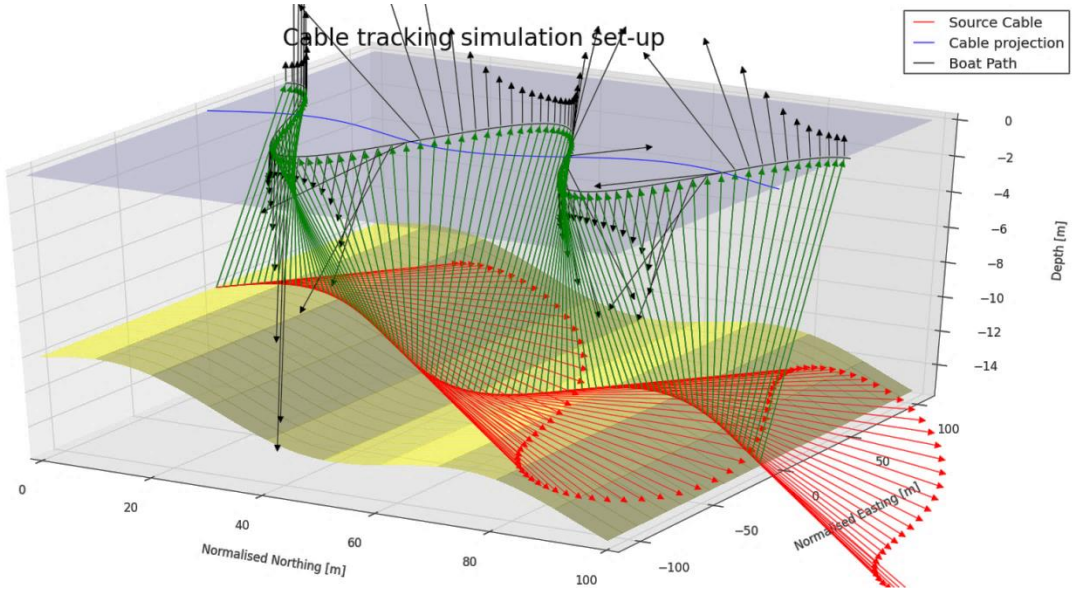

Figure 99 Visualisation of vectors directions

The system's change depends mainly on the change of the platform's position, hence the position of the platform P_k can be taken as the input to the system.

$$x_k = \begin{bmatrix} P_k \\ \widehat{\boldsymbol{h}}_k \\ S_k \\ \widehat{\boldsymbol{d}}_k \end{bmatrix} \tag{98}$$

The transition function takes the source point from step $k-1$ to the source point in step k. The transition is made by projection of the boat's movement vector $\boldsymbol{p}_k$ onto the cable's vector direction $\boldsymbol{d}_k$

The transition function $f(P_k, x_{k-1})$ takes the current platform's location P_k as a known input and previous state x_{k-1}.

$$f(P_k, x_{k-1}) + wh_k + wp_k + wd_k = \begin{bmatrix} P_k \\ f_h(\widehat{\boldsymbol{h}}_{k-1}) + wh_k \\ S_{k-1} + (\boldsymbol{p}_k \cdot \boldsymbol{d}_k)\widehat{\boldsymbol{d}}_k + wp_k \\ f_d(S_{k-1}, S_k) + wd_k \end{bmatrix} \tag{99}$$

To investigate equation (99) the vectors can be represented by Cartesian coordinates components:

$$f(P_k, x_{k-1}) + wh_k + wp_k + wd_k = \begin{bmatrix} P_k^{(x)} \\ P_k^{(y)} \\ P_k^{(z)} \\ f_h{}^{(x)}(P_k) + wh_k^{(x)} \\ f_h{}^{(y)}(P_k) + wh_k^{(y)} \\ f_h{}^{(z)}(P_k) + wh_k^{(z)} \\ S_{k-1}^{(x)} + (\boldsymbol{p}_k \cdot \boldsymbol{d}_k)(d_k^{(x)}/|\boldsymbol{d}_k|) + wp_k^{(x)} \\ S_{k-1}^{(y)} + (\boldsymbol{p}_k \cdot \boldsymbol{d}_k)(d_k^{(y)}/|\boldsymbol{d}_k|) + wp_k^{(y)} \\ S_{k-1}^{(z)} + (\boldsymbol{p}_k \cdot \boldsymbol{d}_k)(d_k^{(z)}/|\boldsymbol{d}_k|) + wp_k^{(y)} \\ f_d{}^{(x)}(S_{k-1}, S_k) + wd_k^{(x)} \\ f_d{}^{(y)}(S_{k-1}, S_k) + wd_k^{(y)} \\ f_d{}^{(z)}(S_{k-1}, S_k) + wd_k^{(z)} \end{bmatrix} \tag{100}$$

The noise wp_k relates to the estimation of the position of the source point along the direction of the cable. This noise comes from readings of the platform's position. It can be assumed that the noise is white Gaussian.

In most cases, a short section of the cable path can be described by a straight line. The function $f_d(S_{k-1}, S_k)$ can be linearized by using the direction of the cable from the previous step and assuming the noise wd_k related to the deviation from the straight path. With this assumption equation (100) becomes:

$$f(P_k, x_{k-1}) + wh_k + wp_k + wd_k = \begin{bmatrix} P_k^{(x)} \\ P_k^{(y)} \\ P_k^{(z)} \\ \hat{p}_k^{(x)} + wh_k^{(x)} \\ \hat{p}_k^{(y)} + wh_k^{(y)} \\ \hat{p}_k^{(z)} + wh_k^{(z)} \\ S_{k-1}^{(x)} + (\boldsymbol{p}_k \cdot \boldsymbol{d}_k)(d_k^{(x)}/|\boldsymbol{d}_k|) + wp_k^{(x)} \\ S_{k-1}^{(y)} + (\boldsymbol{p}_k \cdot \boldsymbol{d}_k)(d_k^{(y)}/|\boldsymbol{d}_k|) + wp_k^{(y)} \\ S_{k-1}^{(z)} + (\boldsymbol{p}_k \cdot \boldsymbol{d}_k)(d_k^{(z)}/|\boldsymbol{d}_k|) + wp_k^{(y)} \\ \hat{d}_{k-1}^{(x)} + wd_k^{(x)} \\ \hat{d}_{k-1}^{(y)} + wd_k^{(y)} \\ \hat{d}_{k-1}^{(z)} + wd_k^{(z)} \end{bmatrix} \quad (101)$$

If the cable follows a bend or curve, within small range the path can be approximated by a second order fit. In such cases the function $f_d(S_{k-1},\ S_k)$ can become the nonlinear regression or spline and can incorporate n source points to become $f_d(S_{k-n}, S_{k-n+1}, \dots,\ S_k)$. The noise wd_k will follow the deviation from the straight line and will not be white Gaussian. This situation will be further investigated in subsequent sections.

The nonlinearity in the state equation described in equation (101) occurs only in the projection of the vector of the platform movement $\boldsymbol{p}_k$ onto the direction of the cable $\widehat{\boldsymbol{d}}_k$.

After a description of state transition, the measurement function needs to be characterised.

The state equation allows calculating the MF vector $\boldsymbol{B}_k$ pointing from the measurement point P_k.The MF at the point is measured by two coils. One of the coils is placed horizontally in the direction of the platform path. Second coil is placed vertically to the water surface. This set-up is depicted on Figure 100.

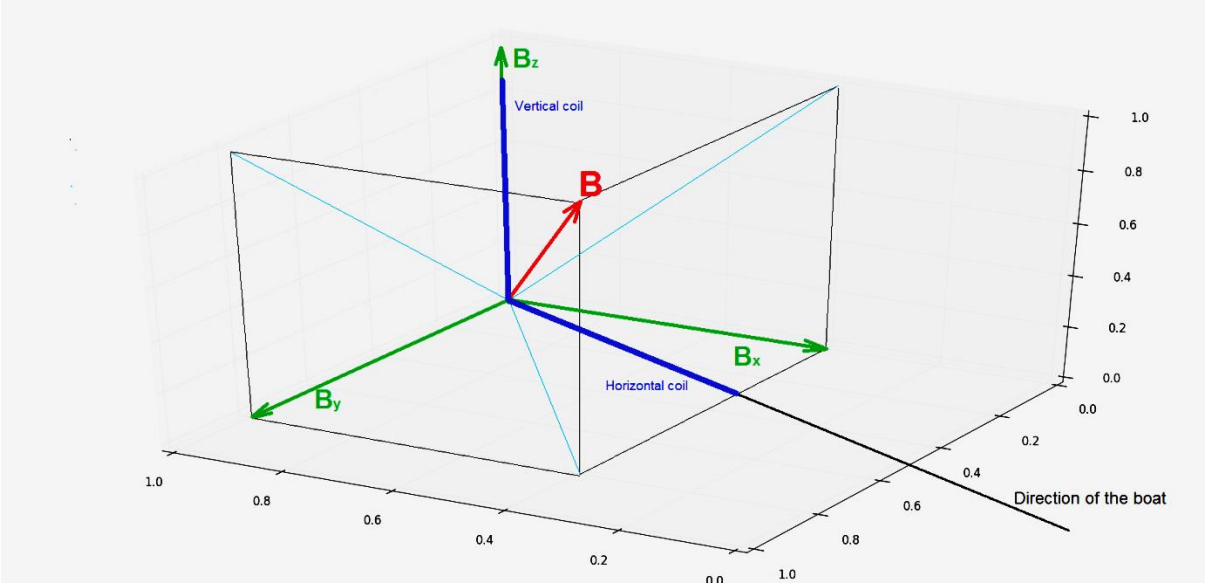

Figure 100 Direction on measurement coils in relation to the vector of MF

The measurement model can be defined as the output from the coils placed in the MF with vector $\boldsymbol{B}$.

Figure 101 shows theoretical readings from both horizontal and vertical coils. The left part of the figure represents the horizontal coil's output with a single peak above the cable. The right part of the figure represents the vertical coil's output. The vertical coil outputs a zero voltage above the cable with two peaks on both sides of the cable.

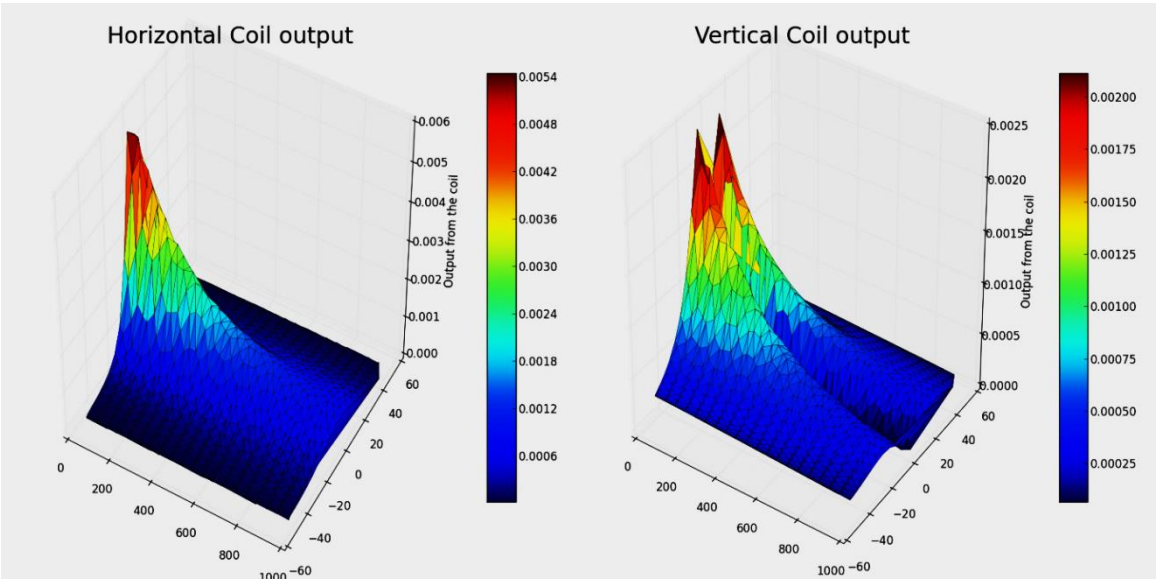

Figure 101 Distribution of readings from horizontal and vertical coils

It must be noted that MF is orthogonal to the cable's vector direction $\boldsymbol{d}_k$ and the vector $\boldsymbol{r}_k$ pointing from the source point S_k to the sample point P_k.

Each measurement data z_k follows the mesurement function $h(x_k)$ and depends upon the MF vector $\boldsymbol{B}_k$ at the sampling point and boat's heading $\widehat{\boldsymbol{h}}_{\boldsymbol{k}}$.

$$z_k = h(x_k) + v_k = \begin{bmatrix} C_H + v_k^H \\ C_V + v_k^V \end{bmatrix} = \begin{bmatrix} \boldsymbol{B}_k \cdot \widehat{\boldsymbol{p}}_{\boldsymbol{k}} + v_k^H \\ \boldsymbol{B}_k \cdot \hat{\boldsymbol{z}} + v_k^V \end{bmatrix} \quad (102)$$

In equation (102) the values $C_H + v_k^H$ are the output from the horizontal coil and the horizontal coil's noise, $C_V + v_k^V$ are the output from the vertical coil and the vertical coil's noise. The vector $\widehat{\boldsymbol{p}}_{\boldsymbol{k}}$ is a unit vector of the boat movement assuming that the centre line of the horizontal coil is placed in the same direction as the vector $\boldsymbol{p}_k$. The vector $\hat{\boldsymbol{z}} = [0,0,1]$ is a unit vector in the z-direction and direction of the vertical coil. In other words the measurement of the coil is the result of the projection of the MF onto the vector of the direction of the coil's centre line.

The measurement noise v_k is related to the output of the coils, precision of the hardware and surrounding magnetic noises. It can be assumed that this is white Gaussian noise.

The magnetic field $\boldsymbol{B}_{\mathbf{k}}$ at the measurement point P_k can be calculated based on Biot-Savart's law and it can be simplified as:

$$\boldsymbol{B}_{\mathbf{k}} = \frac{\mu_0 I}{4\pi r_k^3} \left(\widehat{\boldsymbol{d}}_{k+1} \times \boldsymbol{r}_k \right) = \frac{\mu_0 I}{4\pi r_k^3} \left(\widehat{\boldsymbol{d}}_{k+1} \times [P_k - S_k] \right) = c \frac{\left(\widehat{\boldsymbol{d}}_{k+1} \times [P_k - S_k] \right)}{r_k^3} \quad (103)$$

In equation (103) $\mu_0 I/4\pi$ is constant along the cable and can be written as a constant c. Thus combining equation (102) and (103) gives the measurement function in terms of state variables.

In the case in which the survey platform moves along the path perpendicular to the direction of the cable equation (102) reduces to trigonometric functions of the MF strength.

$$z_k = \begin{bmatrix} cos(|B_k|) + v_k^H \\ sin(|B_k|) + v_k^V \end{bmatrix} \quad (104)$$

This simplified relation in equation (104) will be used in the implementation of a PF where the boat path can be assumed to be a straight line perpendicular to the cable. In this case the magnetic source can be assumed to be the centre point of cross section of the cable. Translating equation (104) to measured quantities leads to :

$$z_k = \begin{bmatrix} c\dfrac{\left(\hat{\boldsymbol{d}}_{k+1} \times [P_k - S_k]\right)}{|[P_k - S_k]|^3} \cdot \hat{\boldsymbol{p}}_{\boldsymbol{k}} + v_k^H \\ c\dfrac{\left(\hat{\boldsymbol{d}}_{k+1} \times [P_k - S_k]\right)}{|[P_k - S_k]|^3} \cdot [0,0,1] + v_k^V \end{bmatrix} \quad (105)$$

Equation (105) can be represented by the Cartesian components of the vectors:

$$z_k = \begin{bmatrix} \dfrac{c}{|[P_k - S_k]|^3} \begin{bmatrix} \hat{x} & \hat{y} & \hat{z} \\ \hat{d}_{k+1}^{(x)} & \hat{d}_{k+1}^{(y)} & \hat{d}_{k+1}^{(z)} \\ P_k^{(x)} - S_k^{(x)} & P_k^{(y)} - S_k^{(y)} & P_k^{(z)} - S_k^{(z)} \end{bmatrix} \cdot \begin{bmatrix} p_k^{(x)} \\ p_k^{(y)} \\ p_k^{(z)} \end{bmatrix} + v_k^H \\ \dfrac{c}{|[P_k - S_k]|^3} \begin{bmatrix} \hat{x} & \hat{y} & \hat{z} \\ \hat{d}_{k+1}^{(x)} & \hat{d}_{k+1}^{(y)} & \hat{d}_{k+1}^{(z)} \\ P_k^{(x)} - S_k^{(x)} & P_k^{(y)} - S_k^{(y)} & P_k^{(z)} - S_k^{(z)} \end{bmatrix} \cdot \begin{bmatrix} 0 \\ 0 \\ 1 \end{bmatrix} + v_k^V \end{bmatrix} \quad (106)$$

where in equation (106), the vector product can be expanded as:

$$\begin{bmatrix} \hat{x} & \hat{y} & \hat{z} \\ \hat{d}_{k+1}^{(x)} & \hat{d}_{k+1}^{(y)} & \hat{d}_{k+1}^{(z)} \\ P_k^{(x)} - S_k^{(x)} & P_k^{(y)} - S_k^{(y)} & P_k^{(z)} - S_k^{(z)} \end{bmatrix} = \quad (107)$$

$$(\hat{d}_{k+1}^{(y)}\left(P_k^{(z)} - S_k^{(z)}\right) - \hat{d}_{k+1}^{(z)}(P_k^{(y)} - S_k^{(y)}))\hat{x} +$$

$$\left(\hat{d}_{k+1}^{(x)}\left(P_k^{(z)} - S_k^{(z)}\right) - \hat{d}_{k+1}^{(z)}\left(P_k^{(x)} - S_k^{(x)}\right)\right)\hat{y} +$$

$$(\hat{d}_{k+1}^{(x)}\left(P_k^{(y)} - S_k^{(y)}\right) - \hat{d}_{k+1}^{(y)}(P_k^{(x)} - S_k^{(x)}))\hat{z}$$

Using the fact that the vertical coil output is the dot product of unit $\hat{z}$ vector, the expression (106) can be simplified to:

$$z_k = \begin{bmatrix} \frac{c}{|[P_k - S_k]|^3} \begin{bmatrix} \hat{x} & \hat{y} & \hat{z} \\ \hat{d}_{k+1}^{(x)} & \hat{d}_{k+1}^{(y)} & \hat{d}_{k+1}^{(z)} \\ P_k^{(x)} - S_k^{(x)} & P_k^{(y)} - S_k^{(y)} & P_k^{(z)} - S_k^{(z)} \end{bmatrix} \cdot \begin{bmatrix} p_k^{(x)} \\ p_k^{(y)} \\ p_k^{(z)} \end{bmatrix} + v_k^H \\ \frac{c}{|[P_k - S_k]|^3} \ (\hat{z} + \hat{d}_k^{(z)} + (P_k^{(x)} - S_k^{(x)})) + v_k^V \end{bmatrix} \quad (108)$$

where in equation (108) the denominator $|[P_k - S_k]|$ is the length of the distance vector $\boldsymbol{r}_k$ from the source to the measurement point and the platform path movement respectively. The modulus are defined as follows:

$$|[P_k - S_k]| = \left(\sqrt{\left(P_k^{(x)} - S_k^{(x)}\right)^2 + \left(P_k^{(y)} - S_k^{(y)}\right)^2 + \left(P_k^{(z)} - S_k^{(z)}\right)^2} \right) \quad (109)$$

The above model was implemented in two different setups. One of them follows a three-dimensional model (3D) and equations (101) and (108). The more simplified set-up reduces the readings taken from the experiments to two-dimensional space (2D). This simplification was possible as each survey line crossed the cable in a perpendicular direction. It can be assumed that the MF at each sample point is a result of the field emitted from a single point on the cable. In this case, the state equation reduces to a point representing the source and a point representing the platform's position.

$$x_k = \begin{bmatrix} P_k \\ S_k \end{bmatrix} \quad (110)$$

and the measurement equation reduces to:

$$z_k = \begin{bmatrix} \frac{c}{|[P_k - S_k]|^3} \begin{bmatrix} \hat{x} & \hat{y} \\ P_k^{(x)} - S_k^{(x)} & S_k^{(y)} \end{bmatrix} \cdot \begin{bmatrix} p_k^{(x)} \\ p_k^{(y)} \end{bmatrix} + v_k^H \\ \frac{c}{|[P_k - S_k]|^3} \ (\hat{z} + (P_k^{(x)} - S_k^{(x)})) + v_k^V \end{bmatrix} \quad (111)$$

where $P_k^{(y)} = 0$ and the distance from sample point to the source point can be calculated as:

$$|[P_k - S_k]| = \left(\sqrt{\left(P_k^{(x)} - S_k^{(x)}\right)^2 + \left(S_k^{(y)}\right)^2} \right) \quad (112)$$

The next section presents the result implementing the PF algorithm using the 2D hypothesis and equations (110) and (111).

8.1.2 Single point implementation 2D case

Traditionally tracking methods are based on processing the MF sampled at a single measurement point. Although the sensors configuration can be treated as a sensor array, often sensors are set in different position or angles to each other to support better signal inversion. Usually, sensing coils are set in a different direction or separated by some fixed small distance. On each sample point, readings from all available sensors are treated as a single measurement coming from one array of information. The information is processed, the position is updated and the iteration step progresses onto the next sample point. In a similar fashion, PFs were implemented during a first research phase. Two coils, horizontal and vertical, were treated as the sensors array and particle filtering was performed at every step.

On the start of the line, a region of possible source localisation was chosen. The particles representing state variables in equation (110) were drawn at random in the region of interest (ROI). After every sample point, the weights of all existing particles were calculated following equation (111) in accordance with the new measurement output.

During the survey the platform moves from the position of P_k at time step k to the new position P_{k+1} but the source of the MF and particles stays at the same location hence $S_k = S_{k+1}$.

In the measurement function, the new distance is calculated between the source and new boat position P_{k+1} which leads to the new values of MF strength and new theoretical outputs from the coils.

Figure 102 to Figure 106 show iteration steps after initialisation and five samples, twenty samples, forty samples, sixty samples and after finishing the line.

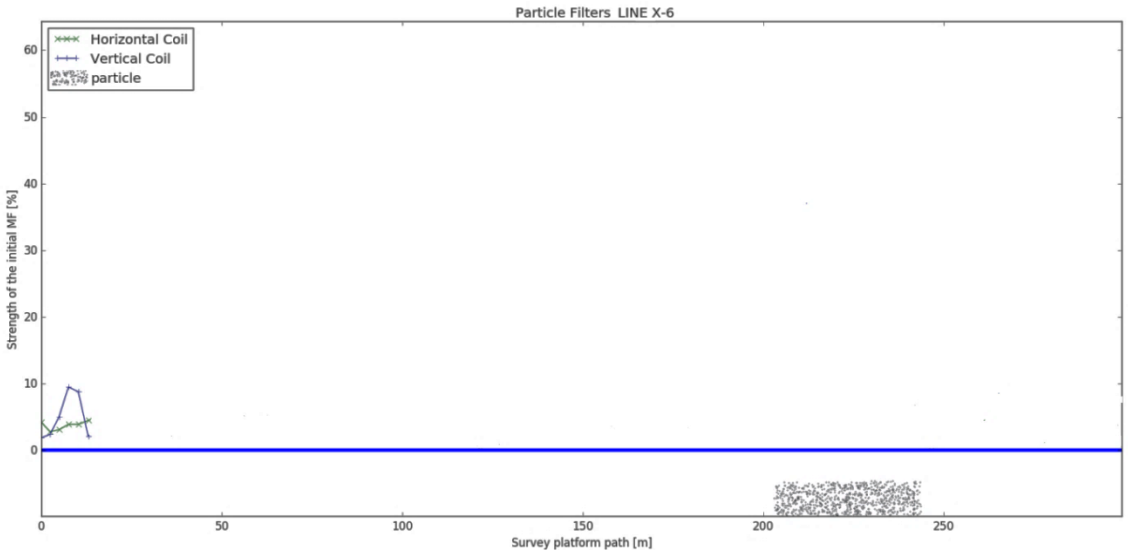

Figure 102 PF algorithm after initialisation and iteration over five samples

At first, the particles were drawn at random over the ROI. The first initial iteration did not change the particles distribution.

After twenty iterations shown in Figure 103, the distribution of particles starts to group into some more condensed regions.

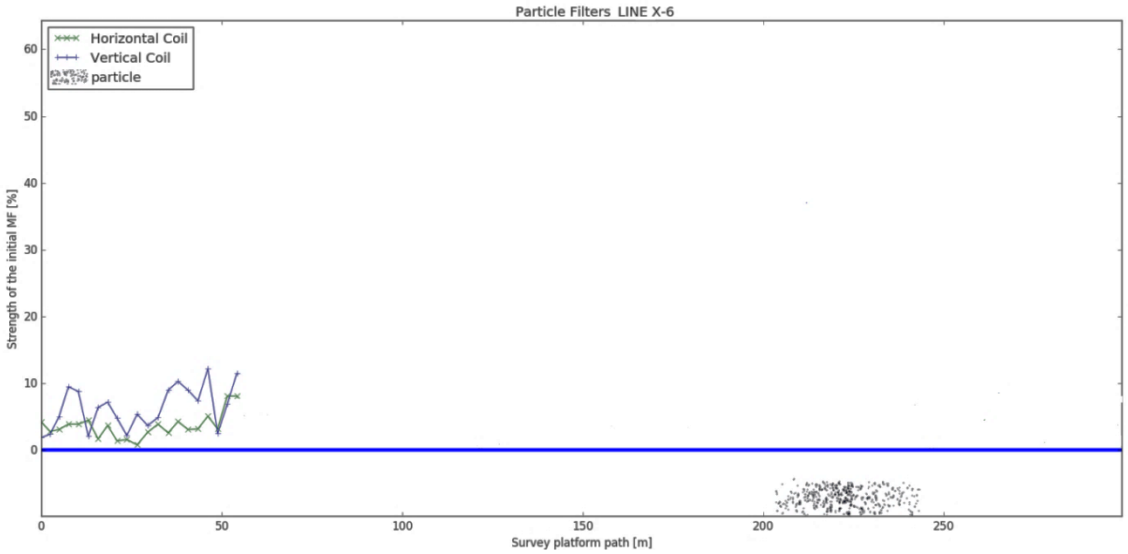

Figure 103 PF algorithm and particles after iteration over twenty samples

After forty iterations shown in Figure 104 the particles diverge from the region were the true source is localised and move into the position much further from the water line.

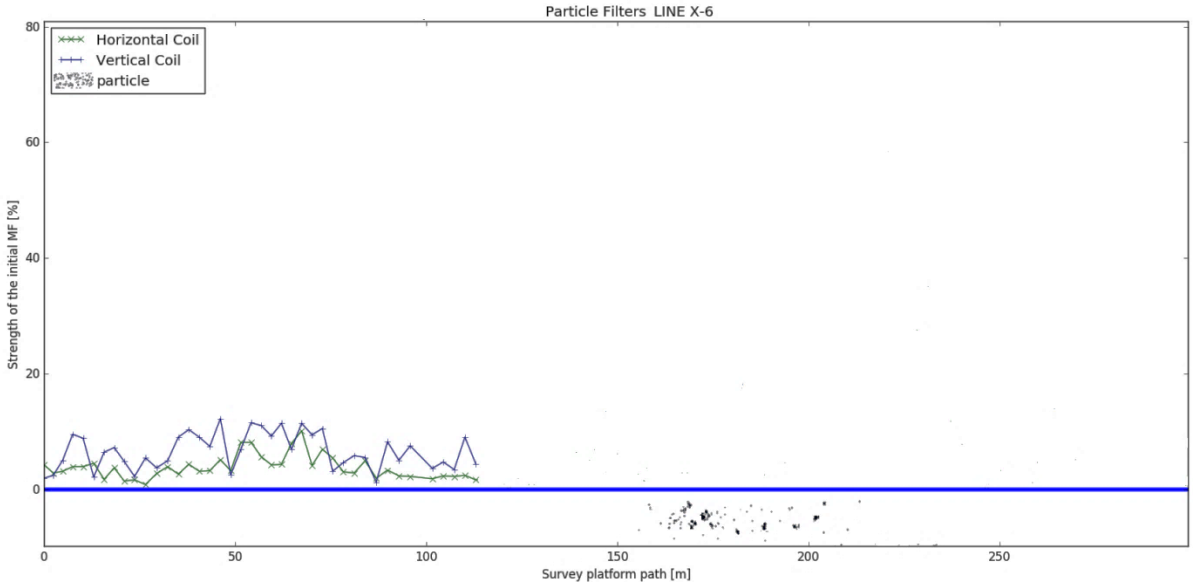

Figure 104 PF algorithm and diverges of particles after iteration over forty samples

The tendency of divergence persists during the entire process.

Figure 105 shows algorithm's performance after sixty iterations. The particles diverge to a position far from the true value. Most of the particles are already outside of plot's boundaries.

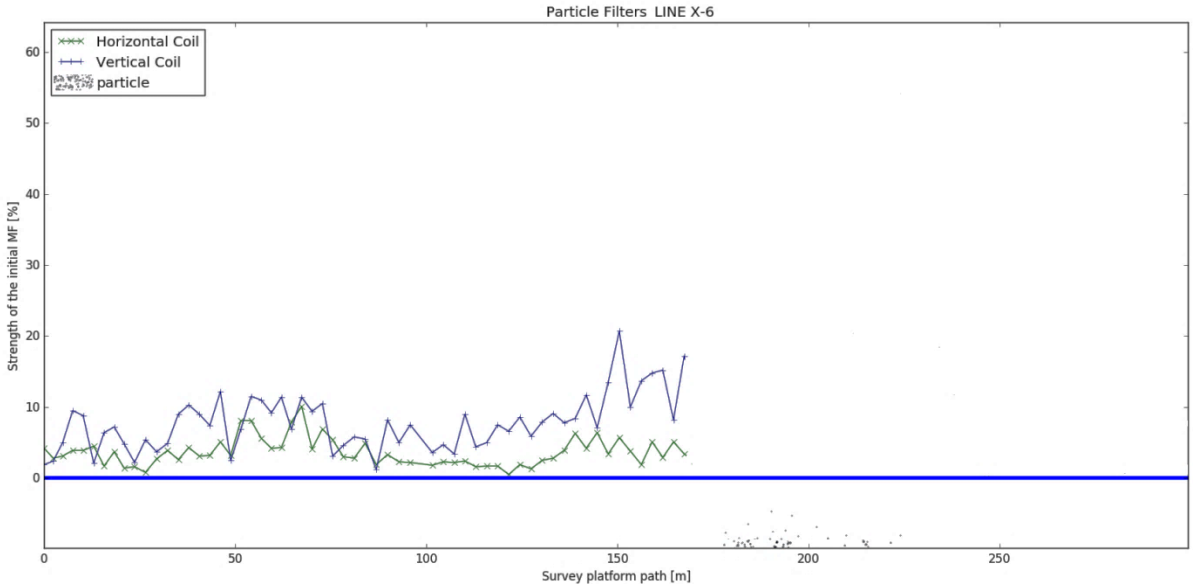

Figure 105 PF algorithm and particles diverged from the plot scales after sixty samples

After iterating over the whole line the particles diverged from the true position. On the plot shown in Figure 106, there is no particle left in the ROI.

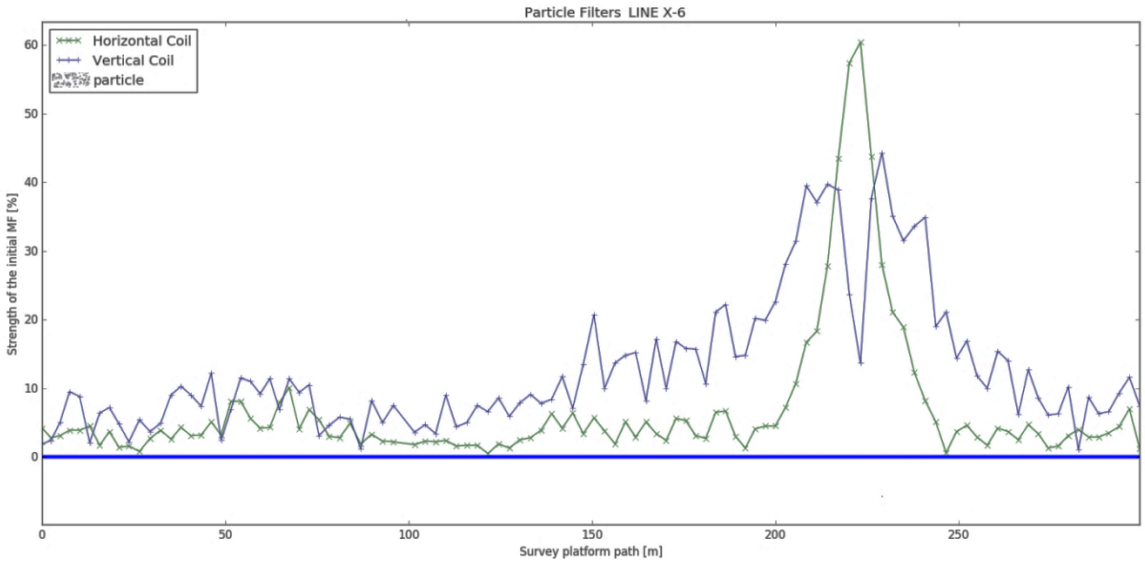

Figure 106 Iteration over the whole line with particles diverged from the plot's scale

As can be seen, the first approach to PF did not finish with satisfactory results. The particles diverged from the true position.

The procedure was repeated and tested on different lines with different ROI localisation. None of the trials brought satisfactory results and convergence to the true position.

To explain this situation it has to be noted that particle's iteration starts when there is no signal presented in the samples. Starting from the beginning of the line the coils readings provide only the noise.

To overcome this problem a different approach is taken and presented over next part. Instead of iterating over each sample point, the line is treated as a whole. In such a configuration all samples are taken as a single sensor's array and complete line is fed into algorithm at each iteration.

8.1.3 Batch Particle Filter 2D case – single line

In the previous section a PF algorithm was implemented during iteration over a single point fed to the system according to the boat's dynamics. Such an approach is similar to the SLAM process where the sensors placed on a moving robot provide readings over the time of operation. The main problem with this scheme is a large amount of samples in which the presented signal is very weak or does not occur at all.

To overcome this problem, the procedure was changed to present all sample points at the initialisation of the PF algorithm.

The idea behind this scheme comes from surveying practice. The boat's path and surveying line are determined before the cable is detected. Finding the exact position of the utility does not change the boat's steering and rarely affects the survey plan. The position of the cable can be calculated after the line is finished, hence all sample points can be fed into PF algorithm as one batch. To distinguish this procedure the algorithm will be called the BPF.

Simulation of the BPF scheme is presented in Figure 107, Figure 108 and Figure 109. The MF from a known source was simulated at discrete locations. The reading from the horizontal coil is related to the signal's MF through the cosine function. It means that the output from the horizontal coil reaches its peak above the cable. The reading from the vertical coil is related through the sine function. The vertical coil placed directly above the cable should give a zero reading. The ROI region was calculated based on a peak in horizontal sensor readings and low value in the vertical sensor and is around the region of the biggest difference between two coils.

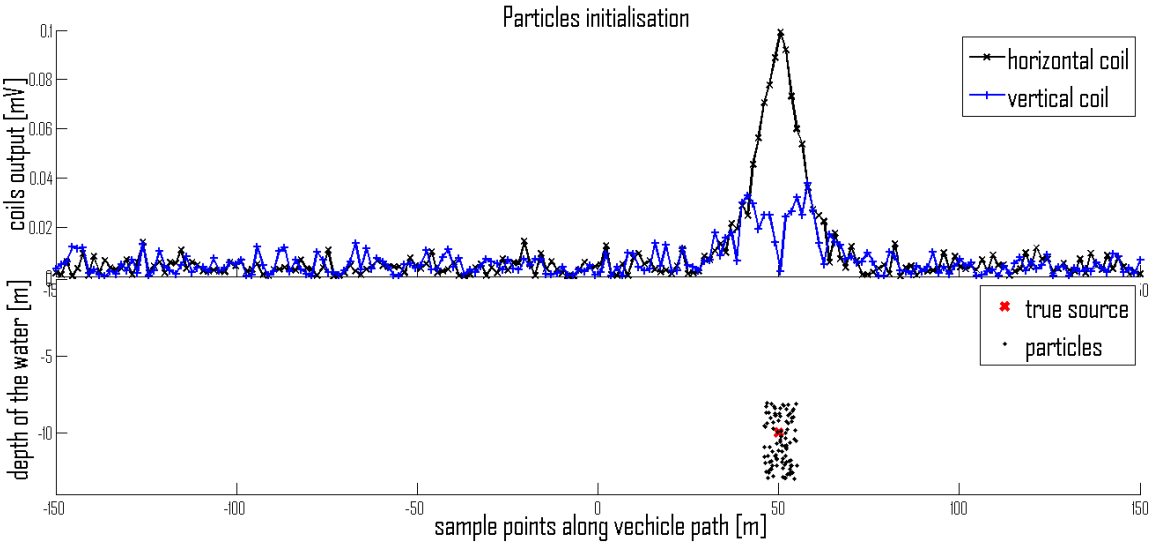

Figure 107 Batch Particle Filters simulation- initialisation

In the initialisation step, 100 theoretical source positions are drawn. Each point has randomly chosen x and y coordinates in range of ROI. In additions the attenuation constant c is drawn at random for each particle. After initialisation the particles had calculated their weight value.

Particles were resampled according to their weights and a new distribution of particles was drawn.

Figure 108 shows convergence of particles after only two iterations. In each iteration, the new set of particles is drawn at random and new hypothetical source with their weights are calculated.

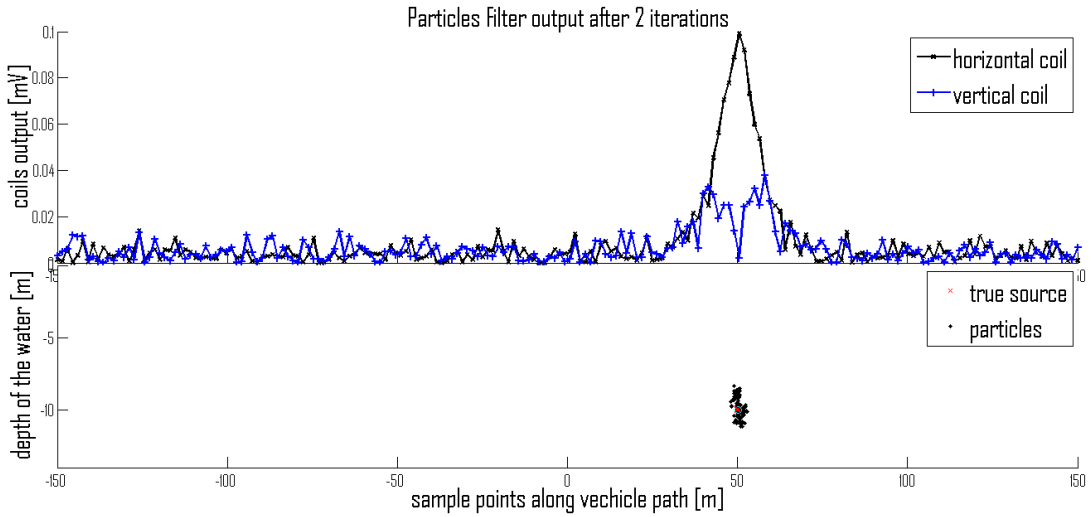

Figure 108 Batch Particle Filters simulation- after two iterations

Figure 109 shows the convergence of all particles to true source position after 20 iterations.

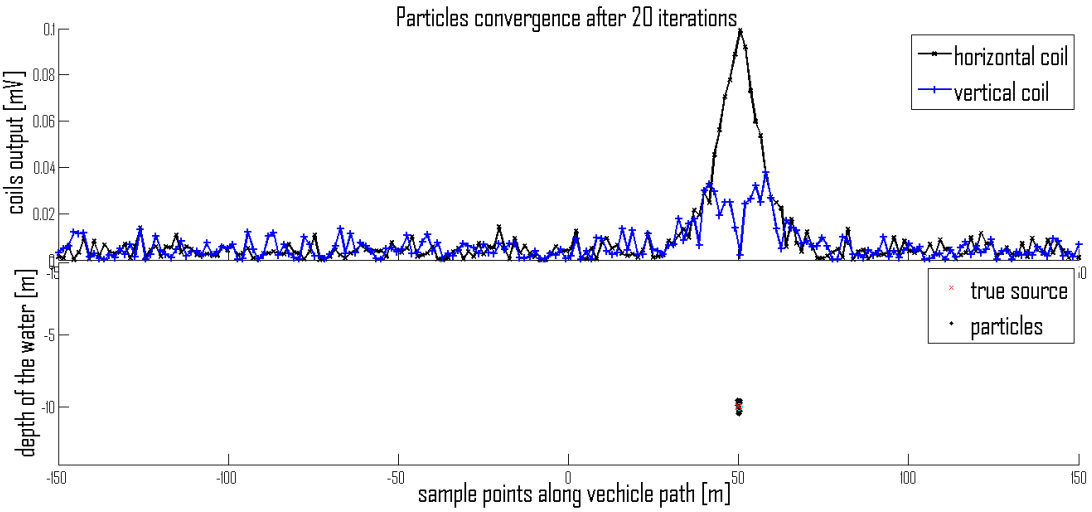

Figure 109 Batch Particle Filters simulation- after twenty iterations

After successful source tracking in simulation, the BPF procedure was applied to real data. For this purpose, the samples from the Denmark experiments were utilised.

The BPF implementation is shown in Figure 110, Figure 111 and Figure 112. First based on the readings from vertical and horizontal coils, the ROI is evaluated.

In BPF algorithm the ROI is calculated as the square area below the sample point with the maximum distance between the horizontal and vertical coils.

The sample is not necessarily taken above the cable and the reading is corrupted by noise. In practice the sample points are taken every two to three metres and the cable can be at any point between the sample points. For this reason, the ROI is extended to cover twenty sample points before and twenty sample points after the initial source.

For each sample point the depth of the water column is measured by an echo sounder. The cable can lie on the sea bottom, can be buried up to three metres or can be suspended in the water. The height of the ROI is taken from three metres below the floor level, up to two metres above.

Each particle represents a hypothetical source. For calculating the distribution of the MF, not only the position of the source is important but also the attenuation of the MF. The attenuation is related to the water conductivity whose general value is known before the survey. The conductivity of the sea water varies from about $1\ S/m$ in the Baltic Sea to $5\ S/m$ in the ocean. The estimated value for the survey area was $1.6\ S/m$. Each particle in the ROI has randomly assigned conductivity which is bound by $0.5\ S/m$ below and above the estimated value.

In an initialisation step N particles are drawn. The number of particles is arbitrary chosen as $N = 1000$. In later work different number of particles were tested, but aside of computational intense there is no significant difference in BPF performance. Appendix C shows performance of the BPF algorithm executed on different data with different initial number of particles.

For each particle the theoretical distribution of the MF is calculated. From this distribution the theoretical readings of the horizontal and vertical coils are calculated for each data point.

Figure 110 shows the initialisation of the BPF. The boat's path shown in Figure 110 (E) crosses the cable's path perpendicularly and can be described as a straight line for two-dimensional calculation.

The left image of Figure 110 (a) shows the ROI and 1000 hypothetical sources. The dark green line with an $\times$ symbol represents the horizontal coil readings for each sample point. Dark blue line with a $+$ symbol represents the vertical coil readings. Light green and blue lines represent theoretical output for horizontal and vertical coil respectively.

The random distribution of particles is shown in Figure 110 (b) cover all the ROI.

After the particles' initialisation, particle weights Figure 110 (c) are assigned to each theoretical source. The square root distances between the experimental and calculated coil readings are normalised and assigned to particles.

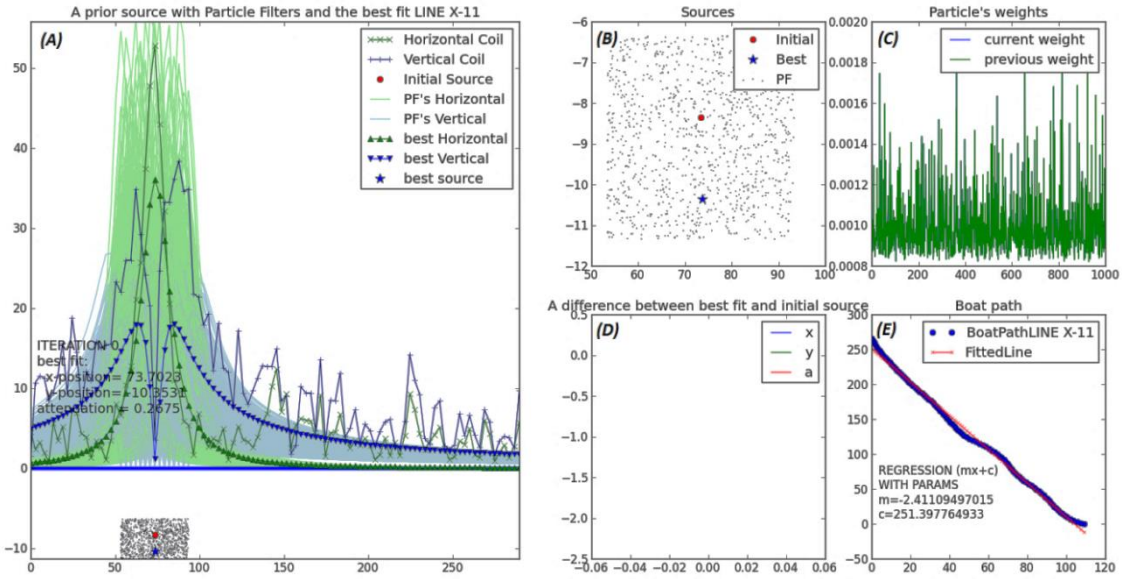

Figure 110 Initialisation of Particle Filter; (a): A prior source with Particle Filters and the best fit LINE X-11; (b): Sources; (c): Particle's weights; (d): A difference between best fit and initial source; (e): Boat path

In the next, resampling step new sources are drawn. A particle's probability of being chosen depends upon its weight and is higher if the distance between the particle distribution and the experimental readings is lower.

After the resampling procedure the particles are recalculated. A random number from a Gaussian distribution is added to the position and an attenuation parameter is assigned to the particle. The value of random number depends upon the particle weight. The bigger weight comes from the particle with smaller distance, hence closer to the real source. If the weight of the particle is bigger, the added random number is smaller to test an area in close proximity to the particle. Figure 111 shows the convergence of sources after ten iterations. The hypothetical sources concentrate in the region most plausible to be the true source.

Figure 111 (B) shows particles convergence. The particles represent the true distribution, hence the value can be obtained by taking the mean of the distribution. The standard deviation can give the error's prediction.

In addition, the particle representing the source with the smallest distance from the experimental readings is represented as a blue star point. The distribution of theoretical horizontal and vertical readings is represented as green and blue lines with triangles at the sampling points.

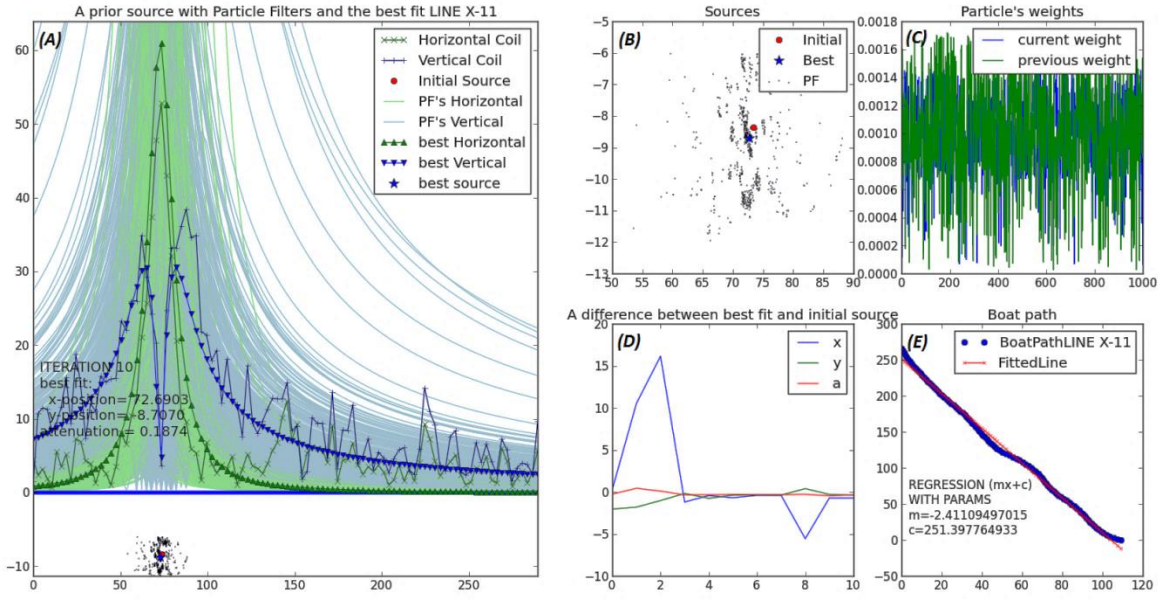

Figure 111 Particle Filter after 10 iterations; (a): A prior source with Particle Filters and the best fit LINE X-11; (b): Sources; (c): Particle's weights; (d): A difference between best fit and initial source; (e): Boat path

The resampling procedure is repeated to evaluate the best possible source. Figure 112 shows particles converging after 100 iterations. The particles cumulate in the cloud of highest probability of the true source. Each particle has a different attenuation rate. The source with the smallest distance and the highest weight represents the best estimation of the true source position and attenuation parameter.

Figure 112 (D) shows the convergence of the particles to the true location. The figure presents three parameters, namely x and y coordinates and the attenuation parameter. It can be noted that parameters converge to true location after twenty iterations.

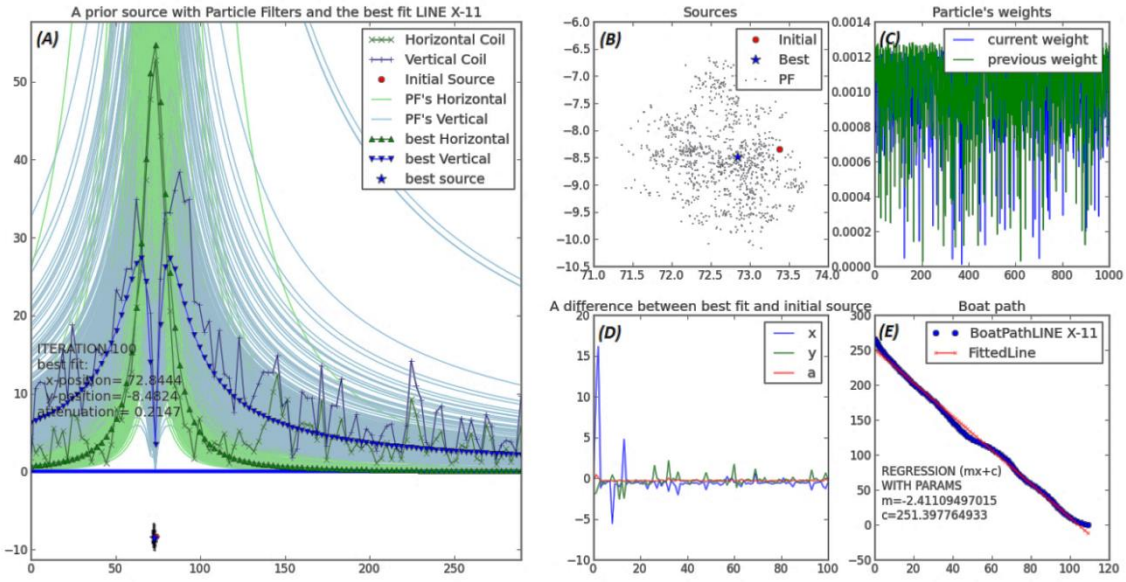

Figure 112 Particle Filter after 100 iterations; (a): A prior source with Particle Filters and the best fit LINE X-11; (b): Sources; (c): Particle's weights; (d): A difference between best fit and initial source; (e): Boat path

Appendix C shows application of the BPF on different lines from Denmark data. The behaviour of the algorithm gives readings which are close to the readings taken by a diver.

The BPF algorithm gives not only the estimation of the best position of the source but also the best estimation of the local attenuation rate. The advantage of the BPF algorithm is that it can find a source even without correctly given parameters. However the algorithm is computationally expensive. In a future study optimisation of algorithm will be investigated.

8.1.4 Batch Particle Filter 3D case

The purpose of the cable survey is to investigate a section of a cable rather than only one position as described above. The one position estimation method of BPF can be extended to locate the section of the cable. The MF distribution from the section of the cable on the sea surface can be sampled and measured by magnetic sensors. The sampled distribution of the MF gives indication of the cable position. For the straight section of the cable, only the initial starting position and the initial direction can be estimated. For the BPF algorithm, all points on the cable corresponding to the sample points are estimated along the cable section starting from the initial position and direction.

The BPF algorithm for cable localisation is initialised by drawing a set of hypothetical sections of the cable in the ROI. The ROI is calculated based on two peaks obtained from the horizontal and vertical searching coils. The peaks are considered on the first and the last survey line.

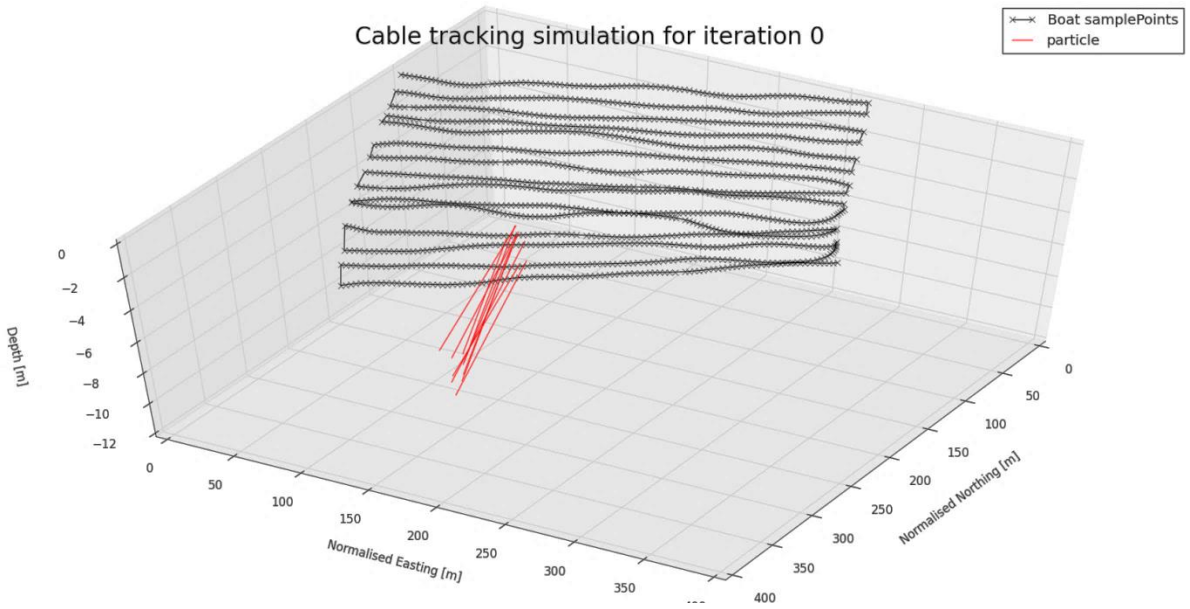

Figure 113 Initialisation of the BPF for cable section

To test the validity of the straight cable assumption, all peaks in the survey area can be regressed with linear regression. The standard goodness of fit test (Smith & Rose, 1995) gives a good indication of the cable path.

After the ROIs are evaluated and the straight cable path assumption holds, the particle cables are drawn with starting and ending points between the ROIs. For each sample point the nearest point on the particle cable is evaluated and a vector of the MF is calculated using equation (103).

Fig 114 shows the PF iteration. Ten hypothetical lines are drawn in between the ROIs region under the peaks. Each particle representing a hypothetical cable contains a possible position of the cable characterised by its directional vector and a starting point but also includes an attenuation parameter. The particles are chosen randomly from a ROI. The distribution of the MF is calculated by means of equation (103) and from this value the sensor readings are calculated by equation (105).

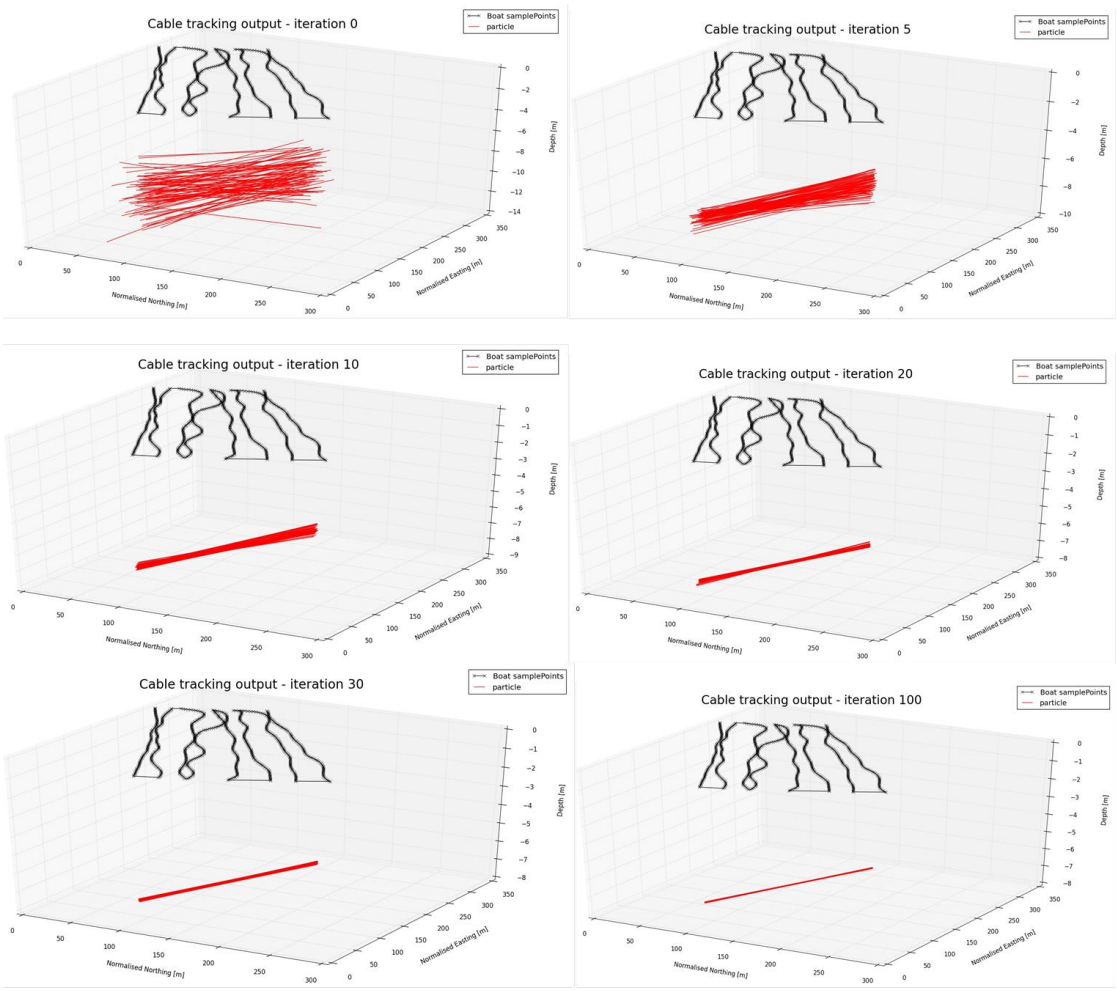

Fig 114 Particle cables iterations

The algorithm becomes sensitive to the initial value of the attenuation parameter and care should be taken to select this parameter as close to its true value by taking into account prevailing environmental conditions. The particles are iterated with the initial parameters. Only a first quartile is propagated to the next step. The distance between the particle's MF distribution and experimental data is calculated. The weights are assigned as an inverse of distances, normalised along all particles. From the set of all particles, one-fourth with the highest weights are chosen to propagate to the first step. Each particle in a chosen quartile propagates with three additional particles. The additional particles cover an area close to the base particle. They are constructed based on the initial particle with an added Gaussian random number. The particles move closer to the true value of the cables location and attenuation parameter after each iteration.

It can be observed that the particles tend to cumulate in the most plausible region after 5 iterations. The particles converge to a small area which is the true location of the straight section of the cable.

Point estimation and location of the straight section of the cable by PF can be used to locate any length and shape of the cable by dividing the whole section of the cable into a number of straight sections with different starting positions.

8.2 Algorithm detailed specifics

The PF algorithms are studied already from different angles. During implementation, subtle nuances need to be considered. In following section detail elements of the BPF will be described. The method can be divided into four parts.

In the first part prior data are used and initial cable position is drawn. The initialisation concludes with setting up particles for PF iteration. The first section will provide an overview of this initialisation step.

The BPF outcome is sensitive to initialisation step, thus additional measures are taken to make sure the procedure successfully converges. Whole section is devoted to this problem describing signal discrimination and initialisation in dynamical process.

After all primary data are obtained, the BPF commences to iteration process. During the process the particles are resampled, recreated and all necessary statistics are calculated. The process requires some consideration described in one of subsections.

After iteration steps the decision about validity of the estimation needs to be taken. The last section of this chapter describes error calculation and validation of the final output.

8.2.1 Region of Interest ROI

The BPF procedure used for cable localisation follows general PF scheme depicted in Figure 95. In the first step, the algorithm is initialised by generation of set of particles. In this prediction step, some prior assumption about cable localisation is used. The process of initialisation needs to be adequate to the problem of cable tracking and include initial prior position. It also needs to incorporate generation of particles drawn at random. The randomness provides coverage of wide range of possibilities.

Those requirements are satisfied by appropriately chosen parameters during particles' initialisation. Although the BPF can converge even if the true cable localisation coordinates are not covered by parameters of originally chosen particles, the well-chosen ROI region with drawn particles plays an important role in algorithm's performance.

In addition to ROI area, the number of generated particles needs to be considered. It needs to be large enough to provide good convergence without risk of particles degeneration but also needs to be adequate to computers processing power and allows fast computation.

Adequate construction of ROI was carefully considered in throughout autonomous navigation. During the initial part of the research, the PF was computed with on-line, sample by sample process. Each sample point position with its corresponding sensor's reading was fed to the algorithm one by one as the point was received from acquisition tools. In this process, the assumption about initial location could be made only with some *a priori* information from a previous survey or already surveyed section.

During such tracking, in the very first line there is no knowledge about the cable's position. The first ROI can be set only with some assumption and cannot be verified until the line is completed. In the following lines the ROI can be estimated based on prediction of cable's direction and projection of the boat's movement into this direction.

In the final method, the PF is performed after the line is completed. All data are available during PF iteration but also for particles initialisation. This solution greatly reduced problems which may be encountered in on-line localisation based on single samples.

In BPF, where all data points are available for PF algorithm, the ROI is set based on collected sensors' readings. The horizontal and vertical configuration gives a distinct pattern above the cable if the signal is presented.

As it was already described, the horizontal coils reading give a peak value directly above the cable, the vertical coil readings give increasing readings when the boat moves towards the cable, to fall down to a null value directly above the cable, sharply increase after crossing and slowly decrease when the boat moves away from the utility.

From the readings pattern, it was deduced that the best horizontal approximation of the cables position is the point with the largest difference between horizontal and vertical readings.

It needs to be noted that the noise incorporated in the readings can impact the point of biggest difference. In addition, the readings are not necessarily taken above the cable and it can happen that two readings are symmetrically on both sides of the utility. For this reasons different ranges of ROI were investigated. The optimal choice depends on factors such quality of acquired data, distance to the cable

In Denmark data, the horizontal range of ROI is expanded to five samples taken before and after the biggest difference. In practical terms it means that the ROI covers area of about 20 metres of each side of the cable but it depends on the specification of the survey.

The first assumption about vertical distance to the cable can be made by the distance to the seabed read by depth sensors. The range of vertical positions of the cable can be inferred from the subsea cable's nature and properties. In deep water areas, the cable is laid on the sea bottom. In shallow water, the cable installers aim to bury the cable up to two metres in the seabed. In practice it is not always possible and sometimes cable can even be suspended between the rocks.

For above reason, the ROI's depth is calculated from three metres below the seabed up to two metres above. It gives five metres of vertical range to draw theoretical position and particles.

The ROI and particle characteristics are not only confined to particle's coordinates. The important part of the algorithm is an estimation of the attenuation factor. As it was already pointed out, the attenuation factor depends upon characteristics of the water such as salinity but also on the parameters of the induced tone and magnitude of the current.

The initial attenuation of the particles is estimated with best fit method for the single point in ROI area. This Best Estimation Point (BEP) is located on the sea bottom level directly under the biggest difference. If the cable would be on the sea floor and the readings would be perfect, this point would also be the position of the cable.

After establishing the BEP the readings are calculated according to equation (111), where the only unknown is the attenuation factor c.

To find the best fit the simple calculation of the theoretical values in the range of different attenuation rates were sufficient. For each of attenuation the least square fit was calculated between the theoretical values and experimental data. The rate with the smallest distance was chosen as the most appropriate.

As the calculation between the theoretical output and noisy readings are not perfect, the range of the attenuation factor is set as 15% below the best fit and 15% above.

The percentage was established empirically mainly on Denmark data. The best fit was calculated if the cables be position on the top of the ROI range, its bottom and corners. For different position and different lines the attenuation did not fall more than 10%. As Denmark data may not be representative for all possibilities, it was decided that the initial range will be between 15% space above and below.

The example of ROI region and convergence of particles is shown in Figure 115, Figure 116 and Figure 117.

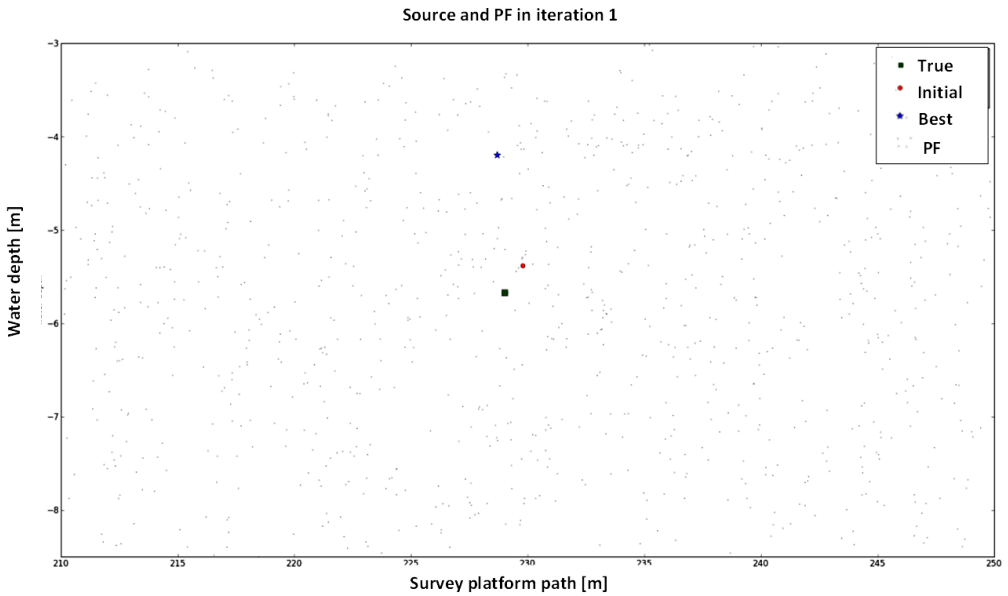

Figure 115 Initialisation of ROI and 1000 particles

In the initialisation step random set of 1000 particles are drawn in ROI area. Each particle has its coordinates but also its randomly chosen attenuation step. After initialisation, the particles start to converge into areas of more plausible for cable location.

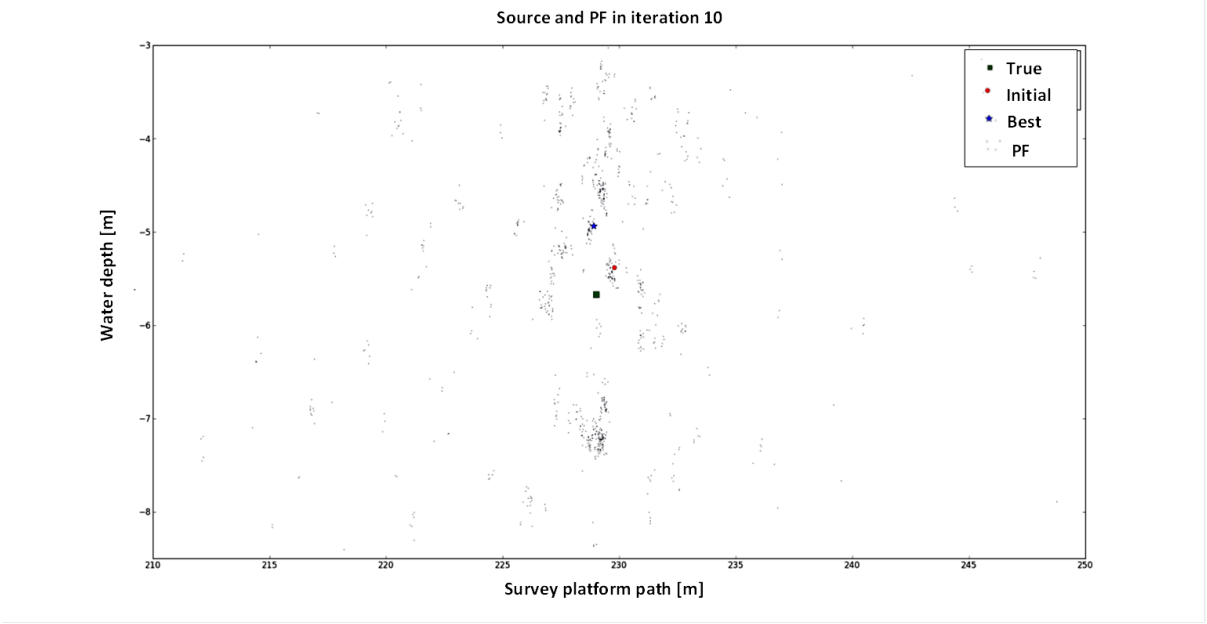

Figure 116 The ROI region and convergence of particles after 10 iterations

After 100 iterations shown in Figure 117, particles tend to concentrate in the area of the true location of the utility.

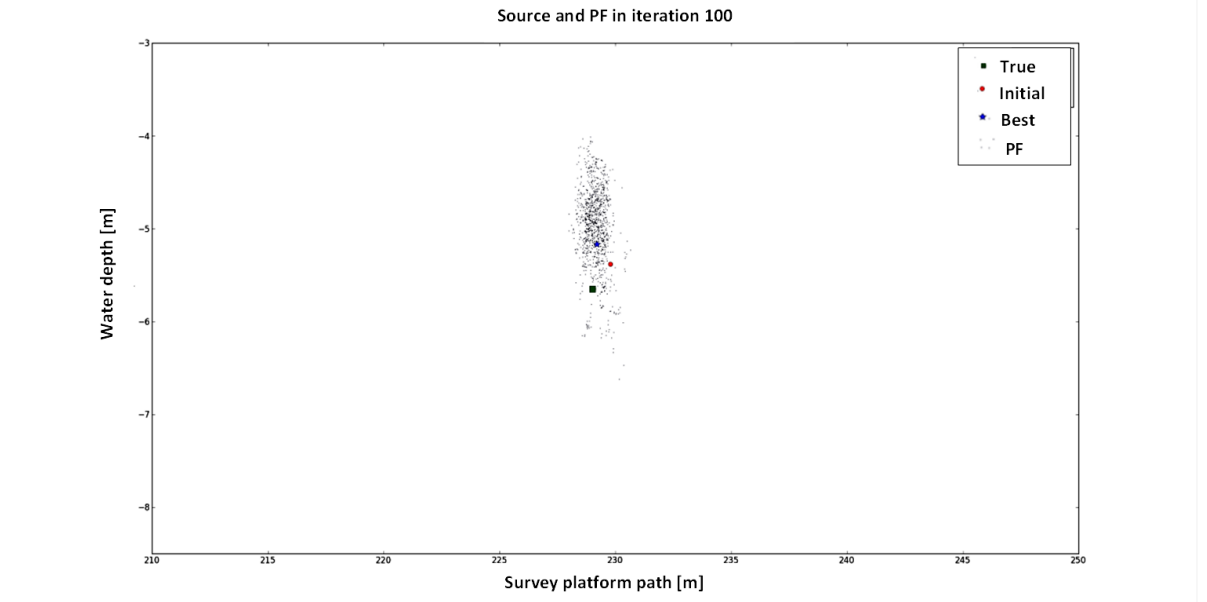

Figure 117 The ROI region and convergence after 100 iterations

The ROI area was tested by conducting different runs on collected data and on simulations. On all runs the described choice of ROI gave convergence to the mean values in the range of standard deviation.

Beside BPF for a single line with 2-dimensional space, the BPF was applied to three-dimensional problems where instead of a single point, the section of the cable is estimated by line equation.

Two different solutions were tested with satisfactory result.

In one of the tested solutions, the cable is described as parametric equation (113) in three-dimensional space.

$$x - x_0 = at \qquad (113)$$

$$y - y_0 = bt$$

$$z - z_0 = ct$$

The above equation describes a line through the point (x_0, y_0, z_0) and parallel to non-zero vector $v = (a, b, c)$. During BPF iteration process readings in each sample points were calculated according to the shortest distance between the sample point and particle represented by the parametric line equation.

The particles were initiated by choosing the points in a similar fashion as in 2-dimensional problem. The coordinates of the point were made in the plane under a regression line fitted to the boat path with the depth of the points two metres above and three metres under the sea floor.

To estimate the initial direction vector v the initial vector was built between two BEP points located under the first and last survey line.

In similar fashion to the 2-d problem, the initial attenuation factor was estimated by the best fit between the readings and their estimation with different attention. For attenuation estimation the first survey line was used and the theoretical output was calculated in accordance with parametric line between the BEP on the first and last survey line.

The autonomous navigation system uses a combined approach. The autonomous platform requires some indication of the *a priori* cable position. At first, the ROI is projected to find next place of interest. The platform moves to cross this position, collecting data points along the line. Based on the reading the ROI is corrected and the BPF algorithm proceeds as above.

8.2.2 Fuzzy Logic based Region of Interest selection

A tracking algorithm needs to be robust in a survey environment. It needs to perform tracking in all conditions and provide accurate localisation despite survey circumstances. The choice of ROI described above gave good results but does not guarantee robustness in every situation. Problems can occur if there are anomalies in the data such as large noise or unpredicted spikes.

Another situation where the algorithm can mislead the cable's localisation is a situation when there is no signal in the cable. Such situations can occur for different reasons and sometimes are difficult to predict. It was witnessed during the trials at a Cornish site – Sennen Cove 2013.

The tone in the cable was provided by a cable station in London. During the survey everything was arranged beforehand. The cable's signal was tested on the beach a day before the sea trials. The following day, during the boat operation it was impossible to locate a cable by any means. After consultation with the cable station it turned out that they experienced difficulties, had to switch off the tone during the night shift and did not pass this information to the surveying team. As a result, during the survey, the coil's readings presented only noise without a signal.

Although the biggest difference between horizontal and vertical coils readings most often arises above the searched utility, experimental data suggest it not always might be the case.

During experiments conducted locally in Hooe Lake in Plymouth, the data showed singular anomalies and occurrences of large spikes in one of the readings. The false readings came from different sources such as equipment defects or external interference such as the boat's engine sparks.

The false readings can lead to ROI set in the wrong position, under the areas where there is no signal coming from the utility. This situation was tested and is presented in the following section.

Figure 118 shows correctly established ROI in the area where the signal is presented. The vertical lines on the graph separate the signal to the area of the noise only on the left, signal in the middle and noise on the right.

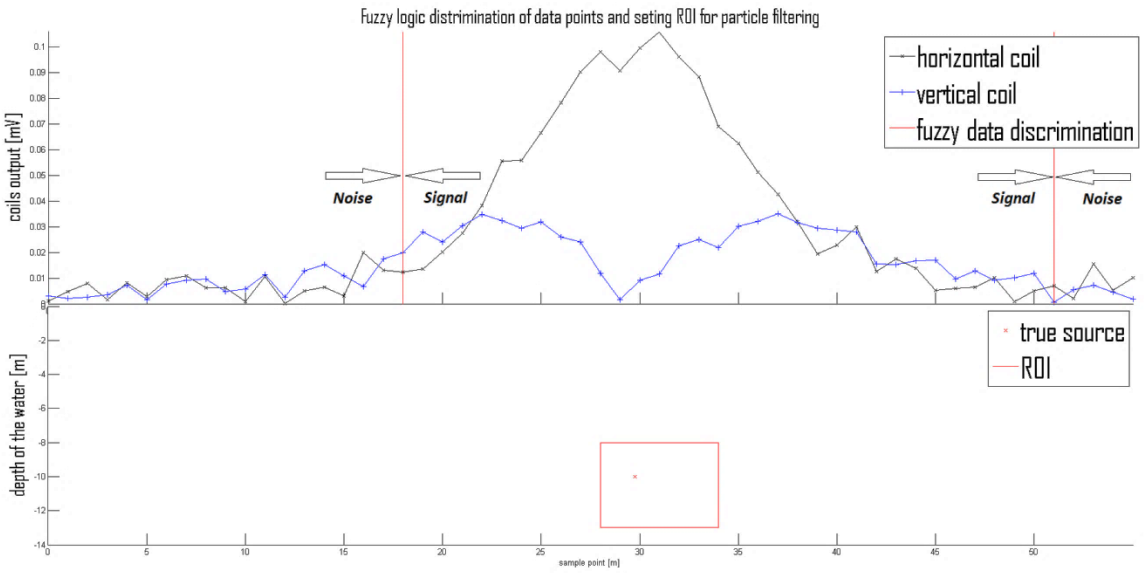

Figure 118 Correctly set ROI in area of the signal

The correctly positioned ROI guarantees convergence of the BPF. Different set-ups were tested with ROIs scaled to cover wider or smaller areas and started in different positions. Even if the ROI does not initially include the true location but it is aligned in the area of the signal, it does converge to the true location.

The convergence is not guaranteed if the ROI starts in the area where no signal is presented. Figure 119 presents ROI initialisation outside of the signal area.

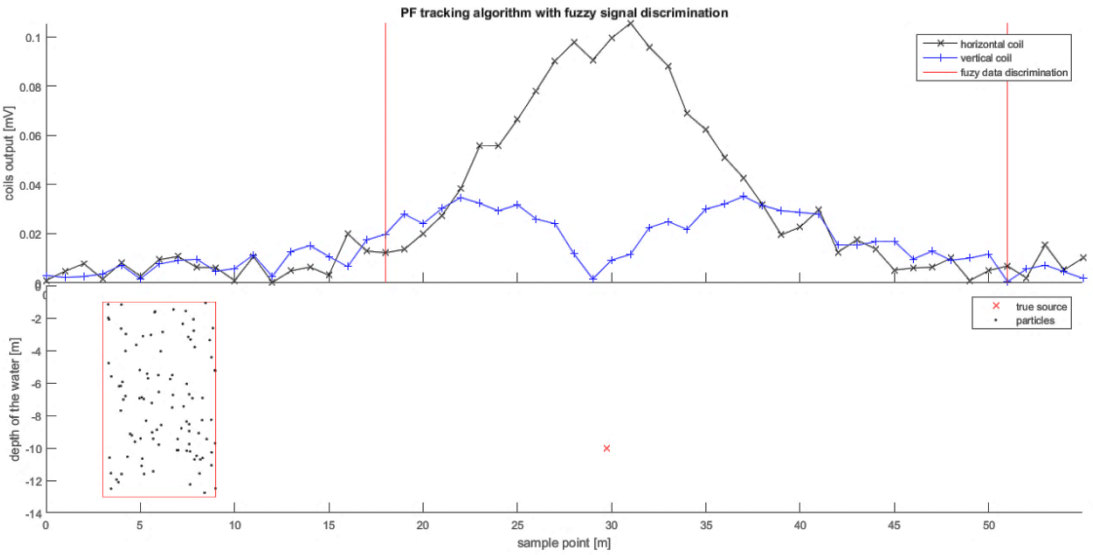

Figure 119 Initialisation of PF outside signal range

After BPF iteration, particles start to diverge from the true location. Figure 120 shows particles' localisation after ten iterations.

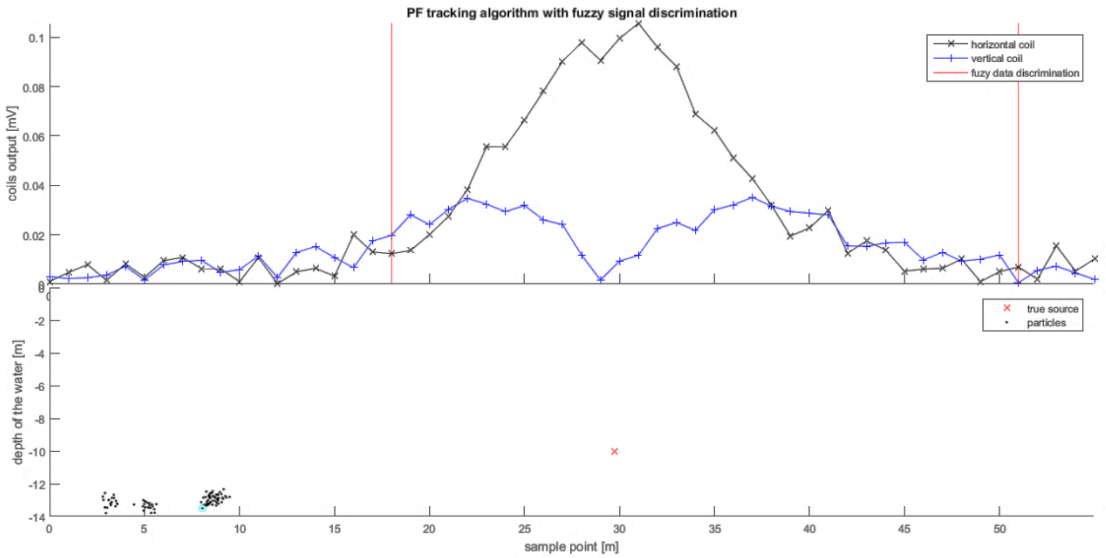

Figure 120 BPF divergence after 10 iterations

After 20 iterations shown in Figure 121 all particles start to diverge from the correct location. It needs to be noted that BPF algorithm includes random process. Although in most cases checked in simulation, the BPF with outside set ROI diverged, it does not have to be a case.

Cases of divergence were not noted if the ROI was set correctly under the area of presented signal.

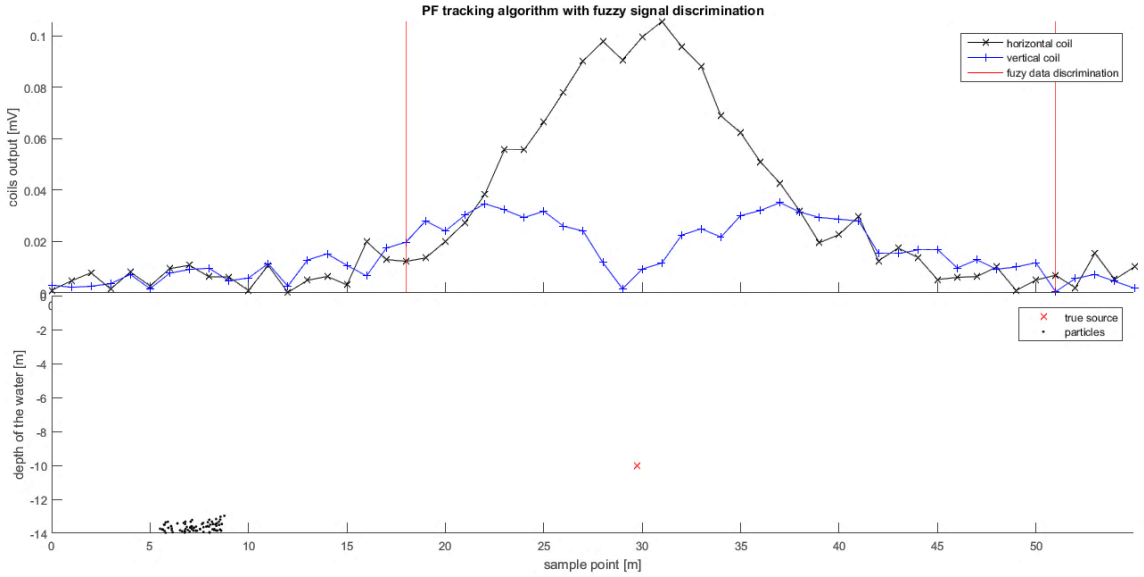

Figure 121 BPF divergence after 20 iterations

To overcome the problems related to the presence of the signal, additional measures were proposed. The data were categorised into three parts, the noise only before the cable, the signal above the cable and the noise only after the cable. The classification relied mainly on simple moving average (SMA) and noise average value used as discriminatory filter built on Fuzzy Logic System decision-making (FLS).

The SMA statistic was calculated for each line criss-crossing the cable. After starting the line the survey platform collected horizontal and vertical coils readings. If there was no signal presented in collected data, properties of the white noise indicated that the SMA should have no change thus be equal to zero.

When the platform approaches the cable the moving average should show positive incline. It should increase up to the point of crossing then start to decrease when the boat departure to the cable.

The average signal magnitude gave the second statistic used in the calculation of a threshold value of the signal. The threshold M was calculated as double of the noise average value.

The 10-samples SMA computed from the coil readings were fed as input to the membership function shown in Figure 122.

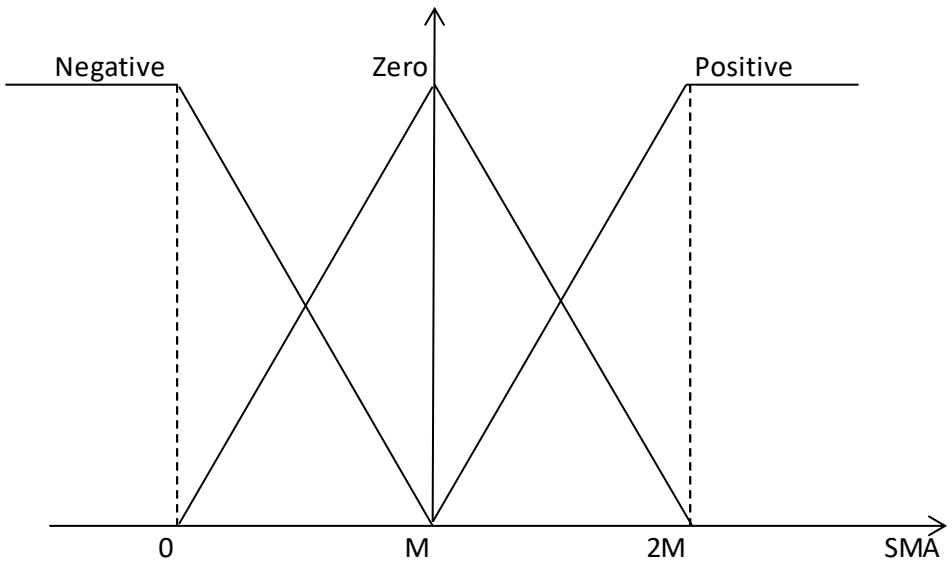

Figure 122 Fuzzy classifier - input membership function

The following fuzzy rules were applied during decision-making process:

- Rule 1: If SMA is negative, then ff is negative
- Rule 2: If SMA is zero, then ff is zero
- Rule 3: If SMA is positive, then ff is positive

The output of the system is fuzzy flag ff. The crisp value of classifier is obtained from the output membership function shown in Figure 123. The flag ff is Boolean value zero or one and it is used to indicate whether or not the coil readings were meaningful.

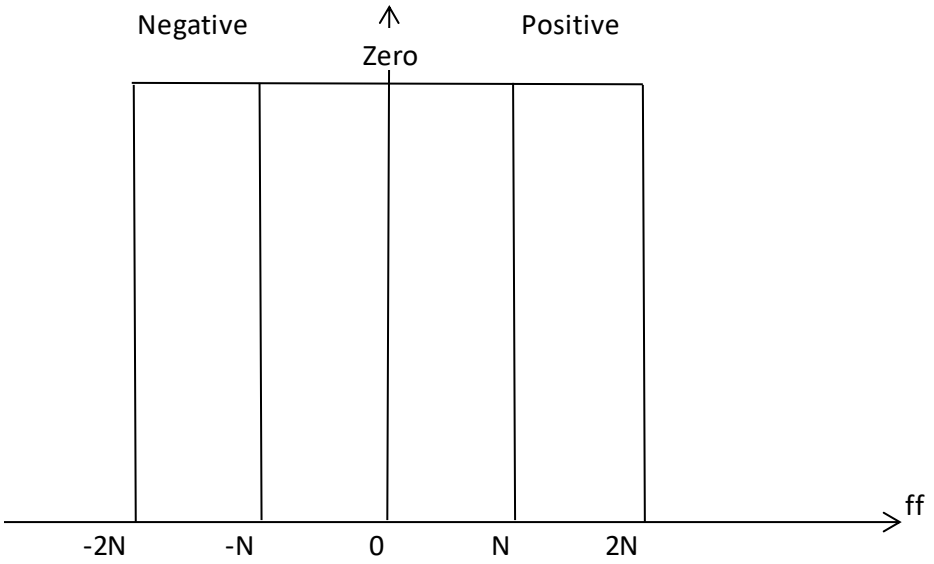

Figure 123 Fuzzy classifier - output membership function

The classifier flag is reset to zero at the beginning of every surveying line. After the flag changes to 1, the readings are considered relevant to the signal and those readings are taken to initialise BPF algorithm.

The computer implementation of the classifier is presented in Appendix D.1.

In addition to signal discrimination fuzzy classifier ff can be used in autonomous navigation. The rise of the flag indicates that the vehicle is approaching the cable. The data collection process can be started and the meaningful data are fed into the algorithm.

The drop of the flag indicates that the vehicle is departing from the cable into the area where the readings are irrelevant as there is too weak or no signal in the noise. In such situation, the vehicle can abandon the surveying line and start manoeuvre to source data in next survey line.

8.2.3 PF resampling and weighting

After the ROI initialisation and particles draw, the BPF algorithm iterates to produce the localisation result. In each iteration the particles have their weights determined, are resampled, their mean and error covariance are recalculated and the decision about new iteration is made. In addition to normal procedure an extra adaptive step is introduced. After importance sampling, the particles are regenerated to guarantee more precise convergence.

In the first initialisation step, N number of particles are generated in the area of ROI. N random numbers are drawn with random number generator. As most generators produce the numbers in the range of zero to one. The numbers are scaled to cover ROI and create an array of N random sources with positional and attenuation components.

For each random source an importance weight is calculated. The theoretical values of sensors readings are computed in the way the readings would be taken in the sample points if the true cable position and attenuation would be the same as the given source.

The Euclidian distance between the theoretical readings and experimental data is computed to give a single sum corresponding to a particular source. The bigger number means there is more difference between the experimental and theoretical data, thus the smaller numbers correspond to more plausible locations.

The array of all weights is normalised and theoretical sources are recreated and resampled accordingly to the weights.

In many PFs presented in the literature, the algorithm resamples from the same set of particles and propagates particles through a system model. Arulampalam et al., (2002) and Cappe et al., (2007) point out that the PF algorithm tends to degenerate and leads to sample impoverishment. The resampling procedure propagates only a small set of samples with high weights; particles with small weights do not contribute to the process.

Fu & Jia (2010) proposed a new resampling algorithm in which particles with low weights are eliminated and the particles with high enough weight are used as mother particles to generate new particles.

For BPF an algorithm custom generation method was introduced. Before resampling the particles are ordered accordingly to their weights. First, 25% of samples propagate to the next step and 75% samples with low weights are eliminated. For each source from remaining particles, three new sources are created. Each newly created source differs from the mother particle by some random number r. The difference depends upon preserved original weight. If the original weight was high, hence the particle's output was closer to experimental data, the difference is smaller. If the original weight was on another side of the scale, hence lower weight and larger contrast between particle's output and empirical data, the spread of newly created particles is larger.

After recreation of the particles, their weights are reconstructed and particles are resampled into a new set. The recreation procedure eliminates the risk of samples impoverishment and introduces diversity in particles. As this major drawback of PF was taken care of, the BPF can implement a straight forward resampling algorithm.

There exist many resampling algorithms having different advantages in speed, intensity and built in prevention of weight degeneration. The most commonly used resampling algorithm called Roulette Wheel Sampling (RWS) (Vavak & Fogarty, 1996) is often considered as perfect but computationally intensive method.

The RWS samples one particle at the time. It selects the first sample such that the sum of weights in the input up to and including this sample by uniform random sampling from the distribution [0 1]. Although RWS is computationally intensive, the algorithm is easy to implement and parallelise (Massey, 2008). As the name suggests the procedure follows selection on a roulette wheel. The whole roulette is partitioned into several sections corresponding to different particles. After the spun wheel stops, a pointer points to a winning section. The magnitude of a central angle of each section is proportional to the weights of the particle, thus the probability of the sector to be chosen is related directly to the particle's weight (Zhong et al., 2005).

Massey (2008) provides a description of the algorithm as shown in Figure 124. Computer implementation of the algorithm can be found in Appendix D.2

to *sample-one* (μ)*:*

$t \leftarrow 0$

for i **from** 1 **to** m **do**

$t \leftarrow t + w(s_i)$

if $t > \mu$ **then**

return s_i

to *sample:*

for i **from** 1 **to** n **do**

$\mu \leftarrow random\text{-}real\ ([0..1])$

$s_i \leftarrow sample\text{-}one\ (\mu)$

Figure 124 Algorithm of resampling with Roulette Wheel

Whole resampling procedures together with particle regeneration is shown in Figure 125. It was tested on both simulated data and samples collected during experiments. The algorithm performed with satisfactory results and provided an outcome with sufficient performance.

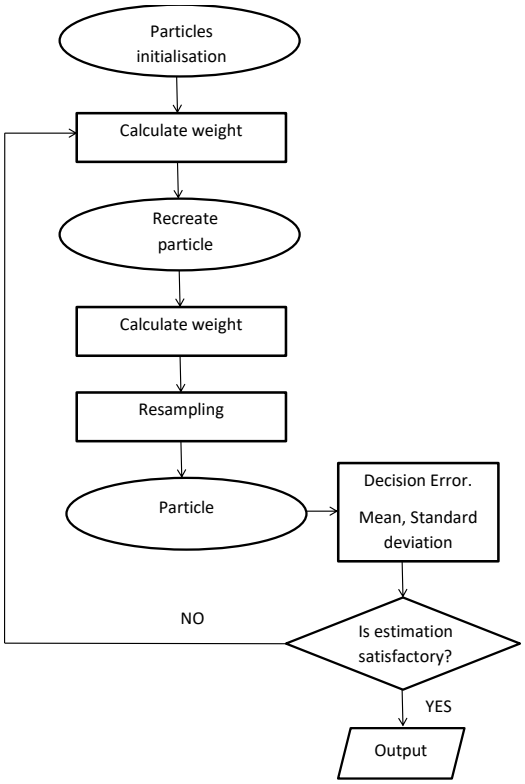

Figure 125 Batch Particle Filter iteration procedure

The process of iteration finishes with the estimation of the outcome. The outcome includes all positional data together with an estimation of the error, the standard deviation

8.2.4 Error decision

The final outcome of BPF algorithm is estimation of cable localisation. The position of the cable is given by probability distribution function. The mean of the distribution serves as the cable location. The standard deviation of this distribution gives an insight into the estimation error. In other words, it provides a precision of the localisation algorithm.

The BPF is an iterative process. During estimation, the resampling and particle regeneration repeats up to a point when the break decision is made. The judgment relies on the distributions' mean, its change during iteration and its standard deviation.

After initialisation, the particles cover large ROI region. In the first iterations they start converging quickly into more plausible regions.

The iteration stops when the error variance for each positional parameter doesn't change by more than a given value in ten consecutive runs. For practical implementation, the standard deviation is set to be below 0.3. It can be translated to thirty centimetres of BPF accuracy. The variance of the standard deviation in ten consecutive runs needs to be below 0.01. It means that the particles reached their position and do not converge anymore. The values were set experimentally by analysing the data.

Although there were no cases of divergence found, the performance of the algorithm depends upon number of iterations and number of particles. The algorithm tested on different data shows that given correct ROI selection, the algorithm will converge to the similar distribution of particles. The BPF algorithm convergence behaves in a stable manner despite the number of iterations or number of particles, the algorithm gives good results with 1000 particles and 50 iterations.

Figure 126, Figure 127 and Figure 128 show the behaviour of the algorithm performed on the same survey line but initialised with a different number of particles. As the algorithm includes random process, the outcome of each BPF instance behaves differently. Calculated variance of the statistics in iterations after convergence, illustrate change in the distribution.

Figure 126 presents three examples of BPF initialised only with ten randomly chosen sources. The BPF converge to anticipated value but the mean of the distribution is not stable. The variation of the second half, where the distribution should already have converged, exceeds the established threshold of 0.01.

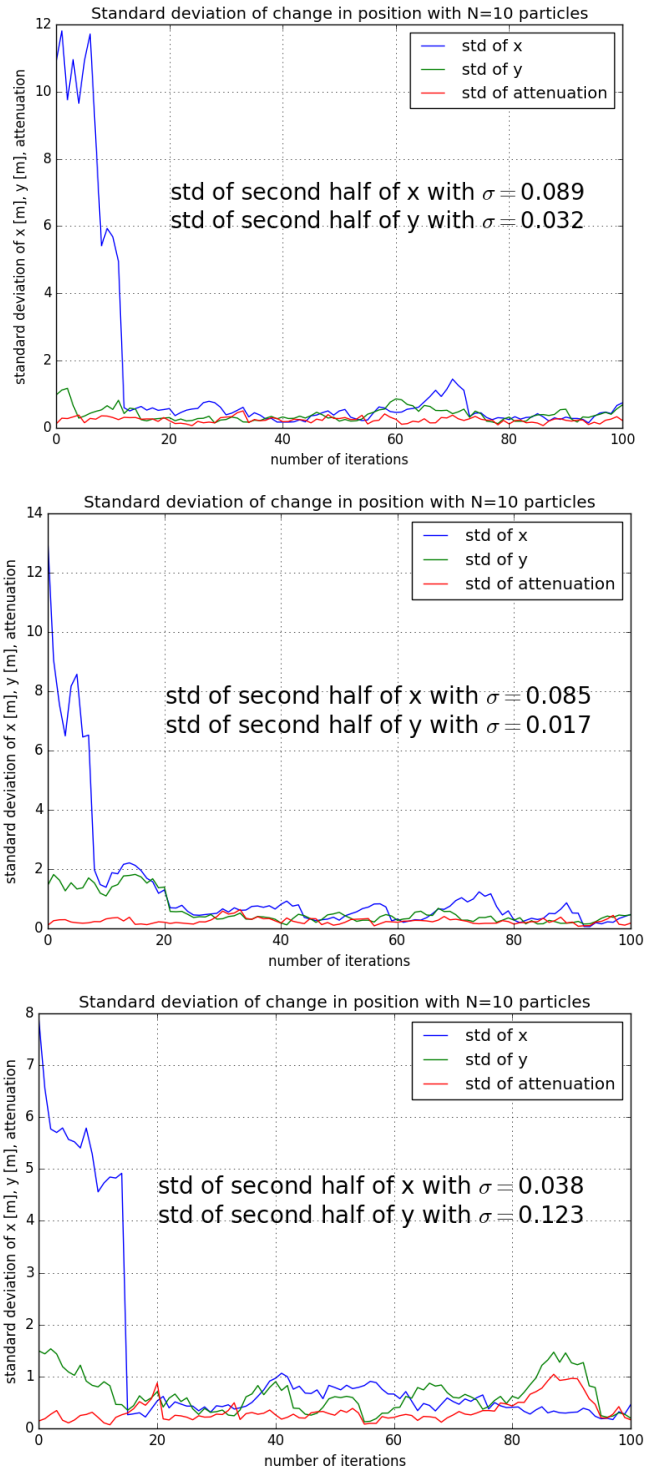

Figure 126 Convergence examples: standard deviation of coordinates with BPF initiated by 10 particles

Much better behaviour is given by a BPF initialised with 100 particles. Figure 127 shows that the particles behave in more stable manner. After convergence, the mean persists on the stable level. The variation of the mean changes is still inadequate.

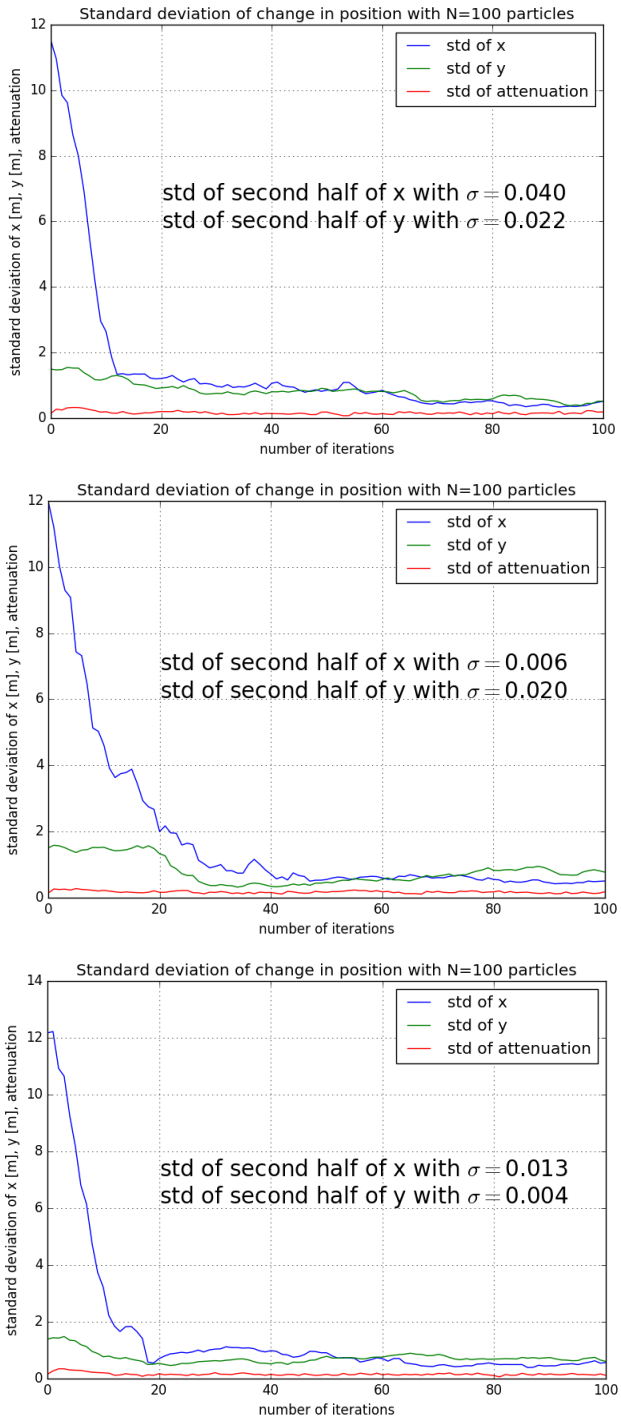

Figure 127 Convergence examples: standard deviation of coordinates with BPF initiated by 100 particles

Figure 128 shows BPF initialised with 1000 particles. It smoothly convergences in the initial iterations and stays at a similar level after first 50 iterations.

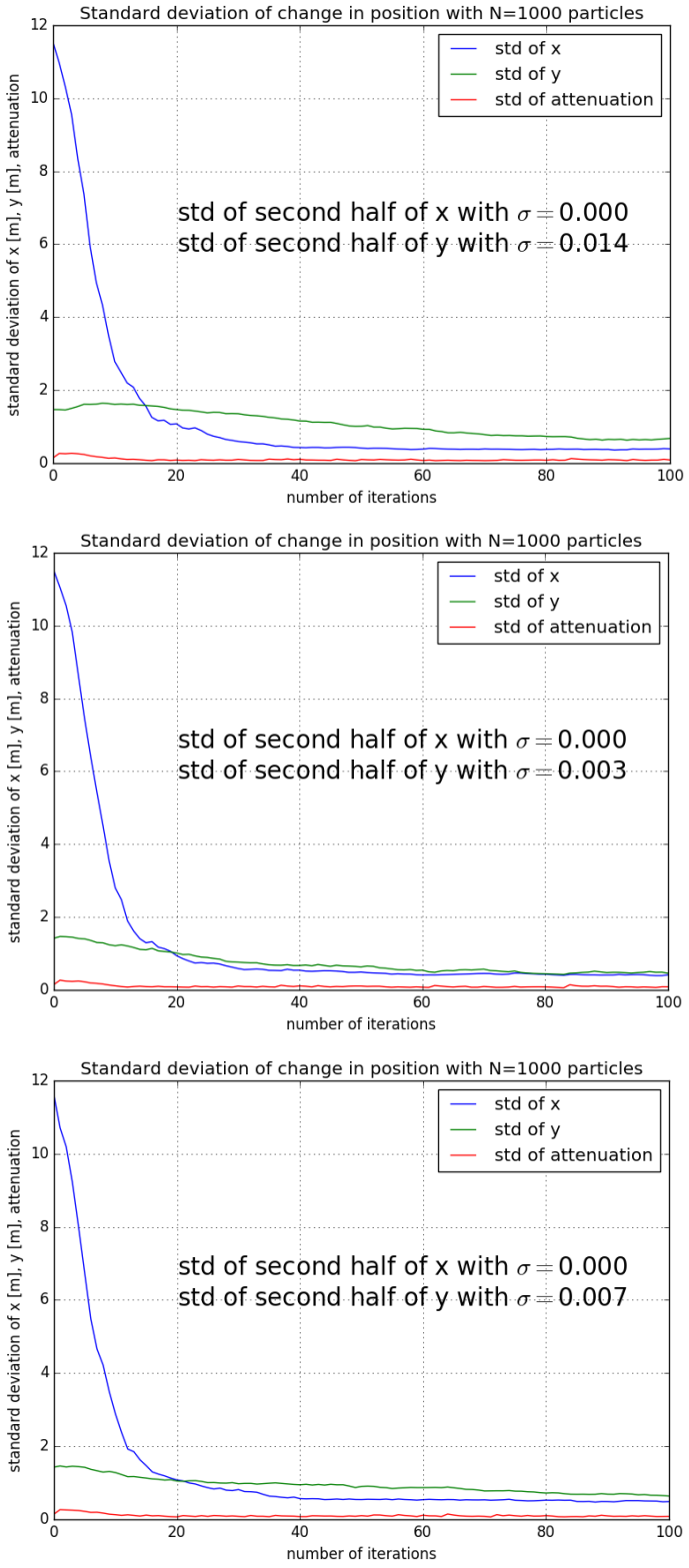

Figure 128 Convergence examples: standard deviation of coordinates with BPF initiated by 1000 particles

The final output is given by the mean and standard deviation calculated after ten iterations with variance less than 0.01 under the condition that standard deviation is less than 0.3 metre.

8.3 Batch Particle Filter Final method

The method of BPF was applied to localise and estimate the burial depth of the cable near the Danish town Korsør. The data from performed survey were collected by navigation software and grouped into survey lines. Each line was fed to BPF algorithm performing the cable's positioning. Figure 129 shows the final cable's position as a connection of estimated points.

Figure 129 Cable location - Korsør, Denmark 2011

During the estimation, the cable positions were analysed in the iterating process as one survey line at the time. Each line was fed into the algorithm to calculate easting, northing and vertical distance of the cable's position.

For the purpose of the estimation, the survey line was projected onto a two-dimensional plane. For this reason, the survey line was estimated as a straight line equivalent to a regression fit through all surveying

points. The plane was set to include the survey fit and have vertical direction $z = 0$. In the short distances the cable can be considered as a straight section and analysing the signal source in the two dimensional plane reduces computational expense.

Figure 130 shows three-dimensional visualisation of the survey lines, water depth as read by single beam echo sounder and cable line connecting the survey points.

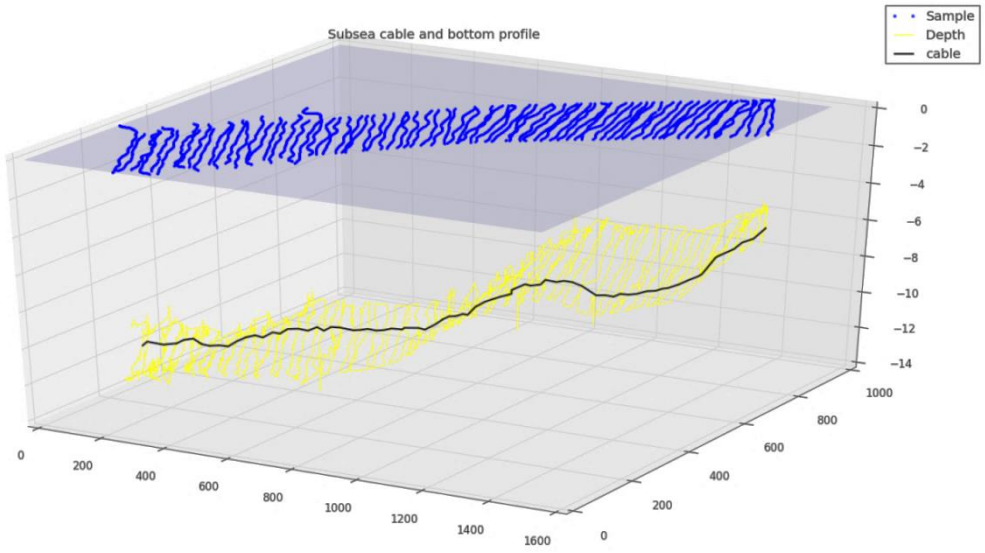

Figure 130 Cables position after performing localisation on all surveying lines

The data from the cable are presented in a tabulated form where for each line single source position in easting and northing is provided with corresponding water depth and distance to the cable.

Figure 131 presents a section of the data showing first eight lines.

Date	Time	Name	Easting	Northing	Ceeducer	CableDepth
11/05/2011	14:27:58	X-76	635043.1	6131438	-10.66	-10.768
11/05/2011	14:35:33	X-75	635048.5	6131446	-10.5	-10.596
11/05/2011	14:38:46	X-74	635080	6131467	-10.74	-10.8288
11/05/2011	14:42:46	X-73	635082.8	6131472	-10.75	-10.8301
11/05/2011	14:45:19	X-72	635106.2	6131482	-10.74	-10.7996
11/05/2011	14:49:05	X-71	635116.3	6131494	-10.43	-10.5275
11/05/2011	14:51:27	X-70	635134	6131507	-10.55	-10.6217
11/05/2011	14:54:42	X-69	635144.5	6131523	-10.95	-11.078
…	…	…	…	…	…	…

Figure 131 Example of tabulated data presenting source position and depth

The BPF calculates the depth to the cable as the distance from the water line. The burial depth can be obtained by subtraction of the vertical distance to the cable and measurement of water depth provided by the echo sounder.

It needs to be noted that all positional data are taken with sampling of 1 Hz, hence the spacing between the points is equal to distance covered by the boat in time of one second. The correct evaluation of the water depth needs to be left to the judgment of the surveyor. In practice, the seabed is often flat over small sections. Closest readings from the transducer can give good depth approximation and were used for this purpose. Figure 132 gives graphical presentation of the cable position, water depth and burial depth.

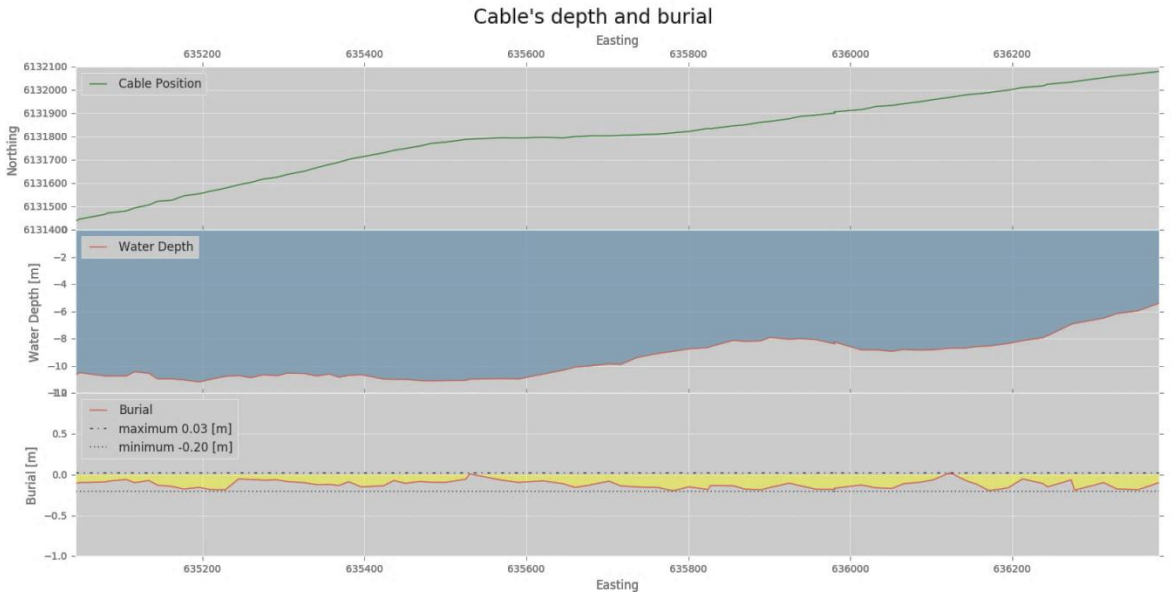

Figure 132 Profile of the cable depth and burial

Although the BPF algorithm was developed for surveys by manned platform, the method of detection was tested for use by an autonomous vehicle. Investigation of possibility of autonomous tracking was performed on the experimental cable path. Collected data were smoothed and interpolated to cover all survey area. The data were provided to simulated guided navigation.

The autonomous platform was modelled based on an unmanned surface vehicle (USV) “Springer” developed at Plymouth University (Motwani et al., 2013). The USV is equipped with a system of positioning and heading directed to the navigation control.

The movement of the vehicle was dynamically planned to follow a cable's route with a vehicle's path criss-crossing the cable in perpendicular directions.

At first, some, deliberately incorrect, assumption about the cable position and direction were made. The navigation guidance system determined the waypoints of the USV path in such the way that the USV crossed assumed cable portion perpendicularly to its direction. After the data were collected from the criss-crossing line, the readings were given to BPF algorithm to estimate exact crossing localisation and obtain correct cable's position. Using this information, the position of the cable in some distance downstream was estimated. Based on corrected data the guidance system determined next crossing point and further waypoint for the vehicle's control and the survey path was re-planned. The combination of BPF and autonomous navigation yield good results and the USV was able to correctly localise the utility.

The USV tracking brought additional challenges. During manned inspections, qualified surveyors and the vessel's crew constantly monitored streamed data, review them and make decisions about the further course of the survey. During the autonomous operation, the vehicle needs to make decision about quality of data and adjust the path dynamically.

The use of BPF in autonomous navigation raised problems, barely present during manned survey. Opposed to the manned survey when the skipper can react to survey's conditions and changes in searched signal, USV navigation is more uncompromised. Although the survey lines are planned dynamically, once set the USV aims to follow its waypoints. The USV has a bigger chance to align with the line which is not accurately perpendicular to the cable's direction. To overcome the problem additional readings correction was introduced.

Though vertical coils readings are not affected if the USV deviates from the perpendicular line, the horizontal readings are altered. To adjust the readings, collected data are adjusted by a cosine between required direction and actual USV heading. In practical terms, the corrected readings are reduced by small fraction depending on the path error. The correction is described in Equation (114)

$$C_H(k) = \frac{C_H'(k)}{\cos(\alpha)} \qquad (114)$$

where the $C_H'(k)$ is actual reading, $\cos(\alpha)$ represents the correction depending on an angle α between planned line and actual heading and $C_H(k)$ is corrected horizontal coil reading.

The setup is depicted in Figure 133.

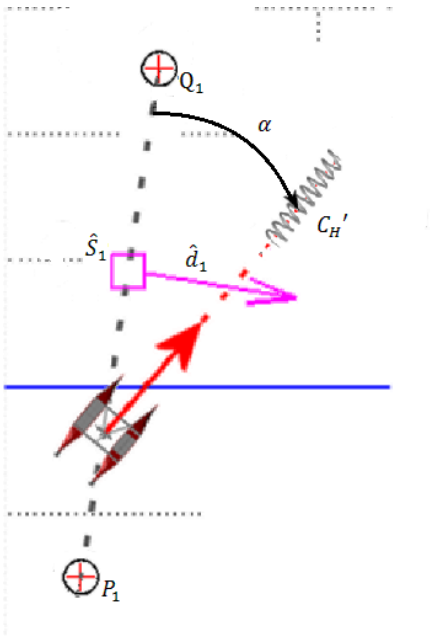

Figure 133 Horizontal coil readings correction

The BPF and the USV navigation and guidance system need to closely cooperate during the survey. Figure 134 shows initial set-up with cable assumptions and vehicles trajectory. Before operation commences, some prior statement about cable position is made. Prior position $\hat{S}_1$ and prior cables direction $\hat{d}_1$ give a way to set initial waypoints. The USV aims to conduct straight line $l_1 = \overline{P_1 Q_1}$ between starting point P_1 and finishing point Q_1. The data from sensors readings are fed to the acquisition system with FLS signal discrimination described previously. The FLS raises a flag when the USV enters region with strong signal presented. After USV crosses the cable and departures form the area covered by meaningful signal the FLS drops the flag and the data are passed to BPF for processing.

The completion of data gathering leads to two processes. The prior estimation of the cable's position is corrected and the guidance system estimates new crossing points furthermore determining USV path.

Based on gathered data the BPF algorithm calculates new, posterior location S_1. With all previous available data, the best cable direction is obtained. In the initial line, without previous cable points the prior direction

is assumed to be correct. The posterior position is projected forward by surveying line spacing, usually 30 metres. Obtained new prior position $\hat{S}_2$ is fed to a guidance system and USV path is recalculated.

The FLS flag drop indicates that the current surveying line is no longer adequate. There will be no more meaningful data collection along the straight line and the USV can abandon the current path in favour of a new direction. Figure 134 indicates this situation giving new waypoint Q_1' where the vehicle started its turn.

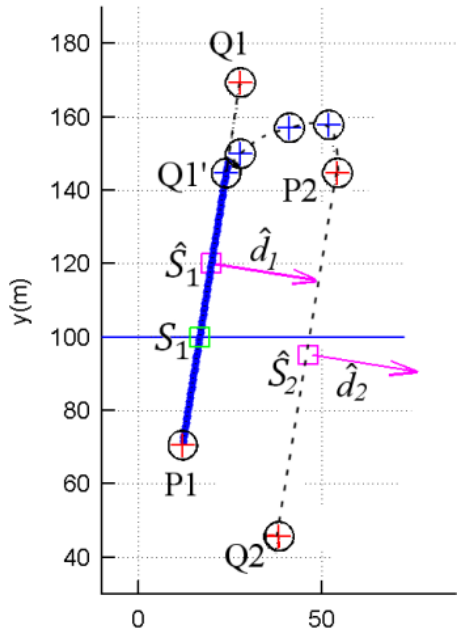

Figure 134 Initial cable estimation, USV trajectory and resulting path planning

After completing each survey lien l_k a new prior crossing position $\hat{S}_{k+1}$ is presented to the USV control system. The crossover point is calculated as the previous *post-priori* point S_k projected by some line spacing distance ρ into direction of the cable d_k 30 m in this case. Equation (115) describes the procedure.

$$\hat{S}_{k+1} = S_k + \rho\, d_k \qquad (115)$$

The guidance system sets new waypoints and determines the vehicle path to reach entry point of the line l_{k+1} The line is indicated by its starting point P_{k+1} and ending point Q_{k+1} in such a way that that the points span 50 m distance on each sides of the crossing point $\hat{S}_{k+1}$ and the vector between the points is perpendicular to prior vector direction of the cable $\hat{d}_{k+1}$.

After a few lines are completed and the cable position is charted correctly, the cable direction $\hat{d}_{k+1}$ can be obtained more precisely. The subsea cables are rigid body stretched on the seabed. The cable is modelled with a parabolic function extrapolating last three source estimates $(S_{k-2}, S_{k-1}S_k)$. The cable's direction $\hat{d}_{k+1}$ at $\hat{S}_{k+1}$ is estimated to be that of the tangent of the parabola at that point. Figure 135 USV trajectory with complete cables estimation process is shown in Figure 135. It shows a simulation of the cable localisation and tracking process for 300 m section.

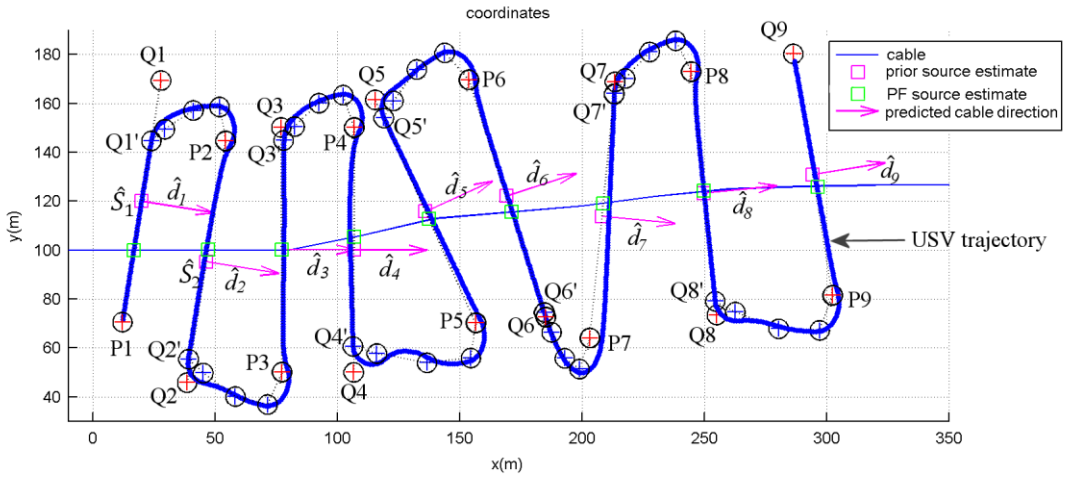

Figure 135 USV trajectory with complete cables estimation process

Combination of BPF with well-designed autonomous navigation and guidance system gives good perspective for reducing costs and safety consideration in subsea cable inspection. The system is able not only to chart the cable and follow its direction but also estimated vertical distance to the cable which in combination with water depth indicates its burial depth.

Chapter 9. Discussion, Conclusion and Recommendation for Future work

In this chapter, the main aspects of the work described in this thesis are summarised and discussed. During the project a new algorithm was developed. Although the algorithm was tested in simulation and in experimental trials there is still room for further improvements. Proposals for future research are given.

9.1 Discussion and Conclusions

The focus of this thesis has been on the study and development of a new method for tracking and estimating the burial depth of subsea cables. The task of underwater cable tracking is very important and also demanding and difficult to perform.

In the first chapters of this work the existing methods were reviewed and their ability to track the buried subsea cables was analysed.

After setting the aim and objectives of this work in Chapter 1, the following four chapters focused on different aspects of marine surveys, cable detection and tracking.

Chapter 2 described visual and hydro acoustic underwater detection. The visual methods were divided into deterministic and stochastic approaches. A Review of the subsea environment revealed that the deterministic approach encounters drawbacks difficult to overcome in marine surroundings. In this chapter the particle filter methods were presented for the first time. The particle filter was applied to visual cable tracking, where the utility line was modelled by particles representing possible cable parameters. The random process of particle creation and their Gaussian distribution proved to be better suited for underwater tracking. Aside from visual methods this chapter described hydro acoustic techniques are the choice for many marine applications. Acoustic surveys are well developed and provide tools for penetrating the seabed but in the current technological state it still cannot localise thin cable lines.

Chapter 3 focused on magnetic and electromagnetic detection. The magnetic field of the subsea cable penetrates different substances and does not suffer the limitation of not being visible if the cable is buried in the seabed. The chapter presented the theory behind the distribution of the field emitted from the cable. This theory is later used in the BPF algorithm hence, it was described in much detail. The publicly available literature does not cover much research on subsea cables. For this reason aerial power lines and underground cables were reviewed.

Chapter 4 gave a market analysis and presented available methods. In recent years the marine industry has undergone many transformations and is struggling with the economic crisis. On the contrary, the subsea cable market is experiencing an expansion and new investment. Cable tracking, periodical inspection and maintenance is a sought-after service. It is also demanding and difficult to perform, and especially in shallow water, difficult to be accessed by a specialised support vessel.

Tools existing on the market were developed decades ago and do not follow recent technological advances. An analysis of the market proves that the new method for cable tracking can be a good alternative to the existing methods, filling the gap between the market's demands and the offer.

Chapter 5 describes the prototype of the new system. Its modular design ensures flexibility and promotes its expansion. The chapter is divided into three sections. The first section focuses on sensor improvements, the second describes the hardware and the third section focuses on the user interface and the method of operation.

After these five chapters the work describes the algorithm for cable tracking. Traditionally cable localisation is made by an inverse method. The possibility of estimating the cable position from the EMF readings taken by a stationary sensor is investigated at first. The inverse method is difficult to apply for distances greater than three metres. To reduce this limitation, Neural Networks were investigated. The results did not give a satisfactory outcome and the approach was changed to analyse multiple sample points.

Chapter 7 focused on modelling of the EMF emitted from the cable based on collected sample points. The resulting models were enhanced with Kalman and unscented Kalman filter algorithms for the linear and non-linear case respectively. The main disadvantage of this approach is the need of good quality data prior to the survey.

All the work and analysis led to the development of a Particle Filter algorithm based on the whole distribution of the data samples. Chapter 8 describes the BPF in detail. It starts with the simplest two dimensional case where the coordinate system is reduced to the cable depth as the vertical axis and distance along the survey line as the horizontal axis. From this point the BPF is extended to the three dimensional case with all information from the sample point and the cable line described in the geographical coordinate system. The cable can be modelled as sections of straight lines and such was investigated in the most developed case. The BPF was tested in simulation and on real data collected in experiments and during the repair work. Those investigations conclude the chapter and verify the method.

9.2 Recommendation for future work

The following lists several suggestions for future work that because of time limitations were not possible to investigate further or improve in the current work.

The BPF localisation algorithm proves to be the good tool for localisation of subsea cables. It estimates the position of the utility giving its longitude and latitude coordinates and the vertical distance between the cable and the water surface were the sample points were taken. The method was investigated in experiments conducted in a shallow subtidal lake with a test cable. Although simulations show that the experiment finding can be transferred to bigger depths and real cables, the measurements were not verified with alternative methods.

The verification can prove to be costly and difficult. Expensive equipment would need to be deployed and the exact measurements would require cooperation of a larger team. It is believed that such situations can take place during some of the real work in the future. Verification of the methods would provide full approval and confirmation of the academic work. It cannot be done with the academic funding but in future commercial work the method can be arbitrarily tested and verified.

From the start the BPF was design as part of a wider hydrographic survey. The method is designed to read data along the survey line, traditionally criss-crossing the utility. With few modifications and additional developments to employ a sensor array, the time and cost of the cable survey can be considerably improved.

In future work the acquisition hardware can be extended to read not just one three-axis coil but a suite of sensors deployed as a tow fish or mounted across the survey boat as a long array. Such a configuration

would require a modification and possibly optimisation of the algorithm but can be a worthwhile alternative for traditional surveys covering large paths and consuming expensive survey time.

A natural extension of the above recommendation would be to deploy the method on a fully autonomous platform where the survey plan would take into account the BPF requirements and optimisation of the platform's parameters such an operation time or power consumption.

Lastly the BPF is designed for shallow water surveys where the boat in naturally in short distance to the cable. The deep ocean exploration demands different approach and deploying underwater vehicles. The BPF can serve as the main tool for cable tracking in deep oceans and integration into underwater vehicle. Implementation of the algorithm to such applications would relax the requirements of keeping the vehicle close to the seabed and risking its damage in underwater features.

Finally the BPF algorithm can be extended to other principles and serve as the main localisation tool in geomagnetic detection or visual and hydro acoustic surveys. The author of this work hopes the method will be fully commercialised and will bring more positive results in the future.

Bibliography

Abdou, A. A., A. Shaw, A. Mason, A. Al-Shamma'a, J. Cullen, and S. Wylie. “Electromagnetic (EM) wave propagation for the development of an underwater Wireless Sensor Network (WSN).” *2011 IEEE SENSORS Proceedings*, no. 1 (2011): 1571-1574.

Alen, G. I., G. Sulzberger, J. Bono, J. S. Pray, and T. R. Clem. “Initial Evaluation of the New Real-time Tracking Gradiometer Designed for Small Unmanned Underwater Vehicles.” Brest: Proceedings of OCEANS 2005 MTS/IEEE, 2005.

Al-Shamma'a, A.I., A Shaw, and S Saman. “Propagation of Electromagnetic Waves at MHz Frequencies Through Seawater.” *IEEE Transactions on Antennas and Propagation* 52, no. 11 (2004): 2843-2849.

Antich, Javier, and Alberto Ortiz. “Evolutionary Tuning of the Control Architecture of an Underwater Cable Tracker.” *Artificial intelligence research and development* 100 (2003b): 65.

Antich, Javier, and Alberto Ortiz. “Underwater cable tracking by visual feedback.” *Pattern Recognition and Image Analysis*, 2003a: 53-61.

Araujo, Teresa, and Dinis Rui. “Analytical evaluation and optimization of the analog-to-digital converter in software radio architectures.” *IEEE transactions on vehicular technology* 56, no. 4 (2007): 1964-70.

Arulampalam, M. S., S. Maskell, N. Gordon, and T. Clapp. “A tutorial on particle filters for online nonlinear/non-Gaussian Bayesian tracking.” *IEEE Transactions on Signal Processing* 50, no. 2 (2002): 174-188.

Asif, M., and M. R. Arshad. “An active contour and kalman filter for underwater target tracking and navigation.” *Mobile Robots Towards New Applications* 1 (2006): 373-392.

Bagnitsky, Andrey, Alexander Inzartsev, and Alexander Pavin. “Side scan sonar using for underwater cables amp; pipelines tracking by means of AUV.” *nderwater Technology (UT), 2011 IEEE Symposium on and 2011 Workshop on Scientific Use of Submarine Cables and Related Technologies (SSC).* France, 2011. 1-10.

Balasuriya, Arjuna, and Tamaki Ura. “Autonomous target tracking by Twin-Burger 2.” *Intelligent Robots and Systems, 2000. (IROS 2000).* Takamatsu, Japan: 2000 IEEE/RSJ International Conference on, 2000.

Balasuriya, B. A.A.P., M. Takai, W. C. Lam, Tamaki Ura, and Y. Kuroda. “Vision based autonomous underwater vehicle navigation: underwater cable tracking.” *OCEANS '97.* Halifax, Nova Scotia, Canada: MTS/IEEE Conference Proceedings, 1997. 1418 -1424 vol2.

Bartington Instruments. *Datasheets Mag690.* 2014. http://www.bartington.com/Literaturepdf/Datasheets/Mag690%20DS2604.pdf (accessed 11 07, 2014).

Batista, Pedro, Carlos Silvestre, and Paulo Oliveira. “Single range aided navigation and source localization: Observability and filter design.” *Systems & Control Letters* 60, no. 8 (2011): 665-673.

Bech, Mogens, Andres Bjerrum, and Geoffery Arthur Shippey. “A system for underwater survey operations.” *Patent Europe WO1996003662 A2*, 1996.

Bogie, I.S. “Conduction and magnetic signalling in the sea a background review.” *Radio and Electronic Engineer* 42, no. 10 (1972): 447.

Brandstein, Michael Shapiro, and Harvey F. Silverman. “A practical methodology for speech source localization with microphone arrays.” *Computer Speech & Language* 11, no. 2 (1997): 91–126.

Cappe, Olivier, Simon J. Godsill, and Eric Moulines. “An Overview of Existing Methods and Recent Advances in Sequential Monte Carlo.” *Proceedings of the IEEE* 95, no. 5 (2007): 899-924.

Capus, Chris, Yan Pailhas, Keith Brown, and David Lane. “Detection of buried and partially buried objects using a bio-inspired wideband sonar.” Sydney: OCEANS 2010, 2010.

Caruso, M J, T Bratland, C H Smith, and R Schneider. “A new perspective on magnetic field sensing.” *SENSORS-PETERBOROUGH-* 15 (1998): 34-47.

Chen, Hsin Hung, Wen Ning Chuang, and Chau Chang Wang. “Vision-based line detection for underwater inspection of breakwater construction using an ROV.” *Ocean Engineering* 109 (2015): 20-33.

Chen, Z H E. “Bayesian Filtering: From Kalman Filters to Particle Filters, and Beyond.” *Statistics* 182, no. 1 (2003): 1-69.

Clausi, David A. “An advanced computational method to determine co-occurrence probability texture features.” *IEEE International Geoscience and Remote Sensing Symposium.* Toronto, 2002. 2453-2455.

Clem, T. R., and J. L. Lopes. “Progress in the development of buried minehunting systems.” San Diego, USA: Oceans 2003. Celebrating the Past ... Teaming Toward the Future (IEEE Cat. No.03CH37492), 2003.

Cloutier, Paul A, Delbert R. Oehme, and Ronald F. Stebbings. “Apparatus and method for locating and tracking magnetic objects or sources.” *Patent United States of America US4427943 A*, 2008.

Cloutier, Paul A., Delbert R. Oehme, and Ronald F. Stebbings. “A Vector Magnetometer System for Detection, Tracking, and Survey of Submerged and Buried Transmission Cables and Lines from Controlled Submersible Vehicle.” Washington: OCEANS '76, 1976.

Cloutier, Paul A., Timothy I. Marzolf, Delbert R. Oehme, and Ronald F. Stebbings. “Method and apparatus for providing permanent magnetic signatures in buried cables and pipes to facilitate long-range location, tracking and burial depth determination.” *Patent United States of America US6369679 B1*, 2002.

Colnet, B, and J Di Martino. “Source localisation with recurrent neural networks.” Atlanta, Georgia, USA: 1996 IEEE International Conference on Acoustics, Speech, and Signal Processing Conference Proceedings, 1996. 3073-3076.

Corbyn, J. A. “Pulse induction metal detector.” *Wireless World*, 1980.

Cowls, S., and S Jordan. “The enhancement and verification of a pulse induction based buried pipe and cable survey system.” *OCEANS'02 MTS/IEEE*, 2002: 508-511.

Crisan, D., and O. Obanubi. “Particle filters with random resampling times.” *Stochastic Processes and their Applications* 122, no. 4 (2012): 1332–1368.

Cui, G, K Ren, C Li, and Z Wang. “Odor source localization research of mobile robot based on neural network.” Guiyang, China: 2011 International Conference on System science, Engineering design and Manufacturing informatization, 2011. 130-133.

Dahab, A.a., F.K. Amoura, and W.S. Abu-Elhaija. “Comparison of Magnetic-Field Distribution of Noncompact and Compact Parallel Transmission-Line Configurations.” *IEEE Transactions on Power Delivery* 20, no. 3 (2005): 2114-2118.

Das, Yogadhish, John E. McFee, and Robert H. Chesney. “Determination of Depth of Shallowly Buried Objects by Electromagnetic Induction.” *IEEE Transactions on Geoscience and Remote Sensing* GE-23, no. 1 (1985): 60-66.

Dehkordi, M, H Abutalebi, and H Ghanei. “A compressive sensing based compressed neural network for sound source localization.” Tehran, Iran: 2011 International Symposium on Artificial Intelligence and Signal Processing (AISP), 2011. 6-10.

Dezelak, K., G. Stumberger, and Franc Jakl. “Arrangements of overhead power line conductors related to the electromagnetic field limits.” Wroclaw: Modern Electric Power Systems (MEPS), 2010 Proceedings of the International Symposium, 2010.

Dorrington, A, and R Kunnemeyer. “A simple microcontroller based digital lock-in amplifier for the\ndetection of low level optical signals.” Christchurch, New Zealand: Proceedings First IEEE International Workshop on Electronic Design, Test and Applications '2002, 2002. 0-2.

Dunbar, Robin M., Michael R. Frater, Michael J. Ryan, and Greg N. Milford. “Undersea electromagnetic networking.” Canberra, ACT: 2011 Military Communications and Information Systems Conference, 2011.

El Dein, Adel Z. “Magnetic-Field Calculation Under EHV Transmission Lines for More Realistic Cases.” *IEEE Transactions on Power Delivery* 24, no. 4 (2009): 2214-2222.

Fallon, Maurice F, and Simon Godsill. “Acoustic Source Localization and Tracking Using Track Before Detect.” *IEEE Transactions on Audio, Speech, and Language Processing* 18, no. 6 (2010): 1228–1242.

Feistel, R.; Weinreben, S.; Wolf, H.; Seitz, S.; Spitzer, P.; Adel, B.; Nausch, G.; Schneider, B. “Density and Absolute Salinity of the Baltic Sea 2006–2009.” *Ocean Science Discussions* 6, no. 2 (2009): 1757-1817.

Fisher, J. W. *jwfishers.* 2016. http://www.jwfishers.com/ (accessed 09 18, 2016).

Flowerdew, Peter M., and Andrezej Z. Regini. “Method and apparatus for tracing conductors using an alternating signal having two components related in frequency and phase.” *Patent United States of America US5260659 A*, 1993.

Floweredew, Peter M., and Andrzej Z. Regini. “Method of and apparatus for tracing faults in electrical conductors.” *Patent United States of America US4896117 A*, 1990.

Fu, Xiaoyan, and Yingmin Jia. “An Improvement on Resampling Algorithm of Particle Filters.” *IEEE Transactions on Signal Processing* 58, no. 10 (2010): 5414-5420.

Gard, M.F. “Magnetic field sensing in the underground construction environment.” 2nd ISA/IEEE Sensors for Industry Conference,, 2002. 57-65.

Gee, Jeffrey S. “A surface-towed vector magnetometer.” *Geophysical Research Letters* 29, no. 14 (2002): 1-4.

Geng, Y, and J Jung. “Sound-Source Localization System for Robotics and Industrial Automatic Control Systems Based on Neural Network.” Goyang-si, Korea (South): 2008 International Conference on Smart Manufacturing Application, 2008. 311-315.

Gordon, N. “A hybrid bootstrap filter for target tracking in clutter.” *IEEE Transactions on Aerospace and Electronic Systems* 33, no. 1 (1997): 353-358.

Gordon, N., D. Salmond, and A. Smith. “Novel approach to nonlinear/non-Gaussian Bayesian state estimation.” *Radar and Signal* 2, no. 140 (1993): 107–113.

Gutowski, M., J. Malgorn, and M. Vardy. “3D sub-bottom profiling; High resolution 3D imaging of shallow subsurface structures and buried objects.” Genova: OCEANS 2015 - Genova, 2015.

Hallset, J. “A prototype autonomous underwater vehicle for pipeline inspection.” Advanced Robotics, 1991. 'Robots in Unstructured Environments', 91 ICAR., Fifth International Conference onnce on, 1991b.

—. “Simple vision tracking of pipelines for an autonomous underwater vehicle.” Sacramento, California: Proceedings. 1991 IEEE International Conference on Robotics and Automation, 1991a.

Health and Safety Executive HSE. *Are you considering a career in diving?* 2015. http://www.hse.gov.uk/diving/carr.htm (accessed April 17, 2017).

Hol, Jeroen D, Thomas B Schon, and Fredrik Gustafsson. “On Resampling Algorithms for Particle Filters.” Cambridge, United Kingdom: 2006 IEEE Nonlinear Statistical Signal Processing Workshop, 2006. 79-82.

Holt, Peter. *Marine Magnetometer Processing.* Plymouth: 3H Consulting, 2014.

Innovatum Ltd. *Innovatum .* 2016. http://www.innovatum.co.uk/ (accessed 09 15, 2016).

International Cable Protection Committee. “About Submarine Telecomunications Cables.” October 2011a. https://iscpc.org/documents/?id=1753 (accessed September 09, 2016).

—. *Publications/About the Cables.* 2011b. https://iscpc.org/publications/ (accessed September 09, 2016).

Inzartsev, A. V, and A. M. Pavin. “AUV Cable Tracking System Based on Electromagnetic and Video Data.” *OCEANS 2008 - MTS/IEEE Kobe Techno-Ocean*, 2008: 1-6.

Isaac, J. C., and R. Goroshin. “Automated cable tracking in sonar imagery.” Sydney: OCEANS 2010, 2010.

Ito, Yoshihiko, Naomi Kato, Junichi Kojima, Satoru Takagi, Kenichi Asakawa, and Yuichi Shirasaki. “Cable tracking for autonomous underwater vehicle.” *Proceedings of IEEE*

Symposium on Autonomous Underwater Vehicle Technology. Slambridge, MA: AUV'94, 1994. 218-224.

J.W. Fisher. “CT-1 Cable Tracker Data Sheet.” 2016. http://www.hawkmarine.co.uk/images/PDF/JWFishers/CT-1DS-3blue1.pdf (accessed 09 18, 2016).

Janosek , Michal. “Parallel Fluxgate Magnetometers.” In *High Sensitivity Magnetometers*, 41-61. Springer International Publishing, 2017.

Johnson, Christopher, Christopher L Wagner, Robert Rebich, Jeffery L Young, and Das Butherus. “Propagation of low frequency signals in oceanic environments; theory, simulation and experimentation.” Spokane, WA: IEEE, 2011. 2395-2398.

Julier, S. J., and J. K. Uhlmann. “Unscented Filtering and Nonlinear Estimation.” *Proceedings of the IEEE* 92, no. 3 (2004): 401-422.

Kim, Phil. *Kalman Filter for Beginners: With MATLAB Examples.* CreateSpace, 2011.

King, Ronold W.P. “Lateral electromagnetic waves from a horizontal antenna for remote sensing in the ocean.” *IEEE Transactions on Antennas and Propagation* 37, no. 10 (1989): 1250-1255.

King, Ronold W.P. “The propagation of a Gaussian pulse in sea water and its applicaiton to remote sensing.” *IEEE Transactions on Geoscience and Remote Sensing* 31, no. 3 (1993): 595-605.

Klein Marine Systems, Inc. *System 3000 Digital Side Scan Sonar.* 2016. http://kleinmarinesystems.com/products/side-scan-sonar/system-3000/ (accessed May 22, 2016).

Kojima, J, Y Kato, K Asakawa, S Matumoto, S Takagi, and M Kato. “Development of autonomous underwater vehicle 'AQUA EXPLORER 2' for inspection of underwater cables.” Halifax, Nova Scotia, Canada: Oceans '97. MTS/IEEE Conference Proceedings, 1997.

Kwok, N.M., and Weizhen Zhou. “Evolutionary particle filter: re-sampling from the genetic algorithm perspective.” Iros: IEEE/RSJ International Conference on Intelligent Robots and Systems, 2005. 2935–2940.

Lehman, Eric A., and C. Robert Williamson. “Particle Filter Design Using Importance Sampling for Acoustic Source Localisation and Tracking in Reverberant Environments.” *EURASIP Journal on Advances in Signal Processing*, 2006: 1-10.

Lenz, J, and S Edelstein. “Magnetic sensors and their applications.” *Sensors Journal, IEEE* 6, no. 3 (2006): 631-649.

Li, Chun Guang, Ying Jian Wang, Gui Li Wang, Rui Qiao Xiao, and Jin Chen. “Study of Submarine Optical Fiber Cable Detection by Interferometric Synthetic Aperture Sonar.” *Applied Mechanics and Materials* 341-342 (2013): 1094-1098.

Ljung, L. “Some Classical and Some New Ideas for Identification of Linear Systems.” *Journal of Control, Automation and Electrical Systems* 24, no. 1-2 (2013): 1-8.

Ljung, Lennart, and Tianshi Chen. “Convexity issues in system identification.” Hangzhou: ICCA 2013, 2013. 1-9.

March, H. W. “The field of a magnetic dipole int the presence of a conducting sphere.” *Geophysics* 18, no. 3 (1953): 671-684.

Massey, Bart. “Fast perfect weighted resampling.” Las Vegas: Citeseer, ICASSP, 2008.

Mathworks. *Fourier Transforms.* 2014. https://uk.mathworks.com/help/matlab/math/fourier-transforms.html (accessed December 3, 2014).

Mitola, J. “The software radio architecture.” *IEEE Communications Magazine* 33, no. 5 (1995): 26-38.

Motwani, Amit, Sanjay K Sharma, Robert Sutton, and Phil Culverhouse. “Interval Kalman filtering in navigation system design for an uninhabited surface vehicle.” *Journal of Navigation* 66, no. 05 (2013): 639-652.

Narimani, Mehdi, Soroosh Nazem, and Mehdi Loueipour. “Robotics vision-based system for an underwater pipeline and cable tracker.” *OCEANS 2009.* Bremen, Germany: OCEANS 2009 - Europe, 2009. 1-6.

National Instruments. “M Series Multifunction DAQ for USB - 16-Bit, 250 kS/s, up to 80 Analog Inputs.” *Specification*, 2014.

National Instruments. “USER GUIDE NI USB-628X OEM.” *user guide*, 2013.

Olsen, R.G., and P.S.K. Wong. “Characteristics of low frequency electric and magnetic fields in the vicinity of electric power lines.” *IEEE Transactions on Power Delivery* 7, no. 4 (1992): 2046-2055.

Olsen, R.G.; Deno, D.; Baishiki, R.S.; Abbot, J.R.; Conti, R.; Frazier, M.; Jaffa, K.; Niles, G.B.; Stewart, J.R.; Wong, R.; Zavadil, R.M. “Magnetic fields from electric power lines: theory and comparison to measurements.” *Power Delivery, IEEE Transactions on* 3, no. 4 (1988): 2127-2136.

Ortiz, A., M. Simo, and G. Oliver. “Image sequence analysis for real-time underwater cable tracking.” Palm Springs, California, USA : Applications of Computer Vision, 2000, Fifth IEEE Workshop on., 2000.

Ortiz, Alberto, and Javier Antich. “Bayesian visual tracking for inspection of undersea power and telecommunication cables.” *Journal of Maritime Research* VI, no. II (2009b): 83-89.

Ortiz, Alberto, Javier Antich, and Gabriel Oliver. “A Bayesian approach for tracking undersea narrow telecommunication cables.” *OCEANS 2009 - EUROPE*, 2009a: 1-10.

Ortiz, Alberto, Javier Antich, and Gabriel Oliver. “A particle filter-based approach for tracking undersea narrow telecommunication cables.” *Machine Vision and Applications* 22 (2011): 283-302.

Pearson, Richard David, Jeffrey Richard Thompson, and Derek James Wong. “Locator for locating a current carrying conductor.” *Patent EP2589988 A3*, 2015.

Pei, Y. H., and H. G. Yeo. “Magnetic Gradiometer Inversion for Underwater Magnetic Object Parameters.” Singapore: OCEANS 2006, 2006.

Pei, Y. H., and H. G. Yeo. “UXO survey using vector magnetic gradiometer on autonomous underwater vehicle.” *OCEANS 2009, MTS/IEEE Biloxi - Marine Technology for Our Future: Global and Local Challenges*, 2009: 1-8.

Pei, Y. H., H. G. Yeo, X. Y. Kang, S. L. Pua, and John Tan. “Magnetic gradiometer on an AUV for buried object detection.” Sydney: OCEANS 2010, 2010.

Radiodetecion Ltd. *Abc & Xyz of Locating Buried Pipes and Cables for the Beginner and the Specialist.* Radiodetection Ltd - SPX Corporation, 2008.

Rullan-Lara, Jose, L., Guillaume Sanahuja, Rogelio Lozano, Sergio Salazar, Ramon Garcia-Hernandez, and Jose, A. Ruz-Hernandez. “Indoor Localization of a Quadrotor Based on WSN: A Real-Time Application.” *International Journal of Advanced Robotic Systems* 10 (2013): 1.

Sabatini, Angelo M. “Quaternion-based extended Kalman filter for determining orientation by inertial and magnetic sensing.” *IEEE transactions on bio-medical engineering* 53, no. 7 (2006): 1346-56.

Said, Ismail, N.A. Rahman, Halil Hussain, Ahmed Farag, and T. Juhana. “Evaluation of magnetic field from different power transmission line configurations in Malaysia.” Canadian Conference on Electrical and Computer Engineering 2004 (IEEE Cat. No.04CH37513), 2004. 393-396.

Salih, Yasir, and Aamir Saeed Malik. “Comparison of stochastic filtering methods for 3D tracking.” *Pattern Recognition* 44, no. 10-11 (2011): 2711–2737.

Schaul, Tom; Bayer, Justin; Wierstra, Daan; Sun, Yi; Felder, Martin; Sehnke, Frank; Ruckstiess, Thomas; Schmidhuber, Jurgen. “PyBrain.” *Journal of Machine Learning Research* 11 (2010): 743-746.

Schock, Steven G., and James Wulf. “Buried object scanning sonar for AUVs.” *Oceans 2003. Celebrating the Past ... Teaming Toward the Future (IEEE Cat. No.03CH37492).* California, 2003.

Schock, Steven G., Arnaud Tellier, Jim Wulf, Jason Sara, and Mark Ericksen. “Buried object scanning sonar.” *IEEE Journal of Oceanic Engineering* 26, no. 4 (2001): 677-689.

Schock, Steven G., James Wulf, Gwendoline Quentin, and Jason Sara. “Synthetic Aperture Processing of Buried Object Scanning Sonar Data.” *OCEANS 2005.* Proceedings of OCEANS 2005 MTS/IEEE, 2005. 1-6.

Scofield, John H. “Frequency-domain description of a lock-in amplifier.” *American Journal of Physics* 62, no. 2 (1994): 129.

Simo, Miquel, Alberto Ortiz, and Gabriel Olivier. “Optimized image sequence analysis for real-time underwater cable tracking.” *OCEANS 2000.* MTS/IEEE Conference and Exhibition, 2000.

Smith, EP, and KA Rose. “Model goodness-of-fit analysis using regression and related techniques.” *Ecological Modelling* 77 (1995): 49-64.

Somaraju, R., and J Trumpf. “Frequency, Temperature and Salinity Variation of the Permittivity of Seawater.” *IEEE Transactions on Antennas and Propagation* 54, no. 11 (2006): 3441-3448.

Sonnaillon, Maximiliano Osvaldo, and Fabián Jose Bonetto. “A low-cost, high-performance, digital signal processor-based lock-in amplifier capable of measuring multiple frequency sweeps simultaneously.” *Review of Scientific Instruments* 76, no. 2 (2005).

SPX Corporation. *radiodetection about-us.* 2016. http://www.spx.com/en/radiodetection/about-us (accessed October 10, 2016).

Sturim, D. E., M. S. Brandstein, and H. F. Silverman. “Tracking multiple talkers using microphone array measurements.” Munich, Bavaria, Germany: Proc. Int. Conf. Acoust., Speech, Signal Process. (ICASSP), 1997. 371-374.

Sulzberger, G., J. Bono, G. I. Allen, T. Clem, and S. Kumar. “Demonstration of the real-time tracking gradiometer for buried mine hunting while operating from a small unmanned underwater vehicle.” Singapore: OCEANS 2006, 2006.

Sun, Keli, K. O'Neill, Fridon Shubitidze, Shah A. Haider, and Keith D. Paulsen. “Simulation of electromagnetic induction scattering from targets with negligible to moderate penetration by primary fields.” *IEEE Transactions on Geoscience and Remote Sensing* 40, no. 4 (2002): 910-927.

Szyrowski, Tomasz, Sanjay K Sharma, Rober Sutton, and Gareth A Kennedy. “Developments in subsea power and telecommunication cables detection : Part 1 – Visual and hydroacoustic tracking.” *Underwater Technology* 31, no. 3 (2013a): 123-132.

Szyrowski, Tomasz, Sanjay K Sharma, Robert Sutton, and Gareth A Kennedy. “Developments in subsea power and telecommunication cables detection : Part 2 – Electromagnetic detection.” *Underwater Technology* 31, no. 3 (2013b): 133-143.

Takagi, S, J. Kojima, and K. Asakawa. “DC cable sensors for locating underwater telecommunication cables.” *OCEANS 96 MTS/IEEE Conference Proceedings. The Coastal Ocean - Prospects for the 21st Century*, 1996: 339-344.

Tao, R. J., and A. Zahedi. “Proceedings of the 2nd International Conference on Bioelectromagnetism (Cat. No.98TH8269).” Melbourne, Vic., 1998.

Terabit Consulting Inc. “Submarine Cable Industry Report 2014.” 2014. http://www.terabitconsulting.com/downloads/2014-submarine-cable-market-industry-report.pdf (accessed September 20, 2016).

Texas Instruments. “High-Resolution Analog-to-Digital Converter High Resolution : Flexible Digital Filter : Analog Supply :.” *Specification*, 2007.

The Crown Estate. “Submarine Cables .” 2015. https://www.thecrownestate.co.uk/media/5748/ei-cables-and-pipelines-uk.pdf (accessed September 20, 2016).

Tinsley Instrumentation Ltd. *Tinsley.* 2012. http://tinsley.co.uk/wp/?page_id=1785 (accessed 12 13, 2012).

Tumanski, Slawomir. “Induction coil sensors—a review.” *Measurement Science and Technology* 18, no. 3 (2007): R31-R46.

Vallivaara, Ilari, Janne Haverinen, Anssi Kemppainen, and Juha Roning. “Magnetic field-based SLAM method for solving the localization problem in mobile robot floor-cleaning task.” Tallinn: 2011 15th International Conference on Advanced Robotics (ICAR), 2011.

Vavak, F., and T., Fogarty. “Comparison of steady state and generational genetic algorithms for\nuse in nonstationary environments.” Nagoya: Proceedings of IEEE International Conference on Evolutionary Computation, 1996.

Vermaak, J., and A. Blake. “Nonlinear filtering for speaker tracking in noisy and reverberant environments.” Salt Lake City, UT: 2001 IEEE International Conference on Acoustics, Speech, and Signal Processing. Proceedings (Cat. No.01CH37221), 2001. 3021–3024.

Vermaak, J., C. Andrieu, A. Doucet, and S. J. Godsill. “Particle methods for Bayesian modeling and enhancement of speech signals.” *IEEE Transactions on Speech and Audio Processing* 10, no. 3 (2002): 173-185.

Walden, R. H. “Analog-to-digital converter survey and analysis.” *IEEE Journal on Selected Areas in Communications* 17, no. 4 (1999): 539-550.

Wang, P, P Lewin, K Goddard, and S Swingler. “Design and testing of an induction coil for measuring the magnetic fields of underground power cables.” *2010 IEEE International Symposium on Electrical Insulation*, no. 1 (2010): 1-5.

Wang, X. L., L. Li, and Y. X. Cui. “Detection and Location of Underwater Pipeline Based on Mathematical Morphology for an AUV.” *Key Engineering Materials* 561 (2013): 591-596.

Ward, Darren B., Eric A. Lehmann, and Robert C. Williamson. “Particle filtering algorithms for tracking an acoustic source in a reverberant environment.” *IEEE Transactions on Speech and Audio Processing* 11, no. 6 (2003): 826-836.

Ward, Richard Frederick, and Denise Louise Harris. “Receiver.” *Patent United States of America USD631893 S1*, 2011.

Wargo, Robert, and Tara Davenport. *Submarine Cables The Handbook of Law and Policy.* Leiden, Boston: Martinus Nijhoff Publishers, 2014.

Weiss, Eyal; Ginzburg, Boris; Cohen, Tsuriel Ram; Zafrir, Hovav; Alimi, Roger; Salomonski, Nizan; Sharvit, Jacob “High Resolution Marine Magnetic Survey of Shallow Water Littoral Area.” *Sensors* 7 (2007): 1697-1712.

Whitcomb, Louis L. “Underwater robotics: out of the research laboratory and into the field.” *Robotics and Automation, 2000. Proceedings. ICRA '00. IEEE International Conference on.* 2000. 709 -716 vol.1.

Wirth, Stephan, Alberto Ortiz, Dietrich Paulus, and Gabriel Olivier. “Using particle filters for autonomous underwater cable tracking.” Killaloe, Ireland: IFAC Workshop on Navigation, Guidance and Control of Underwater Vehicles, 2008.

Won, I.J. “Characterization of UXO-like targets using broadband electromagnetic induction sensors.” *IEEE Transactions on Geoscience and Remote Sensing* 41, no. 3 (2003): 652-663.

Worzyk, Thomas. *Submarine power cables: design, installation, repair, environmental aspects.* Berlin: Springer Science & Business Media, 2009.

Yardim, Caglar, Zoi-heleni Michalopoulou, and Peter Gerstoft. “An Overview of Sequential Bayesian Filtering in Ocean Acoustics.” *IEEE Journal of Oceanic Engineering* 36, no. 1 (2011): 71-89.

Zhang, Xiaoming, and Lizhen Gao. “A novel auto-calibration method of the vector magnetometer.” Beijing: th International Conference on Electronic Measurement & Instruments, 2009.

Zhong, J., X. Hu, M. Gu, and J. Zhang. “Comparison of Performance between Different Selection Strategies on Simple Genetic Algorithms.” Vienna: International Conference on Computational Intelligence for Modelling, Control and Automation and International Conference on Intelligent Agents, Web Technologies and Internet Commerce (CIMCA-IAWTIC'06), 2005.

Appendix A Neural Networks results

Appendix A.1 Single input, distance out

```
** DEBUG_171 [  7.82066510e+01   6.70532327e-02   3.11364228e+01]
** DEBUG_172 [[  1.68037748e+00   6.85588592e-04  -4.14159299e-01]
 [  6.85588592e-04   1.53764768e-05   4.93267890e-03]
 [ -4.14159299e-01   4.93267890e-03   1.91544093e+00]]
RMS error:  0.0933771892823

FeedForwardNetwork-13

   Modules:
<BiasUnit 'BiasUnit-6'>,
<LinearLayer 'LinearLayer-5'>,
<SigmoidLayer 'SigmoidLayer-14'>,
<SigmoidLayer 'SigmoidLayer-15'>,
<LinearLayer 'LinearLayer-16'>

   Connections:
<FullConnection 'FullConnection-10': 'BiasUnit-6' -> 'LinearLayer-16'>,
<FullConnection 'FullConnection-11': 'SigmoidLayer-15' -> 'LinearLayer-
16'>, <FullConnection 'FullConnection-12': 'LinearLayer-5' ->
'SigmoidLayer-14'>, <FullConnection 'FullConnection-7': 'SigmoidLayer-
14' -> 'SigmoidLayer-15'>, <FullConnection 'FullConnection-8':
'BiasUnit-6' -> 'SigmoidLayer-14'>, <FullConnection 'FullConnection-9':
'BiasUnit-6' -> 'SigmoidLayer-15'>

'Module:', 'SigmoidLayer-14'
'-connection to', 'SigmoidLayer-15'
'- parameters', [ 1.25552287,  3.08761871, -0.27919971, -0.58007289]
'Module:', 'BiasUnit-6')
'-connection to', 'LinearLayer-16'
'- parameters', [-0.26543242]
'-connection to', 'SigmoidLayer-14'
'- parameters', [ 0.96178813,  0.9577808 , -0.08787658, -0.3210907 ]
'-connection to', 'SigmoidLayer-15'
'- parameters', array[-1.66114057]
'Module:', 'SigmoidLayer-15'
'-connection to', 'LinearLayer-16'
'- parameters', [ 1.63921786]
'Module:', 'LinearLayer-16'
'Module:', 'LinearLayer-5'
'-connection to', 'SigmoidLayer-14'
- parameters'[-2.45539964, -2.41240208, -3.8545287, -3.37947589,
6.35023324, 3.70740613, 0.37915656, -0.56434287]

Network weights:
[-0.26543242  0.96178813  0.9577808  -0.08787658 -0.3210907  -1.66114057
 -2.45539964 -2.41240208 -3.8545287  -3.37947589  6.35023324  3.70740613
  0.37915656 -0.56434287  1.25552287  3.08761871 -0.27919971 -0.58007289
  1.63921786]
```

Appendix A.2 Horizontal and Vertical Coils in, distance out

```
create_network(n_inputs, n_outputs, n_hidden)

    biasUnit = pybrain.structure.BiasUnit()
    inputLayer = pybrain.structure.LinearLayer(n_inputs)
    hiddenLayer = pybrain.structure.SigmoidLayer(n_hidden)
    outputLayer = pybrain.structure.SigmoidLayer(n_outputs) # Can be
sigmoid as well
    scaleLayer = pybrain.structure.LinearLayer(n_outputs)

net = create_network(2, 1, 5)

maxDist = 50



RMS error:  0.121171626242



Network weights:
[-0.81914361 -0.55833185 -0.73403965 -0.66965543  2.7195965   0.03035565
  5.31788925  3.00051523 -3.50652571 -2.79282305  5.41642672  4.10075056
  2.55233747  2.13376936 -1.84528701  1.49743694 -2.26427737 -1.45041042
  1.20081275]
RMS error:  0.12988225508



** DEBUG_184 Network weights:
[-0.20300881  0.70246178 -0.92341091 -0.90144267  0.31562741  0.1091253
  2.8005306   2.97649771 -3.90213381 -3.57686118  2.10156366 -0.15351526
  5.48743462  2.20244966 -1.15061144  2.58111701 -0.01480434 -2.7068741
  1.40626334]
RMS error:  0.133928378075



** DEBUG_184 Network weights:
[ 0.04121834  0.2729105   0.18685401 -0.86609046 -0.57342052 -0.07553261
  4.29528676  1.92968147 -4.3207564  -2.85558067 -3.86311161 -3.6451136
  3.60340473  2.40239024 -1.70573818  1.52890314  1.90807653 -0.07818886
  1.94371683]
RMS error:  0.124420357357

Network weights:
[ 1.02810561  0.25251216  0.42452392  0.18451693  0.59841889 -0.82723992
  0.54290499  4.28757527  3.29959234 -5.54637966 -4.22389584 -4.90539053
 -5.85247109 -5.9669799  -4.07134758 -4.10472763 -3.01057049  0.84908906
 -1.29725788 -1.27642928 -2.51857323 -1.71052499 -1.15437502]
```

Appendix B Kalman Filter computers output for model

Appendix B.1 Modelling a cable in relation to magnetic field read by searching coil

```
  Model for output "Distance": A(z)y_1(t) = B(z)u(t) + e_1(t)
    A(z) = 1 - 1.274 z^-1 + 0.4084 z^-2

    B1(z) = 3.247 z^-1 + 5.312 z^-2

    B2(z) = 1.226 z^-1 - 4.055 z^-2

  Model for output "Attenuation": y_2(t) = - A_i(z)y_i(t) +  B(z)u(t) +
e_2(t)
    A_1(z) = -8.646 z^-1 - 5.953 z^-2

    B1(z) = 446.8 z^-1 + 367.8 z^-2

    B2(z) = 133.1 z^-1 + 167.2 z^-2

  Model for output "Deviation": y_3(t) = - A_i(z)y_i(t) +  B(z)u(t) +
e_3(t)
    A_1(z) = -2.186 z^-1 + 1.709 z^-2

    B1(z) = -4.321 z^-1 - 0.4342 z^-2

    B2(z) = 9.924 z^-1 - 8.01 z^-2

Sample time: 1 seconds

Parameterization:
   Polynomial orders:   na=[2 0 0;2 0 0;2 0 0]
   nb=[2 2;2 2;2 2]   nk=[1 1;1 1;1 1]
   Number of free coefficients: 18

Status:
Estimated using ARX on time domain data "inputData".
Fit to estimation data: [47.91;28.91;52.64]% (prediction focus)
FPE: 1049, MSE: 500

ss_arxMimo =
   a =
            x1       x2       x3       x4       x5       x6
   x1    1.274        0        0        1        0        0
   x2    8.646        0        0        0        1        0
   x3    2.186        0        0        0        0        1
   x4  -0.4084        0        0        0        0        0
   x5    5.953        0        0        0        0        0
   x6   -1.709        0        0        0        0        0

  b =
            HmV      VmV
   x1    3.247    1.226
```

```
    x2    446.8    133.1
    x3   -4.321    9.924
    x4    5.312   -4.055
    x5    367.8    167.2
    x6  -0.4342    -8.01

  c =
                x1  x2  x3  x4  x5  x6
    Distance     1   0   0   0   0   0
    Attenuation  0   1   0   0   0   0
    Deviation    0   0   1   0   0   0

  d =
                HmV  VmV
    Distance      0    0
    Attenuation   0    0
    Deviation     0    0

Sample time: 1 seconds
Discrete-time state-space model.
```

Appendix B.2 Modelling a cable in relation to a platform's position

```
Discrete-time ARX model:
  Model for output "Distance":     A(z)y_1(t) = B(z)u(t) + e_1(t)
    A(z) = 1 - 1.318 z^-1 + 0.5792 z^-2
    B1(z) = 0.09624 z^-1 + 0.1272 z^-2
    B2(z) = 1.659 z^-1 - 0.05871 z^-2

  Model for output "Attenuation": y_2(t) = - A_i(z)y_i(t) +  B(z)u(t) + e_2(t)
    A_1(z) = -9.568 z^-1 - 12.29 z^-2

    B1(z) = 2.039 z^-1 + 2.835 z^-2
    B2(z) = 56.37 z^-1 + 24.93 z^-2

  Model for output "Deviation": y_3(t) = - A_i(z)y_i(t) +  B(z)u(t) + e_3(t)
    A_1(z) = -2.599 z^-1 + 2.068 z^-2
    B1(z) = -0.04084 z^-1 - 0.072 z^-2
    B2(z) = 0.2589 z^-1 - 1.009 z^-2

Sample time: 1 seconds

Parameterization:
   Polynomial orders:   na=[2 0 0;2 0 0;2 0 0]   nb=[2 2;2 2;2 2]   nk=[1 1;1 1;1 1]
   Number of free coefficients: 18

Status:
Estimated using ARX on time domain data "inputData".
Fit to estimation data: [33.63;-9.21;49.53]% (prediction focus)
FPE: 5016, MSE: 1179


ss_arxMimo =

  a =
             x1      x2      x3      x4     x5     x6
```

x1	1.318	0	0	1	0	0
x2	9.568	0	0	0	1	0
x3	2.599	0	0	0	0	1
x4	-0.5792	0	0	0	0	0
x5	12.29	0	0	0	0	0
x6	-2.068	0	0	0	0	0

b =

	PathTraveled	BasisBoatAng
x1	0.09624	1.659
x2	2.039	56.37
x3	-0.04084	0.2589
x4	0.1272	-0.05871
x5	2.835	24.93
x6	-0.072	-1.009

c =

	x1	x2	x3	x4	x5	x6
Distance	1	0	0	0	0	0
Attenuation	0	1	0	0	0	0
Deviation	0	0	1	0	0	0

d =

	PathTraveled	BasisBoatAng
Distance	0	0
Attenuation	0	0
Deviation	0	0

Sample time: 1 seconds
Discrete-time state-space model.

Appendix B.3 MATLAB scripts for UKF

SigmaPoints.m

```
%% Sigma points to create points for unscented transformation
function [Xi, W] = SigmaPoints(xm, P, kappa)

    if nargin < 3
        kappa = 2;
    end
    n = numel(xm);
    Xi = zeros(n, 2*n+1);
    W = zeros(n, 1);

    Xi(:, 1) = xm;
    W(1) = kappa / (n + kappa);

    U = chol((n+kappa)*P);
```

```
    for k=1:n
        Xi(:, k+1) = xm + U(k, :)';
        W(k+1) = 1/(2*(n*kappa));
    end
    for k=1:n
        Xi(:, n+k+1) = xm - U(k, :)';
        W(n+k+1) = 1/(2*(n+kappa));
    end
end
```

UT.m

```
%% Unscented transformation to run points through transform
function [xm, xcov] = UT(Xi, W, noiseCov)
    [n, kmax] = size(Xi);
    xm = 0;
    for k=1:kmax
        xm = xm +W(k)*Xi(:, k);
    end
    xcov = zeros(n, n);
    for k=1:kmax
        xcov = xcov + W(k)*(Xi(:, k) - xm)*(Xi(:, k) - xm)';
    end
    xcov = xcov + noiseCov;
end
```

Appendix C Batch Particle Filter single line outputs

Appendix C.1 Line X-2

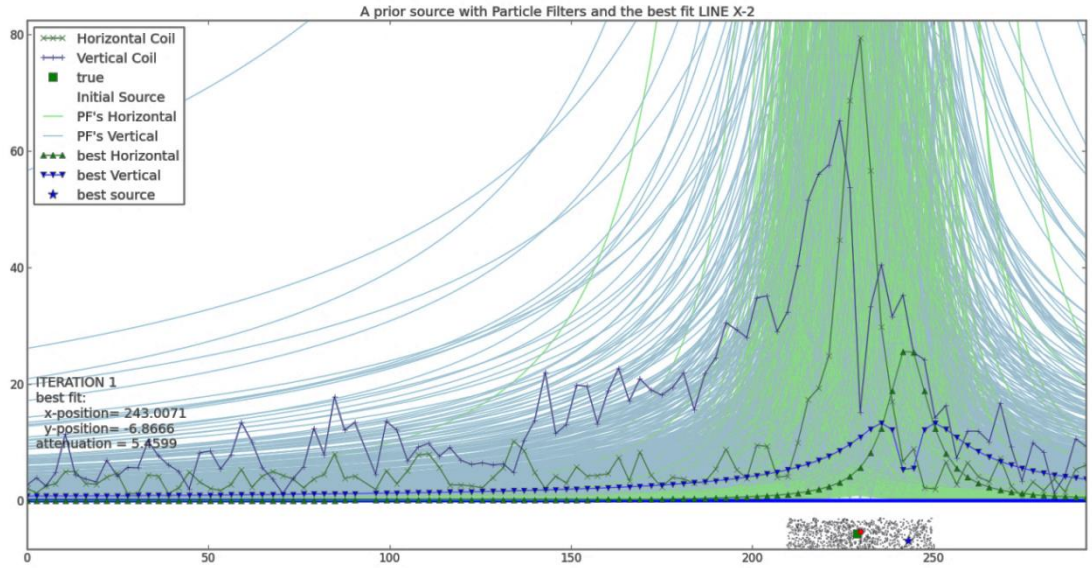

Figure 136 A prior source with Particle Filters and the best fit LINE X-2 Iteration 1

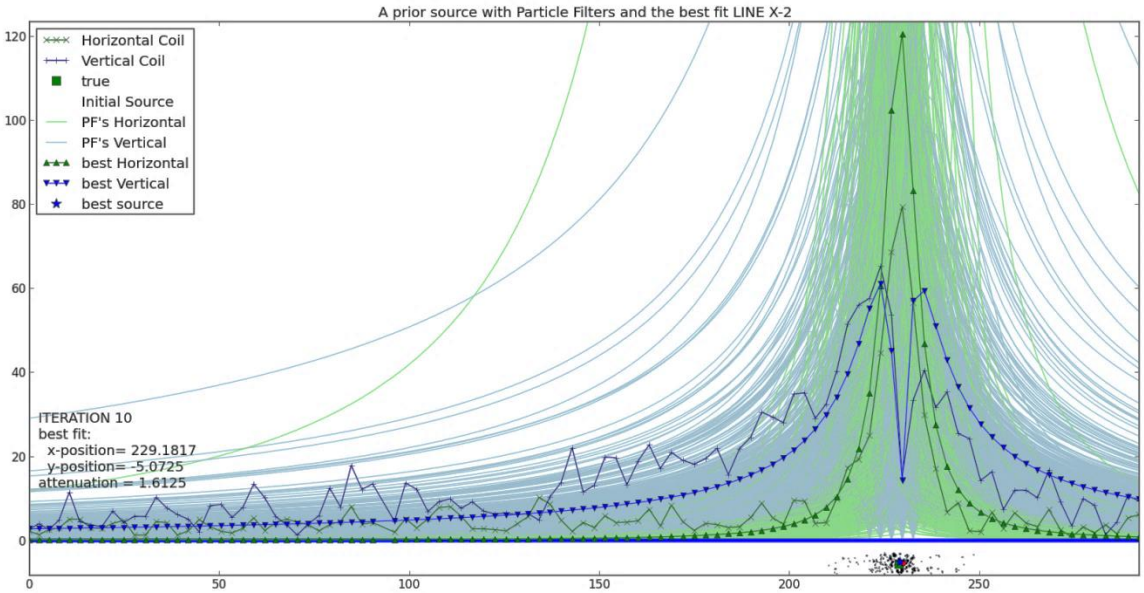

Figure 137 A prior source with Particle Filters and the best fit LINE X-2 Iteration 10

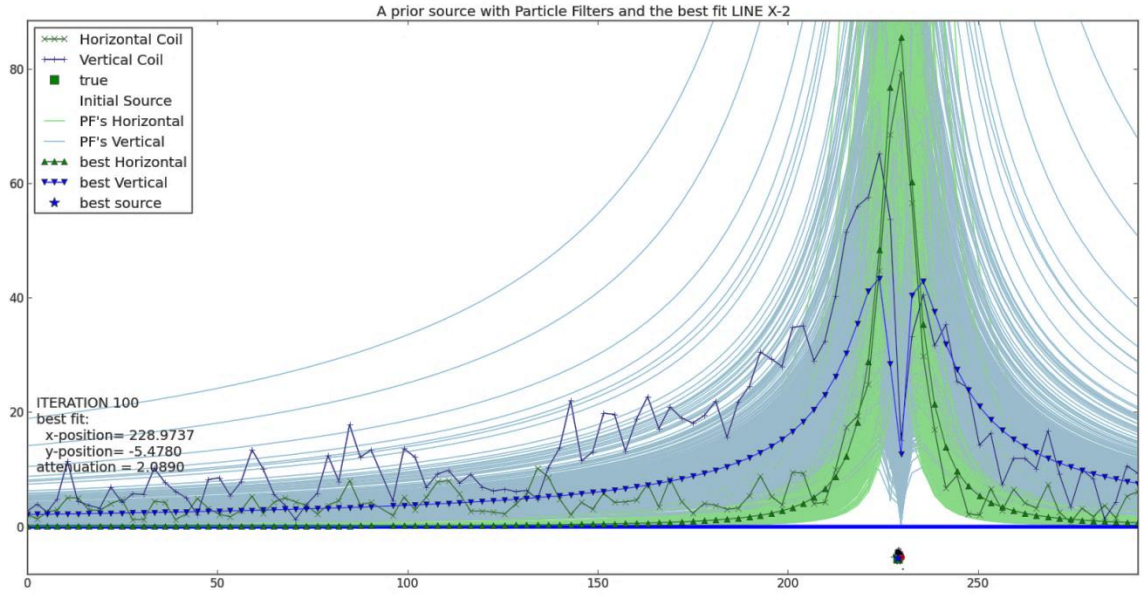

Figure 138 A prior source with Particle Filters and the best fit LINE X-2 Iteration 100

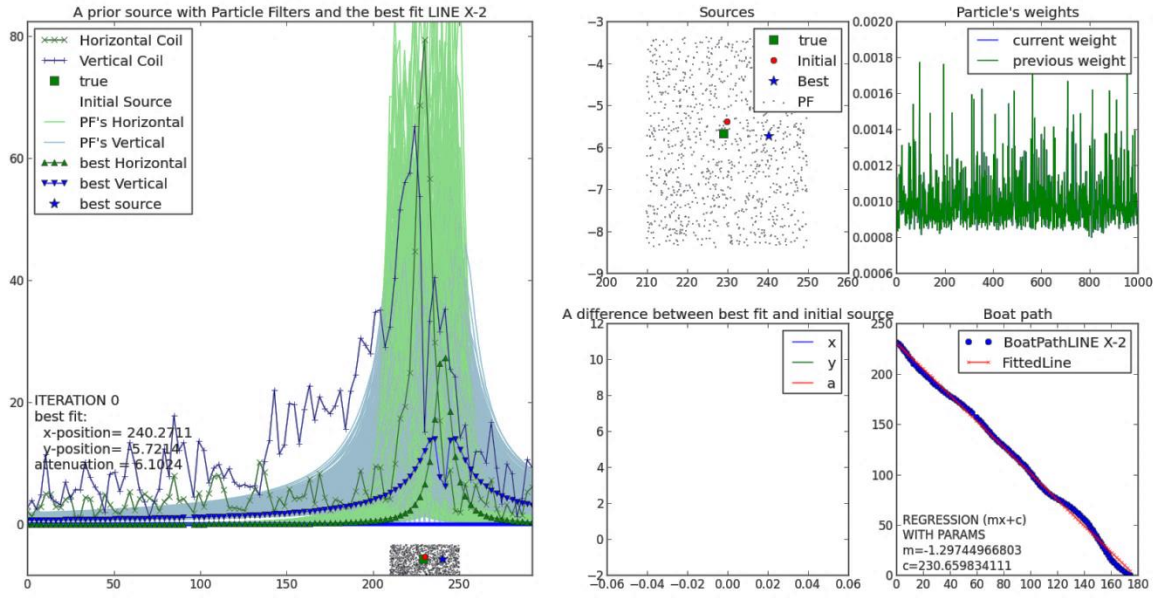

Figure 139 A prior source with Particle Filters and the best fit LINE X-2 Iteration 0

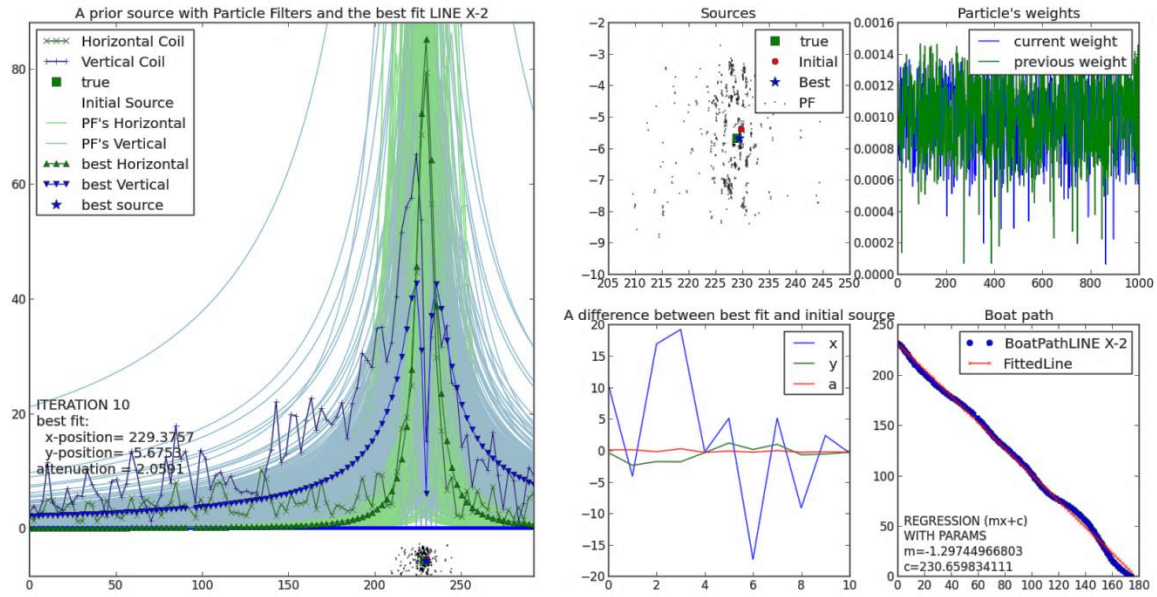

Figure 140 A prior source with Particle Filters and the best fit LINE X-2 Iteration 10

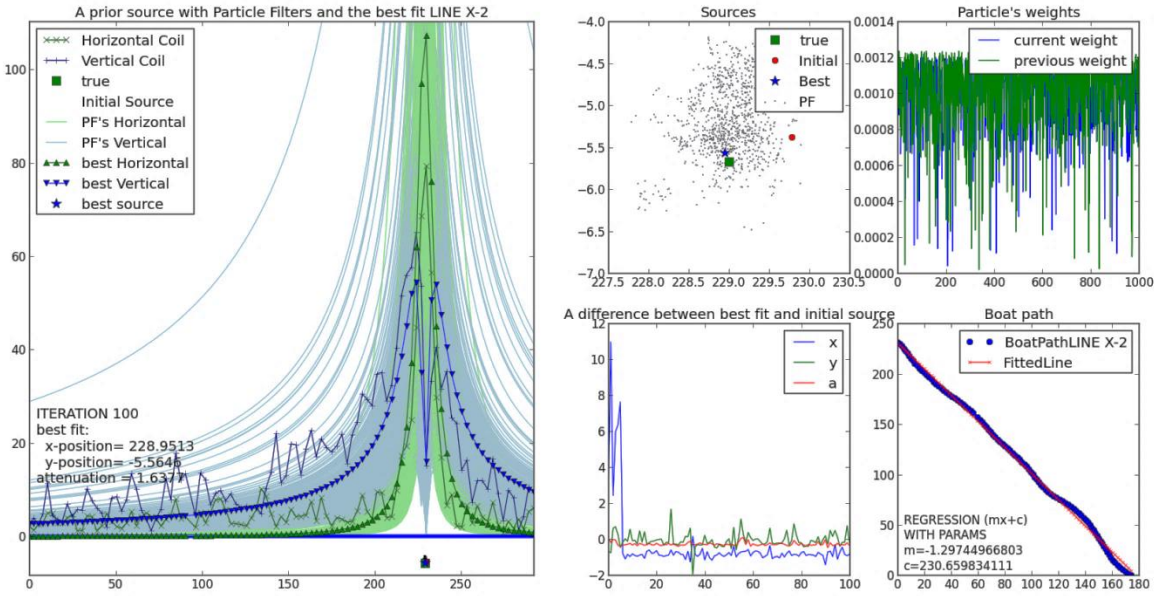

Figure 141 A prior source with Particle Filters and the best fit LINE X-2 Iteration 100

Appendix C.2 Line X-6

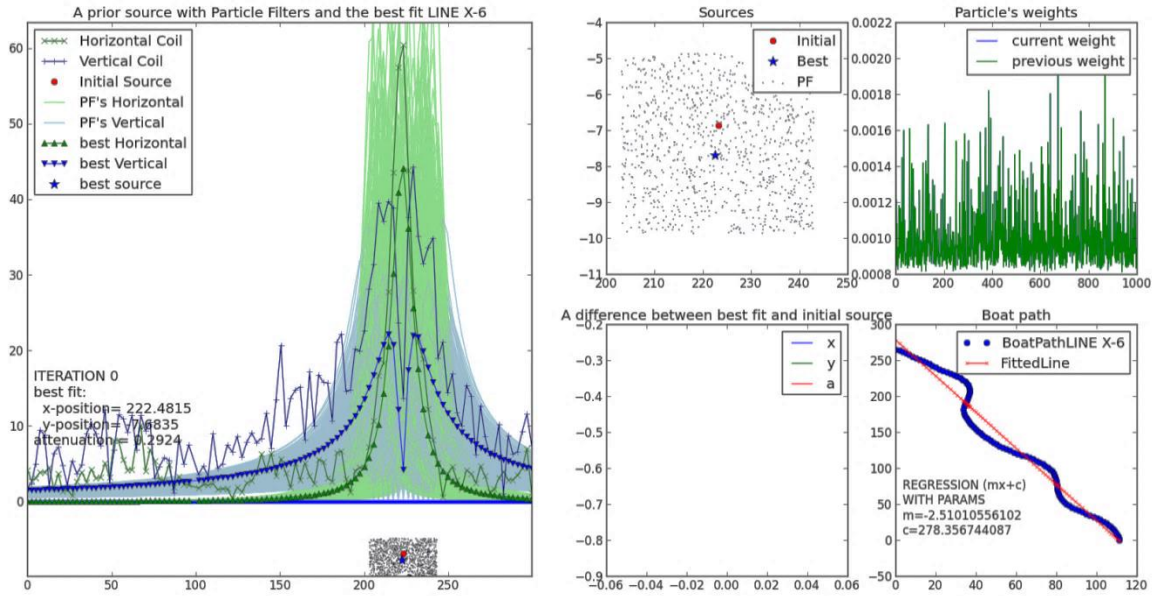

Figure 142 A prior source with Particle Filters and the best fit LINE X-6 Iteration 0

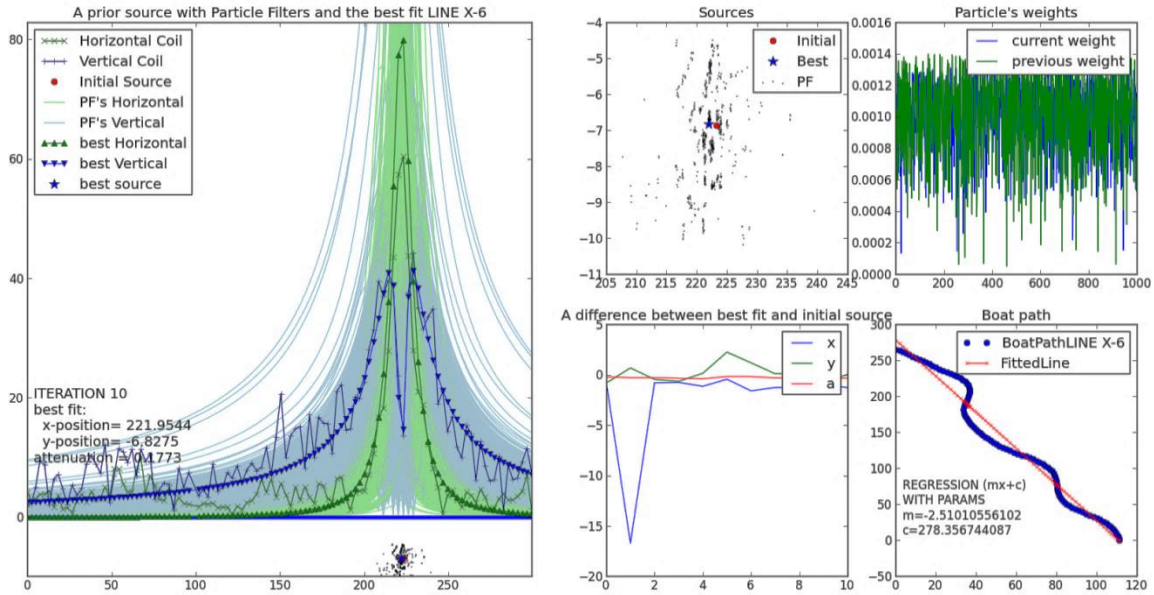

Figure 143 A prior source with Particle Filters and the best fit LINE X-6 Iteration 10

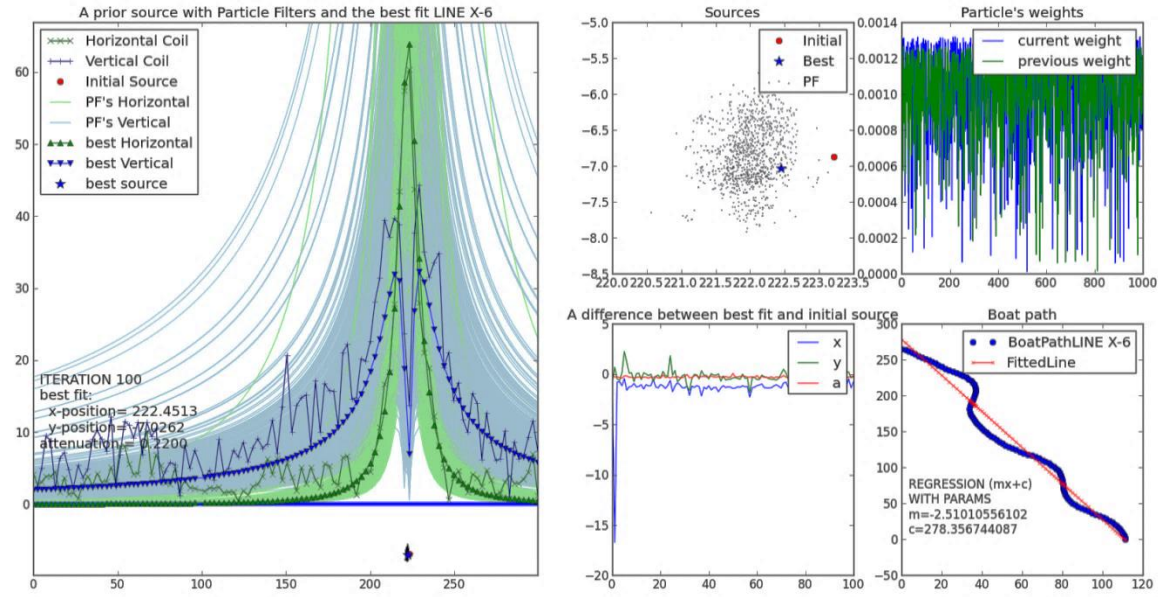

Figure 144 A prior source with Particle Filters and the best fit LINE X-6 Iteration 100

Appendix C.3 Line X-65

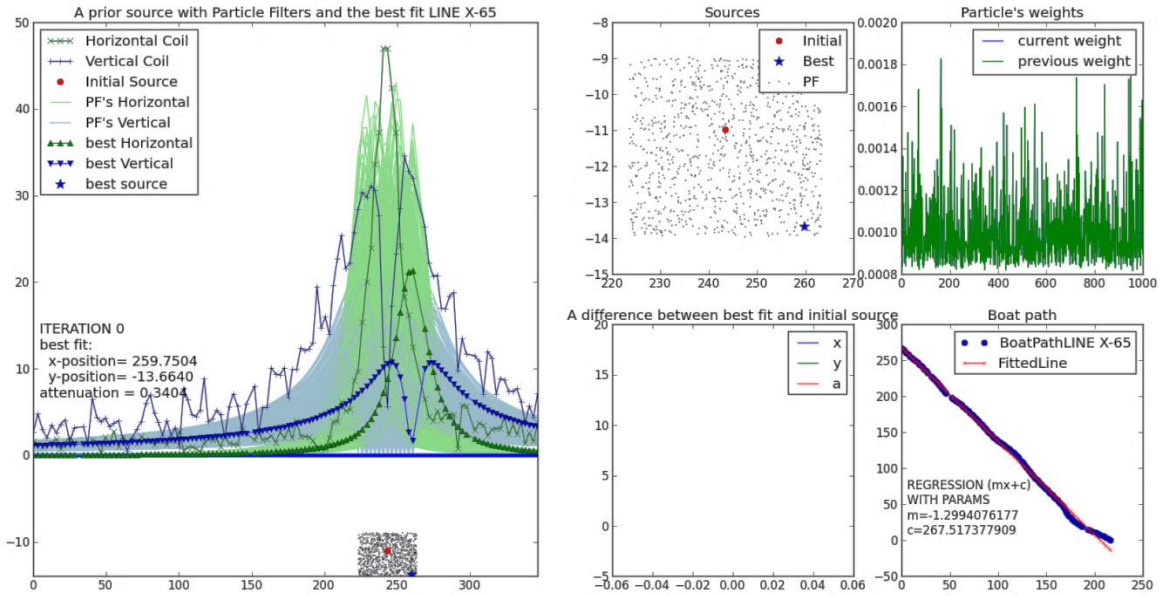

Figure 145 A prior source with Particle Filters and the best fit LINE X-65 Iteration 0

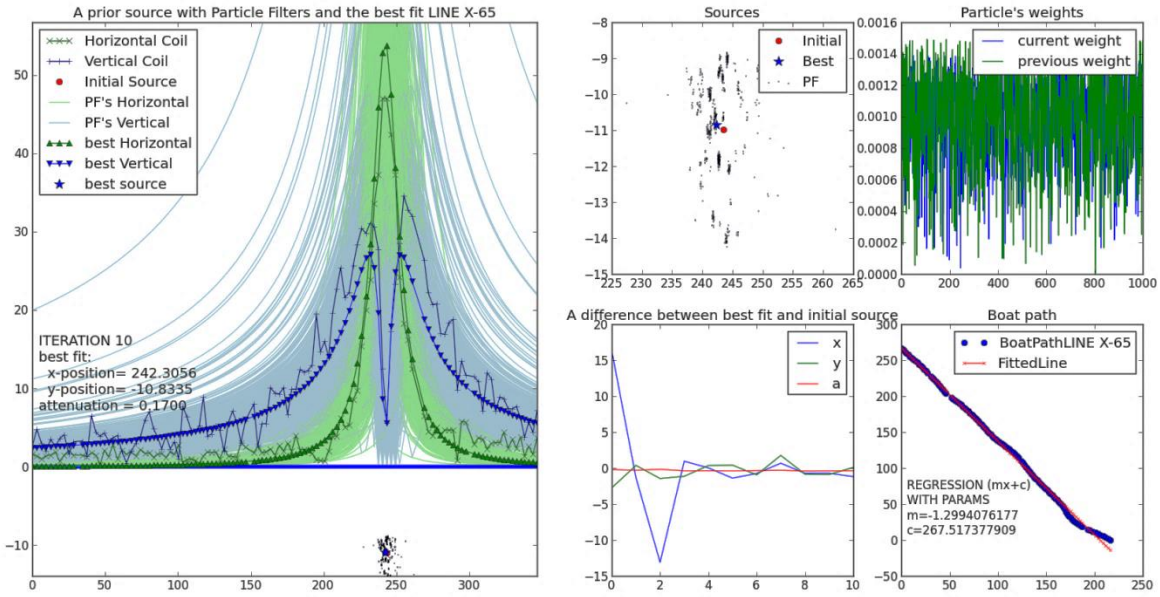

Figure 146 A prior source with Particle Filters and the best fit LINE X-65 Iteration 10

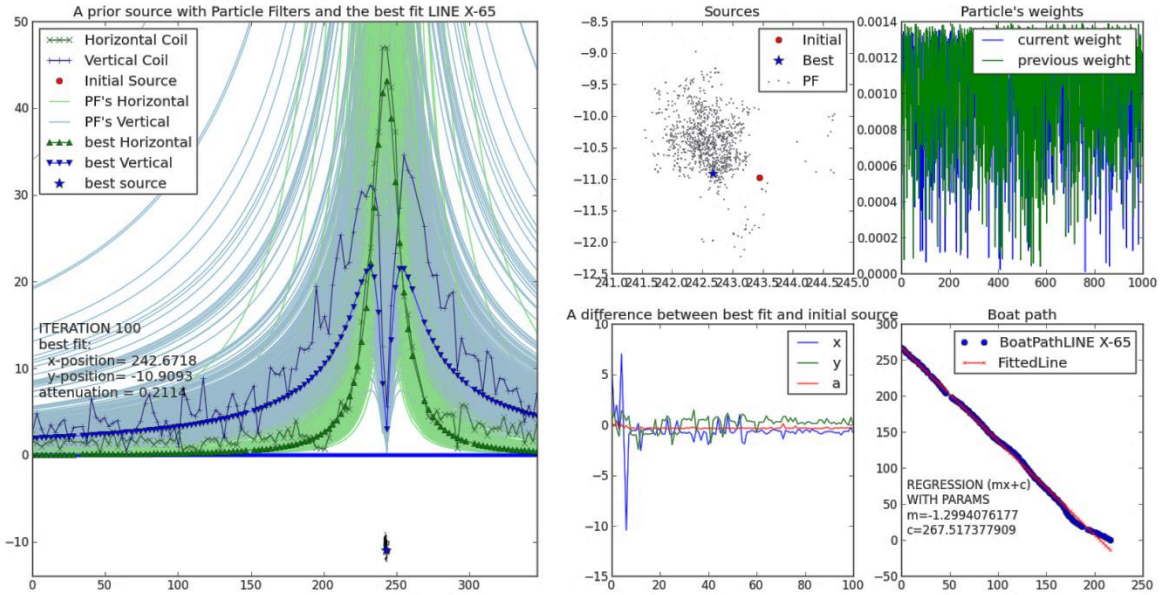

Figure 147 A prior source with Particle Filters and the best fit LINE X-65 Iteration 100

Appendix D BPF various problems

Appendix D.1 Fuzzy classifier – Matlab implementation

```
classdef FUZZY_MS < handle


    % FUZZY class for detecting relevant coil readings
    % the fuzzy flag (ff) is turned on (positive) if the coil readings
are
    % relevant and off (<=0) if the coil readings are made up solely of
    % noise and hence are discarded for estimating the magnetic source.

    properties (Access = private)

    end

    properties (SetAccess = public)
        M
        N
    end

    properties  (Dependent = true)

    end

    methods  % get and set methods
        function set.M(obj,value)
            obj.M = value;
        end

        function value = get.M(obj)
            value = obj.M;
        end

        function set.N(obj,value)
            obj.N = value;
        end

        function value = get.N(obj)
            value = obj.N;
        end

    end

    methods (Access = public)

        function obj = FUZZY_MS  %class constructor

        end

        function ff = calculate(obj,SMA)
```

```
            if SMA <= 0
                ff = -obj.N;
            elseif SMA > 0 && SMA <= obj.M
                mu_z = SMA/obj.M;
                mu_n = 1-SMA/obj.M;
                ff = -obj.N*mu_n;
            elseif obj.M < SMA && SMA < obj.M*2
                mu_p = (SMA-obj.M)/obj.M;
                mu_z = 1-(SMA-obj.M)/obj.M;
                ff = obj.N*mu_p;
            elseif SMA >= obj.M*2
                ff = obj.N;
            end
        end

    end

end
```

Appendix D.2 Particles resampling –implementation

Matlab implementation:

```
function newSources = resampleParticles2d(particles)
%% resampling particles with roulette wheel
%     Function takes N random sources and distances as weights
%     draws N new samples according to the weights
%     First newSources vector is initiated
%     from pldSources the points are drawn and append into new sources
    weights = particles(:,4);
    newSources=zeros(size(particles));
    % Resampling Wheel implementation
    % First index as random in oldSources
    N = length(weights);
    index = randi(N);
    beta = 0.0; % initialise to zero, change value after
    [maxWeight] = max(weights); % maximum weights from weights in
oldParticles

    for k = 1:N
        % can be as large as twice maximum from all weights
        beta = beta + rand * 2.0 * maxWeight;

%         while beta > weights(index)
%             beta = beta - weights(index);
%             index = (index + 1); %
%         end
        % adding whole position to NewSources
        while beta > weights(index)
          beta = beta - weights(index);
          index = index+1;
          if index > N
            index = 1;
          end
        end
        newSources(k,:) = particles(index,:);
```

```
    end
```

Python implementation:

```
    def importanceSampling(self, sources):
        '''Function takes N random sources and distances as weights
        draws N new samples according to the weights
        First newSources vector is initiated
        from pldSources the points are drawn and append into new
sources'''

        weights = sources[:,3]
        newSources=[]
        # Resampling Wheel implementation
        # First index as random in oldSources
        index = int(np.random.random() * self.N)
        beta = 0.0 # initialise to zero, change value after
        maxWeight = max(weights) # maximum weights from weights in
oldSources
        index = np.argmax(weights)
        for i in range(self.N):
            # can be as large as twice maximum from all weights
            beta += np.random.random() * 2.0 * maxWeight
            while beta > weights[index]:
                beta -= weights[index]
                index = (index + 1) % self.N
            # adding whole position to NewSources
            newSources.append(sources[index,:])
        newSources = np.asarray(newSources)
        return newSources
```

Appendix E Notation

$P_k(P_k^{(x)}, P_k^{(y)}, P_k^{(z)})$ measurement point k along the platform path

$S_k(S_k^{(x)}, S_k^{(y)}, S_k^{(z)})$ the source point on the cable for the measurement point k.

$p_k(p_k^{(x)}, p_k^{(y)}, p_k^{(z)})$ Vector of the movement along the platform path from the measurement point P_{k-1} to the point P_k

$h(h_k^{(x)}, h_k^{(y)}, h_k^{(z)})$ The vector of platform heading. The vector also describes the orientation of the magnetometers.

$d_k(d_k^{(x)}, d_k^{(y)}, d_k^{(z)})$	Vector of the movement along the platform path from the measurement point S_{k-1} to the point S_k
$f(S_{k-1}, S_k, d_k)$	Function describing path of the cable from the point S_{k-1} to S_k (linear regression, spline)
$\bar{d}_{k+1}$	*A priori* direction of the cable in the next step
$r_k(r_k^{(x)}, r_k^{(y)}, r_k^{(z)})$	Vector of the distance from the source point S_k to the measurement point P_k.

Appendix F Implementation Lock-in amplifier

Python implementation of Lock-in amplifier

```
'''

@author: Tomasz
'''
from __future__ import division
from numpy import *
from scipy.integrate import *
import pylab as pl

def reference(t, *args):
    f, phi = args
    return sin(2*pi*f*t + phi)

def signal(t):
    # fs = fl*0.9
    # return sin(2*pi*fs*t)
    # ee = 1
    # return (1-mod(floor(t),2))*(1-exp(-ee*mod(t,1))) + mod(floor(t),2)*(exp(-
ee*mod(t, 1))-exp(-ee))
    return 1 + mod(floor(t),2)*0.1

def lockin(t, *args):
    return reference(t, *args)*signal(t)
```

```
phl = linspace(0,90,6)/180*pi
for phi in phl:
    T = 10
    fl = 0.5
    # phi = 20/180*pi
    t = linspace(0, 10, 45)
    out = array([quadrature(lockin, tt-T, tt, args=(fl, phi), maxiter=60) for tt in
t])/T
    pl.plot(t, out[:,0], label='%d' %(phi/pi*180))

pl.legend(loc='best')
pl.show()
```

C – IMPLEMENTATION

LockAmp.c

```
#include "LockAmp.h"

void LockAmp::GetValue(double *amp,double *phase,int *samples,int *errors)
{
        //Take the lock
        pthread_mutex_lock(&mutexLock);

                for(int i=0;i<3;i++)
                {
                        amp[i] = sqrt(sinSumm[i]*sinSumm[i]+cosSumm[i]*cosSumm[i]);
                        phase[i] = atan2(sinSumm[i],cosSumm[i]);
                        sinSumm[i] = 0.0;
                        cosSumm[i] = 0.0;
                }

                *samples = summNumber;
                *errors = errNumber;
                //*errors = lineNumber;

        errNumber=0;
        summNumber=0;
        msTime=0;
        lineNumber=0;

        //Give back the lock
        pthread_mutex_unlock(&mutexLock);
}

void LockAmp::NewSample(char *line)
{
        static int lastSampleTime=0;

        char *pch = line;
        char *pos[10];
        int i=0;

        lineNumber++;
        while((pch=strchr(pch+1,',')) != NULL) //locate ',' positions brake if no more
        {
                *pch = ' ';                             //change ',' to SPACE
                if(i<10) pos[i++] = pch;    //save positions
        }
```

```
	if(i>7)
	{
		int time = (int)strtol(pos[1],NULL,10); //extract time stamp from
sample
		int Coil[3];
		Coil[0] = (int)strtoul(pos[5],NULL,16);	//extract coil 0
sample at 16 base
		Coil[1] = (int)strtoul(pos[6],NULL,16);	//extract coil 1
sample at 16 base
		Coil[2] = (int)strtoul(pos[7],NULL,16);	//extract coil 2
sample at 16 base

		if(time<1000)
		{

		int timeStep = time-lastSampleTime;
		if(timeStep<0)
		{
			//printf("jump %i %i \n",lastSampleTime,time);
			timeStep+=1000; //when jump from 99 to 0 occurs
		}
		lastSampleTime = time;
		//if(timeStep<20)
		//{

		//if(timeStep>1)
		//	printf("jump %i \n",timeStep);

		//Take the lock
		pthread_mutex_lock(&mutexLock);

			errNumber += (timeStep-1);  //if time step is bigger then 1
sample has beem missed
			msTime += timeStep;			//update ms time base
on sample

			double angle =
(((double)msTime)/1000)*2*M_PI*(double)frequency;
			for(int i=0;i<3;i++)
			{
				sinSumm[i] += ((double)Coil[i]) *sin( angle );
				cosSumm[i] += ((double)Coil[i]) *cos( angle );
			}


			summNumber++;

		//Give back the lock
		pthread_mutex_unlock(&mutexLock);

		//printf("%i %i %i %i\n",time,C[0],C[1],C[2]);
		}//}
	}
}

void LockAmp::SetFrequency(int freq)
{
	frequency = freq;
}

LockAmp::~LockAmp(void)
{
	pthread_mutex_destroy(&mutexLock);
}
```

```
LockAmp::LockAmp(void)
{
	sinSumm[0]=0.0;
	cosSumm[0]=0.0;
	sinSumm[1]=0.0;
	cosSumm[1]=0.0;
	sinSumm[2]=0.0;
	cosSumm[2]=0.0;

	lineNumber=0;
	errNumber=0;
	summNumber=0;
	frequency = 80;
	msTime=0;
	pthread_mutex_init(&mutexLock, NULL);
}
```

LockAmp.h

```
#ifndef LOCK_AMP_H
#define LOCK_AMP_H

#include <stdio.h>
#include <stdlib.h>
#include <unistd.h>
#include <string.h>
#include <pthread.h>
#define _USE_MATH_DEFINE
#include <math.h>

class LockAmp
{
	private:
		double sinSumm[3],cosSumm[3];
		unsigned int errNumber,summNumber,lineNumber;
		unsigned int frequency;
		unsigned int msTime;
		pthread_mutex_t mutexLock;
	public:
		void SetFrequency(int freq);
		void GetValue(double *amp,double *phase,int *samples,int *errors);
		void NewSample(char *line);
		LockAmp(void);
		~LockAmp(void);
};
#endif
```